Nanoparticules métalliques@polymères poreux : matériaux hybrides innovants pour la catalyse supportée

Romain Poupart

Thèse de Doctorat

présentée par :

Romain Patrick POUPART

pour obtenir le grade de Docteur de l'Université Paris-Est

École doctorale Sciences, Ingénierie et Environnement

Spécialité : Sciences des Matériaux

Nanoparticules Métalliques@Polymères Poreux :
Matériaux Innovants pour la Catalyse Supportée

Soutenue le 26 Octobre 2017 devant un jury composé de :

Rapporteurs

Christophe SINTUREL	*Professeur, Université d'Orléans*
Jean-François LAHITTE	*Maître de Conférences HDR, Université Toulouse III Paul Sabatier*

Examinateurs

Pascale MASSIANI	*Directrice de Recherche, CNRS*
Benjamin LE DROUMAGUET	*Maître de Conférences, Université Paris-Est Créteil*

Directeurs de thèse

Daniel GRANDE	*Directeur de Recherche, CNRS*
Benjamin CARBONNIER	*Professeur, Université Paris-Est Créteil*

Thèse réalisée au Institut de Chimie et des Matériaux Paris-Est

Equipe Systèmes Polymère Complexes

2-8 rue Henri Dunant

94320 Thiais

Tel : +33 (0)1

Fax : +33 (0)1 49 78 11 66

Web : http://www.icmpe.cnrs.fr/

Sous la direction de	Dr. Daniel GRANDE	grande@icmpe.cnrs.fr
Co-direction	Pr. Benjamin CARBONNIER	carbonnier@u-pec.fr
Co-encadrement	Dr. Benjamin LE DROUMAGUET	ledroumaguet@icmpe.cnrs.fr

“I've been running all my lives... through time and space.
Every second of every minute of every day for over nine hundred years.
I fought for peace in a universe at war.
Now the time has come to face the choices I made in the name of the Doctor.
Our future depends on one single moment of one impossible day.
The day I've been running from all my life.
The day of the Doctor.”

Doctor Who

Avant-Propos

Cette thèse a été rédigée sous la forme de différents articles acceptés ou parus dans des revues à comité de lecture mais aussi en cours de rédaction. L'indulgence du lecteur est donc sollicitée pour les répétitions et redites inhérentes à cette forme de rédaction choisie.

Remerciements

Mon premier et très sincère remerciement sera bien évidemment pour l'Université de Paris-Est qui, par le bénéfice d'une bourse du Ministère de l'Enseignement supérieur de la Recherche, a alloué le financement nécessaire à ces travaux de recherche et m'a ainsi permis de réaliser cette thèse.

Mon deuxième, et néanmoins tout aussi important, remerciement ira directement au personnel de l'Institut de Chimie et des Matériaux Paris-Est (ICMPE), et plus particulièrement à l'équipe Système Polymères Complexes (SPC) pour leur gentillesse, leur professionnalisme et pour m'avoir si chaleureusement accueilli parmi eux. L'environnement de travail et les personnes venus d'horizons différents m'ont aidé à apprendre plus et de tout le monde. J'associe à ces chaleureux remerciements Madame la Pr. Valérie LANGLOIS pour m'avoir accueilli au sein de l'équipe durant ces trois années.

Je tiens maintenant à remercier tout particulièrement MM. les Pr. Christophe SINTUREL de l'Université d'Orléans et le Dr. Jean-François LAHITTE de l'Université Toulouse III Paul Sabatier pour examiner et juger ensemble ce travail de recherche ainsi qu'à Madame la Dr. Pascale MASSIANI de l'Université Pierre et Marie Curie pour avoir accepté d'examiner ce travail.

Je souhaiterais aussi exprimer par ces quelques mots un énorme remerciement et une réelle reconnaissance pour ceux qui ont encadré ma thèse, le Dr. Daniel GRANDE, le Pr. Benjamin CARBONNIER et le Dr. Benjamin LE DROUMAGUET, pour m'avoir généreusement transmis leur intérêt dans de nombreux et divers domaines des polymères et de la chimie. Je leur suis grandement reconnaissant de tout ce qu'ils m'ont apporté et de ce que je suis devenu, principalement grâce à l'opportunité de faire cette thèse à leurs côtés. De plus j'aimerais associer à ce remerciement le Dr. Mohamed GUERROUACHE pour ses conseils avisés sur les capillaires et pour m'avoir si bien transmis son savoir dans ce domaine.

Je suis aussi très reconnaissant au Pr. Nicola PINNA et au Dr. Jörg POLTE pour m'avoir accueilli dans leur laboratoire de la Humboldt Universität à Berlin de janvier à mars 2017. Ils m'ont offert l'opportunité d'apprendre des choses nouvelles sur la chimie inorganique. Je me permets d'avoir ici une pensée bienveillante et une reconnaissance particulière envers Alexander BIRNBAUM, pour m'avoir ainsi supporté et aidé durant ces trois mois de stage, avec les autres étudiants, au laboratoire et au bureau, Dr. Frider KETTEMANN, Steffen WITTE, Sinem PALANTÖKEN, Sebastian WAHL, Rui ZHANG et Andréa MARTIN pour nos discussions, leur aide et l'ambiance qui y régnait là-bas. Je n'oublierai donc pas ces agréables moments « never, ever ».

Maintenant, il est de mon devoir d'exprimer ma reconnaissance et de remercier bien sincèrement le Dr. Davy-Louis VERSACE, pour m'avoir accepté en stage à l'ICMPE dès mon envie et mon souhait de « chercher ». Il m'a ainsi permis de développer et de concrétiser mon goût de la recherche. La photochimie a été le premier aperçu de la science que j'ai eu l'opportunité d'étudier et elle aura toujours une place spéciale dans ma tête.

J'aimerais enfin remercier le personnel de l'IUT de Créteil-Vitry avec lesquels j'ai interagi durant mes vacations, plus particulièrement, Marie-Laure TEYSSIER, Jean-Philippe COUZINIER et Nathalie BULTINCK. Ces journées d'enseignement, domaine qui me tient à cœur, m'ont permis de pratiquer et de connaître cette effervescence et ce merveilleux sentiment qui est la transmission du savoir.

Pour mener à bien cette thèse, j'ai eu l'occasion de travailler avec des stagiaires et plus directement avec Deena CHELLAPERMAL, Hadja DIAKHITE. Merci à vous. Un remerciement spécial à Nour El Houda DJERIR pour l'excellent travail dont elle a fait preuve et tous mes souhaits de réussite pour sa thèse à venir.

Que seraient les remerciements sans une mention spéciale à mes collègues doctorants ? Aussi mercis à Hai Bang LY, Gaëlle LE FER, Iurii ANTONIUK, Clément ROBIN, Seydina Ibrahima KEBE, Van Son VO, Tina MODJINOU, Erica Gea RODI, Marina ANDREEVA, Pierre PUBELLIER, Carine MANGEON, Antoine BENLAHOUES, Sarra MEZHOUD, Etienne DESSAUW, Alina VASHCHUK, Azad ERMAN, Aline-Sarah GLAIVE, Thibault LEROUGE, Pauline SAUTROT et Vierajitha « Viera » SRIKANTHAN du SPC mais aussi Jérôme PAUL et Priscilia KUTUDILA de l'équipe ESO. Les fructueuses et moins productives discussions ont rendu ces années mémorables ! Puis pour tous ceux qui ont dû me supporter dans l'enceinte de notre bureau, je leur adresse non seulement une dédicace spéciale mais aussi toutes mes excuses en retard pour les avoir malmenés.

Finalement, et je terminerai par ces derniers mots, j'aimerais remercier mes amis et ma famille, spécialement mes parents Christine et Patrick POUPART. Vous avez toujours été là pour moi et j'espère que vous serez fiers de ce que je suis devenu. Aucun mot dans aucune langue ne serait assez pour décrire à quel point je suis fier d'être votre fils.

Figure Captions

Table Captions

Table of Contents

Introduction

Depuis une cinquantaine d'années, la catalyse a pris un nouveau tournant avec le développement de synthèses de nanoparticules diverses et variées. Auparavant, les catalyseurs étaient majoritairement des complexes en solution. Il fallait donc les extraire et ces étapes, longues et fastidieuses, étaient aussi coûteuses. Compte tenu de la facilité à les isoler et éventuellement les recycler, couplée à l'essor des « nanos » dans les années 2000, les nanoparticules ont réussi à s'imposer dans le domaine de la catalyse hétérogène. A l'instar des complexes de métaux de transition, les nanoparticules métalliques peuvent être utilisées dans la plupart des réactions de chimie fine, avec la possibilité d'être récupérables *via* une filtration par exemple. Au cours des dernières années, les recherches se sont focalisées sur l'amélioration de la recyclabilité des nanoparticules. Si la force des nanoparticules est leur petite taille – permettant un excellent rapport surface sur volume et leur conférant ainsi des propriétés intrinsèques uniques –, elle peut aussi devenir leur faiblesse. En effet, l'étape de filtration nécessaire à leur récupération se complique avec la faible taille de pores requise pour des filtres efficaces. Une alternative à la filtration est de supporter les nanoparticules sur des matrices poreuses. Ces supports catalytiques, de taille macroscopique, sont donc facilement récupérables et l'étape de recyclage est facilitée. Pour être efficaces, ces supports doivent être particulièrement adaptés aux particules qu'ils devront accrocher. Différentes techniques pour pallier ce problème ont été développées. D'une part, des nanoparticules de types cœur/écorce avec un cœur de γ-Fe_2O_3 magnétique permettant la récupération par une simple aimantation et une enveloppe externe composé du métal d'intérêt pour la réaction catalytique envisagée. D'autre part, le développement de nouveaux types de supports notamment des matériaux inorganiques comme des silices poreuses ou des oxydes de titane, des assemblages organo-métalliques plus communément connus sous leur nom anglais de « metal-organic frameworks » (MOFs), mais aussi des polymères fonctionnels. Ces derniers sont d'un très grand intérêt comme supports catalytiques. Facilement synthétisables, modifiables et fonctionnalisables, ils offrent aussi une large gamme de porosités accessibles.

Différentes techniques sont disponibles pour générer des pores dans une matrice polymère et permettent d'en choisir la forme et la taille. Une méthode simple pour obtenir des macropores de taille supérieure à 1 µm est l'addition d'un agent porogène, qui peut être est un solvant, une macromolécule ou bien une particule solide de taille micrométrique qui servira d'empreinte. Par ailleurs, une méthode largement développée pour obtenir des nanopores (10-100 nm) est l'utilisation de segments polymères sacrificiels à partir de copolymères à blocs. Il peut également être envisagé la création de matériaux biporeux – combinant macro- et nanoporosité –, éventuellement à porosité hiérarchisée, en faisant

appel à des techniques telles que celle des émulsions concentrées en phase inverse (polyHIPEs), ou en combinant l'empreinte de particules de sel et l'usage d'un solvant porogène. La fonctionnalisation des matrices polymères, quant à elle, s'effectue généralement par modification chimique post-polymérisation en utilisant différents monomères possédant des groupements chimiques spécifiques et permettant une réaction simple et totale avec des molécules fonctionnelles. On peut citer par exemple les monomères chlorés, comme le 4-chlorure de vinylbenzyle pour des substitutions nucléophiles ou bien le méthacrylate de glycidyle pour des ouvertures de cycles avec des molécules aminées possédant une fonction spécifique à l'accrochage de nanoparticules comme une autre amine, un thiol ou bien un acide carboxylique. Réparties à la surface des pores fonctionnalisés, les nanoparticules joueront ainsi le rôle de catalyseurs supportés. Elles sont préparées soit directement sur la surface du support, par déposition précipitation dans une procédé dit *in situ*, soit en dehors puis immobilisée suite à une mise en contact entre le polymère fonctionnalisé et une solution colloïdale, respectivement *ex situ*.

Ce travail de thèse s'inscrit dans ce contexte et vise à développer la conception et l'élaboration de matériaux poreux polymères originaux en vue de leur future utilisation comme supports catalytiques. L'idée qui sous-tend ces recherches est d'exploiter une gamme variée de morphologies poreuses pour immobiliser des nanoparticules métalliques de différentes natures et valoriser les matériaux hybrides résultants en catalyse hétérogène supportée.

Le premier chapitre de cette thèse sera consacré à une étude bibliographique présentant dans un premier temps un état de l'art sur les polymères poreux. L'accent est mis sur les différents modes d'élaboration en lien étroit avec le niveau de porosité (macro- et nanoporosité ; porosité mono- *vs*. bimodale) recherché ainsi que les principales méthodes de caractérisation. Une seconde partie détaillera les approches utilisées pour l'immobilisation de nanoparticules à la surface des pores ainsi que les principaux usages de tels hybrides comme catalyseurs supportés rapportés dans la littérature.

Le deuxième chapitre traitera des polymères monolithiques macroporeux développés durant cette thèse. Un monomère original, le disulfure de bis(2-méthacryloyl)oxyéthyle, a été synthétisé et utilisé pour l'élaboration de monolithes massiques susceptibles de présenter des fonctions thiol à la surface des macropores. Ce monomère difonctionnel contient un pont disulfure aisément clivable en conditions réductrices, libérant ainsi les fonctions thiol désirées. Celles-ci permettent d'attacher des nanoparticules d'or générées *in-situ* et ainsi de catalyser la réduction d'un colorant, l'éosine Y. D'autre part, un polymère à base de méthacrylate de glycidyle contenant des fonctions amine superficielles, après aminolyse, a aussi été utilisé pour chélater des ions métalliques. Ces ions ont été réduits selon un procédé peu courant pour les polymères, en utilisant l'hydrogène gazeux. Les nanoparticules supportées ainsi formées ont été utilisées comme catalyseurs de réactions modèles de couplage de Suzuki.

Le troisième chapitre traite de la catalyse supportée en flux continu, une technologie avant-gardiste en pleine expansion dans le domaine pharmaceutique et qui répond aux exigences de développement durable et de chimie verte. Des polymères monolithiques macroporeux ont été confinés dans des microcanaux, *i.e.* des capillaires de silice fondue, dans le but de développer des microréacteurs catalytiques. Les avantages de la chimie en flux ont, dans un premier, été mis à profit pour d'une part, éliminer l'agent porogène et générer une porosité interconnectée compatible avec des utilisations à hauts débits, et d'autre part, fonctionnaliser la surface des pores par des groupements chélatants. L'étape de fonctionnalisation s'effectue dans des conditions dynamiques permettant une élimination des réactifs en excès par simple rinçage. L'interface des monolithes a été judicieusement ajustée en fonction de la nature du métal utilisé pour les réactions catalytiques. Ces microréacteurs, qui ont l'avantage de pouvoir traiter de faibles volumes en un temps très court, servent lors de réactions chimiques en flux continu. Ce domaine se prête très bien à la catalyse car lors de ces réactions, les réactifs sont introduits en tête de microréacteur et, lorsque les paramètres sont optimisés, seul le produit souhaité est récupéré. Dans ce chapitre, nous utiliserons tout d'abord une matrice déjà rapportée par notre groupe, à base de *N*-acryloxysuccinimide (NAS). Différents approches de fonctionnalisation seront utilisés. La première voie concernera une fonctionnalisation en deux étapes, *via* (*i*) le greffage de l'allylamine par une réaction l'addition-élimination des unités *N*-hydroxysuccinimide (NHS) suivie (*ii*) d'une réaction d'addition radicalaire de type thiol-ène pour greffer un diacide carboxylique permettant l'immobilisation de nanoparticules de cuivre. Par ailleurs, les unités NHS par différents ligands dérivés de l'éthylènediamine. L'influence de la nature chimique du ligand polyamine sur la répartition et la morphologie des nanoparticules et, *in fine*, sur l'efficacité de la réduction catalytique de composés aromatiques nitrés sera examinée. Nous nous intéresserons finalement à un monomère méthacrylate original contenant une fonction carbonate cyclique. La préparation et la caractérisation poussée de monolithes au sein de microcanaux seront présentées, tout comme l'application à la catalyse en flux continu.

Enfin, le quatrième chapitre sera dévolu à une méthode originale d'obtention de supports poreux en utilisant des copolymères à blocs possédant une jonction clivable telle qu'un pont disulfure ou bien un acétal cyclique. Ces polymères à architecture et fonctionnalité contrôlées ont été synthétisés à partir d'amorceurs difonctionnels asymétriques spécifiquement conçus à cet effet par des méthodes de polymérisations contrôlées comme la polymérisation radicalaire contrôlée par transfert d'atome (ATRP) du styrène et la polymérisation par ouverture de cycles (ROP) du D,L-lactide. Les copolymères diblocs ont ensuite été orientés par différentes techniques : par cellule de cisaillement mais aussi par recuit par vapeur de solvant. Après élimination quantitative du bloc sacrificiel de polylactide par clivage sélectif de la jonction spécifique entre les deux blocs, des pores fonctionnalisés ont été formés, ce qui a permis l'immobilisation de nanoparticules d'or générées *in-situ*. De tels catalyseurs supportés hétérogènes ont été utilisés avec une bonne efficacité dans différentes réactions

organiques modèles, et notamment de manière tout à fait originale dans une réaction en cascade combinant l'homocouplage d'un acide boronique, suivie de la réduction du composé aromatique nitré intermédiaire.

A la suite d'une conclusion générale mettant en lumière les faits saillants de ce travail de thèse, des perspectives seront exposées en ouvrant sur les futurs développements envisageables de matériaux hybrides à base de nanoparticules métalliques et de polymères poreux.

Chapter 1:

State of the Art

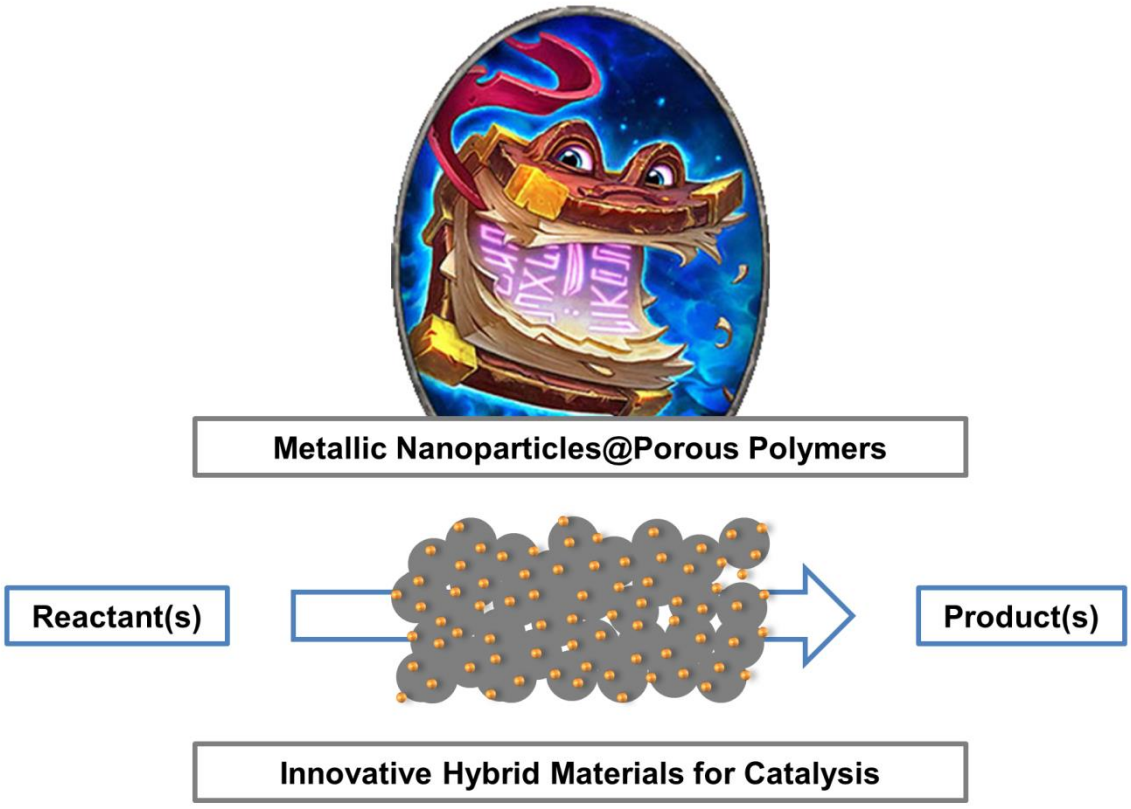

Contexte

Ce chapitre a pour objectif une mise au point bibliographique concernant les matériaux poreux polymères utilisés pour la catalyse supportée. Il y est décrit tout d'abord les principales voies de synthèse des matériaux poreux polymères, classées selon la taille des pores et la morphologie poreuse. Après une brève description de la synthèse des nanoparticules, différents exemples de matériaux hybrides polymères/nanoparticules issus de la littérature seront décrits. Ayant pour objectif d'être proposés comme revue bibliographique dans un journal traitant des matériaux fonctionnels. A ce titre, les résultats publiés et issus de mon travail de thèse sont également présentés comme autant d'exemples représentatifs de l'état de l'art.

Metallic Nanoparticles@Porous Polymers: From Porous Supports to Supported Catalysts

Abstract: Over the past recent years, nanoparticles have been the subject of numerous studies, due to their unique intrinsic properties. In particular, they have found widespread interest in heterogeneous catalysis, and their development in this area is growing. Nevertheless, they still display drawbacks and, among them, the question of their recyclability may arise. Instead of resourceful filtration, metallic nanoparticles may be advantageously supported on miscellaneous porous materials. Polymer materials can be envisaged as versatile and effective supports, due to their low production cost and easy functionalization. This review will first focus on different types of porous polymers developed in view of their further use as catalytic supports. Then, a brief description of the nanoparticles synthesis will be addressed, before a presentation of typical examples reported in the literature about metallic nanoparticles immobilized on porous polymers meant for heterogeneous supported catalysis.

1.1 Introduction

A catalyst is commonly described by the International Union of Pure and Applied Chemistry (IUPAC) as a substance that increases the rate of a reaction without modifying the overall standard Gibbs energy change in the reaction. Two different types of catalytic processes actually exist: *(i)* one type based on homogeneous catalysis, namely the catalyst is present in the same phase as the reactants, mostly a liquid phase,[1] while *(ii)* the other type is named as heterogeneous when the catalyst and the reactants are in different phases. Though, the frontier between both kinds of processes can be sometimes really thin in particular cases.[2] The metal-based catalyst is mostly in the solid state, finely divided, and the reactants are in the liquid or gaseous one. Nevertheless, some examples of heterogeneous biphasic catalysis reported that the catalyst remains in one liquid phase (*i.e.* water) and reactants in another one (*i.e.* oil), such as for the hydroformylation of propene, for instance.[3] One such example illustrates very well the possibility to perform catalysis by phase transfer. Recent developments in this research area notably demonstrated that catalytic reactions, especially organometallic-based ones, can be carried out in more environmentally-friendly conditions than a few years ago.[4] Such catalytic reactions more and more call upon green and sustainable chemistry, and efforts have been put forward in this direction to address specific issues related to the recycling of the catalysts.

In this context, supported metallic nanoparticles present some undeniable advantages regarding heterogeneous catalysis. They have actually shown an increasing interest in the last decade. Such nanometer-sized metallic particles, immobilized on high surface area materials, can now be relatively well characterized by different techniques and have shown some great catalytic performances. The preparation of such hybrid materials involves the design and development of still novel and efficient catalysts, and thus the improvement of (in)organic supports in terms of specific surface area, porosity, surface functionality and chemical inertness towards a wide variety of versatile or harsh reaction conditions.[5] Catalytic systems are commonly used in various industrial techniques[6] as well as in our common life, as demonstrated by automotive catalytic converters for instance.[5] While a serious drawback has been encountered with suspended nanoparticles, *i.e.* the recycling of the nanometal catalyst through time-consuming and non-environmentally friendly tedious purification processes, miscellaneous solutions exists. First, a recently reported solution to address this issue relies on the use of nanoparticles bearing a magnetic core, generally γ-Fe_2O_3. In this case, the nanometal recovery step can be achieved by harvesting with the help of a magnet.[7] Then, another solution consists in using macroscopic porous matrices as supports for the immobilization of metallic nanoparticles at the pore surface. The robust and straightforward immobilization of nanoparticles at the pore surface of suitable supports, notably by tuning the nature of the interface, enables to further avoid such purification processes, as the supported catalyst can be readily removed from the reaction mixture by mere filtration.

Hybrid catalysts based on supported metallic nanoparticle generally consist of (in)organic/hybrid porous frameworks presenting a rather high specific surface area that allows for a large amount of metallic nanoparticles to be immobilized in a straightforward and robust fashion. Among such high specific surface area supports, inorganic materials like zeolites[8] or ordered mesoporous silicas[9] can be found. On the other hand, organic polymer-based supports as well as carbon nanotubes[10] have been recently developed. Finally, hybrid structures, *i.e.* Metal-Organic Frameworks[11] (MOFs) have been deeply investigated in heterogeneous supported catalysis applications, due to their versatility and remarkably high surface area. In the case of polymeric materials, some advantages rapidly come to mind. They can first be easily functionalized so as to tune the pore surface chemistry; the porosity can also be readily varied in terms of pore size, ratio, and shape. Finally, such polymer-based porous supports have mechanical properties tunable in a useful range, and their production cost is lower than their inorganic analogues. On the opposite, some drawbacks can be noticed with such porous polymers: they cannot generally resist to high pressure and temperature, making some catalytic chemical reactions on these supports difficult to envision. However, they still remain common porous supports for metallic nanoparticles immobilization and are thus the subject of widespread interest in the field of heterogeneous catalysis.

In the light of this general introduction, this review will focus onto the design and synthesis of hybrid materials consisting of metallic nanoparticles immobilized at the pore surface of porous polymers for catalytic reaction purposes. A first section will be devoted to general features about porous polymer-based materials; then the main strategies to prepare such porous supports and the associated techniques of characterization will be presented. The reader should bear in mind that this section will not give a full overview of all strategies implemented for the synthesis of porous polymers, but it will rather focus on those mainly used for the preparation of porous polymeric systems meant for supported catalysis applications. It is thus recommended for casual readers to refer to more general reviews on porous polymers to get a full overview of their preparation routes.[12] A second section will then be directed towards the use of hybrid porous materials obtained after metallic nanoparticles immobilization at the pore surface of polymeric supports, and their further implementation in heterogeneous catalysis.

1.2 Porous Polymers: General features, synthesis, and characterization

1.2.1 Generalities on porous polymers

According to the International Union of Pure and Applied Chemistry,[13] porous solid materials can be classified into three main categories. Firstly, microporous materials are characterized by pore diameters below 2 nm. Secondly, the term “mesoporous” is used to qualify materials with pore

diameters between 2 and 50 nm. Finally, macroporous materials can be distinguished by a pore diameter larger than 50 nm. However, in the areas of materials science and nanotechnologies, the term "nanoporous" is commonly applied to materials containing pore sizes lower than 100 nm. Likewise, materials with porosity in the micrometer range (or more) are often called macroporous materials. This general classification can be applied to any type of porous material, namely inorganic, hybrid or organic ones.

1.2.2 Macroporous polymers

Macroporous materials may be prepared by different techniques through the use of miscellaneous porogens. In 1967, Seidl *et al.*[14] distinguished three main synthetic strategies to prepare porous polymeric matrices: *(i)* by using a porogenic solvent, *(ii)* by using a non-solvent as the porogen or *(iii)* by adding a linear polymer as a macromolecular porogen. According to Svec and Fréchet, these synthetic strategies are the most commonly used, but above all they are easy to implement.[15]

When a solvent is used as a porogenic agent, the initiator, monomer(s) and cross-linker are dissolved in a solvent or in a solvent mixture. When the polymerization is triggered by photochemical or thermal decomposition of the initiator, polymeric particles nucleate, grow, and coalesce in the solvent. Depending on the affinity of the solvent for the growing cross-linked polymer, the former will be ejected more or less promptly from the polymer matrix, creating voids filled with solvent. Upon porogenic solvent removal, these voids generate the porosity within the polymeric material. As the moment of the solvent ejection is closely related to the solvent and polymer compatibility, the pore size of the resulting materials can be thus easily tuned by merely changing the solvent polarity. In addition, the porosity ratio will also be dictated by the comonomers/(co)solvent(s) volume ratio. Finally, the porosity can be open or closed, depending on the amount of porogenic agent chosen. For very low porogenic solvent(s) to (co)monomers ratio, it is particularly true.

Such a way of generating porosity within polymeric materials has been widely implemented notably for preparing polymer-based monolithic columns with an interconnected porosity. This enables liquids or gases to easily flow through such monolithic columns, depending on the average pore size of the material as well as on the viscosity of the solvent, to avoid too high back pressures. Different monolithic columns have been prepared so far following this synthetic strategy, whatever the nature of the monomer used. Generally, the monomer is functional, that is to say it possesses a chemical moiety that can be easily chemically modified through a post-polymerization step consisting of a reaction occurring at the interface of the pore with the surrounding fluid, allowing for the interfacial properties of the pore surface to be easily tuned. Historically, the first monolithic capillaries were prepared by Svec's research group in the mid-1990's using glycidyl methacrylate (GMA) as a

functional monomer.[16] GMA bears an epoxide moiety that can be easily functionalized through ring-opening reaction with rather strong nucleophiles like amines.[16] Later on, the same research group has deeply expanded his pioneering works on the exploitation of GMA monomer, notably for chromatographic applications.[17] It is now used in other laboratories,[18,19] allowing for a plethora of potential applications to be envisioned. In the late 1990's, 4-chloromethyl styrene, also known as 4-vinylbenzyl chloride (4-VBC or VBC), was investigated in applications related to monolithic columns.[20] This styrenic monomer gave birth to highly hydrophobic columns, while the pore surface of the resulting materials can be easily tuned by nucleophilic substitution of the benzylic chlorine. It is worth mentioning that such functionalization reactions can lead to hypercrosslinked materials, provided that the chemical graft to anchor possesses two identical reactive groups.[21] 2-Vinyl-4,4-dimethylazlactone (VDMA) is another interesting monomer used for the preparation of porous materials.[22] Indeed, VDMA can be readily incorporated into the composition of polymerization mixtures in conjunction with diverse hydrophilic monomers, *e.g.* 2-hydroxyethyl methacrylate and acrylamide, to prepare functional in-capillary monoliths that can be functionalized with amine bearing bio(macro)molecules.[22] Finally, *N*-acryloxysuccinimide (NAS) and glycidyl carbonate methacrylate (GCMA) have been more recently implemented for the design of innovative functional porous in-capillary columns, as shown in **Figure 1-1 A**.[23] NAS can undergo nucleophilic substitution due to the presence of pendant activated ester moieties and has been widely used for chromatographic applications, such as capillary electrochromatography (CEC) separations[24–29] or for flow through catalysis applications.[30] Alternatively, oligomeric or polymeric chains have also been used as porogens in other studies (**Figure 1-1 B**).[31,32]

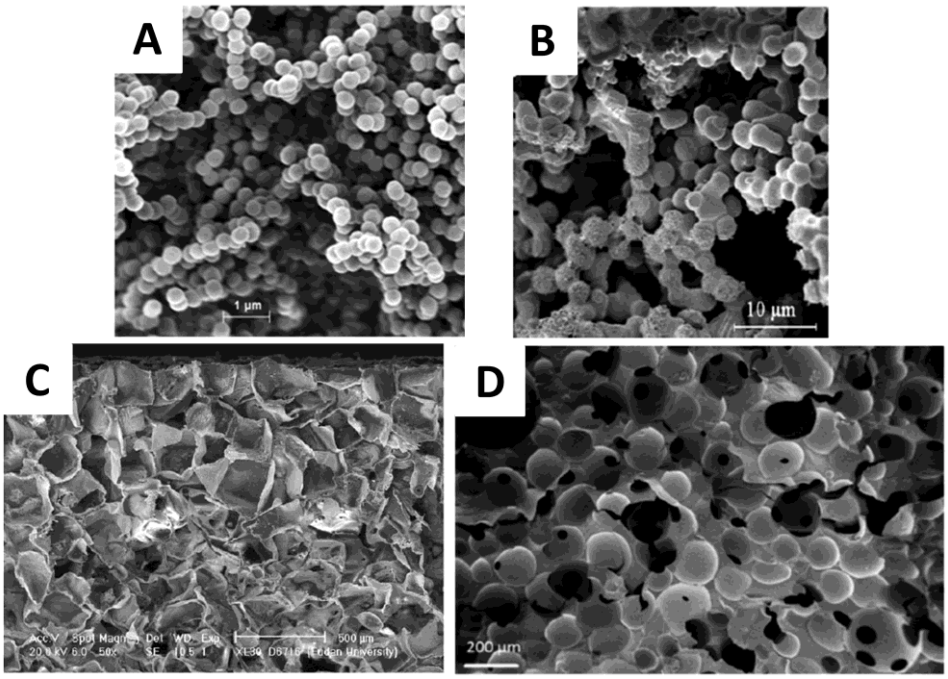

Figure 1-1: Examples of macroporous polymeric materials derived from the use of *A)* a porogenic solvent, *B)* a linear polymer, *C)* NaCl cubic particles and *D)* PMMA beads as macroporogens.

Other porogens than those defined by Seidl and coworkers are nowadays commonly used for different purposes. Especially, macroporogen templating has gained a tremendous interest in the last years. It relies on the use of a so-called template which acts as a macroporogen. It is added to the initial polymerization mixture (consisting of the initiator, the (co)monomer(s) and the cross-linker(s)) and immediately removed after the polymerization completion. The judicious choice of this porogenic template notably allows for tuning the pore morphology as the pores will present a shape that perfectly matches the template imprint. Such porogenic templates are based on solid, mostly inorganic crystal particle, such as sodium chloride (NaCl),[33] calcium carbonate ($CaCO_3$)[34] or ammonium bicarbonate (NH_4HCO_3)[33] particles, for instance. The use of such a methodology presents some non-negligible advantages as it permits to vary the size (by particle sieving) and morphology (depending on the shape of selected porogen) of the pores, while their removal is generally simple to achieve through easy template leaching into an appropriate aqueous solution. In fact, they are usually dissolved in pure water through particle leaching, such as for the extraction of NaCl particles. Alternatively, $CaCO_3$ particle-based templates require an acidic aqueous solution to be removed from the polymer matrix. It is worth mentioning that the porogenic template could also be prepared with the desired shape[35] (**Figure 1-1 C**). As a matter of fact, other investigations reported on the use of different sacrificial templates derived from organic (macro)molecules, such as paraffin or poly(methyl methacrylate) (PMMA) beads. In this case, the porogen could also be dissolved *via* Soxhlet extraction with an

appropriate organic solvent. LaNasa *et al.*[36] and Le Droumaguet *et al.*[37] independently demonstrated that it is possible to successfully use sintered polymeric PMMA beads as an original porogenic template (**Figure 1-1 D**). Such sintered PMMA beads could further be extracted in organic solvent, while the porous polymeric matrix remains intact, due to permanent cross-linking. These sintered spherical beads allowed for the generation of interconnected spherical pores upon removal of the macroporogen.

1.2.3 Nanoporous polymers

Miscellaneous approaches have been developed so far to prepare nanoporous polymer-based materials. These materials are mostly used as filtration membranes. In this particular case, the process is subtler than for the preparation of macroporous materials, and it usually involves the removal of a sacrificial polymer segment from nanostructured precursors, thus generating pores at the nanoscale level. Techniques like track-etching which lead to nanopores will not be discuss here, but reviews discussing the subject may be easily found.[38]

A largely investigated strategy consists in specifically removing one sacrificial block from oriented block copolymers (BCPs), thus leading to ordered nanoporous materials *via* a process milder than that used with other strategies. BCPs and especially diblock copolymers develop very precise equilibrium domain morphologies depending on three main critical parameters, *i.e.* the volume fraction of both blocks *f*, the number of repeating units *N* in the copolymer and χ_{AB}, the Flory-Huggins interaction parameter between both alien blocks.[39] According to theoretical phase diagrams, body-centered spheres, hexagonally close-packed cylinders, bicontinuous gyroids or alternating lamellae can be obtained (**Figure 1-2**).[40] Additionally, it is worth mentioning that the molar mass distribution of the copolymer should also be as narrow as possible in order to obtain highly ordered structured materials. So far, different natures of sacrificial blocks have been implemented to prepare nanoporous materials from this strategy. Historically, the first diblock copolymer precursors used were constituted of a degradable polyisoprene (PI) block and of a stable polystyrene-derived (4-vinylphenyl)dimethyl-2-propoxysilane) block, both synthetized by anionic polymerization. The former block was removed by ozonolysis that selectively cleaved the carbon-carbon double bonds of the isoprene units, while the polystyrene (PS) segment was simultaneously crosslinked, thus revealing nanoporous PS-based networks.[41] Later on, other research groups have successfully developed other sacrificial blocks by varying the conditions of etching[42]. Herein, we will focus on poly(D,L-lactide) (PLA), which has been widely used in the area of nanoporous polymers.

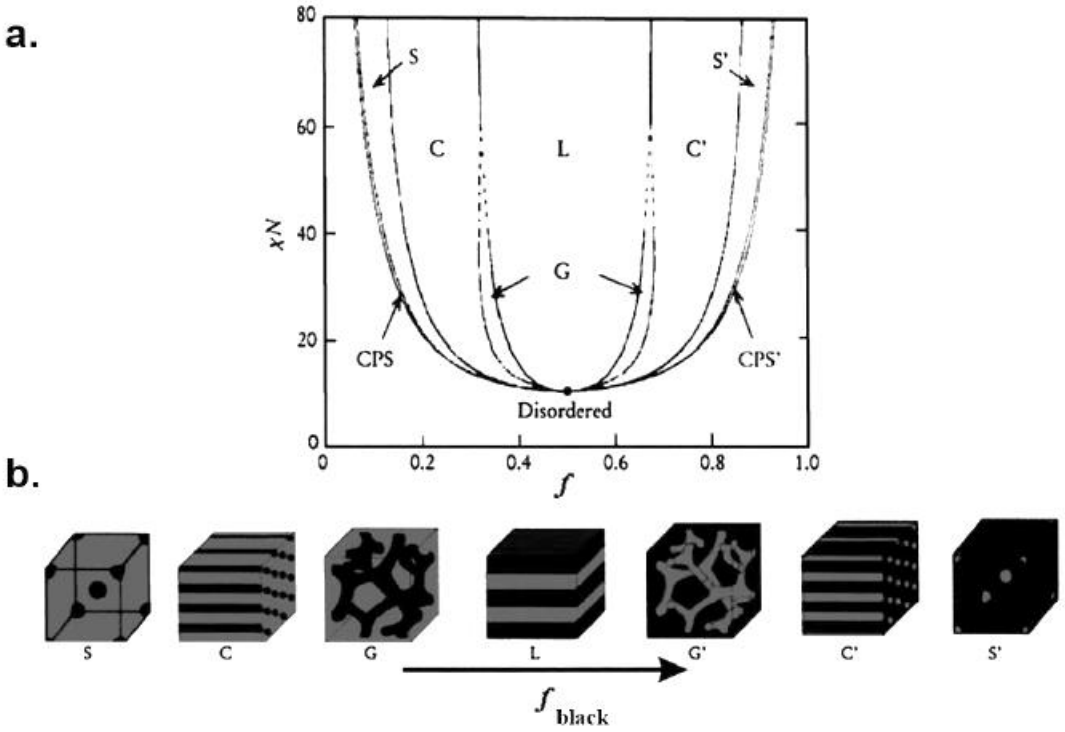

Figure 1-2: *a)* Morphology diagram of AB diblock copolymers obtained upon orientation of respective BCP domains depending on the segregation regime (χN) and of the volume fraction of the minor component (*f*); *b)* Schematic representation of the various possible morphologies depending on f_{black}: S and S': body-centered cubic spheres; C and C': hexagonal close-packed cylinders; G and G': bicontinuous gyroids; L alternating lamellae.

PLA can be synthetized *via* anionic or coordinative ring-opening polymerization (ROP) of 3,6-dimethyl-1,4-dioxane-2,5-dione (usually called D,L-lactide), from alcohol-[43] or amine-based initiators[44] in the presence of organic[45] or organo-metallic[46] catalysts. PLA is generally etched in mild conditions, namely in alkaline conditions and especially in NaOH or KOH hydro-alcoholic solutions, as described by numerous studies from Hillmyer and coworkers first in 2001[47] or later on from our research group[48,49](**Figure 1-3 A**). It is worth noticing that PLA can also be degraded in acidic conditions. It is not until recently that such etching conditions have been reported in the literature for PS-*b*-PLA.[50]

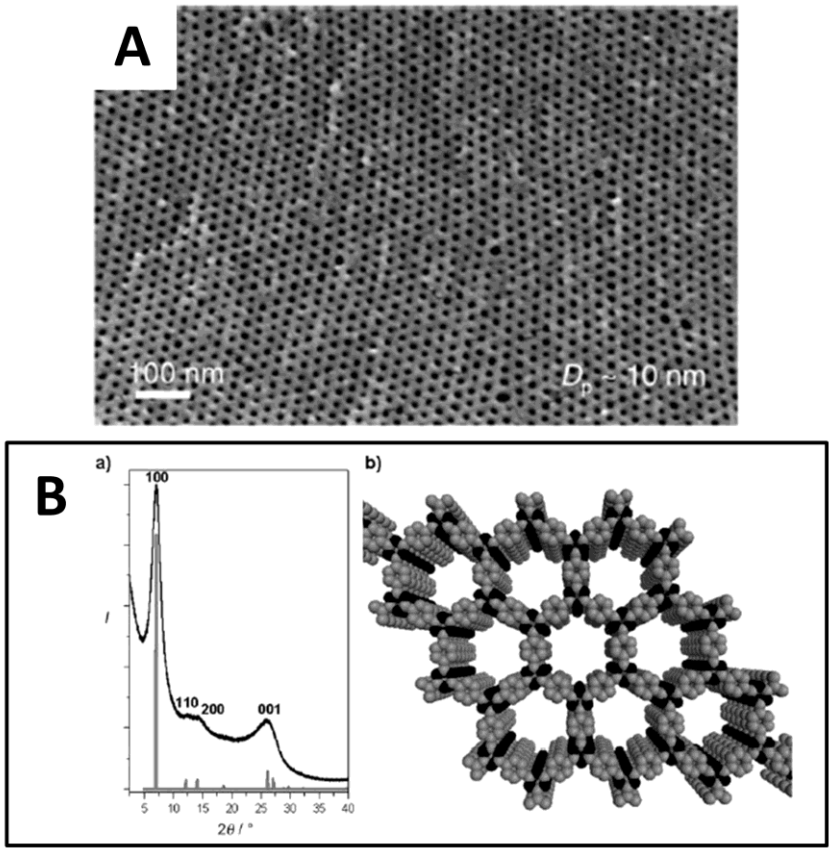

Figure 1-3: Examples of nanoporous polymeric materials with nanopores arising from *A)* selective hydrolysis of the PLA sacrificial block in a PS-*b*-PLA diblock copolymer, and *B)* an intrinsically microporous polytriazine network.

Another somehow smarter strategy to etch the sacrificial block from BCPs relies on the selective cleavage of the junction present between both block. Indeed, the degradable character of such a junction can lead to easy and straightforward removal of the entire sacrificial block in a non-solvent of the remaining block. Such a strategy notably permits to carry out the sacrificial block removal in milder conditions than those employed for the chemical degradation of the block itself and to ensure the presence of a well-defined functional group at the pore surface. Russell's group pioneered this elegant strategy by precisely positioning an anthracene photodimer at the junction between both blocks of a polystyrene-*block*-poly(methyl methacrylate), the PMMA sacrificial block being further released from the oriented diblock copolymers by dissociation of the photodimer under UV or thermal stimuli, thus revealing nanopores.[51] Later on, different selectively cleavable chemical junctions have been used in diblock copolymers. They can be categorized into three main sub-classes. The first one relies on using an irreversibly cleavable junction between both blocks (**Table 1-1**). Trityl ether[52,53] which is easily cleavable by trifluoroacetic acid (TFA), *o*-nitrobenzyl ester[54–57] or carbamate[58] derivative, hemiacetal junction[59] or acetal moiety[60,61] for instance have been successfully implemented

in this context. Other strategies involving reversible junctions have also been put forward, such as the aforementioned [4π+4π] anthracene photodimer,[51,62] disulfide bridges,[63,64] oxi-imines[65] or hetero Diels-Alder adducts arising from RAFT agents,[66] for instance, as depicted in **Table 1-2**. Finally, other investigations reported on the possibility to implement supramolecular junctions to link both blocks in a non-covalent manner, as shown in **Table 1-3**. We can notably mention the use of terpyridine-ruthenium[67] or terpyridine-nickel[68] complexes, ionic interactions[69] or even hydrogen bonds[70] taking place between the two adjacent blocks of oriented copolymers.

Table 1-1: Irreversibly cleavable junctions used for the preparation of functionalized nanoporous polymers.

Type of block junction	Junction formula	Cleavage agent/stimulus	Chemical function remaining after cleavage	References
Trityl ether	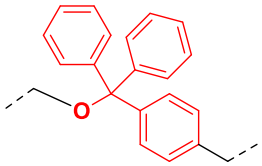	Brønsted or Lewis acid (ex: TFA)	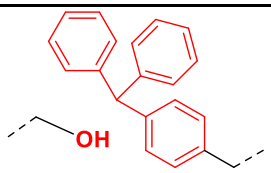 Primary alcohol	52,53
***o*-nitrobenzyl ester**	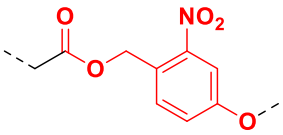	UV light (λ = 350 nm)	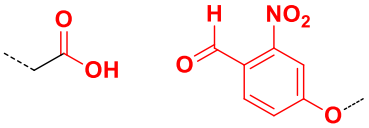 Carboxylic acid	54–57
***o*-nitrobenzyl carbamate**	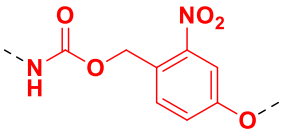	UV light (λ = 300 nm)	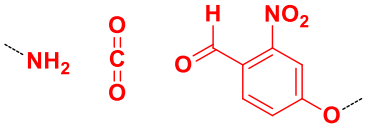 Primary amine	58
Hemiacetal ester	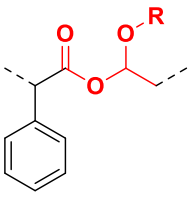	TFA	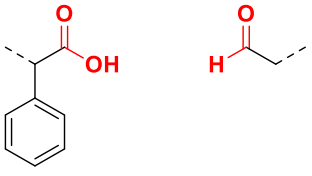 Carboxylic acid	59
Acetal	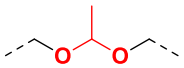	TFA	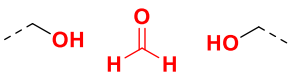 Alcohols	60
Acetal	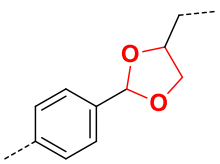	TFA	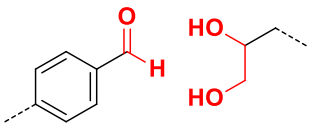 Aldehyde	61

Table 1-2: Reversible junctions used for the preparation of functionalized nanoporous polymers.

Type of block junction	Junction formula	Cleavage agent/stimulus	Chemical function remaining after cleavage	References
[4π+4π] anthracene photodimer	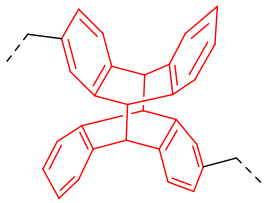	UV light (λ = 280 nm) 130-200 °C	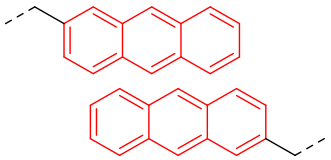 Anthracene	51,62
Disulfide bridge	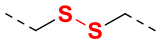	D,L-dithiothreitol, triphnylphosphine, glutathione	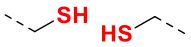 Thiol	63,64
Oxi-imines	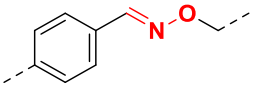	TFA	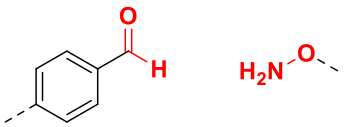 Primary amine	65
Hetero Diels-Alder adduct	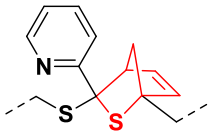	110 °C	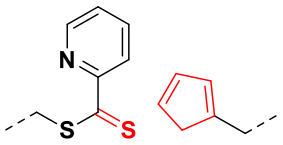 Thio-carbonyl-thio RAFT agent	66

Finally, some polymeric materials develop intrinsic free volume that can be assimilated to micropores; this is the so-called intrinsic microporosity. Such micropore sizes notably allow such types of material to be used for gas-related applications[71–73] especially for separation sciences, gas storage or heterogeneous catalysis in the gaseous phase. Only monomers that offer a good rigidity to the polymer network can prevent them from pore collapse and enable a permanent microporosity. Polymeric microporous polycyanurate,[74] polyisocyanurate,[75] polyurethane,[76] polytriazine[77] (**Figure 1-3 B**), based on Tröger's base[78] or porous aromatics frameworks[79,80] can be found among such innovative materials.

Table 1-3: Supramolecular junctions used for the preparation of functionalized nanoporous polymers.

Type of block junction	Junction formula	Cleavage agent	Chemical function remaining after cleavage	References
Terpyridine-ruthenium complexes	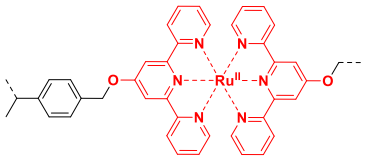	$Ce(SO_4)_2/H_2SO_4$ solution (pH = 1)	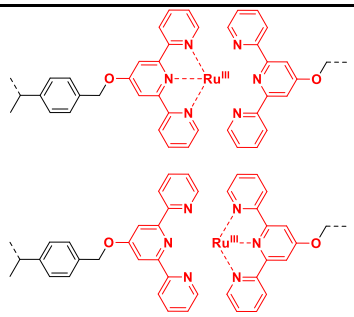 Terpyridine ligand	67
Terpyridine-nickel complexes	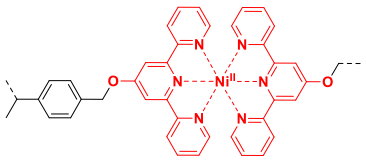	KCN	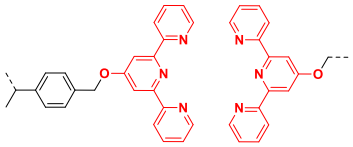 **$K_2[Ni(CN)_4]$** Terpyridine ligand	68
Ionic interactions	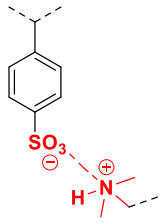	NaCl in $MeOH/H_2O$ solution	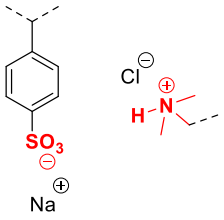 Sulfonate	69
Hydrogen bonds donor-acceptor	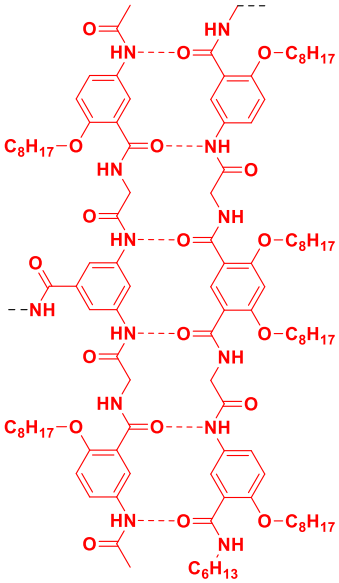	H_2O/MeOH (50/50 % v/v) followed by $CHCl_3$	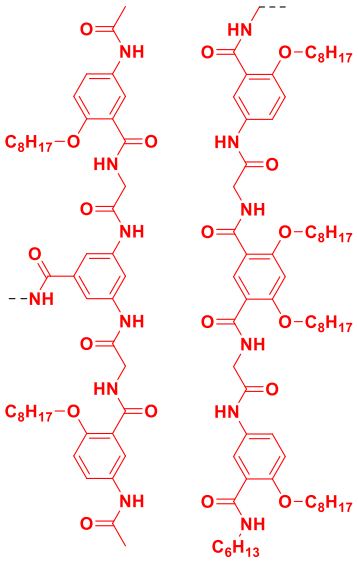 Hydrogen bond building block	70

1.2.4 Biporous polymers

Biporous materials have gained a tremendous interest within the last decades in different research area, such as civil engineering, tissue engineering or even drug delivery. Scientists are now able to prepare porous polymers possessing at least two distinct levels of porosity. Several methods have been so far developed to prepare biporous materials, including rapid prototyping (also called solid free-form fabrication or additive manufacturing) which is underdone by 3D printing[81], gas foaming,[82] temperature-induced phase separation (TIPS),[83] the polyHIPE technique or the double porogen templating approach. Due to purpose considerations, this part will essentially focus on electropsun materials, polyHIPEs, and doubly porous materials derived from the double porogen templating approach, as these three strategies were recently implemented in the literature for the preparation of hybrid polymer-based materials dedicated to supported catalysis.

Closely related to the use of a 3-D printer (*i.e.* rapid prototyping) for constructing biporous materials, electrospinning is a powerful technique that allows for the formation of highly porous scaffolds from solutions of polymeric materials.[84] The electrospinning process was patented by Anton Formhals in 1934,[85] and it was intensively developed by Reneker's research group[86,87] in the 1990's and 2000's with the emergency of nanotechnologies. Electrospun materials are prepared by applying a high voltage electrostatic field (usually in the 10-30 kV range) between a syringe containing a viscous polymeric solution and a collector for the deposition of polymeric fibers. Due to the fiber packing, pores with a wide pore size distribution are generated between fibers, thus allowing for the production of macroporous materials with highly interconnected voids and a large ratio of surface area to volume.[88] Electrospun polymeric fibers present morphological similarities as natural collagen fibrils, and their morphologies can be easily tuned by varying different parameters, such as the voltage, the syringe needle-to-collector distance, the polymer solution flow rate, the solvent volatility and polarity, the polymer solution viscosity and conductivity, *etc.* Therefore, choosing appropriate (co)solvents and electrospinning parameters are crucial to finely control the porous features of resulting polymeric materials.[89] (**Figure 1-4 A**)

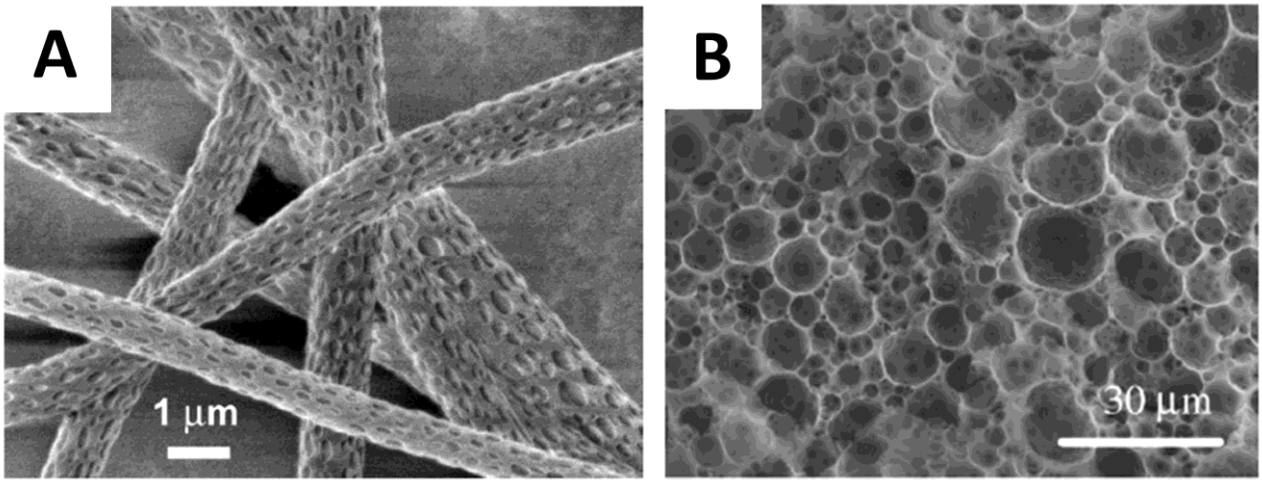

Figure 1-4: Examples of biporous polymeric materials generated by *A)* electrospinning and *B)* polyHIPE process.

Alternatively, polymerization of High Internal Phase Emulsions (HIPEs) is a technique of choice to prepare biporous polymeric frameworks.[90,91] Such materials were first designed by Barby and Haq from Unilever in the early 1980's.[92] In this patent, the authors reported on the preparation of a biporous polymer network obtained after the polymerization of a high internal phase emulsion, the porous polymer being subsequently called polyHIPE. In such polyHIPE-based scaffolds, the higher porosity level arises from drops of the discontinuous phase of the emulsion, while the lower one originates from the interconnections between adjacent pores. PolyHIPEs can be prepared from water-in-oil (w/o)[93], oil-in-water (o/w)[94] emulsions or from emulsified biphasic systems constituted by two immiscible liquids[95] in the presence of surfactants that help to the emulsion stabilization. Due to monomers and cross-linkers remaining in the external continuous phase, w/o emulsions are appropriate to yield hydrophobic polymers such as styrenic polyHIPEs[96] while o/w emulsions are suitable for the production of more hydrophilic polymers.[94] (**Figure 1-4 B**)

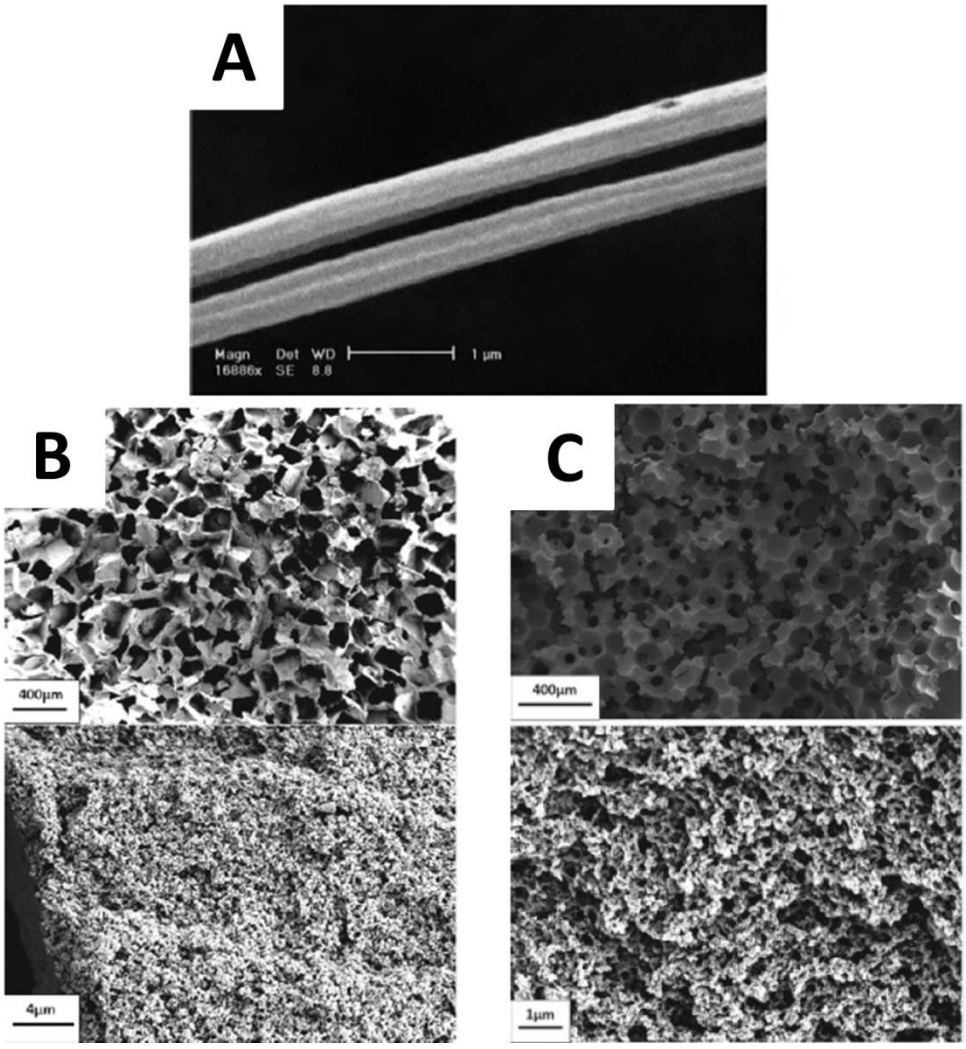

Figure 1-5: Examples of doubly porous materials made by a double porogen approach: *A) via* a combination of electrospinning and $CaCO_3$ particle leaching; *B) via* a combination of NaCl particle leaching and the use of a porogenic solvent; and *C) via* extraction of PMMA beads and a porogenic solvent.

Last but not least, the double porogen templating approach consists in using two different types of porogenic agents, *i.e.* one for the generation of pores within the micrometer range and the other one to obtain pores within the nanometer range. For instance, the use of electrospinning and particle leaching[97] (**Figure 1-5 A**) allowed for the preparation of materials with a macroporosity generated by the fibers organization and a nanoporosity revealed by calcium carbonate particle leaching using g 1, 3, and 5% v/v of HCl aqueous solution, increasing the specific surface area of the porous scaffolds. Another interesting approach using two different porogens was described by Ly *et al*. Poly(HEMA-*co*-EGDMA) monoliths were synthetized using macroporogenic agents consisting of fused PMMA beads[98] or NaCl particles[98–101] and different porogenic solvents (**Figure 1-5 B & 1-5**

C).[99] The fused macroporogens allow for the pores generated after particle leaching to be interconnected, while the porogenic solvent gives rise to a lower porosity level, thus enhancing the specific surface area of the resulting doubly porous materials. Different experimental conditions such as the particle sintering conditions (Spark Plasma Sintering *vs.* vacuum oven), the particle morphology (spherical *vs.* cubic) as well as the porogenic solvent nature were carefully investigated. Such studies have led to optimized materials on which were immobilized gold nanoparticles, thus leading to porous hybrid materials meant for heterogeneous supported catalysis.[101]

1.2.5 Characterization techniques of porous materials

Different techniques have been so far developed for the fine characterization of porous materials. In this way, critical information, including pore size, pore size distribution, pore connectivity (open *vs.* closed, *i.e.* presence or absence of interconnections between adjacent pores), and specific surface area, can be accurately determined using complementary physico-chemical techniques in the laboratory.

Two different techniques are mainly used to determine the pore size of porous polymeric materials. Such techniques rely on the type of porous materials under investigation. Mercury intrusion porosimetry (also shortened as MIP, **Table 1-4**) is a specific technique consisting in intruding a non-wetting liquid, *i.e.* mercury, into a porous sample placed within a penetrometer. Upon applying an increasing pressure, mercury is forced to intrude into the pores of the material.[102] Mercury does not wet materials, and so it will not penetrate pores by capillary action, excepted if it is forced to do so by applying the said pressure. The pore size can then be determined by correlating the pressure required for mercury intrusion into the pores to the pore size *via* the Washburn equation[103] (**Equation 1**):

$$P = \frac{-4\gamma \cos\theta}{D} \qquad \textbf{Equation 1}$$

where P is the pressure applied for the mercury intrusion, γ is the mercury surface tension, θ is the contact angle between the mercury and the pore wall, and D stands for the diameter of the pore being intruded.

It is noteworthy that the pores are supposed to by cylindrical in this equation, while most of the real porosity is not. As said before, for MIP analyses, the porosimeter apply a pressure to force mercury intruding the pores, and the Washburn equation allows for determining the pore diameter.[104] Applying an increasing pressure indeed pushes known amounts of mercury into the porosity of the material, and it thus allows for determining the pore volume for a precise pore size. Additionally, knowing the distribution of the pore volume with respect to its pore size provides the pore size

distribution.[105] However, this technique has some limitations especially regarding pore sizes in the nanometer range.

For materials exhibiting pore sizes within the few nanometer range, gas sorption is much more appropriate, especially for accuracy reasons.[13] Gas sorption measurements can use different gases: mostly N_2[106] is used, but CO_2[107] or Kr[108] can also be employed at a precise temperature to obtain isotherms. Gas sorption porosimetry is now routinely used to determine the specific surface area of porous materials, using the Brunauer-Emmett-Teller (BET) method,[109] whose equation is given below (**Equation 2**):

$$\frac{P}{n^a(P_0-P)} = \frac{1}{n_m^a C} + \frac{(C-1)}{n_m^a C} \times \frac{P}{P_0} \qquad \textbf{Equation 2}$$

where n^a is the gas amount adsorbed at the relative pressure $\frac{P}{P_0}$, n_m^a is the monolayer capacity, and C is a constant, which is function of the isotherm shape. According to this equation, a linear relation exists between $\frac{P}{n^a(P_0-P)}$ and $\frac{P}{P_0}$ so it is possible to determine n_m^a, thus leading to (**Equation 3**):

$$A(BET) = n_m^a \times L \times a_m \qquad \textbf{Equation 3}$$

where *A(BET)* is the specific surface area, L the Avogadro constant, and a_m the average area occupied by each adsorbed molecule in the complete monolayer (*i.e.* the molecular cross-sectional area).

Gas sorption measurements can also give pore sizes for porous materials exhibiting a porosity from the microporous range to 300 nm using the so-called Barrett-Joyner-Halenda (BJH) method (**Table 1-4**).[110] Similarly to MIP, this calculation method leads to a pore size distribution, but it is limited for materials exhibiting pores higher than 0.1 µm.

Alternatively, a less widespread characterization technique can be used for the porosity characterization of mesoporous materials, namely thermoporometry (**Table 1-4**), based on differential scanning calorimetry (DSC).[111] This technique relies on the Gibbs-Thomson equation[112] (**Equation 4**):

$$D_p = 2\left(A + \frac{B}{T_m - T_{m0}}\right) \qquad \textbf{Equation 4}$$

where D_p is the pore diameter, A and B are constants depending on saturating solvent, pore geometry and measurements on cooling or heating, T_m and T_{m0} are the melting temperatures of confined liquid and bulk liquid, respectively.

If a porous material is filled with a liquid, and then the latter is frozen, the melting temperature T_m of the liquid will not be the same for that confined in the pores and that in the bulk. T_m for the liquid in the pores will be lower, and the difference between T_m and the bulk liquid melting temperature provides the pore diameter according to **Equation 4**. Besides, comparing data from

freezing and melting phenomena leads to precious information regarding the pore shape. The limitation of this technique is due to his principle itself: if the pore size is too high, the liquid confined into the pores will act as a bulk liquid. Therefore, the melting peak of the confined liquid will be hidden into the profile of the bulk liquid melting peak and no differences will be observable. However, DSC-based thermoporometry has been proved to be effective using various solvents, like water,[113] benzene,[113] cyclohexane[114] or acetonitrile[115] that are commonly used solvents. Another variation of the technique relies on the use of nuclear magnetic resonance (NMR).[116]

Table 1-4: Common techniques used for the characterization of pore diameter in porous polymers and their caracteristics.

Technique	Pore diameter range	Principle
Mercury Intrusion Porosimetry (MIP)	≈ 300 µm – ≈ 10 nm	Washburn equation
Gas sorption	300 nm – < 2 nm	Barrett-Joyner-Halenda (BJH) theory
DSC thermoporometry	300 nm – 5 nm	Gibbs-Thomson equation

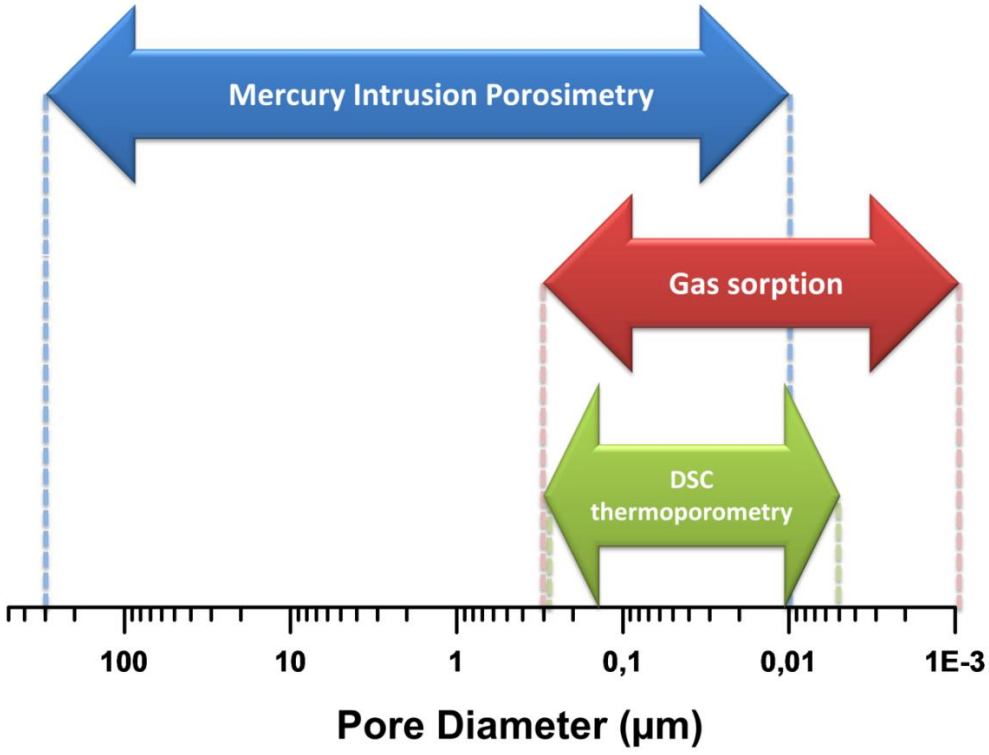

Finally, pycnometry can be used to determine an "apparent density" (more precisely a volume) of a porous solid, which is defined as the ratio between its mass and the total volume enclosed by an envelope of fluid. Pycnometry mostly uses gases, such as helium (He), but it can also be achieved with

liquids, such as water or xylene. A typical pycnometer consists of two sealed chambers connected between them by a valve. The first chamber is used as a reference and the second one holds the sample. The sample chamber is filled with the fluid, while the other one is still under vacuum. Then, the valve is opened and the fluid is allowed to expand into the second chamber at a precise temperature while the pressure is measured, thus giving the volume of the sample V_S, *i.e.* the open porosity volume using the Boyle-Mariotte law[117] (**Equation 5**):

$$V_S = V_C - \frac{V_r}{1-\frac{P_1}{P_2}} \qquad \textbf{Equation 5}$$

where V_C is the volume of the empty sample chamber, V_r is the volume of the second chamber, P_1 is the first pressure in the sample chamber and P_2 is the pressure after expansion into the combined volume of the chambers.

It is important to notice that pycnometry gives the volume of the open porosity. In the case of a closed porosity in the sample, the density will be an effective one. To give access to the closed porosity, two measurements are required: one with a porous system and another with a bulk system. The comparison between both gives access to the volume of the closed porosity.[118] This method has been extended to other porous polymeric systems to enable the characterization of polymer gels for instance.[119]

1.3 Application of metallic nanoparticle@porous polymers as supported catalysts

1.3.1 Key features of nanoparticles

Nanoparticles have been widely used as catalysts in the past decade, as they offer large surface area and consequently enhanced catalytic activity. Well-documented reviews discussing both synthesis and catalysis aspects can be found in the literature[120,121] and, in most cases, these reviews focused on a sole metal type. The reader is kindly referred to the reviews by Takale *et al.*[122] or Daniel & Astruc[123] for critical discussion about gold nanoparticles (Au NPs) and their catalytic uses, while Gawande *et al.*[124] and Ranu *et al.*[125] focused on copper nanoparticles (Cu NPs Chen & Holt-Hindle[126] and Astruc[127] detailed platinum (Pt NPs), and palladium (Pd NPs) nanoparticles, respectively. Herein, we purposely restricted the discussion to the cases of metal NPs supported on organic porous polymers for catalysis in organic chemistry. Although supported catalysts have been much less discussed, reviews present in the literature focused mainly on inorganic materials as supports, and one may cite the comprehensive survey by Corma and Garcia[128] who exclusively summarized recent trends in nanogold supported onto inorganic supports as catalysts for organic synthesis as well as that from Campelo and coworkers[129] describing the synthesis and applications of nanoparticles of various metals.

Regarding the immobilization of nanoparticles onto solid supports, two main ways have been reported to date in the literature, hereafter referred to as *ex-situ* and *in-situ* ways (**Figure 1-6**). It is crucial to mention that in order to achieve robust surface anchoring of metal nanoparticles (MNPs), the supports may preferably bear accessible chemical moieties able to induce specific interactions with the metal in its ionic or reduced forms. Amines, thiols, cyanos, and carboxylic acids are representative exemples ensuring strong interactions with metals, such as gold, copper, palladium. In some cases, the interactions can occur between the chemical units attached on solid surface and the stabilizing agent decorating the NP surface. Porous polymers with chelating ability can be easily designed using monomers incorporating functional side groups that may act as either chelation sites (for example 2-(dimethylamino)ethyl methacrylate) or reactive sites for post-polymerization functionalization. In the latter case, one may cite GMA, 4-VBC, NAS, or GCMA.

The *ex-situ* way requires the synthesis of the NPs prior to their immobilization onto the pore surface. Well-established methods were typically applied for the synthesis of metal colloids. In a further step, the NPs are immobilized onto the solid supports. A major advantage of the *ex-situ* approach is that it offers the possibility to use commercially available nanoparticles. Althoug it makes easier the whole synthesis process and provides fine control over the size distribution and colloidal stability of the NPs, it may be restrictive in terms of available size and shape.

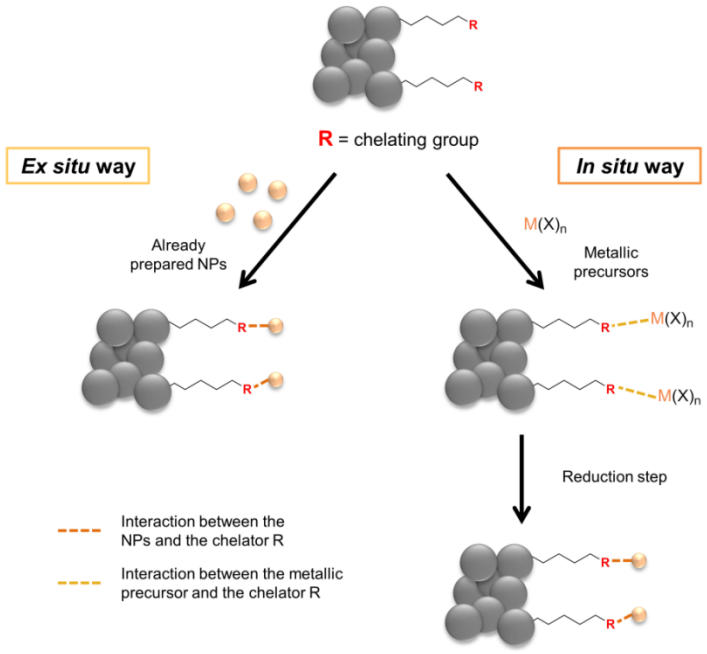

Figure 1-6: Scheme representing both ways of NPs immobilization, namely the *ex situ* way and the *in situ* way, for the immobilization of nanoparticles onto a porous support.

In contrast, the *in-situ* way implies the generation of the NPs in presence of the solid supports and is thus a deposition precipitation process.[130] First, the support is immerged into a solution containing the salt of the metal of interest for impregnation purpose. Then, the metal is reduced to its zero state through a reduction step. Several reducing agents are routinely used in organic synthesis (**Table 1-5**) and can be also envisaged for metal reduction, like $NaBH_4$,[131,132] citrates[133,134] (in the so-called Turkevitch process), hydrazine[135] or even H_2.[136,137] The choice of the reducing agent will depend on the size and shape desired for the NPs and is crucial to achieve controlled synthesis. Indeed, depending on the metal – reducing agent pair, various levels of control on the shape, size and surface distribution will be obtained. Other important parameters are the strength of the interaction between metal ions and the chemical groups at the surface of the support as well as the reducing agent/salt precursor ration.

Table 1-5: Examples of common reducing agents used for the preparation of nanoparticles. Typical conditions for reduction are also provided.

Reducing agent	**Formula**	**Conditions**	**References**
Sodium borohydride	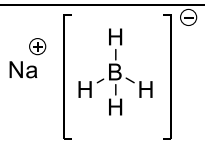	Aqueous solution, r.t.	131,132
Sodium Citrate	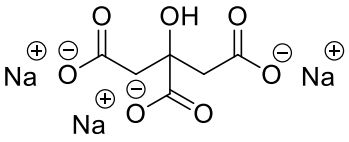	Aqueous solution, heat (reflux)	133,134
Dihydrogen	H_2	Heat	136,137
Hydrazine	H_2N-NH_2	Aqueous solution, heat or ultrasound	135,138

Although easy to implement, successful surface nanostructuration of porous polymers with nanoparticles implies that the NPs are strongly anchored so that leaching phenomenon does not occur. Indeed, the latter is detrimental to product purity as presence of metal, even at the trace levels, may induce toxicity to human beings As such, the choice of the chelating moiety is highly important and must be rationalized with respect to the nature of the metal and stabilizing agents. Generally speaking, the stronger the interaction between the support and the catalyst, the lower the risk of leaching. One should of course keep in mind that the conditions for the immobilization of the NPs may differ

significantly from the conditions for the catalysis applications. Changes such as solvent, pH and temperature may affect the strength of the chelation. Finally, the supported catalyst may be in contact with a variety of chemicals in the course of the catalytic cycles that may pollute the catalyst surface and eventually affect the turnover number and frequency. Thus, regeneration is usually required after several catalytic cycles.

1.3.2 Nanoparticles@macroporous polymers

Supported catalysts have not been widely described in the literature and this is particularly true in the case of porous polymer-based supports. Herein, we purposely opted for a discussion on the basis of the type of polymeric support rather than the type of the catalyzed reaction or nature of the metal NP (**Table 1-6**).

As discussed above, macroporous polymers are essentially generated using a solvent as a porogen.[15] Using such a process, many examples focused on the synthesis of monolithic polymers within microchannels. The as-generated monolithic-based microsystems can be used after immobilization of metal nanoparticles either as sorbents for solid phase extraction or separation purposes or as microreactors for flow through catalysis. One may briefly mention papers from teams of Svec, Buchmeiser, Connolly or Carbonnier who have extended the concept of metal nanoparticules decorating monoliths as chromatographic microcolumns to supported catalysts in continuous flow microreactors.[17,164–166]

In their pioneering work, Nikbin, Ladlow & Ley described in 2007 the synthesis of a vinylbenzyl chloride-based column and its subsequent functionalization with triethylamine to generate ammonium groups at the pore surface.[147] These ammoniums were used to immobilize Pd NPs onto the pore surface through a deposition precipitation process. First, the porous polymer was flushed with an aqueous solution of Na_2PdCl_4 (20 mM) followed by *in-situ* reduction of the surface immobilized Pd ions with sodium borohydride. The reactor was used for the Mizoroki-Heck reaction of different iodobenzyls with styrene and acrylate derivatives providing high yields above 80% (**Table 1-7**). The authors conclusively demonstrated that flow-through processes were superior to batch reaction, notably because of the possibility of processes automation.

Table 1-6: Examples of catalyzed reactions performed using metal nanoparticles supported on polymers.

Name of the reaction	Reactant(s)	General conditions	Catalyst	Products	References
Nitroarenes reduction	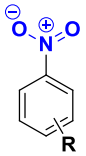	H_2O, $NaBH_4$, r.t.	Au, Ag, Cu, Pt, Pd	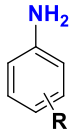	30,61,64,101,138–146
Mizoroki-Heck coupling	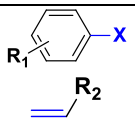 **X = I, Br**	DMF, Base, ≈ 100 °C	Pd	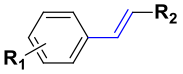	147–149
Suzuki-Miyaura coupling	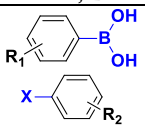 **X = I, Br**	Ethanol or DMF, Base, ≈ 100 °C	Pd	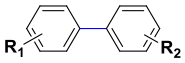	143,148–155
Boronic homocoupling	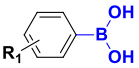	Ethanol, Base, ≈ 65 °C	Au	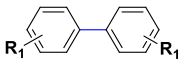	61
Sonogashira coupling	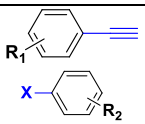 **X = I, Br**	H_2O and THF, Base, ≈ 50 °C	Pd	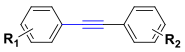	149,150
Hydrosilylation	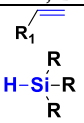	*n*-hexane, 45 °C	Pt	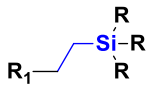	156
Eosin Y reduction	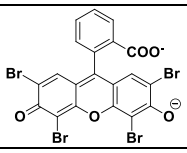	H_2O, $NaBH_4$, r.t.	Au	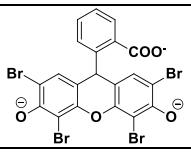	157,158
Reduction of hexacyanoferrate(III)	**$Fe(CN)_6^{3-}$**	H_2O, $NaBH_4$ or thiosulfate, r.t.	Au or Pd/Pt	**$Fe(CN)_6^{3-}$**	19,159
Carbon dioxide conversion	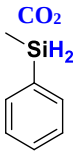	DMSO, r.t.	Pt	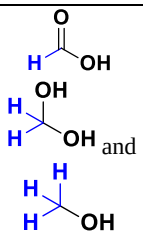 and	160
Hydrogenation of alcohol	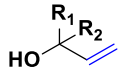 **R_1 = H or CH_3 R_2 = H or alkane group**	THF, H_2 pressure, r.t.	Pd	 **R_1 = H or CH_3 R_2 = H or alkane group**	161,162
Reduction of hexavalent chrome	**Cr^{VII}**	H_2O, formic acid, 50 °C	Au, Pd	**Cr^{III}**	138,163
Reduction of U^{IV}	**U^{VI}**	H_2O, formic acid, 50 °C	Pd	**U^{IV}**	138

The Buchmeiser group worked on the preparation of porous materials into chromatographic columns based on Ring Opening Metathesis Polymerization (ROMP), and suggested several potential applications. Restricting the discussion to supported catalysis, they developed monoliths bearing platinum (**Figure 1-7 A**) or palladium-based nanoparticles, obtained through the *in-situ* reduction of the corresponding salts, and proved their efficiency for several catalytic reactions like hydrosilylation[156] and carbon dioxide conversion[160] or Mizoroki-Heck,[148] Suzuki-Miyaura[148] (**Table 1-7**) and Sonogashira[150](**Table 1-7**). Of particular interest, the authors reported high TurnOver Numbers (TONs, representing the number of moles of reactants that a mole of catalyst can convert before decrease in the catalyst acticity) TONs values higher than 600 000 were reported for the hydrosilylation reaction.

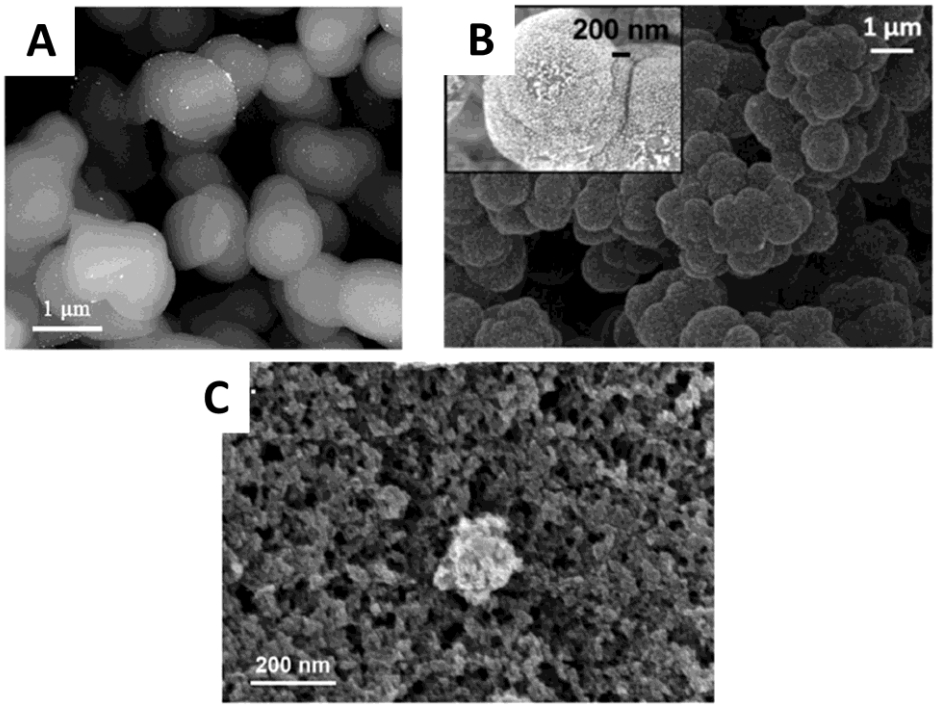

Figure 1-7: Examples of macroporous polymeric materials bearing *A) ex-situ* generated Au NPs onto a NAS-matrix capillary, *B) in-situ* generated Pt NPs onto a ROMP-generated-matrix capillary and *C) in-situ* generated Au NPs onto a DSDMA bulk monolith.

Connolly's team used glycidyl methacrylate- and vinyl azloactone-based monoliths to anchor as-prepared gold nanoparticles[19] as well as bimetallic platinum/palladium nanoflowers.[159] In both cases, the NPs were synthetized *ex-situ* according to literature protocols, and then flushed directly into polymer-filled capillaries or pipette-tips. Amine moieties were grafted onto the polymeric surface using ethylenediamine and were used to anchor both types of nanoparticles. The as-designed supported catalysts were used to reduce a ferric complex, hexacyanoferrate $Fe(CN)_6^{3-}$, into $Fe(CN)_6^{4-}$ using $NaBH_4$ as a co-reagent.

Table 1-7: Examples of C-C coupling reactions achieved using polymer-supported metal nanoparticles. The reactions conditions and yields are also presented.

Reaction name	Specific conditions of the protocol	Catalyst	Yield	References
Suzuki-Miyaura coupling	Solvent: THF/H_2O (50/50 % v/v); 1.5 eq. KO*t*Bu; 1 eq. NBu_4Br; Δ = 50 °C; Time: 24h	Pd	54 % to 99 % (various trials of haloarenes) TONs: 34 400 to 63 000	148
	Solvent: EtOH; 2.5 eq. KO*t*Bu; Δ = 50 °C; Time: 24h	Pd	96 %	151
	Solvent: Dioxane; 0.6 mmol Benzonitrile; Δ = 80-130 °C; Time: 72h	Pd	77 % to 100 %	155
Mizoroki-Heck coupling	Solvent: DMF; Triethylamine = 0.3 mmol; Δ = 130 °C; Flowrate: 0.05 $mL.min^{-1}$	Pd	<50 % to 87 % (various pairs of reactants)	147
	Triethylamine = 5mmol; Δ = 90 °C; Microwave: 300 W	Pd	Acrylate - Time: 1 min → <20 % to 83 % - Time: 5 min → 50 % to >99 % Styrene - Time: 10 min → 35 % to 85 %	149
Sonogashira coupling	Solvent: THF/H_2O (50/50 % v/v); 1.5 eq. KO*t*Bu; 1 eq. NBu_4Br; Δ = 50 °C; Time: 24h	Pd	2 % to 95 % (various trials of haloarenes) TONs: 90 to 4130	150
	DABCO = 2 mmol; Δ = 130 °C; Microwave: 300 W; Time: 2 min	Pd	>90 % to >99 %	149

Our group contributed to the field of supported catalysis for flow-through catalysis by developing a series of chemically modified monolithic supports based on NAS. The generic monolith was initially synthesized within microsized channels and further chemically modified by taking advantage of the reactive of the *N*-hydroxysuccinimide moieties towards nucleophilic species. One of the first examples described the preparation of diacid-decorated porous monolith.[30] Such carboxylic acids were used to anchor copper nanoparticles using two immobilization processes. On the first hand, commercially available copper nanoparticles (with mean diameter in the range 40 – 60 nm) were percolated into the monolithic structure and the microreactor used directly after a rinsing step. On the other hand, Cu^{2+} ions were initially immobilized onto the surface of the functionalized monolith. In a second step, an aqueous $NaBH_4$ solution was injected in the monolithto generating the nanoparticles through reduction. Both microreactors were used to catalyze hydride-mediated reduction of one nitroarene, the *o*-nitrophenol. The best yield (68.5 % at a flow rate of 0.3 $\mu L.min^{-1}$) was obtained when preformed NPs were used while the *in-situ* approach led to slightly lower yields (40 and 55 % for flow rates of 4 and 1.5 $\mu L.min^{-1}$, respectively) (**Table 1-8**).

In another implementation, the NAS-based monolith was used as support for gold nanoparticles. As described in the work of Khalil *et al.*,[145] ethylenediamine was grafted on the monolith surface. The resulting primary amines, in their protonated form, were used as ligands to immobilize Au colloids. Both ways of nanoparticles immobilization, namely *in-situ* and *ex-situ* pathways were investigated. In the former case, an aqueous solution of $HAuCl_4$ was percolated to immobilize Au^{3+} ions followed by reduction using an aqueous $NaBH_4$ solution. For the *ex-situ* way, commercially available Au NPs with a diameter of 20 nm and a citrate stabilization layer were used. Interaction between the carboxylates of the citrates and the ammonium form of the primary amines at the pore surface provided strong interfacial interaction, leading to robust anchoring of the nanoparticles. The microreactors were used for nitroarenes reduction, using *p*-nitroaniline, *o*-nitrophenol, *m*-nitrophenol and *p*-nitrophenol as model molecules. Different parameters were investigated to optimize the reaction yields, like the reactants concentration, the column length, the flow rate allowing for complete conversion of the nitroarenes into the corresponding aromatic aimes. Of particular interest, it was shown that the *in-situ* approach provided higher reaction yields as compared to the *ex-situ* using the same flow conditions.

An extension of this work was provided in the paper by Liu *et al.*[144] were NAS-based monoliths were functionalized with amine moieties derived from histamine. Commercially available Au NPs with different sizes 5 nm, 20 nm (**Figure 1-7 B**) and 100 nm were used. The aggregation behavior of the NPs at the monolith surface as well as the coverage density were found to depend on the chemical nature of the amine ligand and size of the nanoparticles. While the higher diameters (100 and 20 nm) were the most homogeneously and densely covered columns, difficulties were encountered

with the 100 nm Au NPs in the filling and the back pressure obtained from the capillary. The catalytic efficiency of these microreactors was first established for *p*-nitrophenol and then extended to dinitro derivatives, namely 2,5-dinitrophenol, 2,4-dinitroaniline, 2,6-dinitroaniline and 3,5-dinitroaniline. Interestingly, the best results were obtained for the 20 nm nanoparticles, instead of the 5 nm ones, and for a flowrate of 5 $\mu L.min^{-1}$ (**Table 1-8**).

Moreover, Carbonnier's group developed a new monolithic matrix, based on glycerol carbonate methacrylate.[139] Such a carbonate ring can be easily converted into a urethane bond with a suitably chosen amine-bearing molecule. Carboxylic acids were grafted at the surface *via* a two-step process and then used to chelate platinum ions. $NaBH_4$ was used as a reducing agent for the generation of Pt NPs directly onto the pore surface. The as-prepared supported catalyst was further used for the total reduction of *p*-nitrophenol (**Table 1-8**).

Beside the design of porous materials for flow-through applications, our team also prepared bulk polymeric materials using the porogenic solvent approach. A dimethacrylate monomer bearing a disulfide bridge, namely bis(2-methacryloyl)oxyethyl disulfide (DSDMA), was used with the aim to eventually produce thiol-containing monoliths.[157] Such an approach was followed because of the difficulty to polymerize thiol-containing monomers with the occurrence of chain transfer reactions. Herein, we used a protected thiol in the form of disulfide. After polymerization with a dimethacrylate as a cross-linker and using toluene as a porogenic agent, thiols were generated using D,L-dithiothreitol. Gold ions were subsequently anchored to the thiolated surface and further reduced using sodium borohydride to generate Au nanoparticles (**Figure 1-7 C**). Although aggregation trends could be seen onto the SEM pictures, the as-prepared bulk catalysts were used to reduce an organic dye, Eosin Y. Up to six consecutives catalytic cycles were tested with an average yield of about 60 %, thus ascertaining the reusability of the supported catalyst.

Table 1-8: Examples of nitro coupounds reactions achieved using polymer-supported metal nanoparticles. The reactions conditions and yields are also presented.

Reaction name	Specific conditions of the protocol	Catalyst	Yield	References
Nitro reduction	Solvent: Acetonitrile/H_2O (70/30 % v/v); $[NaBH_4] = 1.2 \times 10^{-1}$ M	Cu	Flowrates: - 0.3 µL.min^{-1} → 68.5 % (*ex situ*) - 4 µL.min^{-1} →40 % (*in situ*) - 1.5 µL.min^{-1} → 55 % (*in situ*)	30
	Solvent: H_2O; $[NaBH_4] = 1.2 \times 10^{-1}$ M; Flowrate: 2 µL.min^{-1}	Pt	100 %	139
	Solvent: H_2O; $[NaBH_4] = 1.2 \times 10^{-1}$ M; Flowrate: 5 µL.min^{-1}	Au	100 % (various nitro and dinitro compound)	144
	Solvent: H_2O; $[NaBH_4] = 2 \times 10^{-2}$ M; Time: 25min	Au	95.4 %	141
	Solvent: H_2O; $[NaBH_4] = 0.25$ M; Time: 30 min	Ag	100 %	140
	Solvent: H_2O; $[NaBH_4] = 6.67$ mM; Time: 16 min	Pd	100 %	138
	Solvent: H_2O; $[NaBH_4] = 1.2 \times 10^{-1}$ M	Au	Macroporous - Time: 1 h → 27 % Nanoporous - Time: 1 h → 25 % - Time: 40 min → 71 % Biporous - Time: 1 h → 93 % - Time: 40 min → 83 %	101

1.3.3 Nanoparticles@nanoporous polymers

As previously discussed, pore sizes of nanoporous materials are appealing for catalysis applications, as they can provide a filtration phenomenon occurring simultaneously to the catalytic activity. Few examples in the literatue described the use of nanoporous polymers arising from diblock copolymers. The first example of nanopore decoration with a metal was reported by Ryu *et al.*[63] who generated gold nanorods at the interface of thiolated polymers. Unfortunately, the authors did not mention any application. Recently, Grande's group started to investigate how such pores could be decorated with nanoparticles and considered the use of the resulting composite materials as supported catalysts.

In 2015, the synthesis of a diblock copolymer made of PS and PLA and bearing a disulfide bridge junction between both blocks was first developed.[64] After the synthesis of the dual initiator and both blocks by ATRP and ROP, an orientation step of the resulting functional copolymer was implemented using a channel die process. Cleavage of the disulfide bridge was achieved using triphenylphosphine, revealing the pores as well as the thiol moieties at the pore interface. Au^{3+} ions were then immobilized and further reduced with $NaBH_4$. The as-obtained porous polymer-supported gold nanoparticles were used as efficient catalysts to reduce *p*-nitrophenol. Reaction yields of ≈ 70 % were calculated after 1 h of reaction for five consecutive catalytic runs.

In another implementation, our team used an acetal junction between the two blocks [61]. The dual initiator was synthetized *via* a two-step process, and after the polymerization processes, orientation of the block copolymer structure was performed *via* solvent vapour annealing of films casted onto Si wafers. The acetal link between both blocks could be easily cleaved with trifluoroacetic acid and then, functionalized with amine molecules after reductive amination reaction. Amine-decorated pores were covered with *in-situ* generated gold nanoparticles (**Figure 1-8 A**). First, boronic homocoupling and nitroarene reduction were considered separately. Finally, the two reactions were coupled in a cascade reaction process involving 3-nitrobenzene boronic acid. After formation of the 3,3'-dinitrobiphenyl through homocoupling reaction, the nitro moieties were successfully reduced using $NaBH_4$-mediated reduction yielding 3,3'-diaminobiphenyl as a major product.

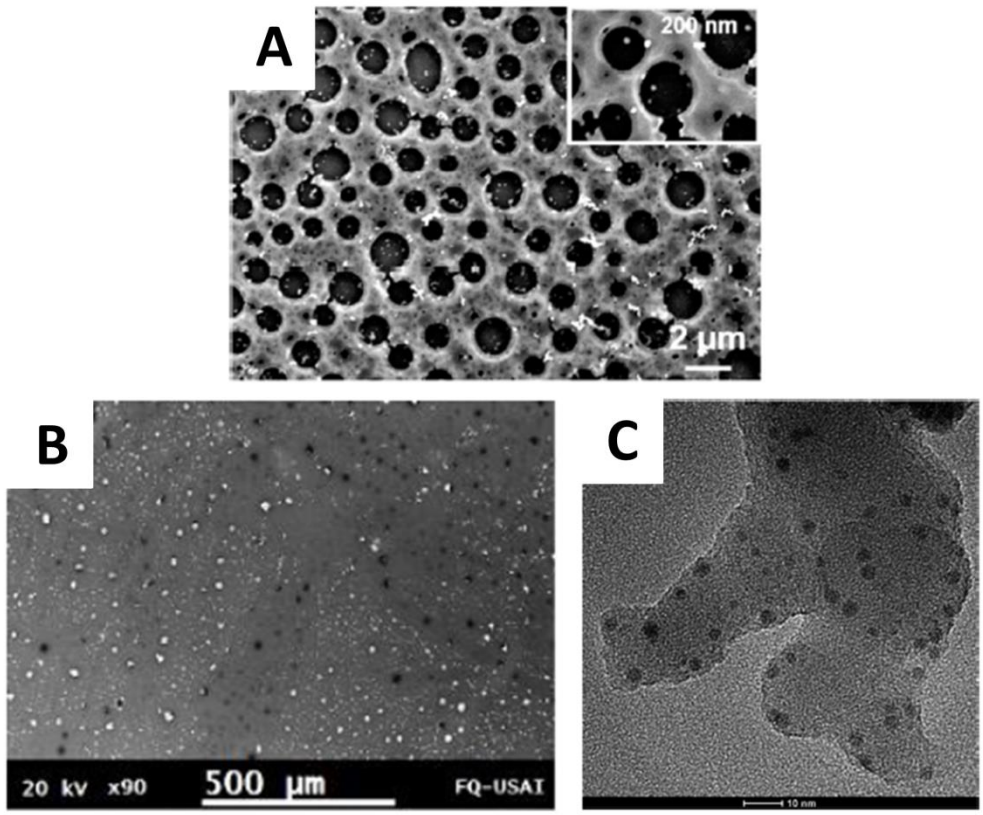

Figure 1-8: Examples of nanoporous polymeric materials bearing *A) in-situ* generated Au NPs onto a PS arising from diblock copolymers, *B) in-situ* generated Au NPs within a cellulose membrane and *C) in-situ* generated Pd NPs into a microporous polyheptazine.

Besides the use of diblock copolymers, several authors have implemented polymer-based membrane materials exhibiting nanoporosity to design supported catalysts. Remigy and Lahitte's group discussed the use of commercially available polyethersulfone membranes with a pore size of 200 nm. The membranes were modified to anchor Pd NPs and further used in several reactions, including nitrophenol reduction,[142,143] Suzuki-Miyaura cross coupling[143,151,152] (**Table 1-7**) or hydrogenation of *trans*-4-phenyl-3-buten-2-one.[162] Interesting comparison was performed considering the use of these membranes in batch mode and under flow-through conditions. The latter conditions proved to be superior providing faster reactions. Indeed, while the reactions could be performed within a 10 s range in flow conditions, the batch mode required 6 h for full conversion. Another interesting result was that no byproducts were observed in the flow-through mode. This was assumedly assigned to a lower kinetic of formation of the side product.

Other research groups focused on using membranes with embedded nanoparticles. One may cite the work from Mora-Tamez *et al.*[141] who considered the use of Au NPs immobilized within cellulose triacetate-based membranes. The originality of the approach lies in the extraction of $Au^{(III)}$

ions by the membranes and their simultaneous *in-situ* reduction with a citrate solution (**Figure 1-8 B**). Such supports with embedded NPs were used for the reduction of *p*-nitrophenol. The authors mentioned reaction yield as high as 95.4 % after 25 min of reaction (**Table 1-8**).

Likewise, Clark's group used biobased nanoporous polymers for catalysis purposes. Starch-based porous supports were obtained by solvent exchange between water and ethanol, and subsequently used to anchor palladium nanoparticles.[149] Palladium acetate was put in the presence of the starch-based materials acting simultaneously as reducing agent and support for the resulting nanoparticles, seemingly self-reducing the precursory metallic ions. Mizoroki-Heck (**Table 1-7**), Sonogashira (**Table 1-7**) and Suzuki-Miyaura reactions were performed under microwave irradiation using the starch-supported Pd NPs. The microwave activation permitted to reduce the reaction time as the reactions could be achieved in less than 10 min. In contrast, thes authors provided a comparison with other data published in the litterature without the use of microwave and for which the reaction times were in the range of 4-12 h. Although the authors concluded on the superiority of the starch-based materials in terms of improved reaction yields, lower reaction times, and renewability of the catalysts, a reliable comparison with traditional catalysts such as Pd/C or silica-supported NPs is, to our point of view, very difficult because most of the studies that the authors referred to did not mention the use of microwave activation.

Finally, microporous polymers (with pores below 2 nm) were used as catalytic supports. Although most of examples in the literature mentioned the direct use of a polymer network as the heterogeneous catalyst due to a specific site like a specific chemical moiety[167] or a metallo-organic complex,[168] some examples about polymer-supported nanoparticles can also be found. Zhang *et al.*[153] designed a porous network *via* a direct Sonogashira coupling of an aromatic trialkyne and 1,4-dibromobenzene. The nanoporous polymer was subsequently immersed into an acetone solution of $Pd(OAc)_2$. After stirring at 90 °C, a Pd NPs-loaded polymer was obtained. Different Suzuki-Miyaura C-C coupling reactions were performed using a large panel of halogenoarenes (iodo and bromo) along with phenylboronic acid. High yields (> 85 %) and short reaction times (less than 4 h) were obtained. Comparison with Pd/C catalysts suggested that such nano Pd-decorated frameworks allowed for a threefold decrease of the reaction times (from 9 h for Pd/C to 3 h) to reach similar reaction yields. Five catalytic cycles were performed and only a limited reduction in catalytic activity was observed as expressed by the decrease of a few percent of the reaction yields, while leaching effect was quantified to be less than 1 % for each cycle.

In their interesting work, Du *et al.*[154] prepared polymer networks through a nucleophilic substitution of chlorines pending on the cyameluric chloride monomer by amines of piperazine. The as-obtained heptazine framework was immersed into an acetone solution of palladium acetate under reflux, allowing for the generation of the Pd NPs by self-reduction (**Figure 1-8 C**). Suzuki-Miyaura

couplings were performed using different pairs of bromoarenes derivatives and phenylboronic acids. Yields above 80 % of conversion were obtained except for the 2-bromonaphtalene along with the arylboronic acid as well as for the 4–nitrobenzene boronic acid along with bromobenzene, for which yields remained below 40 %. A tentative explanation for the obtained yields was provided by the authors based on the large steric hindrance of 2-bromonaphtalene as well as the poor solubility of 4-nitrobenzene boronic acid. Here again, five catalytic runs were performed consecutively showing a limited decrease of the catalytic activity and ICP measurements performed before and after the five cycles showed negligible leaching phenomena.

1.3.4 Nanoparticles@biporous polymers

Macroporous and nanoporous polymers are very different systems in terms or permeability, porosity, surface area which are key features for catalysis applications. Macroporous polymers possess large pores providing enhanced permeability for the liquid to penetrate into the pores but a poor specific surface area. In constrast, nanoporous frameworks afford a larger specific surface area, while a lower accessibility to the pores. A high permeability may favor better accessibility of the reactants to the catalysts, while a large specific surface area should allows for higher density of metal nanoparticles on the support surface. If considered simultaneously, these two criteria may provide more efficient catalytic processes. Based on this simple consideration, biporous materials containing both macropores and nanopores may appear as attractive candidates for nanocatalyst supports.

An easy way of making biporous materials relies on the fabrication of polyHIPEs. One of the pioneering group in the field of polyHIPE preparation and use as catalysts is Deleuze's. In 2005, they described polystyrene-[161] and poly(vinylbenzyl chloride)-based[155] polyHIPEs as supports for *in-situ* generated Pd NPs (**Figure 1-9 A**). The hybrid supports were used for the hydrogenation of an alkene, *i.e.* allyl alcohol, and for Suzuki-Miyaura cross-coupling reactions (**Table 1-7**). The authors reported reaction times of 1 h and 70 h for near-completion hydrogenation and coupling reactions, respectively. The authors discussed their results with respect to other published results obtained with catalysts such as Pd/C using the prepared supported catalysts in powder forms. Polystyrene based polyHIPEs were also used by the same group as supports for gold nanoparticles.[158] In this case, $HAuCl_4$ ions solutions were simply deposited and the PS induced self-reduction. Supported Au NPs were then used for the reduction of a dye, Eosin Y, and the reaction was repeated three times. Near-completion reactions were achieved within one hour and under mild conditions (25 °C).

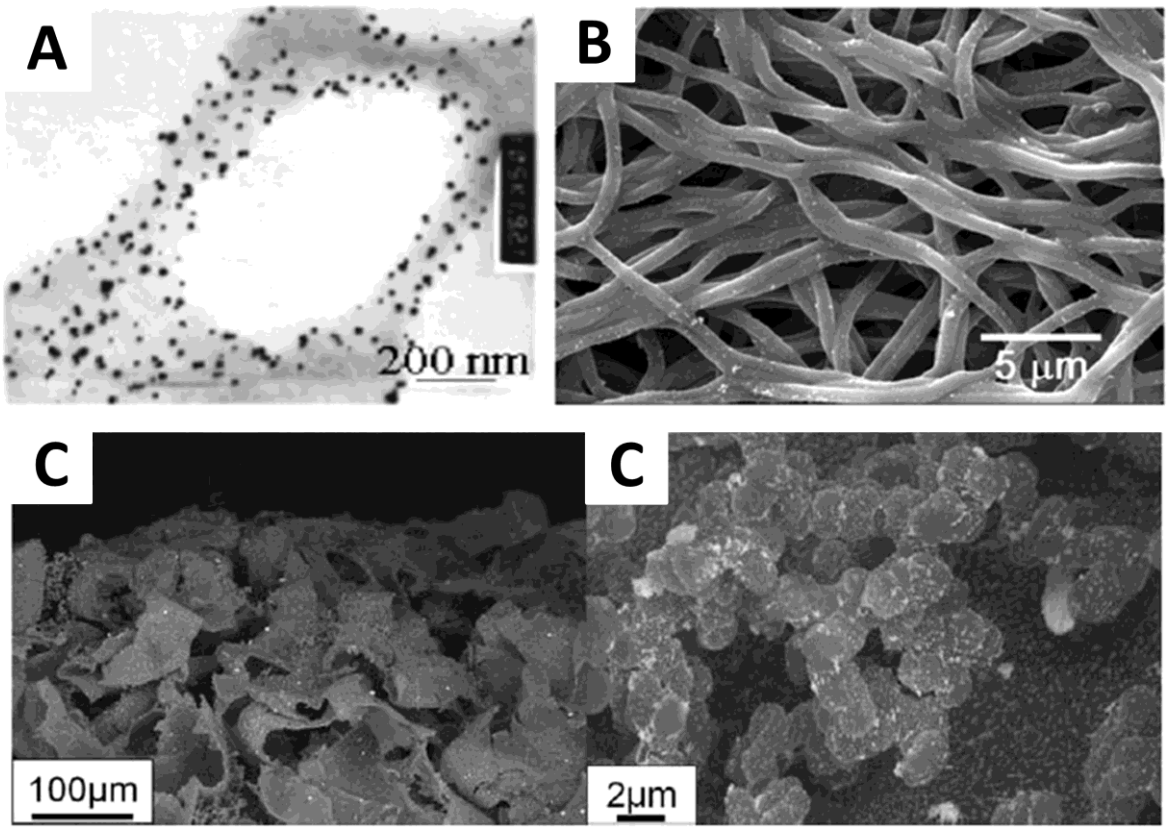

Figure 1-9: Examples of biporous polymeric materials bearing *A) in-situ* generated Pd NPs onto a PS polyHIPE, *B) in-situ* generated Ag NPs onto a poly(acrilic acid) fibers and *C) in-situ* generated Au NPs onto a biporous poly(HEMA-*co*-EGDMA) bulk monolith.

Another way to design nanostructured catalysts relies on the use of electrospun materials. The as-obtained fibers possess several interesting properties for catalytic applications, such as a large surface to volume ratio and superior mechanical properties. Therefore, they are also usually used as membrane-like materials, which can be beneficial to catalysis, as discussed above. To date, electrospun materials have been mostly used for environmental catalytic applications, like hexavalent chromium (Cr^{VI}) or nitro groups reduction. Nevertheless, as-prepared electrospun supports are not widely used as catalyst supports, as most reports in the literature mentioned the use of the polymer mats as precursors for calcination for, as an example, creating titania fibers. Most examples in the literature describe the use of polymer fibers already containing chelating moieties like carboxylic acids or amines. Shi's group described the use of polyethyleneimine (PEI) blended with poly(vinyl alcohol) (PVA) as mats for the support of gold[146] and palladium[163] nanoparticles. Au NPs were used for the successful reduction of nitro compounds, while Pd NPs were applied to the generation of Cr^{III} from Cr^{VI}, which is highly carcinogenic. In the same way, Xiao's group used a blend of polyacrilic acid (PAA) and PVA to chelate *in-situ* generated (sodium borohydride as reducing agent) Ag NPs (**Figure**

1-9 B) for the catalytic reduction of *p*-nitrophenol[140] (**Table 1-8**). Another interesting recent work is that from Pandey's team[138], who used electrospinning to prepare poly(ether sulfone) (PES) fibers and took advantage of the presence of the ether sulfone moieties to perform photolysis under UV irradiation to initiate the growth of polyGMA chains. The pendant oxiran groups were then opened with hydrazine providing directly attachment of the reducing agents on the support surface. A palladium salt was put in contact with the fibers *via* an aqueous solution of palladium chloride and self-reduced. Hybrid fibers were applied to the reduction of hexavalent chromium as well as *p*-nitrophenol (**Table 1-8**) but also the less common reduction of hexavalent uranium (U^{VI}) to U^{IV}.

Last but not least, one may mention the use of the double porogen templating approach allowing for easily combining two levels of porosity and broadening the range of accessible pore shape. Ly *et al.* recently designed doubly porous PHEMA-based materials as supports for gold nanoparticles[101] (**Figure 1-9 C**). They used fused NaCl particles as macroporogens and isopropanol as a porogenic solvent for the production of the nanopores. The surface of the biporous polymers was chemically modified in order to have amines or thiols directly on the surface. $HAuCl_4$ solution was used to load gold ions onto the surface and $NaBH_4$ was used as a reducing agent. Reduction of 4-nitrophenol was performed in order to prove the catalytic efficiency of the as-prepared hybrids. Differences in the size and/or distribution of the nanoparticles were observed as a function of the nature of the chelating group (NH_2 *vs.* SH), thus leading to differences in the reaction yields. It was shown that thiol functions led to bigger nanoparticles, and also surprisingly to leaching of NPs. Monoporous materials were also synthetized in order to highlight the superiority of such doubly porous materials. While monomodal porous polymers, *i.e.* with macroporosity or nanoporosity only, showed rather similar efficiency, the doubly porous homologues exhibited higher catalytic activity. The higher density of nanoparticles associated with the latters along with their higher porosity ratios as compared to the the nanoporous and macroporous materials were assumed to account for such results (**Table 1-8**).

1.3.5 Pros & cons of the strategies

We have reviewed different polymeric materials used in supported heterogeneous catalysis. They were generally used for different purposes; therefore, let us try to define the pros and cons of each type of support.

First, the capillaries filled with polymer monoliths are easy to prepare – each preparation step is conclude in minutes or few hours –, they have the major advantage to give directly the desired product, without any purification step needed. This is in the case of no byproducts generated during the catalytic reactions. Further, they are supposed to be easily scaled up and, as mentioned by Nikbin

et al.,[147] they can be used in automation processes. What a tiny capillary can do, a chromatographic-column size reactor will be able to do. This could compensate one of the drawbacks of the capillaries: the slow flow rates (around microliters per minutes). On top of that, what is a general drawback of the flow-through processes is the backpressure. Too heavy, it will harm the lifetime of the column, reducing its reusability. Moreover, this phenomenon could lead to a higher leaching of nanoparticles, which is not desired.

Concerning the nanoporous polymers arising from diblock copolymers, the main advantage lies in the different controlled morphologies accessible (from cylinders to gyroids or to lamellae), thus enabling to tune the support porosity. Nevertheless, one con is the long step of synthesis required. Besides, depending on the alignment procedure, the quantities of polymeric materials needed and the orientation time are dramatically different. For channel die processing, hundreds of milligrams of polymers are required to determine the best orientation conditions, while for solvent vapour annealing, a diluted polymer solution is enough for film nanostructuration on silicon wafers. Yet, there is no widespread use of these materials for catalysis purposes.

Polymeric membranes seem to be the top choice for efficient catalytic reactions. However, some drawbacks could be found.[169] First, they need a specifically designed and optimized reactor. The cost for a specific reactor chamber must be added to the efforts of creating catalytic membranes, which are not trivial. Moreover, as with capillaries, a specific adjustment of the flow rate with the reaction rate is necessary. Finally, membranes are known to have a limited durability, depending on their thermal, chemical, and mechanical properties. Indeed, the harsher the conditions of use, the quicker they degrade, adding higher costs of renewal.

For the microporous networks, they have one major advantage, namely their specific surface area. Indeed, the pores are the void generated by the monomer assembly, and are in the micropore range. This could logically lead to more gaseous reactions and yet, examples of catalysis reactions in liquid media still exist with such supports. However, they have a low permeability, and this is especially true for pure carbon-based networks.[170] This limitation could prevent reactions from occurring efficiently.

Concerning the polyHIPEs, they display a really accessible high porosity with interconnected pores which enable high flow-through properties. However, since the void size is large (cavities are in the micrometer range), specific surface areas are quite low.[171] Works done by Sherrington's group tried to overcome this issue,[172] using porogenic solvents in addition of the HIPE process, leading to a new limitation, *i.e.* poor mechanical resistance during flow-through processes, even collapsing the monolithic structure.

Electrospun materials have risen since the mid 1990's, where the fibers could be used for nanotechnology applications. As a support for a catalyst, they offer an interconnected porosity due to their generation process. Moreover, they are already used to make filtration membranes, which may be catalytic reactors. Nevertheless, some limitations still exist. It is difficult to produce uniform mats with a diameter inferior to 50 nm.[173] A smaller fiber diameter will lead to a smaller volume of this fiber, enhancing the surface to volume ratio. Progress is already made to overcome this issue by studying the solvent evaporation during the process, among others.

Finally, the double porogen approach may afford high porosity ratios and interconnected pores, provided that the porogens are suitably chosen. However, further investigation needs to be performed to clearly correlate the pore morphology to the mass transfer properties of the resulting materials. Very few of them have been used so far in the area of supported catalysis.

1.4 Conclusions & Prospects

In conclusion, this report critically overviews the main types of polymers used as supports for metallic nanoparticles. The as-prepared hybrid materials have become of crucial interest in the area of heterogeneous catalysis in the recent years, and some notable works have been performed. They are still cheap and quickly generated, making them suitable for various applications, including catalysis. However, progress can and should be made in the near future. As an example, porous polymers arising from diblocks have just recently been used as supports for nanoparticles, starting an interesting new area that could still be explored. Other types of polymer matrices have also been used, while providing many advantages, like capillary columns. In the right conditions, the pure product is totally recovered at the end of the flow-through process.

Based out the state of the art, different key factors need to be considered for porous polymer supports meant for heterogeneous catalysis, in particular porosity range and morphology of the materials, as well as types of moieties present at the pore surface to tune the interactions between the support and the metal. The processes involved (namely batch or flow-through) and the catalytic reaction envisaged are crucial parameters that matter for the appropriate selection of the supports. In this context, we focused our work on developping miscellaneous porous polymeric materials (nano- *vs.* macroporous materials), and we used specific and precise surface chemistry to anchor a large variety of metallic nanoparticles from copper to gold ones and from palladium to platinum counterparts. Such studies allowed us to create new catalytic supports and to understand better the role of aforementioned important structural parameters in reaction processes catalysed by polymer-supported nanoparticles.

1.5 References

(1) Van Leeuwen, P. W. *Homogeneous Catalysis: Understanding the Art*; Springer Science & Business Media, 2006.

(2) Widegren, J. A.; Finke, R. G. A Review of the Problem of Distinguishing True Homogeneous Catalysis from Soluble or Other Metal-Particle Heterogeneous Catalysis under Reducing Conditions. *J. Mol. Catal. Chem.* **2003**, *198* (1), 317–341.

(3) Herrmann, W. A.; Kohlpaintner, C. W.; Manetsberger, R. B.; Bahrmann, H.; Kottmann, H. Water-Soluble Metal Complexes and Catalysts. Part 7. New Efficient Water-Soluble Catalysts for Two-Phase Olefin Hydroformylation: BINAS-Na, a Superlative in Propene Hydroformylation. *J. Mol. Catal. Chem.* **1995**, *97* (2), 65–72.

(4) Pirkanniemi, K.; Sillanpää, M. Heterogeneous Water Phase Catalysis as an Environmental Application: A Review. *Chemosphere* **2002**, *48* (10), 1047–1060.

(5) Bell, A. T. The Impact of Nanoscience on Heterogeneous Catalysis. *Science* **2003**, *299* (5613), 1688.

(6) Copéret, C.; Chabanas, M.; Petroff Saint-Arroman, R.; Basset, J.-M. Homogeneous and Heterogeneous Catalysis: Bridging the Gap through Surface Organometallic Chemistry. *Angew. Chem. Int. Ed.* **2003**, *42* (2), 156–181.

(7) Lu, A.-H.; Salabas, E. L.; Schüth, F. Magnetic Nanoparticles: Synthesis, Protection, Functionalization, and Application. *Angew. Chem. Int. Ed.* **2007**, *46* (8), 1222–1244.

(8) Sachtler, W. M. H.; Zhang, Z. Zeolite-Supported Transition Metal Catalysts. *Adv. Catal.* **1993**, *39*, 129–220.

(9) Opanasenko, M.; Stepnicka, P.; Cejka, J. Heterogeneous Pd Catalysts Supported on Silica Matrices. *RSC Adv.* **2014**, *4* (110), 65137–65162.

(10) Wildgoose, G. G.; Banks, C. E.; Compton, R. G. Metal Nanoparticles and Related Materials Supported on Carbon Nanotubes: Methods and Applications. *Small* **2006**, *2* (2), 182–193.

(11) Liu, J.; Chen, L.; Cui, H.; Zhang, J.; Zhang, L.; Su, C.-Y. Applications of Metal-Organic Frameworks in Heterogeneous Supramolecular Catalysis. *Chem. Soc. Rev.* **2014**, *43* (16), 6011–6061.

(12) Wu, D.; Xu, F.; Sun, B.; Fu, R.; He, H.; Matyjaszewski, K. Design and Preparation of Porous Polymers. *Chem. Rev.* **2012**, *112* (7), 3959–4015.

(13) Rouquerol, J.; Avnir, D.; Fairbridge, C. W.; Everett, D. H.; Haynes, J. M.; Pernicone, N.; Ramsay, J. D. F.; Sing, K. S. W.; Unger, K. K. Recommendations for the Characterization of Porous Solids (Technical Report). *Pure Appl. Chem.* **1994**, *66* (8), 1739–1758.

(14) Seidl, J.; Malinský, J.; Dušek, K.; Heitz, W. Makroporöse Styrol-Divinylbenzol-Copolymere Und Ihre Verwendung in Der Chromatographie Und Zur Darstellung von Ionenaustauschern. *Fortschritte Hochpolym.-Forsch.* **1967**, 113–213.

(15) Svec, F.; Fréchet, J. M. J. New Designs of Macroporous Polymers and Supports: From Separation to Biocatalysis. *Science* **1996**, *273* (5272), 205.

(16) Svec, F.; Fréchet, J. M. J. Modified Poly(Glycidyl Metharylate-Co-Ethylene Dimethacrylate) Continuous Rod Columns for Preparative-Scale Ion-Exchange Chromatography of Proteins. *J. Chromatogr. A* **1995**, *702* (1), 89–95.

(17) Xu, Y.; Cao, Q.; Svec, F.; Fréchet, J. M. J. Porous Polymer Monolithic Column with Surface-Bound Gold Nanoparticles for the Capture and Separation of Cysteine-Containing Peptides. *Anal. Chem.* **2010**, *82* (8), 3352–3358.

(18) Luo, Q.; Zou, H.; Xiao, X.; Guo, Z.; Kong, L.; Mao, X. Chromatographic Separation of Proteins on Metal Immobilized Iminodiacetic Acid-Bound Molded Monolithic Rods of Macroporous Poly (Glycidyl Methacrylate–co-Ethylene Dimethacrylate). *J. Chromatogr. A* **2001**, *926* (2), 255–264.

(19) Floris, P.; Twamley, B.; Nesterenko, P. N.; Paull, B.; Connolly, D. Fabrication and Characterisation of Gold Nano-Particle Modified Polymer Monoliths for Flow-through Catalytic Reactions and Their Application in the Reduction of Hexacyanoferrate. *Microchim. Acta* **2014**, *181* (1), 249–256.

(20) Gusev, I.; Huang, X.; Horváth, C. Capillary Columns with in Situ Formed Porous Monolithic Packing for Micro High-Performance Liquid Chromatography and Capillary Electrochromatography. *J. Chromatogr. A* **1999**, *855* (1), 273–290.

(21) Lv, Y.; Lin, Z.; Svec, F. Hypercrosslinked Large Surface Area Porous Polymer Monoliths for Hydrophilic Interaction Liquid Chromatography of Small Molecules Featuring Zwitterionic Functionalities Attached to Gold Nanoparticles Held in Layered Structure. *Anal. Chem.* **2012**, *84* (20), 8457–8460.

(22) Xie, S.; Svec, F.; Fréchet, J. M. J. Design of Reactive Porous Polymer Supports for High Throughput Bioreactors: Poly(2-Vinyl-4,4-Dimethylazlactone-Co-Acrylamide-Co-Ethylene Dimethacrylate) Monoliths. *Biotechnol. Bioeng.* **1999**, *62* (1), 30–35.

(23) Guerrouache, M.; Carbonnier, B.; Vidal-Madjar, C.; Millot, M.-C. In Situ Functionalization of N-Acryloxysuccinimide-Based Monolith for Reversed-Phase Electrochromatography. *J. Chromatogr. A* **2007**, *1149* (2), 368–376.

(24) Guerrouache, M.; Millot, M.-C.; Carbonnier, B. Functionalization of Macroporous Organic Polymer Monolith Based on Succinimide Ester Reactivity for Chiral Capillary Chromatography: A Cyclodextrin Click Approach. *Macromol. Rapid Commun.* **2009**, *30* (2), 109–113.

(25) Guerrouache, M.; Millot, M. C.; Carbonnier, B. Capillary Columns for Reversed-Phase CEC Prepared via Surface Functionalization of Polymer Monolith with Aromatic Selectors. *J. Sep. Sci.* **2011**, *34* (16–17), 2271–2278.

(26) Dao, T. T. H.; Guerrouache, M.; Carbonnier, B. Thiol-Yne Click Adamantane Monolithic Stationary Phase for Capillary Electrochromatography. *Chin. J. Chem.* **2012**, *30* (10), 2281–2284.

(27) Tijunelyte, I.; Babinot, J.; Guerrouache, M.; Valincius, G.; Carbonnier, B. Hydrophilic Monolith with Ethylene Glycol-Based Grafts Prepared via Surface Confined Thiol-Ene Click Photoaddition. *Polymer* **2012**, *53* (1), 29–36.

(28) Kebe, S. I.; Ben Boubaker, M.; Guerrouache, M.; Carbonnier, B. Thiol-Ene Click Chemistry for the Design of Diol Porous Monoliths with Hydrophilic Surface Interaction Ability: A Capillary Electrochromatography Study. *New J. Chem.* **2016**, *40* (8), 6916–6923.

(29) Mekhalif, T.; Kebe, S. I.; Guerrouache, M.; Belattar, N.; Millot, M. C.; Carbonnier, B. Novel Monolithic Stationary Phase with Surface-Grafted Triphenyl Selector for Reversed-Phase Capillary Electrochromatography. *Chromatographia* **2016**, *79* (19), 1333–1341.

(30) Poupart, R.; Le Droumaguet, B.; Guerrouache, M.; Carbonnier, B. Copper Nanoparticles Supported on Permeable Monolith with Carboxylic Acid Surface Functionality: Stability and Catalytic Properties under Reductive Conditions. *Mater. Chem. Phys.* **2015**, *163*, 446–452.

(31) Lav, T.-X.; Carbonnier, B.; Guerrouache, M.; Grande, D. Porous Polystyrene-Based Monolithic Materials Templated by Semi-Interpenetrating Polymer Networks for Capillary Electrochromatography. *Polymer* **2010**, *51* (25), 5890–5894.

(32) Lav, T.-X.; Grande, D.; Gaillet, C.; Guerrouache, M.; Carbonnier, B. Porous Poly(Styrene-Co-Divinylbenzene) Neutral Monolith: From Design and Characterization to Reversed-Phase Capillary Electrochromatography Applications. *Macromol. Chem. Phys.* **2012**, *213* (1), 64–71.

(33) Lin, H.-R.; Kuo, C.-J.; Yang, C. Y.; Shaw, S.-Y.; Wu, Y.-J. Preparation of Macroporous Biodegradable PLGA Scaffolds for Cell Attachment with the Use of Mixed Salts as Porogen Additives. *J. Biomed. Mater. Res.* **2002**, *63* (3), 271–279.

(34) Chow, K. S.; Khor, E. Novel Fabrication of Open-Pore Chitin Matrixes. *Biomacromolecules* **2000**, *1* (1), 61–67.

(35) Zhang, J.; Wu, L.; Jing, D.; Ding, J. A Comparative Study of Porous Scaffolds with Cubic and Spherical Macropores. *Polymer* **2005**, *46* (13), 4979–4985.

(36) LaNasa, S. M.; Hoffecker, I. T.; Bryant, S. J. Presence of Pores and Hydrogel Composition Influence Tensile Properties of Scaffolds Fabricated from Well-Defined Sphere Templates. *J. Biomed. Mater. Res. B Appl. Biomater.* **2011**, *96B* (2), 294–302.

(37) Le Droumaguet, B.; Lacombe, R.; Ly, H.-B.; Guerrouache, M.; Carbonnier, B.; Grande, D. Engineering Functional Doubly Porous PHEMA-Based Materials. *Polymer* **2014**, *55* (1), 373–379.

(38) Apel, P. Track Etching Technique in Membrane Technology. *Radiat. Meas.* **2001**, *34* (1), 559–566.

(39) Matsen, M. W.; Bates, F. S. Unifying Weak- and Strong-Segregation Block Copolymer Theories. *Macromolecules* **1996**, *29* (4), 1091–1098.

(40) Bates, F. S.; Fredrickson, G. H. Block Copolymers-Designer Soft Materials. *Phys. Today* **1999**, *52* (2), 32–38.

(41) Lee, J. S.; Hirao, A.; Nakahama, S. Polymerization of Monomers Containing Functional Silyl Groups. 5. Synthesis of New Porous Membranes with Functional Groups. *Macromolecules* **1988**, *21* (1), 274–276.

(42) Grande, D.; Le Droumaguet, B. Design of Functional Nanoporous Polymeric Materials from Self-Organized Block Copolymers. In *Nanopores and Nanoporous Materials*; Morton, T., Ed.; Nanotechnology Science and Technology; Nova Science Publishers: Hauppauge, New York, 2016; pp 1–26.

(43) Gorzolnik, B.; Davidson, P.; Beurroies, I.; Denoyel, R.; Grande, D. Novel Functional Mesoporous Materials Obtained from Nanostructured Diblock Copolymers. *Macromol. Symp.* **2010**, *287* (1), 127–134.

(44) Gorzolnik, B.; Penelle, J.; Grande, D. Design of Mesoporous Materials with Controlled Porosity and Functionality from Nanostructured Diblock Copolymers. *Polym. Mater. Sci. Eng.* **2007**, *97*, 223–224.

(45) Chuma, A.; Horn, H. W.; Swope, W. C.; Pratt, R. C.; Zhang, L.; Lohmeijer, B. G. G.; Wade, C. G.; Waymouth, R. M.; Hedrick, J. L.; Rice, J. E. The Reaction Mechanism for the Organocatalytic Ring-Opening Polymerization of l-Lactide Using a Guanidine-Based Catalyst: Hydrogen-Bonded or Covalently Bound? *J. Am. Chem. Soc.* **2008**, *130* (21), 6749–6754.

(46) Cross, E. D.; Allan, L. E. N.; Decken, A.; Shaver, M. P. Aluminum Salen and Salan Complexes in the Ring-Opening Polymerization of Cyclic Esters: Controlled Immortal and Copolymerization of Rac-β-Butyrolactone and Rac-Lactide. *J. Polym. Sci. Part Polym. Chem.* **2013**, *51* (5), 1137–1146.

(47) Zalusky, A. S.; Olayo-Valles, R.; Taylor, C. J.; Hillmyer, M. A. Mesoporous Polystyrene Monoliths. *J. Am. Chem. Soc.* **2001**, *123* (7), 1519–1520.

(48) Grande, D.; Penelle, J.; Davidson, P.; Beurroies, I.; Denoyel, R. Functionalized Ordered Nanoporous Polymeric Materials: From the Synthesis of Diblock Copolymers to Their Nanostructuration and Their Selective Degradation. *Microporous Mesoporous Mater.* **2011**, *140* (1), 34–39.

(49) Majdoub, R.; Antoun, T.; Le Droumaguet, B.; Benzina, M.; Grande, D. Original Route to Polylactide–polystyrene Diblock Copolymers Containing a Sulfonyl Group at the Junction between Both Blocks as Precursors to Functional Nanoporous Materials. *React. Funct. Polym.* **2012**, *72* (8), 495–502.

(50) Sarkar, A.; Stefik, M. Robust Porous Polymers Enabled by a Fast Trifluoroacetic Acid Etch with Improved Selectivity for Polylactide. *Mater. Chem. Front.* **2017**, *1* (8), 1526–1533.

(51) Goldbach, J. T.; Russell, T. P.; Penelle, J. Synthesis and Thin Film Characterization of Poly(Styrene-Block-Methyl Methacrylate) Containing an Anthracene Dimer Photocleavable Junction Point. *Macromolecules* **2002**, *35* (11), 4271–4276.

(52) Yurt, S.; Anyanwu, U. K.; Scheintaub, J. R.; Coughlin, E. B.; Venkataraman, D. Scission of Diblock Copolymers into Their Constituent Blocks. *Macromolecules* **2006**, *39* (5), 1670–1672.

(53) Zhang, M.; Yang, L.; Yurt, S.; Misner, M. J.; Chen, J.-T.; Coughlin, E. B.; Venkataraman, D.; Russell, T. P. Highly Ordered Nanoporous Thin Films from Cleavable Polystyrene-Block-Poly(Ethylene Oxide). *Adv. Mater.* **2007**, *19* (12), 1571–1576.

(54) Kang, M.; Moon, B. Synthesis of Photocleavable Poly(Styrene-Block-Ethylene Oxide) and Its Self-Assembly into Nanoporous Thin Films. *Macromolecules* **2009**, *42* (1), 455–458.

(55) Schumers, J.-M.; Gohy, J.-F.; Fustin, C.-A. A Versatile Strategy for the Synthesis of Block Copolymers Bearing a Photocleavable Junction. *Polym. Chem.* **2010**, *1* (2), 161–163.

(56) Zhao, H.; Gu, W.; Sterner, E.; Russell, T. P.; Coughlin, E. B.; Theato, P. Highly Ordered Nanoporous Thin Films from Photocleavable Block Copolymers. *Macromolecules* **2011**, *44* (16), 6433–6440.

(57) Zhao, H.; Gu, W.; Thielke, M. W.; Sterner, E.; Tsai, T.; Russell, T. P.; Coughlin, E. B.; Theato, P. Functionalized Nanoporous Thin Films and Fibers from Photocleavable Block Copolymers Featuring Activated Esters. *Macromolecules* **2013**, *46* (13), 5195–5201.

(58) Gamys, C. G.; Schumers, J.-M.; Vlad, A.; Fustin, C.-A.; Gohy, J.-F. Amine-Functionalized Nanoporous Thin Films from a Poly(Ethylene Oxide)-Block-Polystyrene Diblock Copolymer Bearing a Photocleavable o-Nitrobenzyl Carbamate Junction. *Soft Matter* **2012**, *8* (16), 4486–4493.

(59) Ouchi, M.; Konishi, A.; Takenaka, M.; Sawamoto, M. Consecutive Living Polymerization from Cationic to Radical: A Straightforward yet Versatile Methodology for the Precision Synthesis of "Cleavable" Block Copolymers with a Hemiacetal Ester Junction. *Polym. Chem.* **2012**, *3* (8), 2193–2199.

(60) Satoh, K.; Poelma, J. E.; Campos, L. M.; Stahl, B.; Hawker, C. J. A Facile Synthesis of Clickable and Acid-Cleavable PEO for Acid-Degradable Block Copolymers. *Polym Chem* **2012**, *3* (7), 1890–1898.

(61) Poupart, R.; Benlahoues, A.; Le Droumaguet, B.; Grande, D. Porous Gold Nanoparticle-Decorated Nanoreactors Prepared from Smartly Designed Functional Polystyrene-Block-Poly(d,l-Lactide) Diblock Copolymers: Toward Efficient Systems for Catalytic Cascade Reaction Processes. *ACS Appl. Mater. Interfaces* **2017**, *article in press*, DOI: 10.1021/acsami.6b16157.

(62) Goldbach, J. T.; Lavery, K. A.; Penelle, J.; Russell, T. P. Nano- to Macro-Sized Heterogeneities Using Cleavable Diblock Copolymers. *Macromolecules* **2004**, *37* (25), 9639–9645.

(63) Ryu, J.-H.; Park, S.; Kim, B.; Klaikherd, A.; Russell, T. P.; Thayumanavan, S. Highly Ordered Gold Nanotubes Using Thiols at a Cleavable Block Copolymer Interface. *J. Am. Chem. Soc.* **2009**, *131* (29), 9870–9871.

(64) Le Droumaguet, B.; Poupart, R.; Grande, D. "Clickable" Thiol-Functionalized Nanoporous Polymers: From Their Synthesis to Further Adsorption of Gold Nanoparticles and Subsequent Use as Efficient Catalytic Supports. *Polym. Chem.* **2015**, *6* (47), 8105–8111.

(65) Rao, J.; De, S.; Khan, A. Synthesis and Self-Assembly of Dynamic Covalent Block Copolymers: Towards a General Route to Pore-Functionalized Membranes. *Chem. Commun.* **2012**, *48* (28), 3427–3429.

(66) Glassner, M.; Blinco, J. P.; Barner-Kowollik, C. Formation of Nanoporous Materials via Mild Retro-Diels-Alder Chemistry. *Polym. Chem.* **2011**, *2* (1), 83–87.

(67) Fustin, C.-A.; Lohmeijer, B. G. G.; Duwez, A.-S.; Jonas, A. M.; Schubert, U. S.; Gohy, J.-F. Nanoporous Thin Films from Self-Assembled Metallo- Supramolecular Block Copolymers. *Adv. Mater.* **2005**, *17* (9), 1162–1165.

(68) Mugemana, C.; Gohy, J.-F.; Fustin, C.-A. Functionalized Nanoporous Thin Films from Metallo-Supramolecular Diblock Copolymers. *Langmuir* **2012**, *28* (5), 3018–3023.

(69) Yu, H.; Stoffelbach, F.; Detrembleur, C.; Fustin, C.-A.; Gohy, J.-F. Nanoporous Thin Films from Ionically Connected Diblock Copolymers. *Eur. Polym. J.* **2012**, *48* (5), 940–944.

(70) Montarnal, D.; Delbosc, N.; Chamignon, C.; Virolleaud, M.-A.; Luo, Y.; Hawker, C. J.; Drockenmuller, E.; Bernard, J. Highly Ordered Nanoporous Films from Supramolecular Diblock Copolymers with Hydrogen-Bonding Junctions. *Angew. Chem. Int. Ed.* **2015**, *54* (38), 11117–11121.

(71) McKeown, N. B.; Budd, P. M. Polymers of Intrinsic Microporosity (PIMs): Organic Materials for Membrane Separations, Heterogeneous Catalysis and Hydrogen Storage. *Chem. Soc. Rev.* **2006**, *35* (8), 675–683.

(72) Dawson, R.; Cooper, A. I.; Adams, D. J. Nanoporous Organic Polymer Networks. *Prog. Polym. Sci.* **2012**, *37* (4), 530–563.

(73) Sakaushi, K.; Antonietti, M. Carbon- and Nitrogen-Based Organic Frameworks. *Acc. Chem. Res.* **2015**, *48* (6), 1591–1600.

(74) Shen, C.; Yu, H.; Wang, Z. Synthesis of 1,3,5,7-Tetrakis(4-Cyanatophenyl)Adamantane and Its Microporous Polycyanurate Network for Adsorption of Organic Vapors, Hydrogen and Carbon Dioxide. *Chem. Commun.* **2014**, *50* (76), 11238–11241.

(75) Zhang, Y.; Riduan, S. N.; Ying, J. Y. Microporous Polyisocyanurate and Its Application in Heterogeneous Catalysis. *Chem. – Eur. J.* **2009**, *15* (5), 1077–1081.

(76) Dey, S. K.; de Sousa Amadeu, N.; Janiak, C. Microporous Polyurethane Material for Size Selective Heterogeneous Catalysis of the Knoevenagel Reaction. *Chem. Commun.* **2016**, *52* (50), 7834–7837.

(77) Kuhn, P.; Antonietti, M.; Thomas, A. Porous, Covalent Triazine-Based Frameworks Prepared by Ionothermal Synthesis. *Angew. Chem. Int. Ed.* **2008**, *47* (18), 3450–3453.

(78) Carta, M.; Croad, M.; Bugler, K.; Msayib, K. J.; McKeown, N. B. Heterogeneous Organocatalysts Composed of Microporous Polymer Networks Assembled by Troger's Base Formation. *Polym. Chem.* **2014**, *5* (18), 5262–5266.

(79) Ben, T.; Ren, H.; Ma, S.; Cao, D.; Lan, J.; Jing, X.; Wang, W.; Xu, J.; Deng, F.; Simmons, J. M.; Qiu, S.; Zhu, G. Targeted Synthesis of a Porous Aromatic Framework with High Stability and Exceptionally High Surface Area. *Angew. Chem.* **2009**, *121* (50), 9621–9624.

(80) Verde-Sesto, E.; Pintado-Sierra, M.; Corma, A.; Maya, E. M.; de la Campa, J. G.; Iglesias, M.; Sánchez, F. First Pre-Functionalised Polymeric Aromatic Framework from

Mononitrotetrakis(Iodophenyl)Methane and Its Applications. *Chem. – Eur. J.* **2014**, *20* (17), 5111–5120.

(81) Zeltinger, J.; Sherwood, J. K.; Graham, D. A.; Müeller, R.; Griffith, L. G. Effect of Pore Size and Void Fraction on Cellular Adhesion, Proliferation, and Matrix Deposition. *Tissue Eng.* **2001**, *7* (5), 557–572.

(82) Ruiz, J. A. R.; Marc-Tallon, J.; Pedros, M.; Dumon, M. Two-Step Micro Cellular Foaming of Amorphous Polymers in Supercritical CO2. *J. Supercrit. Fluids* **2011**, *57* (1), 87–94.

(83) Ly, H. B.; Le Droumaguet, B.; Monchiet, V.; Grande, D. Tailoring Doubly Porous Poly(2-Hydroxyethyl Methacrylate)-Based Materials via Thermally Induced Phase Separation. *Polymer* **2016**, *86*, 138–146.

(84) Huang, Z.-M.; Zhang, Y.-Z.; Kotaki, M.; Ramakrishna, S. A Review on Polymer Nanofibers by Electrospinning and Their Applications in Nanocomposites. *Compos. Sci. Technol.* **2003**, *63* (15), 2223–2253.

(85) Formhals, A. Process and Apparatus for Preparing Artificial Threads. US1975504 A, October 2, 1934.

(86) Reneker, D. H.; Chun, I. Nanometre Diameter Fibres of Polymer, Produced by Electrospinning. *Nanotechnology* **1996**, *7* (3), 216.

(87) Reneker, D. H.; Yarin, A. L.; Zussman, E.; Xu, H. Electrospinning of Nanofibers from Polymer Solutions and Melts. *Adv. Appl. Mech.* **2007**, *41*, 43–346.

(88) Villarreal-Gómez, L. J.; Cornejo-Bravo, J. M.; Vera-Graziano, R.; Grande, D. Electrospinning as a Powerful Technique for Biomedical Applications: A Critically Selected Survey. *J. Biomater. Sci. Polym. Ed.* **2016**, *27* (2), 157–176.

(89) Bognitzki, M.; Czado, W.; Frese, T.; Schaper, A.; Hellwig, M.; Steinhart, M.; Greiner, A.; Wendorff, J. H. Nanostructured Fibers via Electrospinning. *Adv. Mater.* **2001**, *13* (1), 70–72.

(90) Silverstein, M. S.; Cameron, N. R. PolyHIPEs — Porous Polymers from High Internal Phase Emulsions. In *Encyclopedia of Polymer Science and Technology*; John Wiley & Sons, Inc., 2002.

(91) Cameron, N. R.; Sherrington, D. C. High Internal Phase Emulsions (HIPEs) — Structure, Properties and Use in Polymer Preparation. In *Biopolymers Liquid Crystalline Polymers Phase Emulsion*; Springer Berlin Heidelberg: Berlin, Heidelberg, 1996; pp 163–214.

(92) Barby, D.; Haq, Z. Low Density Porous Cross-Linked Polymeric Materials and Their Preparation. EP0060138 A1, September 15, 1982.

(93) Krajnc, P.; Brown, J. F.; Cameron, N. R. Monolithic Scavenger Resins by Amine Functionalizations of Poly(4-Vinylbenzyl Chloride-Co-Divinylbenzene) PolyHIPE Materials. *Org. Lett.* **2002**, *4* (15), 2497–2500.

(94) Krajnc, P.; Štefanec, D.; Pulko, I. Acrylic Acid "Reversed" PolyHIPEs. *Macromol. Rapid Commun.* **2005**, *26* (16), 1289–1293.

(95) Kot, E.; Shirshova, N.; Bismarck, A.; Steinke, J. H. G. Non-Aqueous High Internal Phase Emulsion Templates for Synthesis of Macroporous Polymers in Situ Filled with Cyclic Carbonate Electrolytes. *RSC Adv.* **2014**, *4* (22), 11512–11519.

(96) R. Cameron, N.; C. Sherrington, D. Preparation and Glass Transition Temperatures of Elastomeric PolyHIPE Materials. *J. Mater. Chem.* **1997**, *7* (11), 2209–2212.

(97) Mehraban, M.; Zadhoush, A.; Abdolkarim Hosseini Ravandi, S.; Bagheri, R.; Heidarkhan Tehrani, A. Preparation of Porous Nanofibers from Electrospun Polyacrylonitrile/Calcium Carbonate Composite Nanofibers Using Porogen Leaching Technique. *J. Appl. Polym. Sci.* **2013**, *128* (2), 926–933.

(98) Ly, H.-B.; Le Droumaguet, B.; Monchiet, V.; Grande, D. Designing and Modeling Doubly Porous Polymeric Materials. *Eur. Phys. J. Spec. Top.* **2015**, *224* (9), 1689–1706.

(99) Ly, H. B.; Le Droumaguet, B.; Monchiet, V.; Grande, D. Facile Fabrication of Doubly Porous Polymeric Materials with Controlled Nano- and Macro-Porosity. *Polymer* **2015**, *78*, 13–21.

(100) Ly, H. B.; Halbardier, L.; Grande, D. Biporous Crosslinked Polymers With Controlled Pore Size and Connectivity. *Macromol. Symp.* **2016**, *365* (1), 49–58.

(101) Ly, H. B.; Poupart, R.; Halbardier, L.; Grande, D. Functionalized Doubly Porous Networks: From Synthesis to Application in Heterogeneous Catalysis. *Macromol. Symp.* **2016**, *365* (1), 40–48.

(102) Webb, P. A.; Orr, C.; Corporation, M. I. *Analytical Methods in Fine Particle Technology*; Micromeritics Instrument Corporation, 1997.

(103) Washburn, E. W. Note on a Method of Determining the Distribution of Pore Sizes in a Porous Material. *Proc. Natl. Acad. Sci.* **1921**, *7* (4), 115–116.

(104) Moura, M. J.; Ferreira, P. J.; Figueiredo, M. M. Mercury Intrusion Porosimetry in Pulp and Paper Technology. *Powder Technol.* **2005**, *160* (2), 61–66.

(105) Winslow, D. N. Advances in Experimental Techniques for Mercury Intrusion Porosimetry. In *Surface and Colloid Science: Volume 13*; Matijević, E., Good, R. J., Eds.; Springer US: Boston, MA, 1984; pp 259–282.

(106) Feller, C.; Schouller, E.; Thomas, F.; Rouiller, J.; Herbillon, A. J. N2-BET Specific Surface Areas of Some Low Activity Clay Soils and Their Relationships with Secondary Constituents and Organic Matter Contents. *Soil Sci.* **1992**, *153* (4), 293–299.

(107) Kim, K. C.; Yoon, T.-U.; Bae, Y.-S. Applicability of Using CO2 Adsorption Isotherms to Determine BET Surface Areas of Microporous Materials. *Microporous Mesoporous Mater.* **2016**, *224*, 294–301.

(108) Yanazawa, H.; Ohshika, K.; Matsuzawa, T. Precision Evaluation in Kr Adsorption for Small BET Surface Area Measurements of Less Than 1 M2. *Adsorption* **2000**, *6* (1), 73–77.

(109) Brunauer, S.; Emmett, P. H.; Teller, E. Adsorption of Gases in Multimolecular Layers. *J. Am. Chem. Soc.* **1938**, *60* (2), 309–319.

(110) Barrett, E. P.; Joyner, L. G.; Halenda, P. P. The Determination of Pore Volume and Area Distributions in Porous Substances. I. Computations from Nitrogen Isotherms. *J. Am. Chem. Soc.* **1951**, *73* (1), 373–380.

(111) Iza, M.; Woerly, S.; Danumah, C.; Kaliaguine, S.; Bousmina, M. Determination of Pore Size Distribution for Mesoporous Materials and Polymeric Gels by Means of DSC Measurements: Thermoporometry. *Polymer* **2000**, *41* (15), 5885–5893.

(112) Hay, J. N.; Laity, P. R. Observations of Water Migration during Thermoporometry Studies of Cellulose Films. *Polymer* **2000**, *41* (16), 6171–6180.

(113) Brun, M.; Lallemand, A.; Quinson, J.-F.; Eyraud, C. A New Method for the Simultaneous Determination of the Size and Shape of Pores: The Thermoporometry. *Thermochim. Acta* **1977**, *21* (1), 59–88.

(114) Jones, B. H.; Lodge, T. P. Nanoporous Materials Derived from Polymeric Bicontinuous Microemulsions. *Chem. Mater.* **2010**, *22* (4), 1279–1281.

(115) Wulff, M. Pore Size Determination by Thermoporometry Using Acetonitrile. *Thermochim. Acta* **2004**, *419* (1), 291–294.

(116) Strange, J. H.; Mitchell, J.; Webber, J. B. W. Pore Surface Exploration by NMR. *Magn. Reson. Imaging* **2003**, *21* (3), 221–226.

(117) Dlapka, M.; Danninger, H.; Gierl, C.; Lindqvist, B. Defining the Pores in PM Components. *Met. Powder Rep.* **2010**, *65* (2), 30–33.

(118) Vakifahmetoglu, C.; Colombo, P. A Direct Method for the Fabrication of Macro-Porous SiOC Ceramics from Preceramic Polymers. *Adv. Eng. Mater.* **2008**, *10* (3), 256–259.

(119) Tokuhiro, T. Temperature Dependence of Density of Polymer Gels 1. A Pycnometry Method Applied to Poly(N-Isopropylacrylamide)−Water System. *J. Phys. Chem. B* **1999**, *103* (34), 7097–7101.

(120) Moreno-Mañas, M.; Pleixats, R. Formation of Carbon−Carbon Bonds under Catalysis by Transition-Metal Nanoparticles. *Acc. Chem. Res.* **2003**, *36* (8), 638–643.

(121) Astruc, D.; Lu, F.; Aranzaes, J. R. Nanoparticles as Recyclable Catalysts: The Frontier between Homogeneous and Heterogeneous Catalysis. *Angew. Chem. Int. Ed.* **2005**, *44* (48), 7852–7872.

(122) Takale, B. S.; Bao, M.; Yamamoto, Y. Gold Nanoparticle (AuNPs) and Gold Nanopore (AuNPore) Catalysts in Organic Synthesis. *Org. Biomol. Chem.* **2014**, *12* (13), 2005–2027.

(123) Daniel, M.-C.; Astruc, D. Gold Nanoparticles: Assembly, Supramolecular Chemistry, Quantum-Size-Related Properties, and Applications toward Biology, Catalysis, and Nanotechnology. *Chem. Rev.* **2004**, *104* (1), 293–346.

(124) Gawande, M. B.; Goswami, A.; Felpin, F.-X.; Asefa, T.; Huang, X.; Silva, R.; Zou, X.; Zboril, R.; Varma, R. S. Cu and Cu-Based Nanoparticles: Synthesis and Applications in Catalysis. *Chem. Rev.* **2016**, *116* (6), 3722–3811.

(125) Ranu, B. C.; Dey, R.; Chatterjee, T.; Ahammed, S. Copper Nanoparticle-Catalyzed Carbon-Carbon and Carbon-Heteroatom Bond Formation with a Greener Perspective. *ChemSusChem* **2012**, *5* (1), 22–44.

(126) Chen, A.; Holt-Hindle, P. Platinum-Based Nanostructured Materials: Synthesis, Properties, and Applications. *Chem. Rev.* **2010**, *110* (6), 3767–3804.

(127) Astruc, D. Palladium Nanoparticles as Efficient Green Homogeneous and Heterogeneous Carbon−Carbon Coupling Precatalysts: A Unifying View. *Inorg. Chem.* **2007**, *46* (6), 1884–1894.

(128) Corma, A.; Garcia, H. Supported Gold Nanoparticles as Catalysts for Organic Reactions. *Chem. Soc. Rev.* **2008**, *37* (9), 2096–2126.

(129) Campelo, J. M.; Luna, D.; Luque, R.; Marinas, J. M.; Romero, A. A. Sustainable Preparation of Supported Metal Nanoparticles and Their Applications in Catalysis. *ChemSusChem* **2009**, *2* (1), 18–45.

(130) Munnik, P.; de Jongh, P. E.; de Jong, K. P. Recent Developments in the Synthesis of Supported Catalysts. *Chem. Rev.* **2015**, *115* (14), 6687–6718.

(131) Wuithschick, M.; Paul, B.; Bienert, R.; Sarfraz, A.; Vainio, U.; Sztucki, M.; Kraehnert, R.; Strasser, P.; Rademann, K.; Emmerling, F.; Polte, J. Size-Controlled Synthesis of Colloidal Silver Nanoparticles Based on Mechanistic Understanding. *Chem. Mater.* **2013**, *25* (23), 4679–4689.

(132) Wuithschick, M.; Witte, S.; Kettemann, F.; Rademann, K.; Polte, J. Illustrating the Formation of Metal Nanoparticles with a Growth Concept Based on Colloidal Stability. *Phys. Chem. Chem. Phys.* **2015**, *17* (30), 19895–19900.

(133) Wuithschick, M.; Birnbaum, A.; Witte, S.; Sztucki, M.; Vainio, U.; Pinna, N.; Rademann, K.; Emmerling, F.; Kraehnert, R.; Polte, J. Turkevich in New Robes: Key Questions Answered for the Most Common Gold Nanoparticle Synthesis. *ACS Nano* **2015**, *9* (7), 7052–7071.

(134) Kettemann, F.; Birnbaum, A.; Witte, S.; Wuithschick, M.; Pinna, N.; Kraehnert, R.; Rademann, K.; Polte, J. Missing Piece of the Mechanism of the Turkevich Method: The Critical Role of Citrate Protonation. *Chem. Mater.* **2016**, *28* (11), 4072–4081.

(135) Boutonnet, M.; Kizling, J.; Stenius, P.; Maire, G. The Preparation of Monodisperse Colloidal Metal Particles from Microemulsions. *Colloids Surf.* **1982**, *5* (3), 209–225.

(136) Shim, I.-W.; Kim, J.-Y.; Kim, D.-Y.; Choi, S. Preparation of Rh-Containing Polycarbonate Films and the Study of Their Chemical Properties in the Polymer. *React. Funct. Polym.* **2000**, *43* (1), 71–78.

(137) Groppo, E.; Agostini, G.; Borfecchia, E.; Wei, L.; Giannici, F.; Portale, G.; Longo, A.; Lamberti, C. Formation and Growth of Pd Nanoparticles Inside a Highly Cross-Linked Polystyrene Support: Role of the Reducing Agent. *J. Phys. Chem. C* **2014**, *118* (16), 8406–8415.

(138) Chappa, S.; Bharath, R. S.; Oommen, C.; Pandey, A. K. Dual-Functional Grafted Electrospun Polymer Microfiber Scaffold Hosted Palladium Nanoparticles for Catalyzing Redox Reactions. *Macromol. Chem. Phys.* **2017**, *218* (7), 1600555.

(139) Poupart, R.; Djerir, N. E. H.; Chellapermal, D.; Guerrouache, M.; Carbonnier, B.; Le Droumaguet, B. Novel In-Capillary Polymeric Monoliths Arising from Glycerol Carbonate Methacrylate for Flow-through Catalytic and Chromatographic Applications. *RSC Adv.* **2016**, *6* (17), 13614–13617.

(140) Xiao, S.; Xu, W.; Ma, H.; Fang, X. Size-Tunable Ag Nanoparticles Immobilized in Electrospun Nanofibers: Synthesis, Characterization, and Application for Catalytic Reduction of 4-Nitrophenol. *RSC Adv.* **2012**, *2* (1), 319–327.

(141) Mora-Tamez, L.; Esquivel-Peña, V.; Ocampo, A. L.; Rodríguez de San Miguel, E.; Grande, D.; de Gyves, J. Simultaneous AuIII Extraction and In Situ Formation of Polymeric Membrane-Supported Au Nanoparticles: A Sustainable Process with Application in Catalysis. *ChemSusChem* **2017**, *10* (7), 1482–1493.

(142) Emin, C.; Remigy, J.-C.; Lahitte, J.-F. Influence of UV Grafting Conditions and Gel Formation on the Loading and Stabilization of Palladium Nanoparticles in Photografted Polyethersulfone Membrane for Catalytic Reactions. *J. Membr. Sci.* **2014**, *455*, 55–63.

(143) Gu, Y.; Emin, C.; Remigy, J.-C.; Favier, I.; Gómez, M.; Noble, R. D.; Gin, D. L.; Macanás, J.; Domènech, B.; Lahitte, J.-F. Hybrid Catalytic Membranes: Tunable and Versatile Materials for Fine Chemistry Applications. *Mater. Today Proc.* **2016**, *3* (2), 419–423.

(144) Liu, Y.; Guerrouache, M.; Kebe, S. I.; Carbonnier, B.; Le Droumaguet, B. Gold Nanoparticles-Supported Histamine-Grafted Monolithic Capillaries as Efficient Microreactors for Flow-through Reduction of Nitro-Containing Compounds. *J. Mater. Chem. A* **2017**, *5* (23), 11805–11814.

(145) Khalil, A. M.; Georgiadou, V.; Guerrouache, M.; Mahouche-Chergui, S.; Dendrinou-Samara, C.; Chehimi, M. M.; Carbonnier, B. Gold-Decorated Polymeric Monoliths: In-Situ vs Ex-Situ

Immobilization Strategies and Flow through Catalytic Applications towards Nitrophenols Reduction. *Polymer* **2015**, *77*, 218–226.

(146) Fang, X.; Ma, H.; Xiao, S.; Shen, M.; Guo, R.; Cao, X.; Shi, X. Facile Immobilization of Gold Nanoparticles into Electrospun Polyethyleneimine/Polyvinyl Alcohol Nanofibers for Catalytic Applications. *J. Mater. Chem.* **2011**, *21* (12), 4493–4501.

(147) Nikbin, N.; Ladlow, M.; Ley, S. V. Continuous Flow Ligand-Free Heck Reactions Using Monolithic Pd [0] Nanoparticles. *Org. Process Res. Dev.* **2007**, *11* (3), 458–462.

(148) Bandari, R.; Höche, T.; Prager, A.; Dirnberger, K.; Buchmeiser, M. R. Ring-Opening Metathesis Polymerization Based Pore-Size-Selective Functionalization of Glycidyl Methacrylate Based Monolithic Media: Access to Size-Stable Nanoparticles for Ligand-Free Metal Catalysis. *Chem. – Eur. J.* **2010**, *16* (15), 4650–4658.

(149) Budarin, V. L.; Clark, J. H.; Luque, R.; Macquarrie, D. J.; White, R. J. Palladium Nanoparticles on Polysaccharide-Derived Mesoporous Materials and Their Catalytic Performance in C-C Coupling Reactions. *Green Chem.* **2008**, *10* (4), 382–387.

(150) Bandari, R.; Prager, A.; Höche, T.; Buchmeiser, M. R. Formation of Pd-Nanoparticles within the Pores of Ring Opening Metathesis Polymerization-Derived Polymeric Monoliths for Use in Organometallic Catalysis. *ARKIVOC* **2011**.

(151) Gu, Y.; Favier, I.; Pradel, C.; Gin, D. L.; Lahitte, J.-F.; Noble, R. D.; Gómez, M.; Remigy, J.-C. High Catalytic Efficiency of Palladium Nanoparticles Immobilized in a Polymer Membrane Containing Poly(Ionic Liquid) in Suzuki–Miyaura Cross-Coupling Reaction. *J. Membr. Sci.* **2015**, *492*, 331–339.

(152) Gu, Y.; Bacchin, P.; Lahitte, J.-F.; Remigy, J.-C.; Favier, I.; Gómez, M.; Gin, D. L.; Noble, R. D. Catalytic Membrane Reactor for Suzuki-Miyaura C−C Cross-Coupling: Explanation for Its High Efficiency via Modeling. *AIChE J.* **2017**, *63* (2), 698–704.

(153) Zhang, P.; Weng, Z.; Guo, J.; Wang, C. Solution-Dispersible, Colloidal, Conjugated Porous Polymer Networks with Entrapped Palladium Nanocrystals for Heterogeneous Catalysis of the Suzuki–Miyaura Coupling Reaction. *Chem. Mater.* **2011**, *23* (23), 5243–5249.

(154) Du, Z.-L.; Dang, Q.-Q.; Zhang, X.-M. Heptazine-Based Porous Framework Supported Palladium Nanoparticles for Green Suzuki–Miyaura Reaction. *Ind. Eng. Chem. Res.* **2017**, *56* (15), 4275–4280.

(155) Desforges, A.; Backov, R.; Deleuze, H.; Mondain-Monval, O. Generation of Palladium Nanoparticles within Macrocellular Polymeric Supports: Application to Heterogeneous Catalysis of the Suzuki–Miyaura Coupling Reaction. *Adv. Funct. Mater.* **2005**, *15* (10), 1689–1695.

(156) Bandari, R.; Buchmeiser, M. R. Polymeric Monolith Supported Pt-Nanoparticles as Ligand-Free Catalysts for Olefin Hydrosilylation under Batch and Continuous Conditions. *Catal. Sci. Technol.* **2012**, *2* (1), 220–226.

(157) Poupart, R.; Le Droumaguet, B.; Guerrouache, M.; Grande, D.; Carbonnier, B. Gold Nanoparticles Immobilized on Porous Monoliths Obtained from Disulfide-Based Dimethacrylate: Application to Supported Catalysis. *Polymer* **2017**, *article in press*, DOI: 10.1016/j.polymer.2017.04.034.

(158) Féral-Martin, C.; Birot, M.; Deleuze, H.; Desforges, A.; Backov, R. Integrative Chemistry toward the First Spontaneous Generation of Gold Nanoparticles within Macrocellular PolyHIPE Supports (Au@polyHIPE) and Their Application to Eosin Reduction. *React. Funct. Polym.* **2007**, *67* (10), 1072–1082.

(159) Floris, P.; Twamley, B.; Nesterenko, P. N.; Paull, B.; Connolly, D. Agglomerated Polymer Monoliths with Bimetallic Nano-Particles as Flow-through Micro-Reactors. *Microchim. Acta* **2012**, *179* (1), 149–156.

(160) Taori, V. P.; Bandari, R.; Buchmeiser, M. R. Selective Reduction of CO2 with Silanes over Platinum Nanoparticles Immobilised on a Polymeric Monolithic Support under Ambient Conditions. *Chem. – Eur. J.* **2014**, *20* (12), 3292–3296.

(161) Desforges, A.; Deleuze, H.; Mondain-Monval, O.; Backov, R. Palladium Nanoparticle Generation within Microcellular Polymeric Foam and Size Dependence under Synthetic Conditions. *Ind. Eng. Chem. Res.* **2005**, *44* (23), 8521–8529.

(162) Gu, Y.; Remigy, J.-C.; Favier, I.; Gómez, M.; Noble, R. D.; Lahitte, J.-F. Membrane Reactor Based on Hybrid Nanomaterials for Process Intensification of Catalytic Hydrogenation Reaction: An Example of

Reduction of the Environmental Footprint of Chemical Synthesis from a Batch to a Continuous Flow Chemistry Process. *Chem. Eng. Trans.* **2016**, *47*, 367–372.

(163) Huang, Y.; Ma, H.; Wang, S.; Shen, M.; Guo, R.; Cao, X.; Zhu, M.; Shi, X. Efficient Catalytic Reduction of Hexavalent Chromium Using Palladium Nanoparticle-Immobilized Electrospun Polymer Nanofibers. *ACS Appl. Mater. Interfaces* **2012**, *4* (6), 3054–3061.

(164) Cao, Q.; Xu, Y.; Liu, F.; Svec, F.; Fréchet, J. M. J. Polymer Monoliths with Exchangeable Chemistries: Use of Gold Nanoparticles As Intermediate Ligands for Capillary Columns with Varying Surface Functionalities. *Anal. Chem.* **2010**, *82* (17), 7416–7421.

(165) Connolly, D.; Twamley, B.; Paull, B. High-Capacity Gold Nanoparticle Functionalised Polymer Monoliths. *Chem. Commun.* **2010**, *46* (12), 2109–2111.

(166) Guerrouache, M.; Mahouche-Chergui, S.; Chehimi, M. M.; Carbonnier, B. Site-Specific Immobilisation of Gold Nanoparticles on a Porous Monolith Surface by Using a Thiol-Yne Click Photopatterning Approach. *Chem. Commun.* **2012**, *48* (60), 7486–7488.

(167) Merino, E.; Verde-Sesto, E.; Maya, E. M.; Corma, A.; Iglesias, M.; Sánchez, F. Mono-Functionalization of Porous Aromatic Frameworks to Use as Compatible Heterogeneous Catalysts in One-Pot Cascade Reactions. *Appl. Catal. Gen.* **2014**, *469*, 206–212.

(168) Xie, Z.; Wang, C.; deKrafft, K. E.; Lin, W. Highly Stable and Porous Cross-Linked Polymers for Efficient Photocatalysis. *J. Am. Chem. Soc.* **2011**, *133* (7), 2056–2059.

(169) Vankelecom, I. F. J. Polymeric Membranes in Catalytic Reactors. *Chem. Rev.* **2002**, *102* (10), 3779–3810.

(170) Cheng, G.; Hasell, T.; Trewin, A.; Adams, D. J.; Cooper, A. I. Soluble Conjugated Microporous Polymers. *Angew. Chem. Int. Ed.* **2012**, *51* (51), 12727–12731.

(171) Cameron, N. R. High Internal Phase Emulsion Templating as a Route to Well-Defined Porous Polymers. *Polymer* **2005**, *46* (5), 1439–1449.

(172) Hainey, P.; Huxham, I. M.; Rowatt, B.; Sherrington, D. C.; Tetley, L. Synthesis and Ultrastructural Studies of Styrene-Divinylbenzene Polyhipe Polymers. *Macromolecules* **1991**, *24* (1), 117–121.

(173) Dzenis, Y. Spinning Continuous Fibers for Nanotechnology. *Science* **2004**, *304* (5679), 1917.

Chapter 2:

Metallic Nanoparticles Immobilized on Bulky Macroporous Monoliths

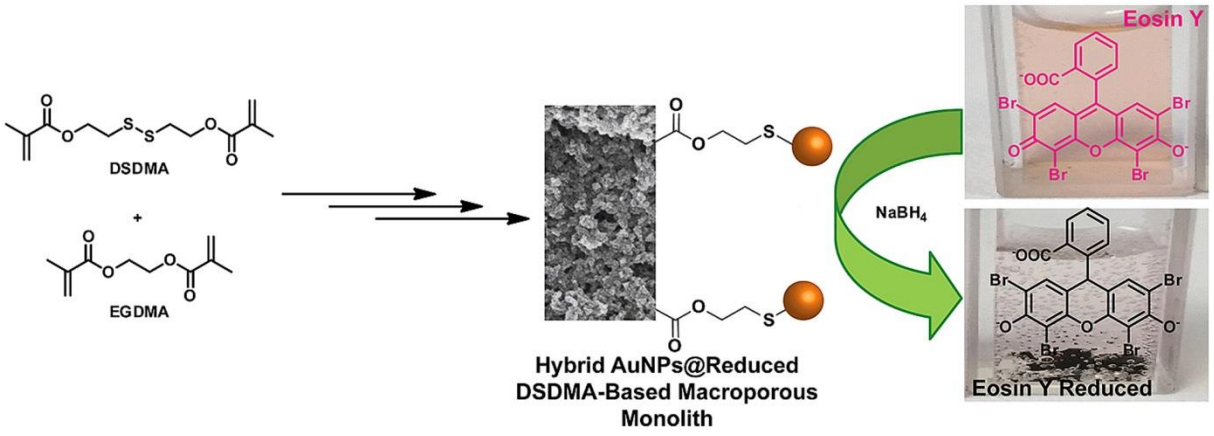

Contexte

Pour immobiliser des nanoparticules sur une surface poreuse, la présence d'interactions entre cette surface et la particule elle-même est nécessaire. Certaines fonctions chimiques sont connues pour être des chélatants de nanoparticules métalliques et/ou de leurs précurseurs ioniques. Parmi elles, nous pouvons citer les amines, les acides carboxyliques, les groupements cyano ou encore les thiols.

Ces derniers présentent un intérêt car ils sont d'excellents chélatants des nanoparticules d'or, malheureusement, leur intégration sur des monomères est délicate. Mis en présence lors d'une polymérisation radicalaire, ils agissent en tant qu'agent de transfert, compromettant la réaction en cours. Afin de les intégrer, les scientifiques ont eu recours à diverses stratégies ingénieuses. La première consiste en une réaction de post-fonctionnalisation. Après la polymérisation, un groupe chimique, pendant sur la chaîne polymère, réagi avec une molécule possédant un groupement –SH, générant le thiol requis. Une autre voie est basée sur une séquence de protection/déprotection. Le thiol peut cette fois-ci être indirectement contenu dans le monomère car protégé par une fonction chimique n'interférant pas avec la polymérisation. Ce nouveau groupement doit être issu d'une réaction réversible, permettant ainsi la régénération du thiol initial. Le pont disulfure correspond à ces critères car, après la polymérisation, son clivage par un agent réducteur chimique régénère ainsi le thiol.

Par ailleurs, un autre phénomène important lors de l'immobilisation des nanoparticules, et plus précisément lors d'une génération *in situ*, est l'accessibilité à l'intérieur du réseau poreux. Les ions ainsi que le réducteur doivent pénétrer au cœur du matériau afin que celui-ci possède un maximum de sites catalytiques. Les réactions en phase liquide dans un milieu poreux peuvent devenir problématiques à cause d'un phénomène non-négligeable: la mouillabilité. Ce phénomène oblige souvent à placer l'échantillon de polymère poreux sous vide et ensuite injecter le liquide, afin d'atteindre le cœur du matériau. Une solution alternative consiste à réaliser ces réactions en phase gazeuse. Les gaz ont la propriété d'occuper tout le volume qui leur est disponible, indépendamment de la taille des pores. Et parmi les gaz, l'un est connu pour être un réducteur des métaux : l'hydrogène. Utiliser l'hydrogène comme réducteur d'ions métalliques est connu dans le milieu de la chimie inorganique, pourtant son utilisation dans le domaine des polymères reste marginale.

Ainsi, pour répondre à ces deux problématiques, nous avons réalisé un monomère possédant un pont disulfure. Nous l'avons utilisé comme comonomère, avec le diméthacrylate d'éthylène glycol, et l'avons polymérisé thermiquement en présence de toluène, afin d'obtenir un polymère monolithique macroporeux. Après clivage du pont disulfure par le D,L-dithiothreitol, des ions auriques (Au^{3+}) ont été immobilisés puis réduits afin de générer les nanoparticules correspondantes. Les matériaux

hybrides ainsi formés ont été testés avec succès comme catalyseurs lors de la réduction de l'éosine Y et ce, sur plusieurs cycles. Ces résultats ont été publiés dans l'article suivant : **Gold nanoparticles immobilized on porous monoliths obtained from disulfide-based dimethacrylate: Application to supported catalysis**, R. Poupart, B. Le Droumaguet, M. Guerrouache, D. Grande, B. Carbonnier, *Polymer*, **2017**, article sous presse, DOI : 10.1016/j.polymer.2017.04.034.

Par ailleurs, nous avons synthétisé des polymères en masse à partir du méthacrylate de glycidyle, dont les cycles oxiranes ont pu être ouverts par l'attaque nucléophile d'une amine, l'éthylènediamine. Imbibés de solutions de sels métalliques - respectivement d'or, de palladium et d'un mélange équimolaire d'or et de palladium - ils ont par ailleurs été réduits par un flux d'argon et d'hydrogène (95/5 % v/v) sous température (100 °C), générant ainsi les nanoparticules correspondantes. Ces dernières expériences ont été effectuées lors d'un séjour de trois mois dans le laboratoire du Professeur N. Pinna de l'Université Humboldt de Berlin. Les matériaux ont ensuite été utilisés afin de catalyser une réaction de Suzuki-Miyaura entre le 4-iodotoluène et l'acide phénylboronique. L'influence de la nature du métal sur les produits de la réaction a ainsi pu être analysée.

Gold nanoparticles immobilized on porous monoliths obtained from disulfide-based dimethacrylate: Application to supported catalysis

Abstract: In this work, we report on the design and synthesis of an original methacrylic monolith bearing selectively cleavable disulfide bridges. One such monolith was prepared by thermally-induced free-radical copolymerization using a disulfide-based labile dimethacrylate, *i.e.* bis(2-methacryloyl)oxyethyl disulfide, and ethylene glycol dimethacrylate as comonomers, as well as toluene as a porogenic solvent. Upon dithiothreitol-mediated reduction of the disulfide moieties within the as-obtained disulfide-bearing monolith, thiol functions were formed at the pore surface of the resulting monolith, which was confirmed by means of *in-situ* Raman spectroscopy, while the pore size distribution was analyzed by mercury intrusion porosimetry. Immersion of the thiol-functionalized porous material in a chloroauric acid solution allowed for successful chelation of Au^{3+} ions. Subsequent hydride-mediated reduction of the latters in the presence of $NaBH_4$ gave rise to the generation of gold nanoparticles (AuNPs) that were immobilized at the monolithic pore surface. The efficiency of this hybrid material based on AuNPs@porous monolith as a heterogeneous supported catalyst was further demonstrated through the reduction of a relatively toxic dye commonly used in textile and dye industries, *i.e.* Eosin Y. Notably, no loss of catalytic activity was observed by using this hybrid supported catalyst after 6 consecutive runs.

2.1 Introduction

In this era of great efforts towards the development of more and more eco-friendly processes, heterogeneous supported catalysis appears as an appealing field of research due to actual ever-growing environmental concerns/requirements.[1,2] Among this field, nanometal-based catalysis has gained a tremendous interest, as supported nanometals present unique properties compared to their bulk material counterparts that make them advantageous in different applications. In the broad area of catalysis, gold nanoparticles are probably the most commonly used nanometals.[3–11] During the last decade, not only gold[12–14] but also palladium-,[15] silver-,[16] platinum-,[17] and copper-based nanoparticles[18] have been applied to heterogeneous catalysis, even though they were considered a few years ago as chemically inert.[19] Different model catalytic reactions have been so far developed with such nanometal-based systems., including (di)nitroarene,[11,12,20,21] hexacyanoferrate[10] or dye reduction,[4,5] and even more interesting Suzuki-Miyaura C-C cross-coupling reactions[6] or cascade reactions.[22] However, inherent properties of immobilized gold nanoparticles do not restrict them only to the catalysis area but can also have interesting applications in diverse research fields, such as chromatographic supports,[23–29] antibacterial systems,[30] drug delivery devices,[31] sensors[32,33] and photovoltaics,[34] supported biocatalysts[35] as well as Surface Enhanced Raman Spectroscopy (SERS).[36]

Thiol functions are prone to chelate gold and are generally used to anchor them in a covalent-like manner.[24] Unfortunately, thiols are also well-known to easily produce corresponding disulfide bridges under mild oxidizing conditions, such as under O_2 atmosphere, thus presenting a serious limitation to their use. However, disulfide moieties (-S-S-) can be selectively cleaved by using appropriate chemical reducing agents, such as phosphine derivatives[12,37] or dithiothreitol (DTT),[38] to cite but a few, thus being considered as protected thiols. Recently, polymeric materials bearing such disulfide bridges have largely been used in diverse applications,[12,39,40] mainly because of the straightforward introduction of such chemical functions within the backbone or the pendant chains of the macromolecules, but also because of the subsequent readily selective cleavage of the -S-S- bond. In this regard, different studies have demonstrated that the reversible character of this chemical junction confers very interesting stimuli-responsive properties to the corresponding materials. Matyjaszewski and Gao research groups notably prepared independently atom transfer radical polymerisation (ATRP) initiators from 2-hydroxyethyl disulfide (also called as bishydroxyethyldisulfide) precursor.[41–43] Such initiators were used to prepare block copolymers that could be further cleaved by selective reduction of the disulfide junction, thus allowing for the production of thiol-functionalized (co)polymers. More recently, Engler *et al.*[39] and Xu *et al.*[40] combined disulfide and carbonate chemistry to produce "smart" stimuli-responsive drug delivery devices. In a similar manner, Lu *et al.*[44] suggested a strategy for synthesizing materials for drug delivery purposes using disulfide and urethane chemistry. Finally, other interesting studies also investigated the properties of disulfide-containing polymer-based systems.[45–48] Recently, some of us

also took advantage of the redox-responsive character of this chemical moiety to produce thiol-functionalized nanoporous materials through the selective triphenyl phosphine-mediated chemical reduction of a disulfide bridge positioned at the junction between both blocks of newly synthesized polystyrene-*block*-poly(D,L-lactide) copolymer precursors.[12] The subsequent immobilization of *in-situ* formed gold nanoparticles permitted the preparation of hybrid supported catalysts with high efficiency towards nitroarene reduction, even after 5 successive catalytic cycles. These few examples highlight the potential of disulfide-based chemicals to produce redox-responsive polymeric systems with unique and tunable properties.

Herein, we report on the development of original monolithic supports relying on the implementation of a cleavable disulfide-based dimethacrylate. Such porous materials can undergo selective and facile disulfide bridge reduction in the presence of DTT to afford thiol-functionalized porous monoliths. Further, the presence of thiols at the pore surface allowed for the immobilization of gold nanoparticles (AuNPs) through the so-called *in-situ* strategy involving the adsorption of Au^{3+} ions at the pore surface and the subsequent hydride-mediated reduction of the metallic cations. Such novel functional monoliths were fully characterized by means of several techniques, including mercury intrusion porosimetry, Raman spectroscopy, TGA, SEM, and EDX spectroscopy. More interestingly, advantage of the presence of immobilized AuNPs within the hybrid monoliths was taken to successfully achieve the supported catalytic reduction of Eosin Y as a model reaction. Indeed, dyes commonly used in textile and dye industry are well-known pollutants of waste water of such industrial sectors. Reduction of some of these dyes using supported or suspended gold nanoparticles may constitute a suitable pathway to transform such toxic species into more eco-friendly products. This was notably demonstrated in the case of different dyes, such as Methylene Blue,[49] Safranin T,[50] Congo Red,[51] and Eosin Y.[4,49–52]

2.2 Experimental

2.2.1 Materials

2-Hydroxyethyl disulfide (technical grade), ethylene glycol dimethacrylate (EGDMA, 98%), methacryloyl chloride (97%), Eosin Y (EY, ≈99%), D,L-dithiothreitol (DTT,≥98%), and sodium borohydride ($NaBH_4$, ≥99%) were obtained from Sigma-Aldrich. Triethylamine (TEA, 99%) and hydrogen tetrachloroaurate (III) hydrate ($HAuCl_4$, 99.9%) were purchased from Alfa Aesar. Toluene (HPLC grade), dichloromethane (DCM, synthesis grade), tetrahydrofuran (THF, HPLC grade), *n*-hexane (Pure), and ethyl acetate (EtOAc, analysis grade) were supplied by Carlo Erba. All reagents were used without further purification, except for 2,2'-azobisisobutyronitrile (AIBN, Acros Organics)

that was recrystallized from methanol prior to use. 18.2 MΩ deionized water was filtered through a Milli-Q Plus purification pack.

2.2.2 Synthesis of disulfide-based dimethacrylate

2-Hydroxyethyl disulfide (3.085 g, 20 mmol, 1 equiv.), triethylamine (8.4 mL, 60 mmol, 3 equiv.) were added to 20 mL of THF in a round-bottom flask immersed in an ice/water bath. Methacryloyl chloride (5.86 mL, 60 mmol, 3 equiv.) was added dropwise to the reaction mixture *via* a dropping funnel. The reaction was stirred at 0 °C for 1 h, and then it was allowed to warm to room temperature overnight. The resulting heterogeneous solution was supplemented with 80 mL of dichloromethane and filtered off to remove triethylamonium salts. The organic phase was washed with 10 mL of a 0.1 M HCl solution, then with 10 mL of a 0.1 M NaOH solution, and with 10 mL of a saturated NH_4Cl solution. This organic phase was finally dried over $MgSO_4$, filtered, and evaporated, while immersed in an ice bath, and then dried under vacuum overnight. The product was purified over a silica gel chromatography column eluting with a 9/1 (v/v) solvent mixture of *n*-hexane/ethyl acetate. The pure disulfide-based dimethacrylate (DSDMA) was obtained in 73 % yield as a yellowish viscous oil. It was stored at −18 °C with some traces of benzophenone as a free-radical inhibitor, as the dimethacrylate may be prone to easily polymerize. ^{1}H NMR ($CDCl_3$, 400 MHz) δ (ppm): 6.12 (s, 2H, *H*-C=C), 5.58 (d, 2H, *H*-C=C), 4.40 (t, 4H, -O-C*H*$_2$-), 2.97 (t, 4H, -CH$_2$-C*H*$_2$-S-S-), 1.94 (s, 6H, *H*$_3$C-). ^{13}C NMR ($CDCl_3$, 400 MHz) δ (ppm):167.25 (s, 2C, *C*=O), 136.11 (s, 2C, CH$_3$-*C*=C), 126.16 (s, 2C, -C=*C*-H), 62.60 (s, 2C, -O-*C*H$_2$-), 37.36 (s, 2C, -CH$_2$-*C*H$_2$-S-S-), 18.41 (s, 2C, *C*H$_3$-).

2.2.3 Synthesis of macroporous disulfide-bearing monolith

The porous monolith was prepared through a free-radical copolymerization reaction of a mixture consisting of the following typical composition: DSDMA as a functional labile crosslinking monomer (0.632 g, 48 mol.%), EGDMA as a permanent crosslinker (0.464 g, 52 mol.%), toluene as a porogenic solvent (2.4 mL, 70 vol.% with respect to the total comonomer amount), and AIBN as a thermal free-radical initiator (1 wt.% with respect of the total amount of monomers).The mixture was sonicated for about 15 min to obtain a homogeneous solution. The mixture was transferred into a glass vial, carefully sealed, and heated during 24 h at 70 °C in order to perform the thermally-induced free-radical copolymerization. The resulting material was subjected to a Soxhlet extraction with dichloromethane as the extracting solvent for 24 h and finally dried under vacuum. Mercury intrusion porosimetry was performed to determine the pore size distribution of the porous monolith.

2.2.4 Selective cleavage of disulfide bridges

200 mg of the synthetized monolith were immersed in 6 mL of a 5 mM phosphate buffer solution (pH = 8) containing 128 mg of DTT during 4 days at 47 °C. *In situ* Raman spectroscopy was used to determine the efficiency of the disulfide bridge cleavage. TGA and SEM were realized before and after cleavage of the accessible disulfide bridges of the DSDMA-based monolith.

2.2.5 *In-situ* generation of gold nanoparticles within macroporous monolith

200 mg of the newly prepared thiol-functionalized monolith were placed in 1 mL of a 0.1 wt.% $HAuCl_4$ solution and let to react overnight. The monolith was removed from the solution, washed five times with 1 mL of water to remove Au^{3+} ions that were non-specifically adsorbed on the material surface. Then, the sample was placed in a $NaBH_4$ aqueous solution (7 mg of $NaBH_4$ in 2 mL of water) for 2 h. The sample was again washed five times with 1 mL of water. The sample was finally dried under vacuum overnight and was examined by SEM to observe the *in-situ* generated AuNPs that were immobilized within the macroporous monolith.

2.2.6 Supported catalytic reduction of Eosin Y

23 mg of the AuNPs immobilized monolith were placed in a freshly prepared aqueous solution containing 35 µL of Eosin Y (5 mg in 10 mL H_2O) and 100 µL of $NaBH_4$ (120 mg in 10 mL H_2O) in 2 mL of water. Reduction of Eosin Y was monitored by UV-Vis spectrophotometry. Six successive catalytic cycles were performed. The solution was withdrawn after only 10 min reaction of each run, placed in a UV quartz cuvette and immediately analyzed *via* off-line UV-Vis spectrophotometry. After each catalytic cycle, the AuNPs adsorbed hybrid material was used after rinsing with milli-Q water and vaccuum drying.

2.2.7 Instrumentation

^{1}H and ^{13}C NMR spectra were recorded at room temperature on a Bruker Avance II spectrometer operating at a resonance frequency of 400 and 100 MHz, respectively. For ^{1}H NMR analysis, the sample concentration was equal to ~10 $mg.mL^{-1}$, while it was equal to ~30 $mg.mL^{-1}$ for ^{13}C NMR. $CDCl_3$ was used as a solvent and internal standard (7.26 ppm in ^{1}H NMR; 77.2 ppm in ^{13}C NMR). UV-Vis spectra were recorded on a Cary 60 UV-Vis spectrophotometer from Agilent Technologies. The chemical structure of monoliths was investigated using a Raman spectrometer

XPloRA PLUS from Horiba Jobin Yvon equipped with a diode laser emitting at 638 nm. Different parts of the samples were investigated in different places to control their homogeneity. The acquisition time was fixed at 1 min. Thermogravimetric analysis (TGA) measurements were performed on a Setaram Setsys Evolution 16 thermobalance by heating the samples at a rate of 10 °C.min^{-1} from 20 °C to 800 °C under argon atmosphere. Mercury intrusion porosimetry was used to determine the pore size distribution of the monolith using a Micromeritics AutoPore IV 9500. The determination of the porosity features was based on the Washburn equation between the applied pressure (from 1.03 to 206.8 MPa) and the pore size into which mercury intruded. Scanning Electron Microscopy (SEM) was performed on a MERLIN microscope from Zeiss equipped with InLens (secondary electrons) and BSD (back-scattered electrons) detectors using low accelerating voltage (2-3 kV). Prior to analyses, the samples were coated with a 4-nm layer of palladium/platinum alloy in a Cressington 208 HR sputter-coater. Energy dispersive X-ray (EDX) spectroscopy was performed using an SSD X-Max detector of 50 mm² from Oxford Instruments (127 eV for the Kα of Mn). Inductively coupled plasma optical emission spectrometry (ICP-OES) analyses were performed using a Varian Vista-PRO CCD Simultaneous spectrometer. Prior to analyses, analysed samples were mineralized in concentrated nitric acid (HNO_3), the resulting solutions were evaporated to dryness and the residue diluted in 10 mL of milliQ water.

2.3 Results and discussion

The synthetic route developed for the preparation of the hybrid supported catalysts is depicted in **Figure 2-1**. It relied on three different successive steps involving: *(i)* the thermally-induced free-radical copolymerization of a disulfide-containing dimethacrylate (DSDMA), *i.e.* bis(2-methacryloyl)oxyethyl disulfide, and ethylene glycol dimethacrylate (EGDMA), in the presence of AIBN as the free-radical initiator and a porogenic solvent, *(ii)* the subsequent DTT-mediated chemical reduction of the disulfide bridges arising from DSDMA, and finally *(iii)* the immobilization of *in-situ* generated gold nanoparticles at the pore surface of the as obtained thiol-modified monoliths.

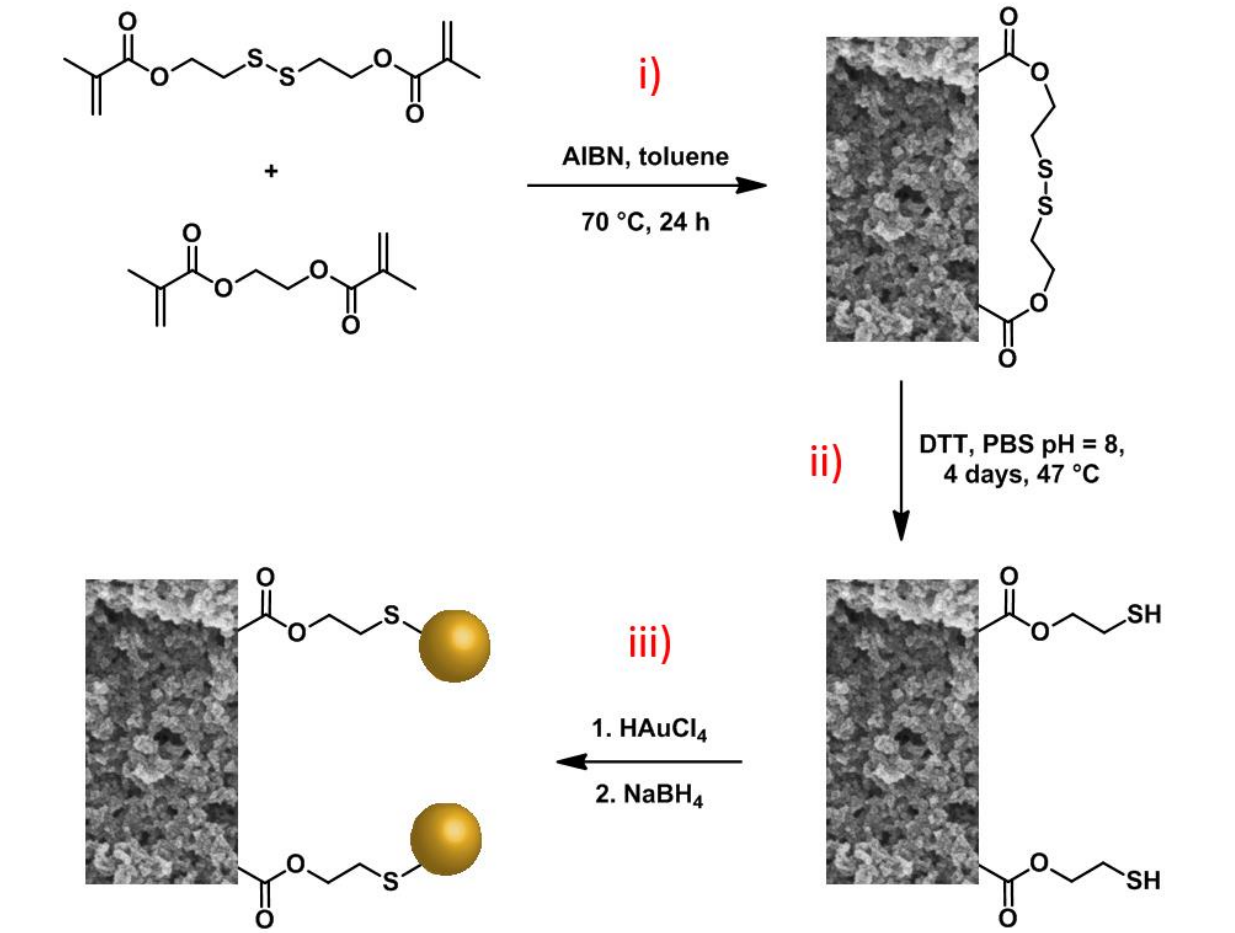

Figure 2-1: Schematic representation of the synthetic route applied for preparing the AuNPs adsorbed monolith *via i)* thermally-induced free-radical copolymerization of DSDMA and EGDMA, *ii)* subsequent reduction of disulfide bridges, and *iii)* final immobilization of AuNPs generated by *in-situ* $NaBH_4$-mediated reduction of corresponding metallic ions.

2.3.1 Synthesis of bis(2-methacryloyl)oxy ethyl disulfide comonomer

Although bis(2-methacryloyl)oxyethyl disulfide is commercially available from different chemical suppliers, it is rather expensive, while its synthesis can be readily achieved in a one-step straightforward procedure. This disulfide-containing dimethacrylate was prepared through a double nucleophilic substitution of 2-hydroxyethyl disulfide with methacryloyl chloride in the presence of TEA. After successive washings with HCl (0.1 M), NaOH (0.1 M) and saturated NH_4Cl, purification over a silica gel chromatography column was necessary in order to isolate the desired product, *i.e.* DSDMA, from unreacted 2-hydroxyethyl disulfide and eventually monosubstituted methacrylate by-product. ^{1}H and ^{13}C NMR analyses of the isolated fraction were performed and demonstrated the

successful synthesis of the desired disulfide-bearing dimethacrylate cross-linking agent. Indeed, the ^{1}H NMR spectrum of the product displayed in **Figure 2-2** clearly showed the presence of methylene protons at 4.40 ppm and 2.96 ppm ascribed to protons in α positions of the ester function and of the disulfide bridge, respectively, as well as methyl protons at 1.93 ppm, and methylidene protons at 6.12 and 5.58 ppm. In the same manner, ^{13}C NMR spectrum of the purified product showed the presence of 6 chemically distinct carbons, due to the symmetrical feature of DSDMA. Especially, carbon chemical shifts were observed at 167.25, and 136.11 and 126.16 ppm, ascribed to carbonyl groups and carbons of both unsaturations, respectively. Finally, the chemical shifts of methylene protons were found at 62.60 and 37.36 ppm, while that of the methylic carbon was found at 18.41 ppm. In addition, no significant impurities were observed on both ^{1}H and ^{13}C spectrum of the as-obtained dimethacrylate, thus enabling its further use for the preparation of the corresponding monoliths. It is worth mentioning that the dimethacrylate was obtained with 73 % yield. It should finally be stressed that DSDMA was stored into an opaque vial at −20 °C and supplemented with tiny quantities of benzophenone as free-radical inhibitor, as it was found to homopolymerize very easily especially when exposed to sunlight irradiation.

2.3.2 Formation of disulfide-bearing monoliths and subsequent surface treatment

A two-step process was involved for the preparation of DSDMA-based bulk monoliths exhibiting thiol functions for further immobilization of gold nanoparticles (see **Figure 2-1**). The first step implied the AIBN-initiated free-radical copolymerization of DSDMA with EGDMA in the presence of a porogenic solvent, *i.e.* toluene. The copolymerization process was conducted at 70 °C for 5 h, and the resulting monoliths were subjected to Soxhlet extraction for 24 h in DCM so as to remove the porogenic solvent. The porous features associated with the monoliths were then analyzed by means of mercury intrusion porosimetry (**Figure 2-3 a**). Pores with an average pore size distribution ranging from 0.01 to 1 µm were observed, while the pore volume was estimated to be equal to 1.22 $mL.g^{-1}$ along with a porosity ratio of 66 %, which is in agreement with the amount of porogenic solvent placed in the polymerization feed, *i.e.* 70 vol.%.

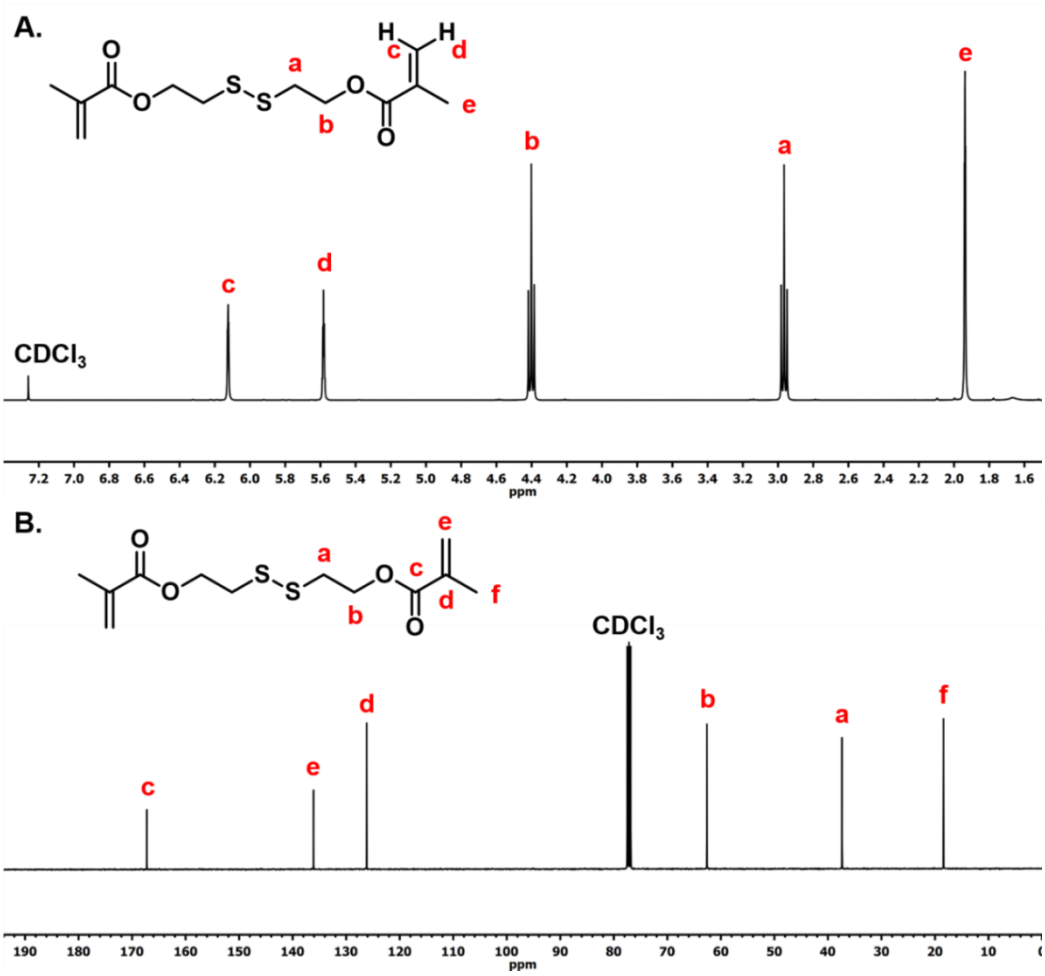

Figure 2-2: *A)* ^{1}H and *B)* ^{13}C NMR spectra of disulfide-based dimethacrylate (DSDMA).

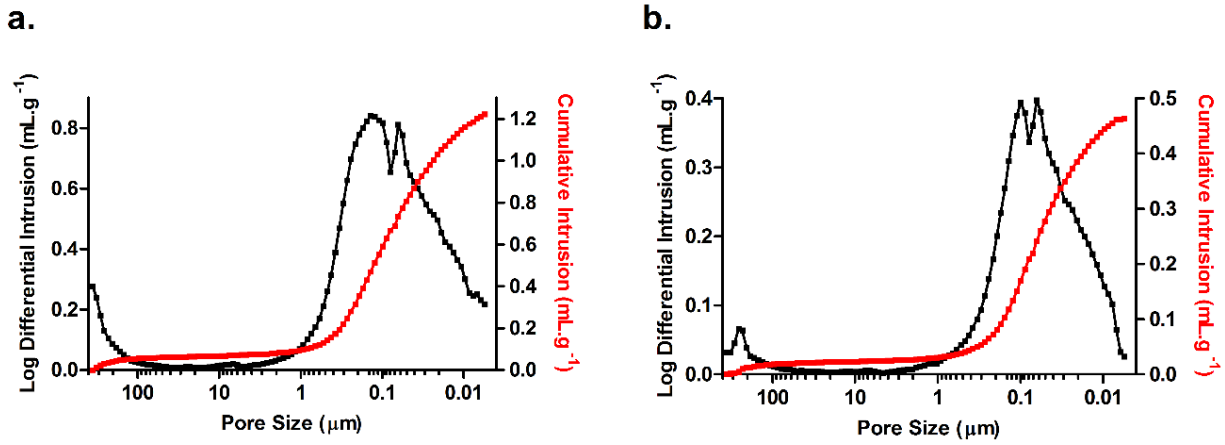

Figure 2-3: Mercury intrusion porosimetry profiles of macroporous DSDMA-based monoliths *a)* before and *b)* after DTT-mediated disulfide reduction.

Different research groups previously reported on the reduction of disulfide bridges within polymers[46,53,54] and polymer-based gels or materials[41] for the generation of corresponding thiol-functionalized products. These polymer-based systems notably relied on 2-hydroxyethyl disulfide or cysteamine precursors, and different reducing agents were successfully applied to allow for the quantitative reduction of disulfide bridges, such as phosphine derivatives or DTT, for instance. The accessibility of the disulfide bridges present within our monolithic systems was assessed by chemical reduction in the presence of DTT. The achievement of the reaction was monitored by *in-situ* Raman spectroscopy, as shown in **Figure 2-4**. The appearance of a band at 2580 cm^{-1} clearly indicated the occurrence of free thiols in the resulting monolith upon DTT-mediated reduction,[55,56] thus highlighting the availability of disulfide functions in the precursory material, even though it seems very difficult to quantify the amount of non-reduced disulfide moieties present in the monolith after the reduction. As shown in **Figure 2-3 b**, the mercury intrusion porosimetry profile of the monolith after DTT-mediated reduction was found to be very similar to that of its oxidized counterpart. Indeed, no great variation was observed in terms of porosity ratio that was found to be equal to 64 %. The porous polymeric materials similarly displayed a porosity consisting of macroporous networks with pore sizes ranging from 0.01 to 1 µm approximatively. This similarity clearly demonstrated that the surface treatment with DTT did not alter significantly the porous structure of the as-obtained materials. Although disulfide bridges of the monoliths were reduced and thus cleaved, the DSDMA-based material was highly crosslinked with EGDMA as a permanent crosslinker (52 mol.% with respect to DSDMA in the copolymerization feed), and thus no dramatic changes in the porous features of the reduced materials were observed.

Further, the possibility to tune the porosity of DSDMA-based monoliths was investigated by varying the nature of the porogenic solvent. Accordingly, methanol, ethanol, and a 50/50 vol.% cyclohexanol/dodecanol mixture were also assessed as porogenic solvents (70 vol.% with respect to the total comonomer amount) in conjunction with the polymerization mixture constituted of DSDMA, EGDMA, and AIBN. After extraction of the porogenic solvents, the as-obtained DSDMA-based monoliths were analyzed by mercury intrusion porosimetry. As shown in **Figure 2-5**, the pore size distribution of DSDMA-based monoliths strongly depends on the porogenic solvent nature.[57] Thus, the use of a polar and hydrophilic solvent like methanol gave rise to a monolith with a relatively narrow pore size distribution centered at 6 µm. Using a slightly less polar and hydrophilic porogenic solvent (*i.e.* ethanol) resulted in a quite narrow porous distribution centered at 500 nm. Finally, much less polar and more hydrophobic solvents, *i.e.* toluene or even a 50 vol.% cyclohexanol/dodecanol mixture, gave rise to broad pore size distributions ranging from about 0.01 to 1 µm.

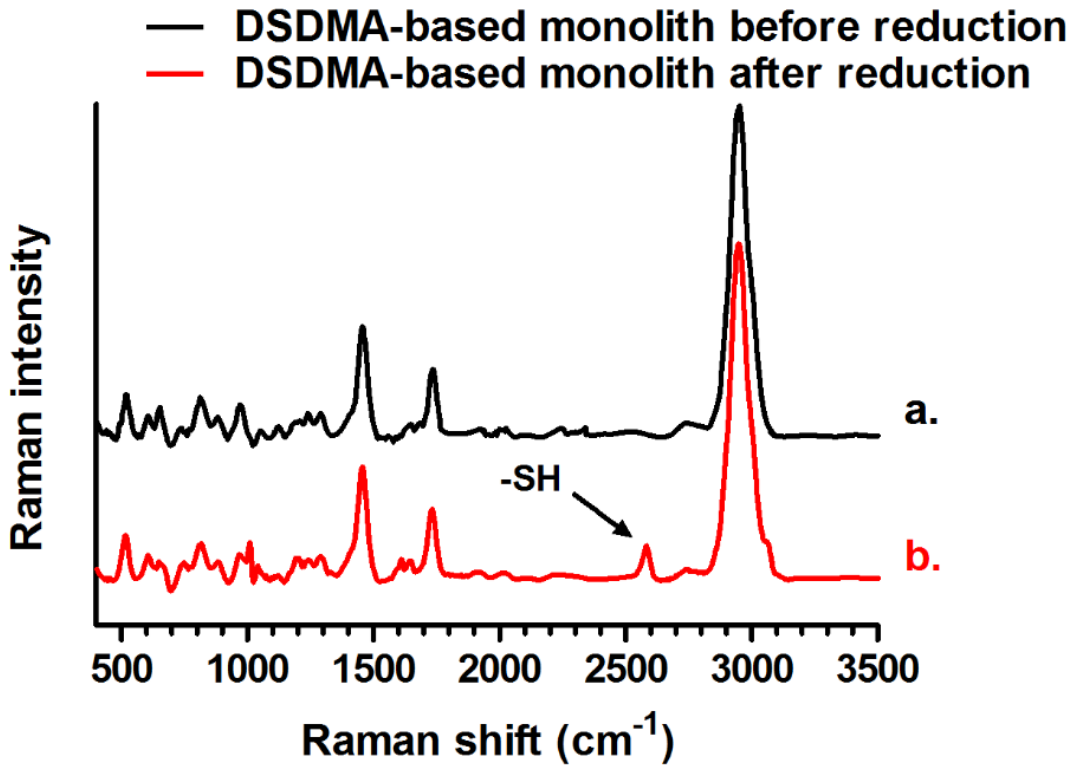

Figure 2-4: Raman spectra of DSDMA-based monoliths *a)* before (black solid line) and *b)* after (red dashed trace) reduction of disulfide bridges with DTT.

TGA measurements were also performed before and after DTT-mediated disulfide reduction (**Figure 2-6**). The thermograms clearly showed that the disulfide-based and corresponding thiol-functionalized monoliths were stable up to 150 °C. Interestingly, this thermal feature might allow the latters to be implemented as catalytic supports for chemical reactions carried out at about 100 °C, such as C-C cross-coupling for instance.[6] Additionally, a first mass loss between 180 °C and 360 °C was attributed to the thermal degradation of DSDMA units in the monolith,[45,58] while the second mass loss between 360 °C and 450 °C was attributed to the thermal degradation of EGDMA units.[59,60] After DTT-mediated reduction of the disulfide bridges, the mass loss corresponding to residual DSDMA units was dramatically reduced, while the appearance of a new mass loss between 125 °C and 150 °C was attributed to the as-cleaved DSDMA units.

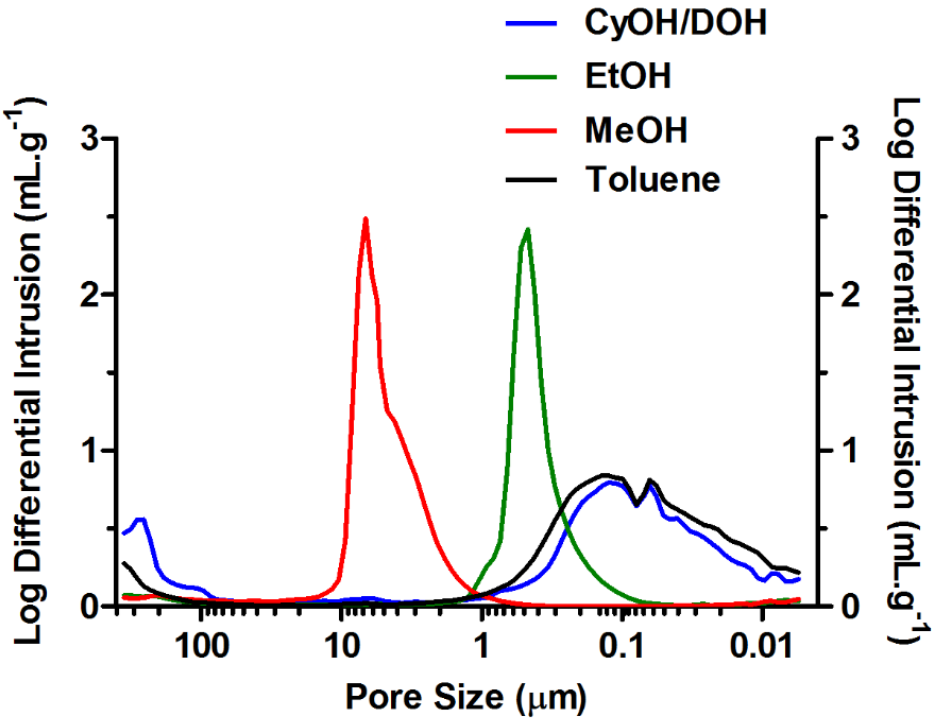

Figure 2-5: Variation of pore size distribution of DSDMA-based monoliths as a function of the porogenic solvent nature used in the polymerization mixture, *i.e.* methanol (MeOH), ethanol (EtOH), 50 vol.% cyclohexanol/dodecanol (CyOH/DOH), or toluene.

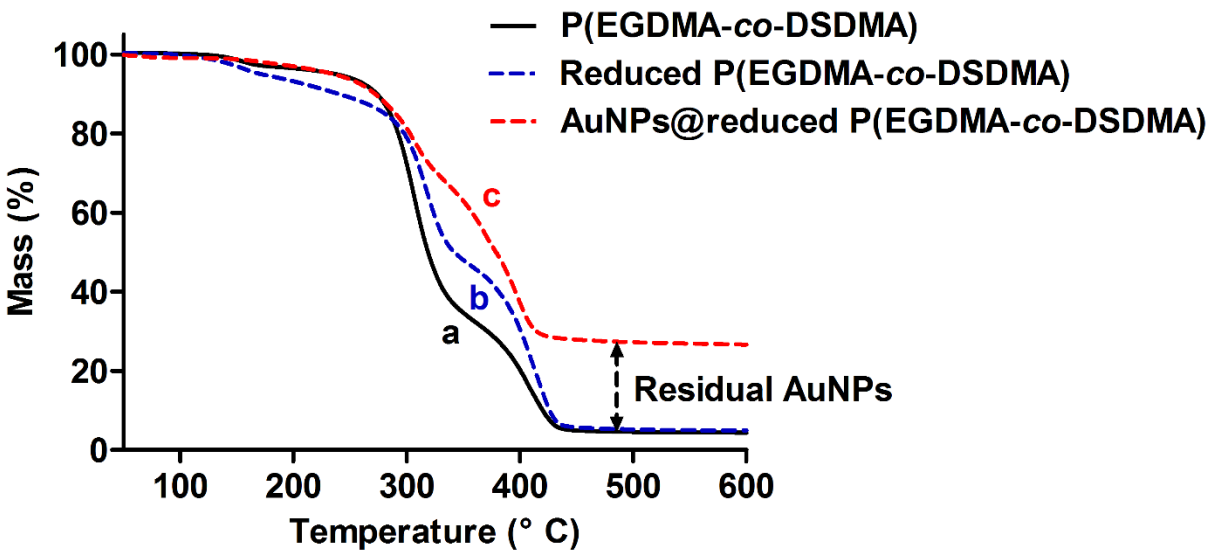

Figure 2-6: TGA curves for DSDMA-based monoliths *a)* before (black plain line) and *b)* after (blue dashed line) reduction of disulfide bridges with DTT, as well as *c)* after subsequent AuNPs immobilization (red dotted line).

2.3.3 Immobilization of *in-situ* generated gold nanoparticles

The benefit of having prepared thiol-modified porous materials notably relies on the possibility to easily immobilize gold nanoparticles through S-Au covalent-like bonds using an *in-situ* strategy. As already mentioned in previous reports from our research group, it is rather difficult to immobilize preformed gold nanoparticles on such polymeric supports (*ex-situ* approach), even under dynamic loading, as aggregation is often observed, preventing some homogeneous and dense nanogold coverage of the pore surface.[13,21] Additionally, commercially available gold nanoparticles are generally coated with surfactants that prevent them to bind to available thiols at the pore surface of the DSDMA-based polymeric scaffolds. The thiol-functionalized monoliths were mixed together with Au^{3+} ions to chelate the latters. These metallic cations were reduced using sodium borohydride to generate *in-situ* metallic AuNPs meant for their subsequent use as supported catalysts. The AuNPs distribution on the pore surface of monoliths was investigated *via* SEM (**Figure 2-7**) coupled with EDX spectroscopy (data not shown). As shown in **Figure 2-7 c**, the presence of metallic nanoparticles was clearly demonstrated by SEM, and such nanoparticles could be observed with a rather homogeneous distribution of diameters, even though a few aggregates were observed. Most of the nanoparticles were lower than 200 nm large, and others composed of aggregates of bigger particles were around 500 nm, likely due to Ostwald ripening. The presence of these AuNPs immobilized at the pore surface of the thiol-modified polymeric monoliths could also be simply observed by the naked eyes. Indeed, a dark strong coloration of the hybrid monolith was observed after reduction of Au^{3+} metallic cations, while the monolith was white upon reduction with DTT and orange upon subsequent impregnation of the thiol-modified monolith with tetrachloroauric acid (see **Figure 2-7 d**).

The chemical nature of these particles was verified by EDX analysis that confirmed the presence of Au element in these hybrid polymer-based monoliths when compared to porous materials before *in situ* generation of AuNPs (data not shown). ICP-OES analyses were also performed to quantitatively determine the amount of gold adsorbed at the pore surface of the thiol-functionalized porous monoliths. To this purpose, samples obtained after impregnation with Au^{3+} ions and after hydride-mediated reduction of the latters were examined. The gold contents were found to be equal to 29.4 and 14.8 wt.% in Au^{3+}-impregnated thiol-functionalized porous monolith and corresponding AuNPs@porous monolith, respectively. Such data meant that half of the quantity of gold cations adsorbed within the thiol-functionalized monolith was immobilized as AuNPs on the pore surface of the corresponding monolith. A TGA analysis was also realized on the hybrid AuNPs@porous monolith (**Figure 2-6 c**), and a gold content of ~19 wt.% could be assessed. This result was in rather good agreement with that previously obtained by ICP-OES.

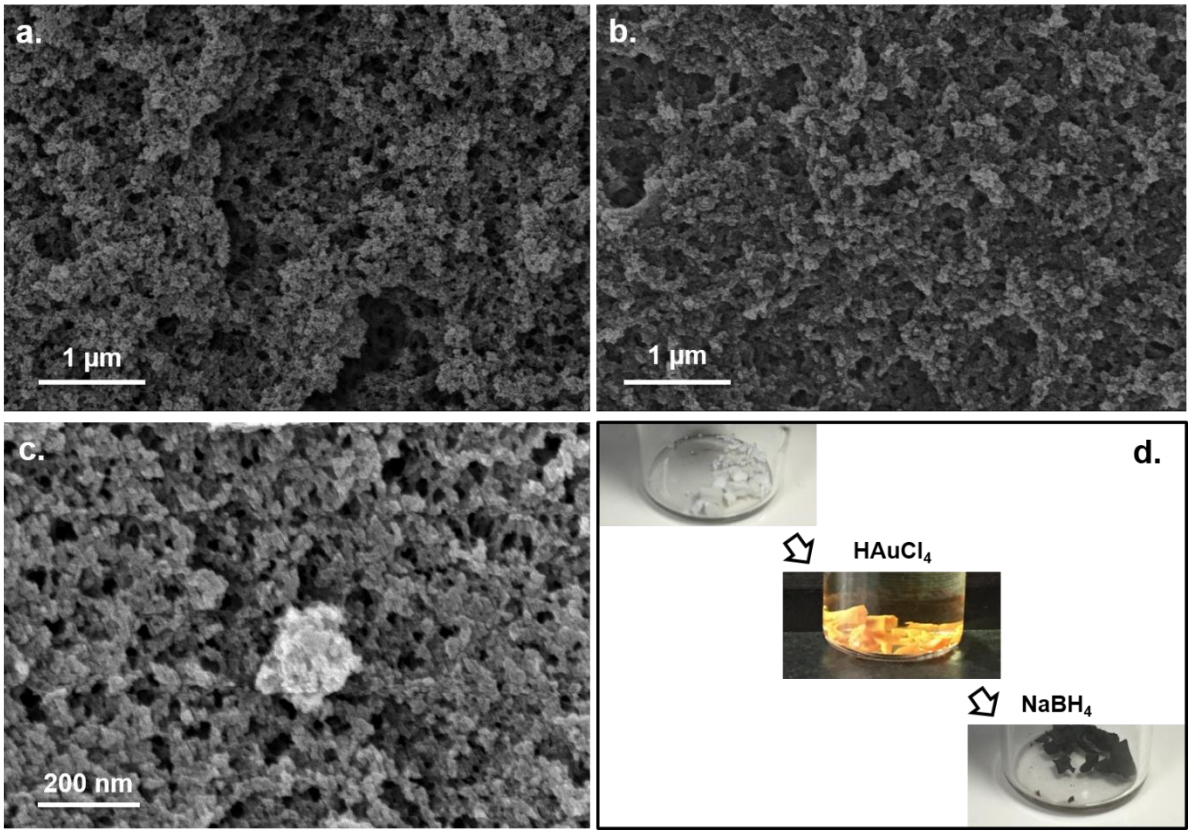

Figure 2-7: SEM micrographs of DSDMA-based monoliths *a)* before and *b)* after reduction with DTT using Inlens detector, as well as *c)* after subsequent AuNPs immobilization using BSD detector (back-scattered electrons provide mass contrast and hence the gold nanoparticle appears brighter than the polymeric porous matrix). *d)* Thiol-modified materials observed by the naked eyes before and after impregnation of the chloroauric salt and subsequent hydride-mediated reduction of metallic cations with $NaBH_4$.

2.3.4 Supported catalytic reduction of Eosin Y dye

To the best of our knowledge, dye reduction is not usually accomplished with such hybrid materials and this could lead to further promising applications. The AuNPs@porous monolith hybrid material was immersed in a freshly prepared aqueous solution of Eosin Y (EY) and $NaBH_4$ as a model system. In only 10 min, the slight pink colour of the EY solution totally vanished as observed in **Figure 2-8 a**. A kinetic study was also performed during the first catalytic cycle by UV-Vis spectrophotometry to monitor the disappearance of the characteristic $\pi \rightarrow \pi^*$ transition band of EY at ~ 520 nm along with the appearance of that of its reduced counterpart at ~ 405 nm. As shown in **Figure 2-8 b**, the reaction was very efficient and quite rapid with 86 % yield after 10 min of reaction time. For the sake of comparison, a blank sample was realized by mixing the EY solution with $NaBH_4$ in the presence of the thiol-modified monolith. No decrease in the characteristic band of EY was observed in

this case, thus highlighting the need for nanogold catalyst so that the reduction reaction might occur. Finally, the recyclability of the hybrid supported catalyst was assessed. To this purpose, 5 additional successive reduction runs were carried out with the same hybrid monolith. Even after 6 catalytic cycles, it was noteworthy that the activity of the supported catalyst was shown to be maintained with rather satisfying yields (~ 60 %), as shown in **Figure 2-8 c**. Thus, reduction of Eosin Y is a model reaction that could be extended to other common industrial polluting dyes such as Methylene Blue, Safranin T, and Congo Red.

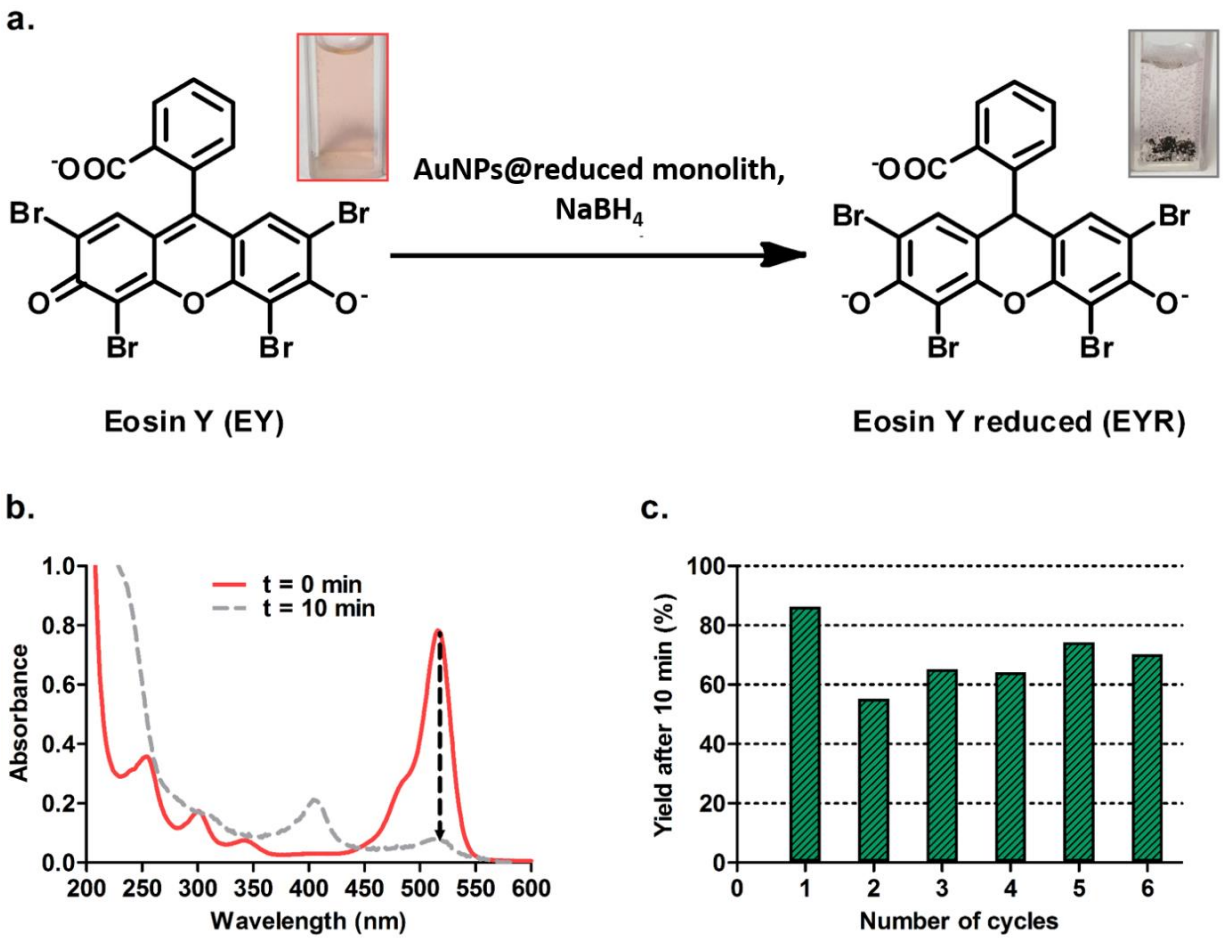

Figure 2-8: UV-Visible spectrophotometric monitoring of hydride-mediated Eosin Y reduction. *a)* Schematic representation of the catalytic reaction occurring at the surface of immobilized nanogold. *b)* UV-Vis spectra of Eosin Y before (black trace) and after 10 min reaction (red trace) in the presence of AuNPs@porous monolith and $NaBH_4$. *c)* Stability of the hybrid supported catalyst after 6 consecutive runs of the same reduction reaction.

2.4 Conclusions

An original porous monolith was prepared from a cleavable disulfide-based dimethacrylate and EGDMA as a permanent crosslinker. Upon disulfide reduction with a suitable reducing agent such as DTT, one such monolith could be decorated with thiol functions at the pore surface, which enabled for subsequent adsorption of *in-situ* generated gold nanoparticles. The presence of immobilized gold nanoparticles permitted their efficient use as supported catalysts. Thus, the reduction of Eosin Y could be easily achieved with a rather high efficiency and good reproducibility over several catalytic cycles. Of particular interest, this original DSDMA-based monolith offers an undeniable advantage over other thiol-functionalized polymer-based counterparts. Indeed, it cannot be oxidized into diverse sulfur-containing species, and it is thus better suited for applications requiring thiol moieties at the pore surface.

This investigation paves the way for further development of innovative hybrid materials based on AuNPs@porous monoliths as efficient supported catalysts in a plethora of organic reactions carried out at room temperature or even higher temperatures, such as for example C-C homo- and cross-couplings.

2.5 References

(1) Allen, D. T.; Shonnard, D. R. Green Engineering: Environmentally Conscious Design of Chemical Processes and Products. *AIChE J.* **2001**, *47* (9), 1906–1910.

(2) Anastas, P. T.; Warner, J. C. *Green Chemistry: Theory and Practice*; Oxford University Press, New York, 1998.

(3) Panigrahi, S.; Basu, S.; Praharaj, S.; Pande, S.; Jana, S.; Pal, A.; Ghosh, S. K.; Pal, T. Synthesis and Size-Selective Catalysis by Supported Gold Nanoparticles: Study on Heterogeneous and Homogeneous Catalytic Process. *J. Phys. Chem. C* **2007**, *111* (12), 4596–4605.

(4) Féral-Martin, C.; Birot, M.; Deleuze, H.; Desforges, A.; Backov, R. Integrative Chemistry toward the First Spontaneous Generation of Gold Nanoparticles within Macrocellular PolyHIPE Supports (Au@polyHIPE) and Their Application to Eosin Reduction. *React. Funct. Polym.* **2007**, *67* (10), 1072–1082.

(5) Sau, T. K.; Pal, A.; Pal, T. Size Regime Dependent Catalysis by Gold Nanoparticles for the Reduction of Eosin. *J. Phys. Chem. B* **2001**, *105* (38), 9266–9272.

(6) Han, J.; Liu, Y.; Guo, R. Facile Synthesis of Highly Stable Gold Nanoparticles and Their Unexpected Excellent Catalytic Activity for Suzuki−Miyaura Cross-Coupling Reaction in Water. *J. Am. Chem. Soc.* **2009**, *131* (6), 2060–2061.

(7) Lopez, N.; Janssens, T. V. W.; Clausen, B. S.; Xu, Y.; Mavrikakis, M.; Bligaard, T.; Nørskov, J. K. On the Origin of the Catalytic Activity of Gold Nanoparticles for Low-Temperature CO Oxidation. *J. Catal.* **2004**, *223* (1), 232–235.

(8) Corma, A.; Garcia, H. Supported Gold Nanoparticles as Catalysts for Organic Reactions. *Chem. Soc. Rev.* **2008**, *37* (9), 2096–2126.

(9) Schimpf, S.; Lucas, M.; Mohr, C.; Rodemerck, U.; Brückner, A.; Radnik, J.; Hofmeister, H.; Claus, P. Supported Gold Nanoparticles: In-Depth Catalyst Characterization and Application in Hydrogenation and Oxidation Reactions. *Catal. Today* **2002**, *72* (1), 63–78.

(10) Floris, P.; Twamley, B.; Nesterenko, P. N.; Paull, B.; Connolly, D. Fabrication and Characterisation of Gold Nano-Particle Modified Polymer Monoliths for Flow-through Catalytic Reactions and Their Application in the Reduction of Hexacyanoferrate. *Microchim. Acta* **2014**, *181* (1), 249–256.

(11) Mora-Tamez, L.; Esquivel-Peña, V.; Ocampo, A. L.; Rodríguez de San Miguel, E.; Grande, D.; de Gyves, J. Simultaneous AuIII Extraction and In Situ Formation of Polymeric Membrane-Supported Au Nanoparticles: A Sustainable Process with Application in Catalysis. *ChemSusChem* **2017**, *10* (7), 1482–1493.

(12) Le Droumaguet, B.; Poupart, R.; Grande, D. "Clickable" Thiol-Functionalized Nanoporous Polymers: From Their Synthesis to Further Adsorption of Gold Nanoparticles and Subsequent Use as Efficient Catalytic Supports. *Polym. Chem.* **2015**, *6* (47), 8105–8111.

(13) Khalil, A. M.; Georgiadou, V.; Guerrouache, M.; Mahouche-Chergui, S.; Dendrinou-Samara, C.; Chehimi, M. M.; Carbonnier, B. Gold-Decorated Polymeric Monoliths: In-Situ vs Ex-Situ Immobilization Strategies and Flow through Catalytic Applications towards Nitrophenols Reduction. *Polymer* **2015**, *77*, 218–226.

(14) Connolly, D.; Twamley, B.; Paull, B. High-Capacity Gold Nanoparticle Functionalised Polymer Monoliths. *Chem. Commun.* **2010**, *46* (12), 2109–2111.

(15) Gallon, B. J.; Kojima, R. W.; Kaner, R. B.; Diaconescu, P. L. Palladium Nanoparticles Supported on Polyaniline Nanofibers as a Semi-Heterogeneous Catalyst in Water. *Angew. Chem. Int. Ed.* **2007**, *46* (38), 7251–7254.

(16) Jiang, Z.-J.; Liu, C.-Y.; Sun, L.-W. Catalytic Properties of Silver Nanoparticles Supported on Silica Spheres. *J. Phys. Chem. B* **2005**, *109* (5), 1730–1735.

(17) Poupart, R.; Djerir, N. E. H.; Chellapermal, D.; Guerrouache, M.; Carbonnier, B.; Le Droumaguet, B. Novel In-Capillary Polymeric Monoliths Arising from Glycerol Carbonate Methacrylate for Flow-through Catalytic and Chromatographic Applications. *RSC Adv.* **2016**, *6* (17), 13614–13617.

(18) Poupart, R.; Le Droumaguet, B.; Guerrouache, M.; Carbonnier, B. Copper Nanoparticles Supported on Permeable Monolith with Carboxylic Acid Surface Functionality: Stability and Catalytic Properties under Reductive Conditions. *Mater. Chem. Phys.* **2015**, *163*, 446–452.

(19) Campelo, J. M.; Luna, D.; Luque, R.; Marinas, J. M.; Romero, A. A. Sustainable Preparation of Supported Metal Nanoparticles and Their Applications in Catalysis. *ChemSusChem* **2009**, *2* (1), 18–45.

(20) Wu, H.; Huang, X.; Gao, M.; Liao, X.; Shi, B. Polyphenol-Grafted Collagen Fiber as Reductant and Stabilizer for One-Step Synthesis of Size-Controlled Gold Nanoparticles and Their Catalytic Application to 4-Nitrophenol Reduction. *Green Chem.* **2011**, *13* (3), 651–658.

(21) Liu, Y.; Guerrouache, M.; Kebe, S. I.; Carbonnier, B.; Le Droumaguet, B. Gold Nanoparticles-Supported Histamine-Grafted Monolithic Capillaries as Efficient Microreactors for Flow-through Reduction of Nitro-Containing Compounds. *J. Mater. Chem. A* **2017**, *5* (23), 11805–11814.

(22) Poupart, R.; Benlahoues, A.; Le Droumaguet, B.; Grande, D. Porous Gold Nanoparticle-Decorated Nanoreactors Prepared from Smartly Designed Functional Polystyrene-Block-Poly(d,l-Lactide) Diblock Copolymers: Toward Efficient Systems for Catalytic Cascade Reaction Processes. *ACS Appl. Mater. Interfaces* **2017**, *article in press*, DOI: 10.1021/acsami.6b16157..

(23) Terborg, L.; Masini, J. C.; Lin, M.; Lipponen, K.; Riekolla, M.-L.; Svec, F. Porous Polymer Monolithic Columns with Gold Nanoparticles as an Intermediate Ligand for the Separation of Proteins in Reverse Phase-Ion Exchange Mixed Mode. *J. Adv. Res.* **2015**, *6* (3), 441–448.

(24) Lv, Y.; Alejandro, F. M.; Fréchet, J. M. J.; Svec, F. Preparation of Porous Polymer Monoliths Featuring Enhanced Surface Coverage with Gold Nanoparticles. *J. Chromatogr. A* **2012**, *1261*, 121–128.

(25) Lv, Y.; Lin, Z.; Svec, F. Hypercrosslinked Large Surface Area Porous Polymer Monoliths for Hydrophilic Interaction Liquid Chromatography of Small Molecules Featuring Zwitterionic Functionalities Attached to Gold Nanoparticles Held in Layered Structure. *Anal. Chem.* **2012**, *84* (20), 8457–8460.

(26) Nesterenko, E. P.; Nesterenko, P. N.; Connolly, D.; He, X.; Floris, P.; Duffy, E.; Paull, B. Nano-Particle Modified Stationary Phases for High-Performance Liquid Chromatography. *Analyst* **2013**, *138* (15), 4229–4254.

(27) Xu, Y.; Cao, Q.; Svec, F.; Fréchet, J. M. J. Porous Polymer Monolithic Column with Surface-Bound Gold Nanoparticles for the Capture and Separation of Cysteine-Containing Peptides. *Anal. Chem.* **2010**, *82* (8), 3352–3358.

(28) Cao, Q.; Xu, Y.; Liu, F.; Svec, F.; Fréchet, J. M. J. Polymer Monoliths with Exchangeable Chemistries: Use of Gold Nanoparticles As Intermediate Ligands for Capillary Columns with Varying Surface Functionalities. *Anal. Chem.* **2010**, *82* (17), 7416–7421.

(29) Currivan, S.; Connolly, D.; Paull, B. Production of Polymer Monolithic Capillary Columns with Integrated Gold Nano-Particle Modified Segments for on-Capillary Extraction. *Microchem. J.* **2013**, *111*, 32–39.

(30) Ehmann, H. M. A.; Breitwieser, D.; Winter, S.; Gspan, C.; Koraimann, G.; Maver, U.; Sega, M.; Köstler, S.; Stana-Kleinschek, K.; Spirk, S.; Ribitsch, V. Gold Nanoparticles in the Engineering of Antibacterial and Anticoagulant Surfaces. *Carbohydr. Polym.* **2015**, *117*, 34–42.

(31) Ghosh, P.; Han, G.; De, M.; Kim, C. K.; Rotello, V. M. Gold Nanoparticles in Delivery Applications. *Adv. Drug Deliv. Rev.* **2008**, *60* (11), 1307–1315.

(32) Saha, K.; Agasti, S. S.; Kim, C.; Li, X.; Rotello, V. M. Gold Nanoparticles in Chemical and Biological Sensing. *Chem. Rev.* **2012**, *112* (5), 2739–2779.

(33) Cao, Y.; Lv, M.; Xu, H.; Svec, F.; Tan, T.; Lv, Y. Planar Monolithic Porous Polymer Layers Functionalized with Gold Nanoparticles as Large-Area Substrates for Sensitive Surface-Enhanced Raman Scattering Sensing of Bacteria. *Anal. Chim. Acta* **2015**, *896*, 111–119.

(34) Giangregorio, M. M.; Losurdo, M.; Bianco, G. V.; Dilonardo, E.; Capezzuto, P.; Bruno, G. Synthesis and Characterization of Plasmon Resonant Gold Nanoparticles and Graphene for Photovoltaics. *Mater. Sci. Eng. B* **2013**, *178* (9), 559–567.

(35) Cao, Y.; Wen, L.; Svec, F.; Tan, T.; Lv, Y. Magnetic AuNP@Fe3O4 Nanoparticles as Reusable Carriers for Reversible Enzyme Immobilization. *Chem. Eng. J.* **2016**, *286*, 272–281.

(36) Tian, F.; Bonnier, F.; Casey, A.; Shanahan, A. E.; Byrne, H. J. Surface Enhanced Raman Scattering with Gold Nanoparticles: Effect of Particle Shape. *Anal. Methods* **2014**, *6* (22), 9116–9123.

(37) Burns, J. A.; Butler, J. C.; Moran, J.; Whitesides, G. M. Selective Reduction of Disulfides by Tris(2-Carboxyethyl)Phosphine. *J. Org. Chem.* **1991**, *56* (8), 2648–2650.

(38) Cleland, W. W. Dithiothreitol, a New Protective Reagent for SH Groups*. *Biochemistry (Mosc.)* **1964**, *3* (4), 480–482.

(39) Engler, A. C.; Chan, J. M. W.; Fukushima, K.; Coady, D. J.; Yang, Y. Y.; Hedrick, J. L. Polycarbonate-Based Brush Polymers with Detachable Disulfide-Linked Side Chains. *ACS Macro Lett.* **2013**, *2* (4), 332–336.

(40) Xu, Z.; Liu, S.; Kang, Y.; Wang, M. Glutathione-Responsive Polymeric Micelles Formed by a Biodegradable Amphiphilic Triblock Copolymer for Anticancer Drug Delivery and Controlled Release. *ACS Biomater. Sci. Eng.* **2015**, *1* (7), 585–592.

(41) Tsarevsky, N. V.; Matyjaszewski, K. Combining Atom Transfer Radical Polymerization and Disulfide/Thiol Redox Chemistry: A Route to Well-Defined (Bio)Degradable Polymeric Materials. *Macromolecules* **2005**, *38* (8), 3087–3092.

(42) Graff, R. W.; Wang, X.; Gao, H. Exploring Self-Condensing Vinyl Polymerization of Inimers in Microemulsion To Regulate the Structures of Hyperbranched Polymers. *Macromolecules* **2015**, *48* (7), 2118–2126.

(43) Min, K.; Gao, H. New Method To Access Hyperbranched Polymers with Uniform Structure via One-Pot Polymerization of Inimer in Microemulsion. *J. Am. Chem. Soc.* **2012**, *134* (38), 15680–15683.

(44) Lu, W.; Wang, X.; Cheng, R.; Deng, C.; Meng, F.; Zhong, Z. Biocompatible and Bioreducible Micelles Fabricated from Novel [Small Alpha]-Amino Acid-Based Poly(Disulfide Urethane)s: Design, Synthesis and Triggered Doxorubicin Release. *Polym. Chem.* **2015**, *6* (33), 6001–6010.

(45) Biradar, S. C.; Shinde, D. B.; Pillai, V. K.; Kulkarni, M. G. Polydentate Disulfides for Enhanced Stability of AuNPs and Facile Nanocavity Formation. *J. Mater. Chem.* **2012**, *22* (19), 10000–10008.

(46) Gao, H.; Tsarevsky, N. V.; Matyjaszewski, K. Synthesis of Degradable Miktoarm Star Copolymers via Atom Transfer Radical Polymerization. *Macromolecules* **2005**, *38* (14), 5995–6004.

(47) Gu, W.; Ting, S. R. S.; Stenzel, M. H. Synthesis of PH-Responsive and Thiol-Degradable Hollow Microspheres. *Polymer* **2013**, *54* (3), 1010–1017.

(48) Li, Y.; Armes, S. P. Synthesis and Chemical Degradation of Branched Vinyl Polymers Prepared via ATRP: Use of a Cleavable Disulfide-Based Branching Agent. *Macromolecules* **2005**, *38* (20), 8155–8162.

(49) Kirillova, A.; Schliebe, C.; Stoychev, G.; Jakob, A.; Lang, H.; Synytska, A. Hybrid Hairy Janus Particles Decorated with Metallic Nanoparticles for Catalytic Applications. *ACS Appl. Mater. Interfaces* **2015**, *7* (38), 21218–21225.

(50) Šimšíková, M.; Bartoš, M.; Čechal, J.; Šikola, T. Decolorization of Organic Dyes by Gold Nanoflowers Prepared on Reduced Graphene Oxide by Tea Polyphenols. *Catal. Sci. Technol.* **2016**, *6* (9), 3008–3017.

(51) Sinha, T.; Ahmaruzzaman, M. A Novel Green and Template Free Approach for the Synthesis of Gold Nanorice and Its Utilization as a Catalyst for the Degradation of Hazardous Dye. *Spectrochim. Acta. A. Mol. Biomol. Spectrosc.* **2015**, *142*, 266–270.

(52) Mahmoud, M. A.; Weng, G. Nanocatalysis Production of Photoactive Radicals. *Catal. Commun.* **2013**, *38*, 63–66.

(53) Chen, J.; Qiu, X.; Ouyang, J.; Kong, J.; Zhong, W.; Xing, M. M. Q. PH and Reduction Dual-Sensitive Copolymeric Micelles for Intracellular Doxorubicin Delivery. *Biomacromolecules* **2011**, *12* (10), 3601–3611.

(54) Tsarevsky, N. V.; Matyjaszewski, K. Reversible Redox Cleavage/Coupling of Polystyrene with Disulfide or Thiol Groups Prepared by Atom Transfer Radical Polymerization. *Macromolecules* **2002**, *35* (24), 9009–9014.

(55) Byler, D. M.; Gerasimowicz, W. V. Normal Coordinate Analysis of Methanethiol and Isotopic Analogs. *J. Mol. Struct.* **1984**, *112* (3), 207–219.

(56) Kieninger, M.; Ventura, O. N. Calculations of the Infrared and Raman Spectra of Simple Thiols and Thiol–water Complexes. *Int. J. Quantum Chem.* **2011**, *111* (7–8), 1843–1857.

(57) Ly, H. B.; Le Droumaguet, B.; Monchiet, V.; Grande, D. Facile Fabrication of Doubly Porous Polymeric Materials with Controlled Nano- and Macro-Porosity. *Polymer* **2015**, *78*, 13–21.

(58) Dong, H.; Mantha, V.; Matyjaszewski, K. Thermally Responsive PM(EO)2MA Magnetic Microgels via Activators Generated by Electron Transfer Atom Transfer Radical Polymerization in Miniemulsion. *Chem. Mater.* **2009**, *21* (17), 3965–3972.

(59) Syu, M.-J.; Nian, Y.-M.; Chang, Y.-S.; Lin, X.-Z.; Shiesh, S.-C.; Chou, T.-C. Ionic Effect on the Binding of Bilirubin to the Imprinted Poly(Methacrylic Acid-Co-Ethylene Glycol Dimethylacrylate). *J. Chromatogr. A* **2006**, *1122* (1), 54–62.

(60) Bayramoğlu, G.; Arıca, M. Y. Synthesis and Spectroscopic Characterization of Superparamagnetic Beads of Copolymers of Methacrylic Acid, Methyl Methacrylate and Ethylene Glycol Dimethacrylate and Their Application to Protein Separation. *Polym. Int.* **2008**, *57* (1), 70–76.

Preparation of Mono- and Bimetallic Nanoclusters Onto Porous Polymers Using Gaseous Hydrogen as Reducing Agent: Application Toward Carbon-Carbon Coupling

Abstract: In this work, we describe an original synthetic pathway to generate metallic nanoclusters at the pore surface of amine functionalized porous crosslinked polymers. Upon synthesis of a porous glycidyl methacrylate-based monolith, the surface exposed epoxide rings were opened by addition of ethylenediamine. The success of this functionalization step was ascertained by *in situ* Raman spectroscopy. Such amine groups at the surface of the polymeric material allowed for the successive chelation of different metallic precursors: tetrachloroauric acid salt, potassium tetrachloropalladate salt and a mixture of both. These surface chelated metallic cations were subsequently transformed into the corresponding nanoparticles through a step consisting in a gas phase reduction under a H_2 stream at 100 °C for 24 h. The as-obtained supported catalysts were assessed for the Suzuki-Miyaura cross-coupling reaction between 4-iodotoluene and phenylboronic acid. Although reaction yields were low (~10 %), results obtained depending on the nanometal or nanometallic alloy immobilized at the pore surface of the amine functionalized porous polymer were very interesting. They notably demonstrated that nanogold only allows for the generation of boronic homocoupling product, palladium only for the desired cross-coupling product, *i.e.* 4-methylbiphenyl, while the immobilized bimetallic nanoclusters did not show any significant selectivity between obtained cross- and homocoupling products.

2.6 Introduction

Over the past decades, heterogeneous catalysis has gained some particular interest from the research community.[1] Since nanoparticles have been used in catalysis, the major issue to overcome relies on the removal of such nanometals from the reaction mixture. An interesting and ingenious solution has been previously based on the implementation of core-shell metallic nanoparticles in which the core is composed of magnetic γ-Fe_2O_3 and a shell that might be devoted to catalysis.[2] Other studies reported the preparation of core-shell metallic nanoparticles composed of an iron oxide core and a polymeric shell in which are embedded organometallic complexes.[3,4] Another alternative solution consists in engineering macroscopic (in)organic supports able to immobilize metallic nanoparticles, that would be easier to remove. To this purpose, porous polymers have been candidates of great interest for the preparation and implementation of such hybrid catalytic supports. Cheap and facile to produce, they can be functionalized in a straightforward and versatile fashion in rather mild conditions. Last but not least, the porosity size and distribution can be finely and easily tuned, depending notably on the nature of the porogenic agent used.[5]

In this context, several strategies have been hitherto reported in the literature to prepare porous polymers so as to subsequently immobilize metallic nanoparticles at the pore surface of such polymeric supports. Impressive developments have been notably reported regarding the preparation of hybrid polymeric capillaries for flow-through catalytic or chromatographic applications. While Svec's research group focused its work onto in-capillary monolith supported gold nanoparticles for chromatographic applications,[6,7] Connolly's team dedicated their studies to porous monolithic capillary columns stemming from glycidyl methacrylate (GMA) or vinyl azlactone for supported catalysis applications. Upon suitable functionalization of the pore surface and subsequent immobilization of *ex situ* generated gold nanoparticles[8] or *ex situ* generated bimetallic nanoparticles (platinum and palladium),[9] the resulting hybrid capillaries were implemented for the reduction of hexacyanoferrate complex. Finally, Carbonnier's group focused onto *N*-acryloxysuccinimide-[10–12] (NAS) and glycerol carbonate methacrylate- (GCMA) based[13] in-capillary monolithic columns decorated with gold nanoparticles for the reduction of nitro compounds. Besides capillaries, interesting studies have been also developed with oriented nanoporous polystyrene regarding the subsequent immobilization of gold nanoparticles for nitroarene reduction[14,15] or boronic homocoupling[15] catalytic applications. Finally, studies carried out by Deleuze's group concerning polystyrenes-based polyHIPEs[16–18] (High Internal Phase Emulsion) at the pore surface of which were immobilized palladium and gold nanoparticles demonstrated that the resulting hybrid materials can be successfully implemented for Suzuki-Miyaura cross-coupling reaction or Eosin Y reduction, respectively.

Even though the intrinsic nature of the porous polymeric support plays a crucial role regarding the immobilization of the metallic nanoparticles, the interface between the nanoparticle and the

support itself as well as the strategy employed for generating the nanoparticles *in situ* should be carefully taken into consideration. Indeed, several chemical agents are prone to reduce metallic cations to the corresponding nanoparticles. Among them, the most commonly used is by far sodium borohydride ($NaBH_4$). It has been used so far to prepare gold,[11,14,15,19] platinum,[13,19] silver[20,21] or palladium[22] nanoparticles. Alternatively, sodium citrate is very well-known for the reduction of chloroauric salts through the so-called Turkevitch reaction. Concerning this reduction process, Polte's group reported on an interesting study describing the mechanism involved in the growth and formation of gold nanoparticles using citrate salt.[23,24] Finally, less commonly used chemicals implemented for the reduction of such metallic cations include notably hydrazine[25,26] or gaseous hydrogen (H_2).[27] Gaseous hydrogen has already been widely used in inorganic chemistry as a candidate of choice for the reduction of metallic cations to synthetize nanoparticles. Examples in the literature show the application of hydrogen gas as a potential reducing agent for the generation of nanoparticles onto silicas,[28–31] or Metal Organic Frameworks (MOFs).[32] However, Such developments onto porous polymeric support only reported very few examples. Shim and coworkers described the use of hydrogen as a reducing agent for different metals precursors to obtain nanoparticles of rhodium,[33] copper[34] or silver[35] in polycarbonate or cellulose acetate films. Groppo *et al.* also used H_2 for the reduction of Pd^{2+} cations into the corresponding nanoparticles at the pore surface of nanoporous polystyrene.[36] The advantage of using H_2 for the reduction of metal salt precursors adsorbed at the surface of polymeric materials relies notably on the easier accessibility of gas into the pores when compared to other chemical reagents solubilized in liquids.

Herein, we decided to investigate the use of gaseous hydrogen as a reducing agent for the *in situ* generation of metallic nanoparticles within porous glycidyl methacrylate (GMA)-based monoliths. To that purpose, macroporous GMA-based polymeric materials were synthetized in presence of porogenic solvents. Upon a ring opening step in the presence of ethylene diamine, the resulting amine functionalized porous monoliths were used as supports for the immobilization of metallic (gold and palladium) nanoparticles *in situ* using a deposition-precipitation process. Experimentally, amine functionalized porous polymers were impregnated with a solution of gold, palladium salt precursor or a mixture of both. Then impregnated porous GMA-based materials were placed in an oven under a H_2 stream that allows for the reduction of metallic cations. To demonstrate the potential of such hybrid systems, the different supported metallic nanoclusters were implemented as catalysts for the Carbon-Carbon coupling of 4-iodotoluene with benzene boronic acid.

2.7 Materials and Methods

2.7.1 Experimental

Gold (III) chloride trihydrate ($HAuCl_4 \bullet 3H_2O$, 99.9 %), perchloric acid ($HClO_4$, 99.999 %) ethylenediamine (EDA, ≥ 99 %), ethylene glycol dimethacrylate (EGDMA, 98 %), glycidyl methacrylate (GMA, ≥ 97.0 %GC) were supplied by Sigma-Aldrich. Potassium tetrachloropalladate (II) (K_2PdCl_4, 99.99 %), potassium carbonate (K_2CO_3, 99 %), benzene boronic acid (98 %+) and 4-iodotoluene (98 %) were furnished by Alfa Aesar. 2,2'-azobisisobutyronitrile (AIBN, 98 %), obtained from Acros Organics, was recrystallized from methanol and stored at 4 °C prior to use. Absolute ethanol was furnished by Carlo Erba while dichloromethane (99.8 %) was furnished by VWR. All chemicals were used as purchased without any further purification, except from AIBN which was recrystallized from methanol prior to use. Milli-Q water (18.2 MΩ.cm) was used as solvent for all inorganic metals salts dissolution. The labware used for the inorganic reactions was cleaned after each synthesic step using aqua regia and Milli-Q water.

2.7.2 Synthesis of the porous poly(glycidyl methacrylate-*co*-ethylene glycol dimethacrylate) (P(GMA-*co*-EGDMA)) material

The porous polymeric monolith was prepared through a photochemically-driven free radical polymerization reaction using the polymerization feed that follows: GMA as a functional monomer (1.2 g, 8.44 mmol), EGDMA as a cross-linker (800 mg, 4.04 mmol), cyclohexanol (1.5 g) and dodecanol (1.5 g) as porogenic solvents and AIBN as an initiator (20 mg, 1 wt % with respect to the total amount of monomers). The polymerization mixture was transferred into glass vials of 1 cm diameter. The latters were placed in a Spectrolinker XL-1500 UV oven (Spectronics, Westburry, NY, USA) equipped with six lamps (6 × 15 W) for 4 h under irradiation at 365 nm to trigger the photo-induced free-radical copolymerization. The as-obtained materials were then subjected to Soxhlet extraction overnight in THF to remove porogens and eventually non-reacted monomers. After this extraction step, porous P(GMA-*co*-EGDMA) samples were dried at room temperature under vacuum. They were then weighed so as to check that monomers or porogenic solvents from the initial polymerization mixture have been removed. Such gravimetric analyses confirmed the complete removal of porogens and monomers.

2.7.3 Chemical functionalization of the pore surface of P(GMA-*co*-EGDMA) porous monoliths with ethylene diamine (EDA)

The functionalization of the newly prepared P(GMA-*co*-EGDMA) was performed *via* a one-step process. 512 mg of the PGMA previously prepared were immersed into 10 mL of a 2 M EDA solution in methanol. The reaction medium was gently stirred on an orbital shaking plate overnight. Samples were abundantly washed with methanol and deionized water, and dried at room temperature under vacuum. Raman spectroscopy was carried out to determine the success of the chemical reaction.

2.7.4 Impregnation of the EDA functionalized porous polymer with metal salt precursors

100 mg of the EDA functionalized polymer were introduced into a vial containing 2 mL of a metal salt precursor solution. These metal salt precursor solutions, either a gold salt solution ($HAuCl_4$ into Milli-Q water), a palladium salt solution (K_2PdCl_4 into a Milli-Q water solution with pH adjusted to 3.3 using $HClO_4$) or a mixture of both metal (K_2PdCl_4 into a $HAuCl_4$-Milli-Q water) had concentrations fixed at 5 mM. The vial was placed under a pressure of 3-bar to ensure the liquid to entirely penetrate into the porous materials and was kept under these pressure conditions for 2 hours. Samples were taken back to atmospheric pressure, then washed thoroughly with Milli-Q water and finally dried under the vacuum line overnight.

2.7.5 Reduction of the metal salt precursors

60 mg of the metal ions-loaded polymer were inserted into a Carbolite Furnaces MTF 12/388 oven streamed with a flux of gas mixture Ar/H_2: 95/5 (v/v). Different parameters were assessed such as the temperature (R.T., 50 °C and 100 °C), the reaction time (12 h and 24 h) and the concentration of the loading metal salt precursor solution (0.5 and 5 mM). For samples treated at 50 °C and 100 °C, the temperature was increased at rate of 2 $°C.min^{-1}$, was then maintained during the time of the reduction step and then decreased at the same rate until room temperature. The metal content in each sample A, B and C (see list in **Table 2-1**) was determined by analysing 5 mg of them by ICP-OES.

Table 2-1: Table presenting the different hybrid samples prepared for catalysis trials.

Metal immobilized	Reduction time (h)	Temperature (°C)	Concentration in metallic salt precursor (mM)	Sample name
Au	24	100	5	A
Pd	24	100	5	B
Au & Pd	24	100	5	C

2.7.6 Heterogeneous supported catalytic trials using the nanoparticles-decorated monoliths

A solution containing prepared by mixing 1 mL of a benzene boronic solution (232 mg dissolved in 64 mL of ethanol), 1 mL of 4-iodotoluene solution (177 mg dissolved in 30 mL of ethanol), 0.6 mL of a K_2CO_3 solution (50 mg dissolved in 0.6 mL of H_2O) was freshly prepared and placed in a round-bottom flask. Three distinct hybrid samples named A, B and C, depending on the nature of the nanometal(s) immobilized, were used as catalysts. The experimental procedure implemented was as follows: 25 mg of the supported catalyst A, B or C were added to the freshly prepared reactant solution in the round bottom flask while the temperature was fixed at 70 °C. The reaction was gently stirred during 24 h before cooling it down to room temperature. The reaction mixture was diluted with CH_2Cl_2 (5 mL) and the supported catalyst was withdrawn from the solution by a readily filtration. Following an extraction step with water to remove inorganic salts, GC-MS analyses were performed on the crude reaction mixtures to determine and quantify the obtained product(s). It is worth noticing that naphthalene was used as an internal standard so as to quantify the product(s).

2.7.7 Instrumentation

The porosity ratios, porous volumes, and pore size distributions of the GMA-based materials were determined by mercury intrusion porosimetry (MIP) using an AutoPore IV 9500 porosimeter from Micromeritics. The determination of the porosity features was based on the Washburn equation between the applied pressure (from 1.03 to 206.8 MPa) and the pore diameter into which mercury intruded. The chemical nature of the pore surface of the prepared polymeric materials was examined using an XPlora One Raman spectrophotometer from Horiba Jobin Yvon equipped with a laser emitting at 638 nm. The acquisition time was fixed at 1 min. Inductively coupled plasma optical

emission spectrometry (ICP-OES) analysis was performed using a Varian Vista-PRO CCD Simultaneous spectrometer. Gas chromatography (GC) was performed using a Shimadzu GC-2025 chromatograph equipped with a Phenomenex ZB-Semi Volatiles capillary column (L = 5.5 m). Azote was used as a carrier gas and column head pressure was fixed at 3 bar. The injector temperature was fixed at 270 °C, whereas that of the FID detector was fixed at 280 °C. The column temperature started at 50 °C and increased at a rate of 10 °C.min^{-1} up to 270 °C, followed by an isotherm during 10 min.

2.8 Results and Discussions

2.8.1 Synthesis and functionalization of the porous glycidyl methacrylate-based monoliths

Glycidyl methacrylate (GMA) functional monomer has been shown in the past to be a candidate of choice for the preparation of porous polymeric monoliths for diverse applications. Sveć and Fréchet notably demonstrated that such monoliths present interesting mechanical properties and tunable porous features and can be easily functionalized in rather mild conditions through ring opening of the epoxide surface functionalities with various nucleophiles such as amines, for instance. All these reasons make these particular monoliths suitable as in-capillary monoliths for chromatographic applications notably. Considering this, we focused our attention on the preparation of GMA-based monoliths. The synthetic pathway, as depicted in **Figure 2-9**, relies on the synthesis of porous polymeric monoliths, their further functionalization with a suitable ligand to ensure in a subsequent chelation of metallic salt precursors that can be in turn reduced to the corresponding nanometals to afford the resulting hybrid porous monoliths.

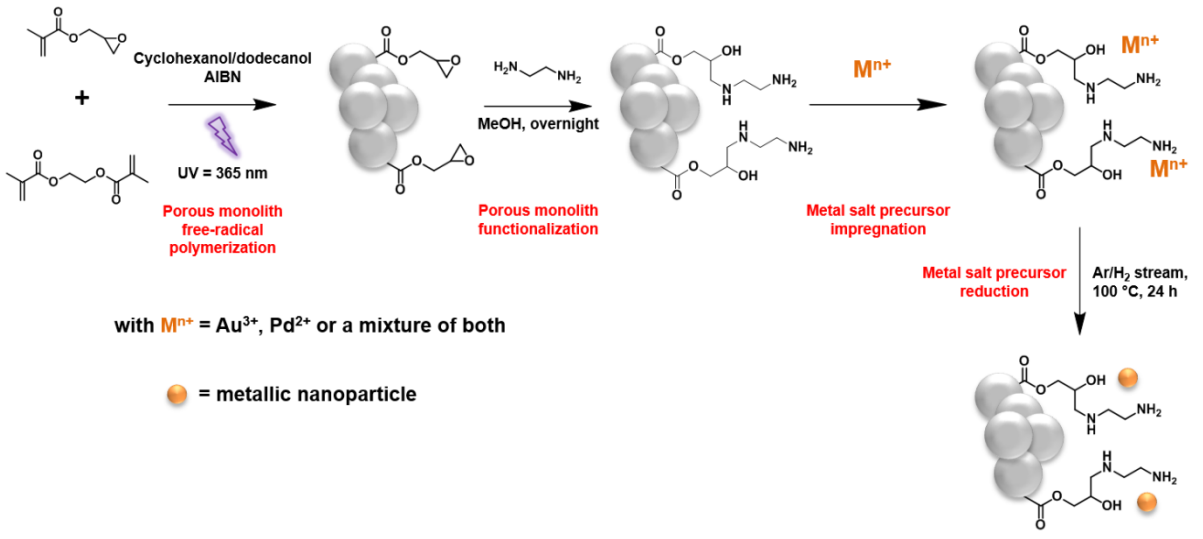

Figure 2-9: Schematic representation of the synthetic pathway applied for preparing porous P(GMA-*co*-EGDMA) supported-metallic nanoparticles.

Experimentally, the porous morphology was generated within the polymeric materials by adding a porogenic solvent mixture constituted of cyclohexanol and dodecanol. It is indeed well-known that such solvents permit the formation of interconnected pores with an average size of ~1 µm, as already reported elsewhere.[37] The porosity of the polymeric frameworks was thus ascertained by mercury intrusion porosimetry that showed a monomodal porous distribution centered on 1 µm, as highlighted in **Figure 2-10**.

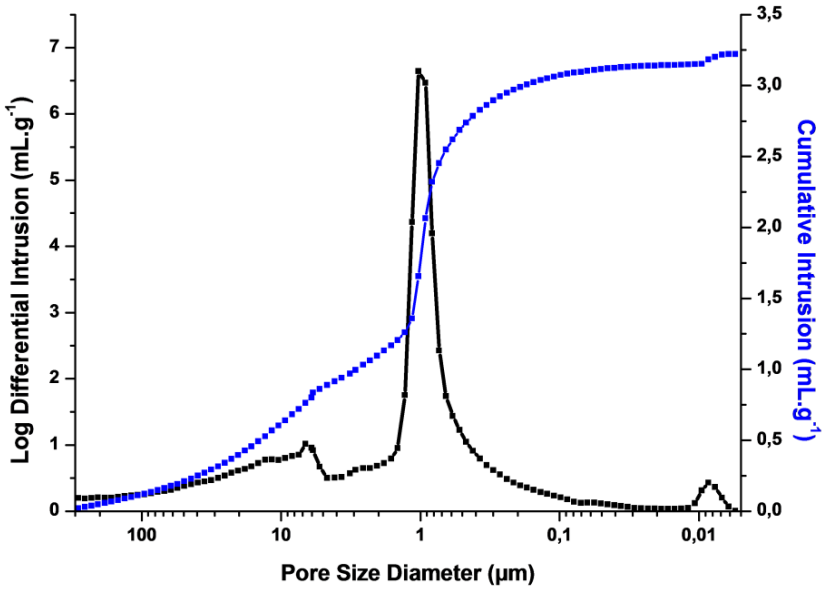

Figure 2-10: Mercury intrusion porosimetry profile of the GMA-based porous monolith.

The chemical nature of the pore surface of such GMA-based monolith was also examined by Raman spectroscopy. **Figure 2-11**, displaying the Raman spectrum of the pristine GMA-based porous material, showed some characteristic bands of the oxiran moiety stemming from the functional GMA monomer at 3000 cm^{-1} and between 800 to 900 cm^{-1}, attributed to the C-H stretching of the epoxide and to the ring vibration of the cycle, respectively.[38] The functionalization of the oxiran moieties pending at the pore surface of the monoliths was conducted in the presence of a diamine, *i.e.* ethylene diamine (EDA), in rather mild conditions (room temperature in THF overnight). The success of the functionalization step was monitored aging by Raman spectroscopy that showed some clear differences when compared to the pristine monolith. Upon ring opening step with EDA followed by thorough rinsing process, the Raman spectrum of the as-functionalized GMA-based monoliths showed a characteristic broad signal at 3300 cm^{-1} ascribed to the -N-H stretching stemming from the grafted amine containing compound, *i.e.* EDA[38] while the signal at 3000 cm^{-1}, typically observed with epoxide containing materials vanished. Finally, a significant decrease of the intensity of the signal at 800 cm^{-1}. All these observations led to the conclusion that the functionalization step was a success. As expected

from the reaction conditions implemented for the functionalization of GMA-based monoliths, the porous profile of the as-obtained EDA functionalized remained unchained when compared to the porous pristine monolith (data not shown).

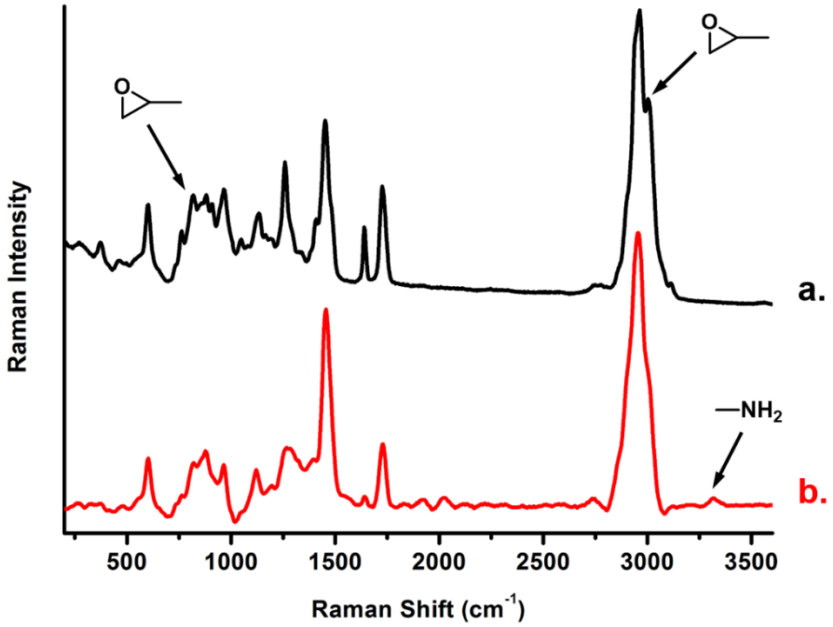

Figure 2-11: Raman spectra of *a)* the pristine GMA-based monolith (black curve) and of *b)* the same monolith after ring opening reaction with ethylene diamine (red curve).

2.8.2 Nanoparticles generation

Even though the reaction conditions required for the reduction of metallic salt precursors within polymers are rather harsh, *i.e.* high temperature in the 90-200 °C range reported in the literature, using gas phase reduction strategy present an undeniable advantage over other liquid phase reductions that are sometimes limited, mainly because of interfacial tensions and wettability concerns due notably to the nature of the polymeric materials. Gases have indeed the advantage of penetrating more easily in confined media than liquids. H_2 was thus selected as a candidate of choice for the gas phase reduction of the metallic precursors adsorbed at the surface of amine functionalized GMA-based porous polymers. Moreover it is known in the literature as a reducing agent of palladium[39] and gold salts,[40] metals we aim to reduce to the corresponding nanoparticles. Finally, H_2 has also been reported as a powerful reducing agent for the preparation of hybrid materials consisting in bimetallic nanoparticles immobilized onto silicas.[41] To evaluate the best conditions for the reduction of metallic cations immobilized at the pore surface of functionalized GMA-based monoliths, different temperature and time were tested. After completion of the process, only samples treated at 100 °C during 24 h showed complete reduction, as can be immediately seen with the naked eye, especially for gold. A clear transformation of the initial yellowish sample into wine red was indeed observed for gold

containing sample after reduction (**Figure 2-12**). In the same way, bimetallic-loaded samples showed their colour turning to purple (data not shown). Finally, the colour of palladium-loaded sample vanished after reduction of Pd^{2+} cations.

Figure 2-12: Pictures with the naked eye of the pristine porous P(GMA-*co*-EGDMA) monolith (white, left), of the same monolith after impregnation with gold salt precursor solution (yellowish, middle) and of the monolith loaded with Au nanoparticles after complete reduction of Au^{3+} cations under Ar/H_2 (v/v : 95/5) stream at 100 °C during 24 h (wine red, right).

ICP-OES analyses of the hybrid materials showed that only tiny quantities of nanometal(s) were immobilized at the pore surface of P(GMA-*co*-EGDMA) polymer. From 3 to 6 µg were found in such as-prepared materials, which represent only from 300 to 600 ppm nanometal when compared to the polymeric support. We also observed that amine immobilized at the pore surface of such P(GMA-*co*-EGDMA) materials are more selective for palladium than for gold as higher molar concentration of the former were found when compared to the latter.

Table 2-2: Gold and palladium contents in hybrid samples A, B and C as determined by ICP-OES.

Sample	m_{Au}[a] (µg)	m_{Pd}[a] (µg)	Au (wt%)	Pd (wt%)
A	6	-	0.06	-
B	-	5	-	0.05
C	3	4	0.03	0.04

[a] Pd and Au mass found in 10 mg of hybrid material A, B or C

2.8.3 Catalytic assays

So as to evaluate the catalytic behaviour of the prepared hybrids materials, C-C cross-coupling reaction were envisioned. On the one hand, palladium (Pd) nanoparticles are widely known to catalyse a plethora of C-C cross-coupling reactions such as Sonogashira[42] and Mizoroki-Heck type reactions,[43] for instance. Pd NPs are also prone to catalyse Suzuki-Miyaura cross-couplings[44] as well as boronic[45] and aryl halide Ullmann-type homocouplings.[46] Moreover, gold (Au) nanoparticles are also able to catalyse such boronic homocoupling reactions, as depicted in numerous articles in the field,[15,47,48] Ullmann-type homocouplings[49] as well as Suzuki-Miyaura reactions. [50] Of particular interest, Suzuki-Miyaura couplings permit to synthesize dissymmetric biphenyl compounds, whose preparation is more interesting to emphasize in the field of organic chemistry than their symmetric analogues. Homocoupling reactions are however also used, mainly because they are able to create symmetric biphenyls.

In our experiments, iodoarene and benzeneboronic acid were used as starting reagents. In the presence of our hybrid materials, the supported catalysis should afford the product expected through Suzuki-Miyaura-type C-C cross-coupling reaction, *i.e.* 4'-methylbiphenyl. The potential influence of the nanometal (Pd, Au or Pd/Au alloy) was in this case investigated. To that purpose, three different hybrid materials were assessed: sample A containing Pd NPs, sample B containing Au NPs and sample C containing a mixture of both nanometals. As boronic and Ullmann-type homocoupling can be closely related to side reaction of the Suzuki-Miyaura reaction, it is important to specify whether one metal is better than the other to carry out such Suzuki-Miyaura reaction in optimal conditions. Also, as the process we used for the generation of nanoparticles implies alloys by mixing both salts in the solution, it is interesting to determine and quantify the potential products that can be obtained with such bimetallic supported systems. For the catalytic tests, a mixture of 4-iodotoluene and benzene boronic acid was used to test the efficiency of the supported hybrid catalysts and to determine the potential outcome of the reaction as boronic acid could be either involved in Suzuki coupling or in boronic homocoupling reaction while arylhalide may be involved in either Suzuki cross-coupling reaction or Ullmann-type homocoupling. To this purpose, the presence of each reactant and product was also thoroughly monitored by GC and GC-MS (data not shown) so as to determine their retention time (**Table 2-3**) and to select the more suitable internal standard.

Table 2-3: Retention time of the reactants, products and internal standard present in the crude products stemming from catalytic reactions carried out in the presence of hybrid samples A, B or C.

Chemical compounds	Reagents		Internal standard	Obtained products		
	4-Iodo-toluene	Phenyl-boronic acid	Naphthalene	Biphenyl	4-Methyl-biphenyl	4,4'-Dimethyl-biphenyl
Retention time (min)	3.18	16.59	3.60	6.00	7.38	8.71

GC chromatogram of the catalytic reaction involving hybrid material A surprisingly shows only one peak at 6.00 min corresponding to the biphenyl (**Figure 2-13**), as determined by GC-MS. Generation of such biphenyl compound means that only boronic homocoupling occurs with immobilized nanogold in the reaction conditions used in thus study. This finding is in agreement with the literature that reported that gold salts and gold nanoparticles[47] are prone to catalyse with high efficiency this aryl boronic acid-based homocoupling reaction. Surprisingly, no cross-coupling product was obtained, meaning that no Suzuki reaction occurred with gold nanoclusters as supported catalyst. On the opposite, reactions carried out in the presence of hybrid samples B and C afforded different products. The catalytic reaction operated in the presence of sample B, on which are immobilized Pd NPs, showed the formation of the expected C-C cross-coupling product, *i.e.* 4-methylbiphenyl whose presence is highlighted by a peak at 7.38 min (**Figure 2-13**). This finding is consistent with the formation of a product obtained through the Suzuki-Miyaura reaction. This notably demonstrated the efficiency of Pd nanoparticle-based catalysts in this reaction. On the other hand, we also observed traces of side-products, as demonstrated by the presence of peaks at 6.00 min and 8.31 min, ascribed to boronic homocoupling product biphenyl and arylhalide homocoupling product 4,4'-dimethylbiphenyl, respectively. This demonstrated the good selectivity of the Suzuki-Miyaura reaction carried out using these hybrid material B incorporating Pd nanoparticles. More interestingly, GC chromatogram of the crude product obtained after reaction in the presence of sample C on which Pd and Au nanoclusters are immobilized presents three distinct peaks. First peak obtained with highest retention correspond to the product arising from boronic homocoupling that is obtained in smaller quantity than the two others. The second one observed at 7.38 min is ascribed, as mentioned earlier, to the product stemming from the Suzuki cross-coupling between 4-iodotoluene and phenylboronic acid. Finally, the last peak at 8.71 min (**Figure 2-13**), was determined by GC-MS analysis to be 4,4'-dimethylbiphenyl, obtained from 4-iodotoluene homocoupling through Ullman-type reaction. Such Ullman-type reaction is indeed promoted by Pd nanoparticles[46] or salts,[51] Au nanoparticles[49] as well as

Au/Pd alloy nanoclusters.[52] Our catalytic results obtained in the presence of both nanometals are thus in good agreement with those reported by Dhital *et al.*[52] in 2012.

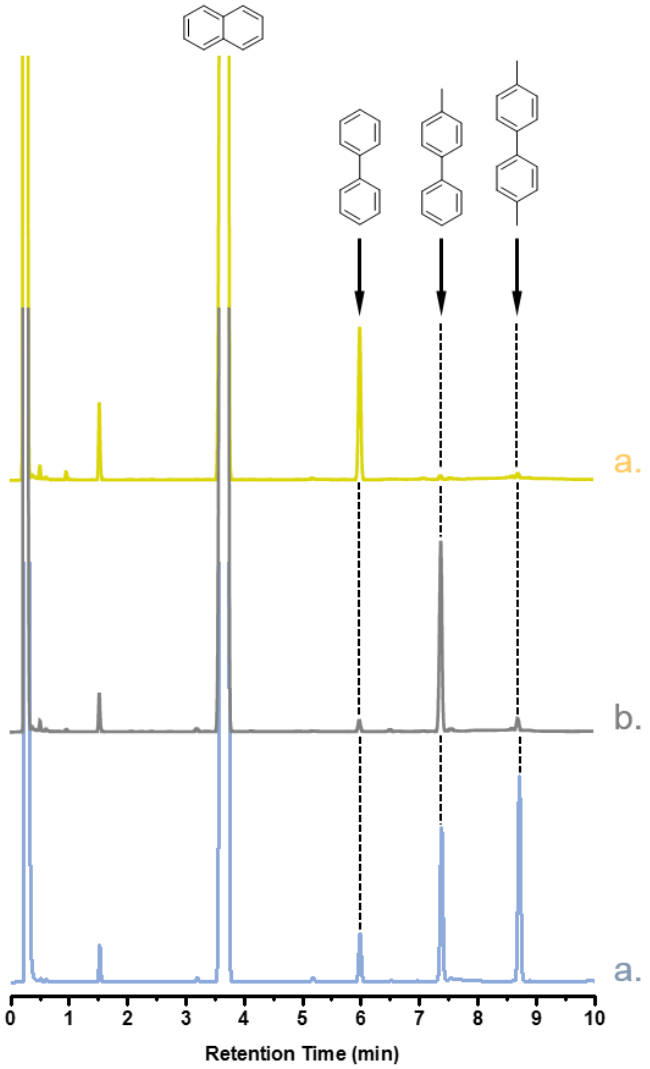

Figure 2-13: GC chromatograms obtained for the C-C coupling reactions realized with hybrid monolithic samples *a)* A, *b)* B and *c)* C.

It is worth noticing that all coupling products were generated with low yields of around 10 %, as listed in**Table 2-4**, likely due to the very low content of (bi)metallic clusters immobilized at the pore surface of EDA functionalized P(GMA-*co*-EGDMA) materials A, B and C. It was notably calculated that the reagents are placed in the reaction mixture with a concentration of 10^{-2} M while the supported catalysts contain quantities of nanometal ranging from 1.5 to 4.7 × 10^{-8} M. This difference of 6 orders of magnitude is thus sufficient to explain the poor yields obtained during these catalytic reactions.

Table 2-4: C-C cross-coupling reaction yields obtained after GC analysis.

Hybrid sample	Product obtained	Concentration (mol.L^{-1})	Yield (%)
A	Biphenyl	8.6×10^{-4} [a]	9
B	4-Methylbiphenyl	1.1×10^{-3} [a]	11
C	Biphenyl	2.6×10^{-4} [a]	3
	4-Methylbiphenyl	8.5×10^{-4} [a]	8
	4,4'-Dimethylbiphenyl	9.2×10^{-4} [a]	9

[a] Concentration of the expected product arising from C-C cross-coupling reaction was calculated to be 1.10^{-2} M in case of total conversion and selectivity equal to 100%

2.9 Conclusions

Hybrid P(GMA-*co*-EGDMA)-based monoliths consisting in Pd, Au or Pd/Au metallic nanoparticles immobilized at the pore surface can be easily engineered in a straightforward fashion. A key step involving the *in situ* reduction of metallic salt precursors at the pore surface of the polymeric matrix is required in this strategy. This step was carried out by placing the material impregnated with metallic salt precursor(s) under H_2 gas stream at 100°C for 24 h. Such prepared hybrid monoliths were successfully used in C-C coupling reactions involving 4-iodotoluene and phenylboronic acid in the presence of K_2CO_3 as the base. It was notably demonstrated that monolith immobilized gold nanoparticles only allow the formation of boronic homocoupling product while monolith immobilized gold nanoparticles gave rise to the production of the C-C cross-coupling product with high selectivity through the Suzuki-Miyaura reaction. Finally, the bimetallic sample shows seemingly no selectivity, giving the desired cross-coupling product as well as the products obtained through the boronic and aryl halide homocoupling reactions. This investigation paves the way for further developments on full understanding of the mechanisms involved such monolith supported metallic nanoparticle-based catalytic reactions.

2.10 References

(1) Bell, A. T. The Impact of Nanoscience on Heterogeneous Catalysis. *Science* **2003**, *299* (5613), 1688.

(2) Lu, A.-H.; Salabas, E. L.; Schüth, F. Magnetic Nanoparticles: Synthesis, Protection, Functionalization, and Application. *Angew. Chem. Int. Ed.* **2007**, *46* (8), 1222–1244.

(3) Stevens, P. D.; Fan, J.; Gardimalla, H. M. R.; Yen, M.; Gao, Y. Superparamagnetic Nanoparticle-Supported Catalysis of Suzuki Cross-Coupling Reactions. *Org. Lett.* **2005**, *7* (11), 2085–2088.

(4) Rosario-Amorin, D.; Gaboyard, M.; Clérac, R.; Vellutini, L.; Nlate, S.; Heuzé, K. Metallodendritic Grafted Core–Shell γ-Fe2O3 Nanoparticles Used as Recoverable Catalysts in Suzuki C-C Coupling Reactions. *Chem. – Eur. J.* **2012**, *18* (11), 3305–3315.

(5) Wu, D.; Xu, F.; Sun, B.; Fu, R.; He, H.; Matyjaszewski, K. Design and Preparation of Porous Polymers. *Chem. Rev.* **2012**, *112* (7), 3959–4015.

(6) Lv, Y.; Lin, Z.; Svec, F. Hypercrosslinked Large Surface Area Porous Polymer Monoliths for Hydrophilic Interaction Liquid Chromatography of Small Molecules Featuring Zwitterionic Functionalities Attached to Gold Nanoparticles Held in Layered Structure. *Anal. Chem.* **2012**, *84* (20), 8457–8460.

(7) Lv, Y.; Alejandro, F. M.; Fréchet, J. M. J.; Svec, F. Preparation of Porous Polymer Monoliths Featuring Enhanced Surface Coverage with Gold Nanoparticles. *J. Chromatogr. A* **2012**, *1261*, 121–128.

(8) Floris, P.; Twamley, B.; Nesterenko, P. N.; Paull, B.; Connolly, D. Fabrication and Characterisation of Gold Nano-Particle Modified Polymer Monoliths for Flow-through Catalytic Reactions and Their Application in the Reduction of Hexacyanoferrate. *Microchim. Acta* **2014**, *181* (1), 249–256.

(9) Floris, P.; Twamley, B.; Nesterenko, P. N.; Paull, B.; Connolly, D. Agglomerated Polymer Monoliths with Bimetallic Nano-Particles as Flow-through Micro-Reactors. *Microchim. Acta* **2012**, *179* (1), 149–156.

(10) Poupart, R.; Le Droumaguet, B.; Guerrouache, M.; Carbonnier, B. Copper Nanoparticles Supported on Permeable Monolith with Carboxylic Acid Surface Functionality: Stability and Catalytic Properties under Reductive Conditions. *Mater. Chem. Phys.* **2015**, *163*, 446–452.

(11) Khalil, A. M.; Georgiadou, V.; Guerrouache, M.; Mahouche-Chergui, S.; Dendrinou-Samara, C.; Chehimi, M. M.; Carbonnier, B. Gold-Decorated Polymeric Monoliths: In-Situ vs Ex-Situ Immobilization Strategies and Flow through Catalytic Applications towards Nitrophenols Reduction. *Polymer* **2015**, *77*, 218–226.

(12) Liu, Y.; Guerrouache, M.; Kebe, S. I.; Carbonnier, B.; Le Droumaguet, B. Gold Nanoparticles-Supported Histamine-Grafted Monolithic Capillaries as Efficient Microreactors for Flow-through Reduction of Nitro-Containing Compounds. *J. Mater. Chem. A* **2017**, *5* (23), 11805–11814.

(13) Poupart, R.; Djerir, N. E. H.; Chellapermal, D.; Guerrouache, M.; Carbonnier, B.; Le Droumaguet, B. Novel In-Capillary Polymeric Monoliths Arising from Glycerol Carbonate Methacrylate for Flow-through Catalytic and Chromatographic Applications. *RSC Adv.* **2016**, *6* (17), 13614–13617.

(14) Le Droumaguet, B.; Poupart, R.; Grande, D. "Clickable" Thiol-Functionalized Nanoporous Polymers: From Their Synthesis to Further Adsorption of Gold Nanoparticles and Subsequent Use as Efficient Catalytic Supports. *Polym. Chem.* **2015**, *6* (47), 8105–8111.

(15) Poupart, R.; Benlahoues, A.; Le Droumaguet, B.; Grande, D. Porous Gold Nanoparticle-Decorated Nanoreactors Prepared from Smartly Designed Functional Polystyrene-Block-Poly(d,l-Lactide) Diblock Copolymers: Toward Efficient Systems for Catalytic Cascade Reaction Processes. *ACS Appl. Mater. Interfaces* **2017**, *article in press*, DOI: 10.1021/acsami.6b16157..

(16) Desforges, A.; Deleuze, H.; Mondain-Monval, O.; Backov, R. Palladium Nanoparticle Generation within Microcellular Polymeric Foam and Size Dependence under Synthetic Conditions. *Ind. Eng. Chem. Res.* **2005**, *44* (23), 8521–8529.

(17) Desforges, A.; Backov, R.; Deleuze, H.; Mondain-Monval, O. Generation of Palladium Nanoparticles within Macrocellular Polymeric Supports: Application to Heterogeneous Catalysis of the Suzuki–Miyaura Coupling Reaction. *Adv. Funct. Mater.* **2005**, *15* (10), 1689–1695.

(18) Féral-Martin, C.; Birot, M.; Deleuze, H.; Desforges, A.; Backov, R. Integrative Chemistry toward the First Spontaneous Generation of Gold Nanoparticles within Macrocellular PolyHIPE Supports

(Au@polyHIPE) and Their Application to Eosin Reduction. *React. Funct. Polym.* **2007**, *67* (10), 1072–1082.

(19) Wuithschick, M.; Witte, S.; Kettemann, F.; Rademann, K.; Polte, J. Illustrating the Formation of Metal Nanoparticles with a Growth Concept Based on Colloidal Stability. *Phys. Chem. Chem. Phys.* **2015**, *17* (30), 19895–19900.

(20) Polte, J.; Tuaev, X.; Wuithschick, M.; Fischer, A.; Thuenemann, A. F.; Rademann, K.; Kraehnert, R.; Emmerling, F. Formation Mechanism of Colloidal Silver Nanoparticles: Analogies and Differences to the Growth of Gold Nanoparticles. *ACS Nano* **2012**, *6* (7), 5791–5802.

(21) Wuithschick, M.; Paul, B.; Bienert, R.; Sarfraz, A.; Vainio, U.; Sztucki, M.; Kraehnert, R.; Strasser, P.; Rademann, K.; Emmerling, F.; Polte, J. Size-Controlled Synthesis of Colloidal Silver Nanoparticles Based on Mechanistic Understanding. *Chem. Mater.* **2013**, *25* (23), 4679–4689.

(22) Kettemann, F.; Wuithschick, M.; Caputo, G.; Kraehnert, R.; Pinna, N.; Rademann, K.; Polte, J. Reliable Palladium Nanoparticle Syntheses in Aqueous Solution: The Importance of Understanding Precursor Chemistry and Growth Mechanism. *CrystEngComm* **2015**, *17* (8), 1865–1870.

(23) Wuithschick, M.; Birnbaum, A.; Witte, S.; Sztucki, M.; Vainio, U.; Pinna, N.; Rademann, K.; Emmerling, F.; Kraehnert, R.; Polte, J. Turkevich in New Robes: Key Questions Answered for the Most Common Gold Nanoparticle Synthesis. *ACS Nano* **2015**, *9* (7), 7052–7071.

(24) Kettemann, F.; Birnbaum, A.; Witte, S.; Wuithschick, M.; Pinna, N.; Kraehnert, R.; Rademann, K.; Polte, J. Missing Piece of the Mechanism of the Turkevich Method: The Critical Role of Citrate Protonation. *Chem. Mater.* **2016**, *28* (11), 4072–4081.

(25) Boutonnet, M.; Kizling, J.; Stenius, P.; Maire, G. The Preparation of Monodisperse Colloidal Metal Particles from Microemulsions. *Colloids Surf.* **1982**, *5* (3), 209–225.

(26) Chappa, S.; Bharath, R. S.; Oommen, C.; Pandey, A. K. Dual-Functional Grafted Electrospun Polymer Microfiber Scaffold Hosted Palladium Nanoparticles for Catalyzing Redox Reactions. *Macromol. Chem. Phys.* **2017**, *218* (7), 1600555.

(27) Lu, L.; An, X. Silver Nanoparticles Synthesis Using H2 as Reducing Agent in Toluene–supercritical CO2 Microemulsion. *J. Supercrit. Fluids* **2015**, *99*, 29–37.

(28) Fukuoka, A.; Araki, H.; Sakamoto, Y.; Sugimoto, N.; Tsukada, H.; Kumai, Y.; Akimoto, Y.; Ichikawa, M. Template Synthesis of Nanoparticle Arrays of Gold and Platinum in Mesoporous Silica Films. *Nano Lett.* **2002**, *2* (7), 793–795.

(29) Overbury, S. H.; Ortiz-Soto, L.; Zhu, H.; Lee, B.; Amiridis, M. D.; Dai, S. Comparison of Au Catalysts Supported on Mesoporous Titania and Silica: Investigation of Au Particle Size Effects and Metal-Support Interactions. *Catal. Lett.* **2004**, *95* (3), 99–106.

(30) Rioux, R. M.; Song, H.; Hoefelmeyer, J. D.; Yang, P.; Somorjai, G. A. High-Surface-Area Catalyst Design: Synthesis, Characterization, and Reaction Studies of Platinum Nanoparticles in Mesoporous SBA-15 Silica. *J. Phys. Chem. B* **2005**, *109* (6), 2192–2202.

(31) Gajan, D.; Guillois, K.; Delichère, P.; Basset, J.-M.; Candy, J.-P.; Caps, V.; Coperet, C.; Lesage, A.; Emsley, L. Gold Nanoparticles Supported on Passivated Silica: Access to an Efficient Aerobic Epoxidation Catalyst and the Intrinsic Oxidation Activity of Gold. *J. Am. Chem. Soc.* **2009**, *131* (41), 14667–14669.

(32) Gu, X.; Lu, Z.-H.; Jiang, H.-L.; Akita, T.; Xu, Q. Synergistic Catalysis of Metal–Organic Framework-Immobilized Au–Pd Nanoparticles in Dehydrogenation of Formic Acid for Chemical Hydrogen Storage. *J. Am. Chem. Soc.* **2011**, *133* (31), 11822–11825.

(33) Shim, I.-W.; Kim, J.-Y.; Kim, D.-Y.; Choi, S. Preparation of Rh-Containing Polycarbonate Films and the Study of Their Chemical Properties in the Polymer. *React. Funct. Polym.* **2000**, *43* (1), 71–78.

(34) Shim, I.-W.; Noh, W.-T.; Kwon, J.; Cho, J. Y.; Kim, K.-S.; Kang, D. H. Preparation of Copper Nanoparticles in Cellulose Acetate Polymer and the Reaction Chemistry of Copper Complexes in the Polymer. *Bull. Korean Chem. Soc.* **2002**, *23* (4), 563–566.

(35) Kwon, J.-W.; Yoon, S. H.; Lee, S. S.; Seo, K. W.; Shim, I.-W. Preparation of Silver Nanoparticles in Cellulose Acetate Polymer and the Reaction Chemistry of Silver Complexes in the Polymer. *Bull. Korean Chem. Soc.* **2005**, *26* (5), 837–840.

(36) Groppo, E.; Agostini, G.; Borfecchia, E.; Wei, L.; Giannici, F.; Portale, G.; Longo, A.; Lamberti, C. Formation and Growth of Pd Nanoparticles Inside a Highly Cross-Linked Polystyrene Support: Role of the Reducing Agent. *J. Phys. Chem. C* **2014**, *118* (16), 8406–8415.

(37) Viklund, C.; Svec, F.; Fréchet, J. M. J.; Irgum, K. Monolithic, "Molded", Porous Materials with High Flow Characteristics for Separations, Catalysis, or Solid-Phase Chemistry: Control of Porous Properties during Polymerization. *Chem. Mater.* **1996**, *8* (3), 744–750.

(38) Socrates, G. *Infrared and Raman Characteristic Group Frequencies: Tables and Charts*; John Wiley & Sons, Inc.: New York, 2004.

(39) Henglein, A. Colloidal Palladium Nanoparticles: Reduction of Pd(II) by H2; PdCoreAuShellAgShell Particles. *J. Phys. Chem. B* **2000**, *104* (29), 6683–6685.

(40) Tsung, C.-K.; Hong, W. B.; Shi, Q. H.; Kou, X. S.; Yeung, M. H.; Wang, J. F.; Stucky, G. D. Shape- and Orientation-Controlled Gold Nanoparticles Formed within Mesoporous Silica Nanofibers. *Adv. Funct. Mater.* **2006**, *16* (17), 2225–2230.

(41) Yang, X.; Chen, D.; Liao, S.; Song, H.; Li, Y.; Fu, Z.; Su, Y. High-Performance Pd–Au Bimetallic Catalyst with Mesoporous Silica Nanoparticles as Support and Its Catalysis of Cinnamaldehyde Hydrogenation. *J. Catal.* **2012**, *291*, 36–43.

(42) Gao, S.; Zhao, N.; Shu, M.; Che, S. Palladium Nanoparticles Supported on MOF-5: A Highly Active Catalyst for a Ligand- and Copper-Free Sonogashira Coupling Reaction. *Appl. Catal. Gen.* **2010**, *388* (1), 196–201.

(43) Luo, C.; Zhang, Y.; Wang, Y. Palladium Nanoparticles in Poly(Ethyleneglycol): The Efficient and Recyclable Catalyst for Heck Reaction. *J. Mol. Catal. Chem.* **2005**, *229* (1), 7–12.

(44) Sawoo, S.; Srimani, D.; Dutta, P.; Lahiri, R.; Sarkar, A. Size Controlled Synthesis of Pd Nanoparticles in Water and Their Catalytic Application in C–C Coupling Reactions. *Tetrahedron* **2009**, *65* (22), 4367–4374.

(45) Prastaro, A.; Ceci, P.; Chiancone, E.; Boffi, A.; Fabrizi, G.; Cacchi, S. Homocoupling of Arylboronic Acids and Potassium Aryltrifluoroborates Catalyzed by Protein-Stabilized Palladium Nanoparticles under Air in Water. *Tetrahedron Lett.* **2010**, *51* (18), 2550–2552.

(46) Monopoli, A.; Calò, V.; Ciminale, F.; Cotugno, P.; Angelici, C.; Cioffi, N.; Nacci, A. Glucose as a Clean and Renewable Reductant in the Pd-Nanoparticle-Catalyzed Reductive Homocoupling of Bromo- and Chloroarenes in Water. *J. Org. Chem.* **2010**, *75* (11), 3908–3911.

(47) Carrettin, S.; Guzman, J.; Corma, A. Supported Gold Catalyzes the Homocoupling of Phenylboronic Acid with High Conversion and Selectivity. *Angew. Chem. Int. Ed.* **2005**, *44* (15), 2242–2245.

(48) Tsunoyama, H.; Sakurai, H.; Ichikuni, N.; Negishi, Y.; Tsukuda, T. Colloidal Gold Nanoparticles as Catalyst for Carbon−Carbon Bond Formation: Application to Aerobic Homocoupling of Phenylboronic Acid in Water. *Langmuir* **2004**, *20* (26), 11293–11296.

(49) Movahed, S. K.; Fakharian, M.; Dabiri, M.; Bazgir, A. Gold Nanoparticle Decorated Reduced Graphene Oxide Sheets with High Catalytic Activity for Ullmann Homocoupling. *RSC Adv.* **2014**, *4* (10), 5243–5247.

(50) Han, J.; Liu, Y.; Guo, R. Facile Synthesis of Highly Stable Gold Nanoparticles and Their Unexpected Excellent Catalytic Activity for Suzuki−Miyaura Cross-Coupling Reaction in Water. *J. Am. Chem. Soc.* **2009**, *131* (6), 2060–2061.

(51) Hennings, D. D.; Iwama, T.; Rawal, V. H. Palladium-Catalyzed (Ullmann-Type) Homocoupling of Aryl Halides: A Convenient and General Synthesis of Symmetrical Biaryls via Inter- and Intramolecular Coupling Reactions. *Org. Lett.* **1999**, *1* (8), 1205–1208.

(52) Dhital, R. N.; Kamonsatikul, C.; Somsook, E.; Bobuatong, K.; Ehara, M.; Karanjit, S.; Sakurai, H. Low-Temperature Carbon–Chlorine Bond Activation by Bimetallic Gold/Palladium Alloy Nanoclusters: An Application to Ullmann Coupling. *J. Am. Chem. Soc.* **2012**, *134* (50), 20250–20253.

Chapter 3:

Metallic Nanoparticles Anchored on Polymeric Capillary Monoliths for Flow-Through Catalysis

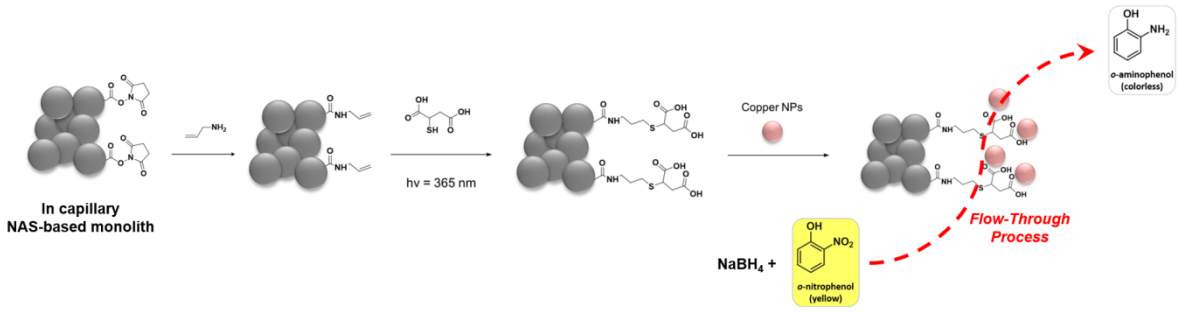

Contexte

La chimie en flux continu intéresse beaucoup les chercheurs et, notamment, depuis les deux dernières décennies. L'avènement de la microfluidique et du concept de « lab-on-a-chip » (laboratoire sur puce) dans les années 1990 et 2000 ont permis le développement de microréacteurs fonctionnels et remis un coup de projecteur sur cette chimie. En effet, elle possède un avantage non négligeable : si la réaction que l'on effectue est totale et qu'elle ne mène à aucun autre sous-produit, alors après injection du (ou des) réactif(s), seul le produit désiré est obtenu après élution et aucune étape de purification n'est donc théoriquement nécessaire.

Dans le cas de la catalyse supportée, une réaction modèle semble se démarquer et répondre à ces critères : la réduction de composés nitrés. Simple à mettre en œuvre et à suivre, sa constante de vitesse est très importante et cette réaction fonctionne avec de nombreuses nanoparticules métalliques. Par ailleurs, elle ne fait intervenir qu'un nitroarène (principalement le 4-nitrophénol), une source d'hydrure (le borohydrure de sodium $NaBH_4$) ainsi que des nanoparticules métalliques comme catalyseur hétérogène. Différents exemples rapportés dans la littérature montre que les métaux comme l'argent, l'or et le platine sont des catalyseurs efficaces de cette réaction, mais il y en a aussi d'autres comme le palladium, le ruthénium ou le cuivre. De plus, les composés aromatiques nitrés utilisés dans cette réaction sont souvent des colorants, alors que les produits obtenus, des dérivés d'anilines sont eux souvent incolores. Cette réaction est ainsi bien adaptée à un suivi cinétique par spectrométrie UV-Visible. Dans le cas d'une chimie en flux continu, en immobilisant les nanoparticules sur une colonne capillaire, il suffit de faire percoler le mélange réactionnel contenant le solvant, l'hydrure et le composé nitré puis de récupérer le produit en sortie de colonne. Une fois un volume suffisant collecté, un simple suivi par UV-Visible permet sa détection, mais aussi d'évaluer le rendement de la réaction.

Dans ce contexte, nous nous sommes intéressés à la réduction catalytique des nitroarènes en flux continu. Nous avons tout d'abord synthétisé des colonnes capillaires macroporeuses à base de *N*-acryloxysuccinimide (NAS). Ce monomère est un ester activé de l'acide acrylique. Il possède un groupe nucléofuge, le *N*-hydroxysuccinimide, permettant une substitution nucléophile par une amine pour créer une liaison amide. Nous avons ainsi pu greffer une amine modèle, l'allylamine, à la surface des pores et effectuer ensuite une réaction d'addition radicalaire thiol-ène avec l'acide mercaptosuccinique, un diacide thiolé. Ces fonctions acide carboxylique ont ainsi permis l'immobilisation de nanoparticules de cuivre *via* deux voies : *ex situ* et *in situ*. Ces catalyseurs supportés ont ensuite été testés pour réduire le 2-nitrophénol. Ce travail a été publié dans l'article suivant : **Copper nanoparticles supported on permeable monolith with carboxylic acid surface**

functionality : Stability and catalytic properties under reductive conditions, R. Poupart, B. Le Droumaguet, M. Guerrouache, B. Carbonnier, *Materials Chemistry and Physics*, **2015**, *163*, 446-452.

De plus, cette même matrice à base de NAS a été utilisée dans le cadre d'une étude plus poussée sur les amines. En effet, si dans la littérature, d'une part, les différences entre les fonctions chimiques et, d'autres parts, les groupements proches des complexes organométalliques sont présentés, peu décrivent l'influence directe de la topologie du ligand dans leurs études. Pourtant, en chimie inorganique, le substrat qui sert à la nucléation est important. Ainsi, différents ligands issus de l'éthylènediamine ont été utilisés pour chélater des ions auriques et les réduire en nanoparticules. Ces capillaires hybrides ont tout d'abord été analysés en microscopie électronique à balayage afin d'observer les différences de morphologie, de taille et/ou de répartition des nanoparticules à la surface des pores entre les échantillons. Par la suite, ces capillaires ont été utilisés pour la réduction de composés nitrés et ce, dans des conditions identiques. Ces résultats ont permis d'observer une certaine influence des différences des caractéristiques des nanoparticules sur le rendement de cette réaction catalytique.

Finalement, nous avons décidé d'utiliser une nouvelle matrice polymère à base de méthacrylate de carbonate de glycérol. Ce monomère étant disponible commercialement est d'un intérêt notable, les carbonates étant connus pour leur capacité à subir des attaques nucléophiles d'amines, entre autres. Après différents essais de mélanges de polymérisation afin de trouver le meilleur porogène et le rapport volumique (co)monomère/solvant adéquat, nous avons sélectionné le mélange qui nous paraissait la plus approprié. Cette matrice a ensuite été caractérisée par spectroscopie Raman afin de déterminer les signaux caractéristiques du carbonate de glycérol, mais aussi par porosimétrie à intrusion de mercure pour déterminer la distribution poreuse de ces monolithes. La surface a ensuite été modifiée par ouverture du cycle carbonate par attaque nucléophile d'une amine, l'allylamine, puis par réaction d'addition radicalaire thiol-ène de l'acide 4-mercaptobutyrique afin d'immobiliser un sel de platine, précurseur des nanoparticules correspondantes. Une fois ces dernières formées, le capillaire hybride a été testé en tant que catalyseur supporté pour la réduction du 4-nitrophénol. Le fruit de ce travail, ainsi qu'une autre partie complémentaire présentant l'application de tels matériaux provenant du méthacrylate de carbonate de glycérol en chromatographique liquide, a été publié dans l'article suivant : **Novel in-capillary polymeric monolith arising from glycerol carbonate methacrylate for flow-through catalytic and chromatographic applications**, R. Poupart, N. E. H. Djerir, D. Chellapermal, M. Guerrouache, B. Carbonnier, B. Le Droumaguet, *RSC Advances*, **2016**, *6*, 13614-13617.

Copper Nanoparticles Supported on Permeable Monolith with Carboxylic Acid Surface Functionality: Stability and Catalytic Properties under Reductive Conditions

Abstract: This work reported on the immobilization of copper metallic nanoparticles at the interface of mercaptosuccinic acid-functionalized *N*-acryloxysuccinimide-based monoliths. Upon photochemically-mediated free radical copolymerization of *N*-acryloxysuccinimide reactive monomer with ethylene glycol dimethacrylate cross-linker, reactive monoliths were obtained. Nucleophilic substitution of the *N*-hydroxysuccinimide moiety with allylamine, allowed for the synthesis of an olefin-functionalized monolith, as demonstrated by Raman spectroscopy. Mercaptosuccinic acid was anchored at the surface of the porous polymeric material through photochemically-driven thiol-ene "click" addition. In a final step, adsorption of copper nanoparticles at the surface of the resulting carboxylic acid functionalized monolith was achieved *via* two distinct pathways. It was either realized by percolation of a suspension of pre-formed copper nanoparticles through the capillary or by *in situ* reduction of $Cu^{(II)}Br_2$ salt solution preliminary flown through the monolith. After characterization of the resulting hybrids by scanning electron microscopy and energy-dispersive X-ray spectroscopy, investigations were further pursued regarding the catalytic behavior of such hybrid materials. The possibility to reduce 2-nitrophenol into the corresponding 2-aminophenol within a few minutes *via* a flow-through process inside the monolithic hybrid capillary was notably successfully demonstrated.

3.1 Introduction

Over the past decade, metallic nanoparticles (NPs) have appealed the research community due to their unique intrinsic properties. Because of their high surface area to volume ratio, they present unexpected enhanced properties compared to those of their bulk material counterparts. Indeed surface effects are predominant in nanometals and confer them with very specific properties. This nano-effect is particularly pronounced in different applications and especially in nanoparticle-based heterogeneous organometallic catalysis. Among the plethora of nanometals declined for heterogeneous catalysis, gold,[1] palladium,[2] platinum[3] and silver[4] are the most reported in the literature. They are largely used for various coupling reactions such as Suzuki-Miyaura,[5,6] Sonogashira[6,7] and Heck[3,6,8] cross-coupling reactions as well as for the reduction of nitroarenes,[1,9–13] to cite but a few. Such nanoparticulate systems require a fine tuning of the functionalities of the (macro)molecules used to stabilize them or of the surfaces on which they are adsorbed so as to increase their reactivity. This has been deeply investigated in the case of Au[14] or Pd[15,16] nanoparticles stabilized with peptides in which the amino-acid sequence was carefully studied for optimal catalytic efficiencies. In the actual context of environmental efforts, reduction of nitroarenes has a great importance because it could notably find applications in the transformation of nitrobenzene derivatives, which are well-known toxic pollutants, into much benign compounds. To the best of our knowledge, copper nanoparticles (CuNPs) have been so far not much investigated in such heterogeneous catalysis applications. CuNPs, that are well-known for their antifungal[17] and antibacterial[18] properties, also possess interesting catalytic behaviour, especially in the Huisgen dipolar azide-alkyne cycloaddition reaction,[6,19] also referred as CuAAC reaction. In addition, these copper-based nanometals have been shown to catalyse the reduction of nitroarenes.[11,20–22] Due to their rather unstable nature, CuNPs colloids are generally stabilized by polymeric species such as poly(*N*-vinylpyrrolidone) (PVP)[23] or poly(vinyl alcohol) (PVA)[24] for instance. Others investigations in the area relied on the immobilization and stabilization of CuNPs onto polyimide (PI) thin layer,[25] into composite films[26–28] based on organic polymers, or onto metal oxides.[29–31] To the best of our knowledge, such CuNPs have never been immobilized at the surface of porous polymers. In this regard, polymer-based monolithic supports may be candidates of choice as they can be easily prepared and functionalized with a variety of different chemical functions such as amine, thiol or carboxylic groups, *etc.*[32,33] This was notably demonstrated a few years ago by our research group regarding the immobilization of gold NPs on the surface of monolithic poly(*N*-acryloxysuccinimide-*co*-ethylene glycol dimethacrylate)-based (P(NAS-*co*-EGDMA)) capillary.[34] Additionally, it avoids a supplementary purification step in order to recover the metal-based catalyst as it is, in this strategy, entrapped within the porous matrix of a capillary.

Herein, we described unprecedented immobilization of copper nanoparticles at the surface of a monolithic capillary column so as to use the resulting hybrid column as microreactor in the reduction of nitrophenols *via* a flow-through process. After chemical modification of the polymer to

functionalize it with an alkene moiety, a photo-induced thiol-ene "click" chemistry reaction was investigated with mercaptosuccinic acid to graft carboxylic acid moieties onto the polymer matrix surface. Carboxylic acid functions are known to chelate copper ions[35] and CuNPs.[26] Additionally, this strategy allowed for performing this functionalization chemical step in mild conditions generally associated with the "click" thiol-ene process. Two strategies were envisioned to ensure the immobilization of copper nanoparticles. In the first strategy, commercially available preformed copper nanoparticles were percolated into the capillary and consequently immobilized onto the monolithic capillary by adsorption. In the second one, copper (II) ions were adsorbed onto the surface of the monolith *via* dynamic loading. A consecutive step consisting in the hydride-mediated reduction of copper ions allowed for the *in situ* formation of copper nanoparticles. Finally, applications of the as-obtained hybrid monolithic capillaries for flow-through microreactors were successfully investigated.

3.2 Materials and Methods

3.2.1 Experimental

N-Acryloxysuccinimide (NAS, >98%) and toluene (99.8%) were obtained from TCI. 3-(trimethoxysilyl)propyl methacrylate (γ-MAPS, 98%), sodium borohydride ($NaBH_4$, ≥98%), sodium hydroxide (NaOH, 1M), hydrochloric acid (HCl, 0.1M for HPCE), mercaptosuccinic acid (97%), 2,2-dimethoxy-2-phenylacetophenone (DMPA, 99%), copper (II) bromide ($CuBr_2$, 99%) and copper nanopowder (40-60 nm, ≥99.5% trace metals basis) were purchased from Sigma Aldrich. Ethylene glycol dimethacrylate (EGDMA, 98%) and 2,2'-azobisisobutyronitrile (AIBN, 98%) were obtained from Acros Organics. 2-nitrophenol (*o*-nitrophenol, 98%) and allylamine (98%+) were purchased from Alfa Aesar. Acetone, HPLC grade acetonitrile (ACN) and absolute ethanol were supplied by Carlo Erba. All reagents were used without any further purification except from AIBN that was recrystallized from methanol prior to use. 18.2 MΩ deionized water was filtered through a Milli-Q Plus purification pack. Fused silica capillaries with a UV-transparent external coating (100 µm I.D.) were obtained from Polymicro Technologies.

3.2.2 Instrumentation

An HPLC pump (Ultimate 3000 Dionex) was used to flush monolithic columns with 2-nitrophenol solutions along with mobile phase. Spectrolinker XL-1500 UV Crosslinker (Spectronics Corporation) equipped with eight lamps (8 × 15W, 365 nm) was used to photoinitiate the polymerization. UV-Vis spectra were recorded in UV quartz cuvette (1 mm length × 10 mm width × 45 mm height) on a Cary 60 UV-Vis Spectrophotometer from Agilent Technologies using a 5 $nm.s^{-1}$

scanning speed. Chemical Structure of the monoliths was investigated using a Raman apparatus XPlora One from Horiba Jobin Yvon equipped with a laser emitting at 638 nm. Cross sections of the monolith were investigated in different places to ensure for the homogeneity of the monoliths. The acquisition time was fixed at 1 min. Scanning Electron Microscopy (SEM) investigations of the materials were performed with a MERLIN microscope from Zeiss equipped with InLens, BSE and SE2 detectors using a low accelerating tension (2-3 kV) with a diaphragm aperture of 30 µm. Prior to analyses, the samples were coated with a 4-nm layer of palladium/platinum alloy in a Cressington 208 HR sputter-coater. Energy-dispersive X-ray spectroscopy (EDX) was performed using a SSD X-Max detector of 50 mm² from Oxford Instruments (127 eV for the Kα of Mn).

3.2.3 Synthesis of the monolithic capillaries

The synthesis of the (NAS-*co*-EGDMA) monolithic columns relies on a three-step process involving *(i)* the synthesis of the porous acrylate matrix ; *(ii)* the chemical modification of the matrix with allylamine and *(iii)* a thiol-ene reaction with mercaptosuccinic acid.

3.2.3.1 Surface pre-treatment of the capillaries

In order to ensure the stability of the monolithic column, the inner wall of the capillaries was submitted to a vinylization step. 3-(Trimethoxysilyl)propyl methacrylate (γ-MAPS) was used as a bifunctional reagent allowing for the covalent attachment of the polymeric material onto the wall of the capillaries. The procedure was as follows: fused silica capillaries were treated with 1 M NaOH for 1h at room temperature and subsequently heated for 2 h at a temperature of 100 °C. Capillaries were flushed with 0.1 M HCl for 10 min, rinsed with deionized water for 10 min and then with acetone for 15 min. Thereafter, capillaries were purged with dry nitrogen gas for 2 h at a temperature of 120 °C. 30% (v/v) 3-(trimethoxysilyl)propyl methacrylate solution in toluene was allowed to react overnight with inner silanols at room temperature. Last, the capillaries were rinsed with toluene for 15 min and dried under a stream of nitrogen gas for 1 h. The capillaries thus treated were stored at 4 °C prior to use.

3.2.3.2 *In situ* synthesis of the porous monolith

The porous monolith was prepared through a photochemically-driven free radical polymerization reaction of a mixture consisting of the following combination: NAS as a functional monomer (200 mg, 1.09 mmol), EGDMA as a crosslinker (110 µL, 0.58 mmol), toluene as a

porogenic solvent (700 µL) and AIBN as an initiator (4 mg, 1% w/w with respect to the total amount of monomers). The mixture was sonicated for about 15 min to obtain homogeneous solution. The pre-treated capillary was completely filled with the polymerization mixture by immersing the inlet of the capillary into a reservoir and by pushing through the solution previously prepared under nitrogen pressure (3 bar). After flushing with a large excess of polymerization solution, both ends of the capillary were sealed with rubber septa and the capillary was placed within a Spectrolinker XL-1500 UV and irradiated under an overall intensity of 8 $J.cm^{-2}$ (800 s). After the polymerization was completed, the septa were removed and the monolith capillary was washed with ACN for 1 h (5 $\mu L.min^{-1}$) to remove the unreacted monomers and the porogenic solvent.

3.2.3.3 *In situ* functionalization of the porous monolith with allylamine

The activated esters stemming from the NAS monomer were functionalized with alkene groups through nucleophilic substitution. The reaction was performed *in situ* by flushing the monolith capillary with a solution of allylamine (1 M = 160 µL in 2 mL of ACN in a reservoir) pushed under nitrogen pressure (50 bars) during 2 h at room temperature. Thereafter, the monolithic capillary was washed with ACN for 1 h in order to remove the unreacted allylamine. The nucleophilic substitution yield was evaluated through *in situ* Raman spectroscopy performed on monolithic capillary samples.

3.2.3.4 Thiol-ene reaction with mercaptosuccinic acid

The capillary was flushed by anhydrous absolute ethanol for 1 h to remove the previous solvent. Then, the surface-grafted alkene moieties provided the reactive sites for the modification by thiol-containing molecules *via* thiol-ene-based "click" chemistry. Photochemical thiol-ene reaction was proceeded as follows: mercaptosuccinic acid (80 mg, 0.27 M) and DMPA (4 mg, 1 wt%) were dissolved in 2 mL of ethanol absolute. The solution was flushed into the capillary during 2 h under UV light (λ = 365 nm). Then the capillary was rinsed with pure absolute ethanol during 1 h to remove unreacted reagents. Conversion of double bonds was evaluated through *in situ* Raman spectroscopy performed on monolithic capillary samples.

3.2.3.5 Adsorption of preformed copper nanoparticles

The adsorption of preformed copper nanoparticles (CuNPs) was performed under dynamic loading of a deoxygenated solution containing 1 mg of CuNPs in 2 mL of ACN and it was considered complete when the liquid coming out from the capillary column appeared in its original colour. The

colour of the monolith became black upon adsorption of CuNPs, whereas it was previously white, and the colour remained upon thorough rinsing with deoxygenated ACN. The monolithic microreactors were sealed at both ends and stored at room temperature.

3.2.3.6 *In situ* formation of copper nanoparticles

The carboxyl-modified capillary was flushed with a solution of 10 mg of $CuBr_2$ into a 2 mL mixture of ACN and water (70/30 v/v) during 1 h. it was then rinsed with a deoxygenated mixture of ACN and water (70/30 v/v) during 1 h to remove the non-adsorbed copper ions. Then a solution of 7 mg of $NaBH_4$ (0.1 M) in the same deoxygenated mixture was flushed during 30 min. Finally the capillary was washed 30 min by a deoxygenated solution of the same solvent mixture. The monolithic microreactors were sealed at both ends and stored at room temperature.

3.2.3.7 Reduction of *o*-nitrophenol by heterogeneous catalysis

A freshly prepared solution containing 200 µL of *o*-nitrophenol (5 mg in 10 mL ACN/H_2O – 70/30 v/v), 200 µL of $NaBH_4$ (114 mg in 10 mL ACN/H_2O – 70/30 v/v) in 5 mL ACN/H_2O (70/30 v/v) was injected in the loop (20 µL, Rheodyne) of a HPLC pump system, the solution coming out from the in-capillary CuNPs decorated monoliths was collected and then analysed by UV-Vis spectrophotometry. This UV study was conducted on both capillary types containing either *in situ* generated CuNPs at different flow rates (1.5 $\mu L.min^{-1}$; 4 $\mu L.min^{-1}$) or containing preformed CuNPs (0.3 $\mu L.min^{-1}$). To undoubtedly evidence the catalytic effect of CuNPs, blank tests were performed with monolithic microreactors without nanoparticles.

3.3 Results and Discussions

3.3.1 Functionalization of the in-capillary polymer monolith

A three-step process was necessary for preparing a –COOH-grafted porous monolith within a fused silica capillary (inner diameter of 100 µm) *via* a thiol-ene “click” chemistry reaction, as shown on **Figure 3-1**.

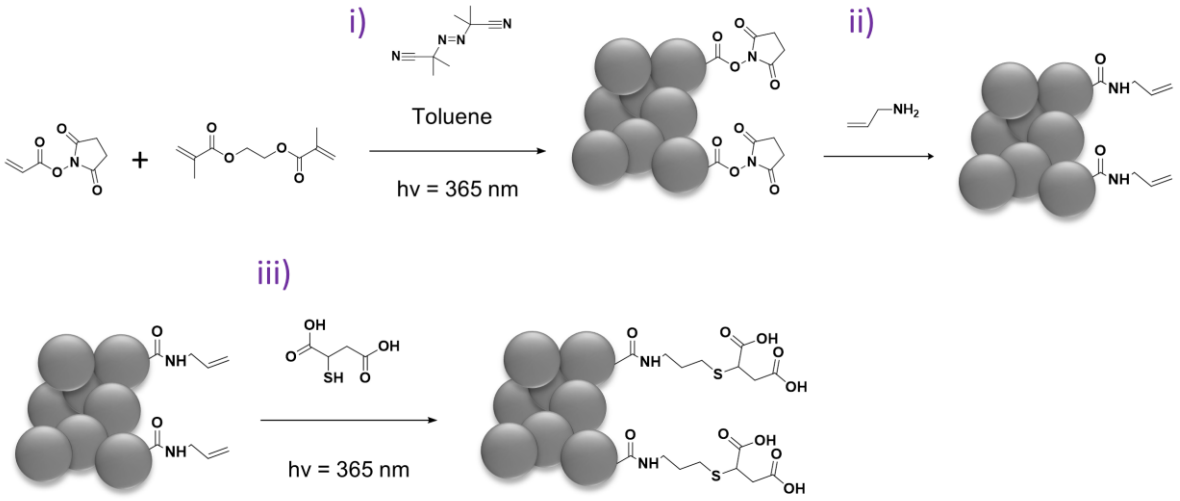

Figure 3-1: Schematic representation of the synthetic route applied to designing monolith with carboxylic acid chelating groups *via* successive *i)* free-radical photopolymerization, *ii)* nucleophilic substitution and *iii)* photo-triggered thiol-ene radical addition.

After activation of the inner wall of the capillary in the presence of 3-(trimethoxysilyl)propyl methacrylate (γ-MAPS), *N*-acryloxysuccinimide (NAS), a functional reactive monomer and ethylene glycol dimethacrylate (EGDMA), a cross-linking agent, were copolymerized in the presence of azobisisobutyronitrile (AIBN, 1% w/w, with respect to the total amount of monomers) and toluene as, a radical initiator and a porogenic solvent, respectively. Upon filling the pre-activated capillary with the polymerization mixture, sealing of the extremities with rubber septa and subsequent photo-initiated copolymerization within a UV oven, an in-capillary poly(*N*-acryloxysuccinimide-*co*-ethylene glycol dimethacrylate) P(NAS-*co*-EGDMA) monolith was obtained with exposed nucleophilic-sensitive *N*-hydroxysuccinimide activated ester functionalities and well-defined interconnected pores in the micrometer-size range as observed by scanning electron microscopy of the monolithic column on **Figure 3-3**. Additionally, the characteristic peaks of the NAS-based activated ester were confirmed by *in situ* Raman spectroscopy as shown on **Figure 3-2 a** that clearly evidenced the presence of the three characteristic bands of NAS at 1730 (imide asymmetric stretching), 1785 (imide symmetric stretching) and 1812 cm^{-1} (activated ester stretching), as reported in previous studies.[34,36–38]

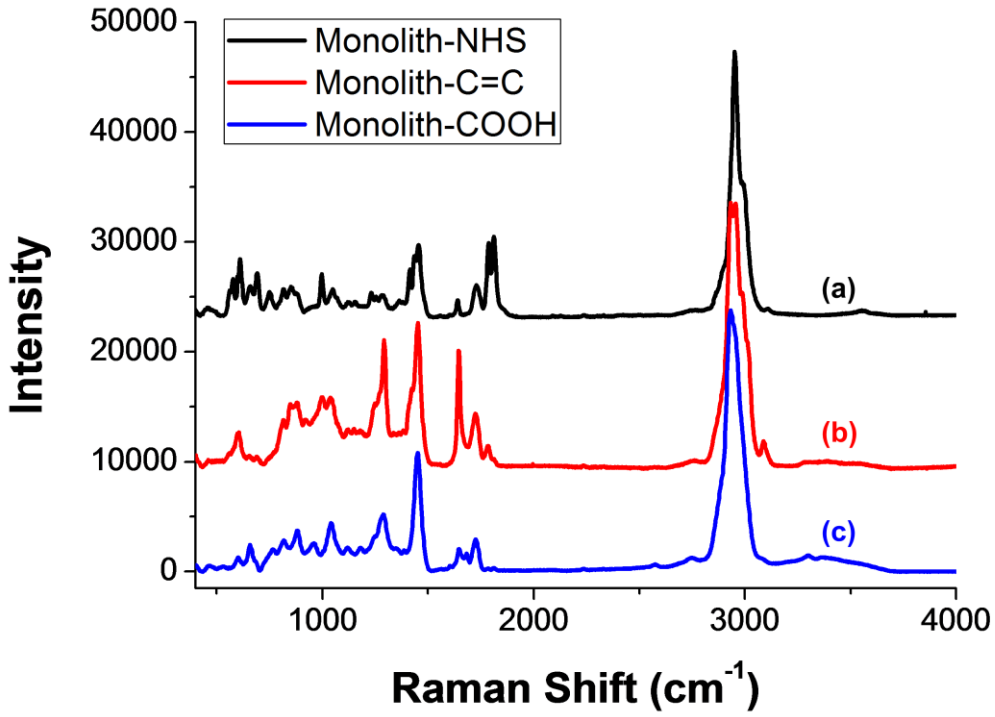

Figure 3-2: Raman spectra of the obtained functionalized in-capillary monoliths: *a) N*-hydroxysuccinimide activated ester containing monolith after polymerization, *b)* alkene functionalized monolith after nucleophilic substitution of the NHS activated esters with allyl amine and *c)* carboxylic acid decorated monolith after thiol-ene addition reaction in presence of mercaptosuccinic acid.

The first modification of the porous polymer consisted in the nucleophilic substitution of the activated ester with allylamine. Indeed, this chemical species presents both nucleophilic amine group for substituting activated ester and an alkene moiety for performing subsequent mild radical thiol-ene addition with selectors/compounds of interest depending on the targeted application. Flushing of allylamine through the capillary allowed, virtually, total consumption of the *N*-hydroxysuccinimide activated ester moieties on the monolith surface, thus permitting the formation of covalent amide bond with the terminal amine function of allylamine. This was notably ascertained by *in situ* Raman spectroscopy of the monolithic capillary. Indeed, disappearance of the NAS characteristic peaks (at 1785 and 1812 cm^{-1}) along with the appearance of a new peak assigned to the allylamine double bond elongation band (ν(C=C) = 1645 cm^{-1}) was observed, as shown on **Figure 3-2 b**, demonstrating the efficient grafting of allylamine onto the porous polymer.[37] Finally, radical thiol-ene addition reaction with mercaptosuccinic acid allowed for the successful anchoring of carboxylic acid functions at the surface of the monolith. This was again demonstrated by *in situ* Raman spectroscopy that evidenced a strong disappearance of the olefin bond signal as shown on **Figure 3-2 c**, thus demonstrating the efficiency of these "click" chemistry reaction for surface chemistry, as reported in previous studies.[37]

The presence of the grafted carboxylic acid functions on the monolith surface should ensure copper ions[35] coordination and, as a consequence, adsorption of copper nanoparticles[26] over the polymeric monolith.

3.3.2 Adsorption of preformed CuNPs and *in situ* formation of CuNPs

Stabilisation and immobilisation of CuNPs in a polymer have been realized in solution and on a polymer film with different functions such as imide,[25] amine[28] or alcohol[24] functions. However, to the best of our knowledge, CuNPs immobilized onto an in-capillary porous polymer matrix is for the first time reported.

Table 3-1: EDX semi-quantitative elemental analysis of the two different hybrid monolithic capillaries prepared *via* the *in situ* or *ex situ* methodologies, respectively.

Element	***ex situ* strategy wt%[a]**	***in situ* strategy wt%[a]**
C	57.99	54.28
N	5.00	6.86
O	20.56	24.55
S	3.95	5.22
Cu	12.50	9.10

[a] Average values determined after three successive measurements

Two pathways were considered. On the one hand, a methodology consisting in the immobilization of percolated preformed CuNPs was adapted. SEM pictures (**Figure 3-3**) demonstrated the efficiency of the immobilization of CuNPs while EDX spectrum (**Table 3-1**, spectrum not shown) corroborate the chemical nature of the nanoparticles, *i.e.* copper. On the other hand, dynamic loading of Cu (II) ions solution followed by their *in situ* hydride-mediated chemical reduction was performed in the presence of $NaBH_4$. SEM pictures, as shown on **Figure 3-3**, revealed the presence of nanoparticles over the surface of both monoliths, *i.e.* those prepared *via* the *in situ* or the *ex situ* methodologies, respectively. More interestingly, careful investigation of the CuNPs adsorbed monolith clearly indicated that a homogeneous and sparse coverage of the polymeric surface was obtained in the case of *in situ* generated NPs, with particle average diameter in the 39 ± 8 nm range. On the other hand, percolation of preformed CuNPs in the carboxylic acid functionalized monolith also allowed for

the adsorption of NPs on the surface. However, in this particular case, a non-negligible quantity of aggregated CuNPs was observed along with a more heterogeneous and dense distribution. In that case, the average diameter of the particles was found to be around 68 ± 16 nm. Elemental semi-quantitative analysis by EDX was also realized on both monoliths so as to ascertain the chemical nature of the NPs. Results gathered in **Table 3-1** indicated that the *ex situ* methodology allows for higher CuNPs adsorption on the monolith surface than with the *in situ* methodology (12.50 wt% *vs.* 9.10 wt%, respectively).

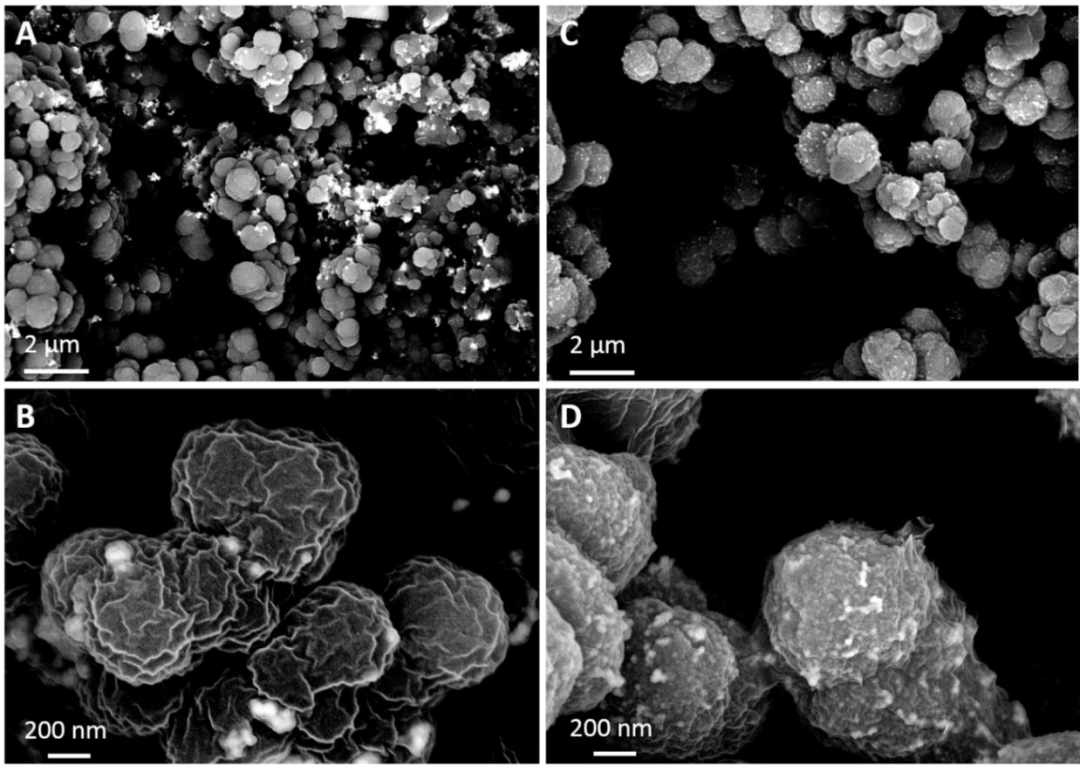

Figure 3-3: Scanning electron micrographs of the hybrid monoliths' surface after *A)* and *B)* immobilization of preformed CuNPs or *C)* and *D) in situ* generation of CuNPs, respectively.

3.3.3 Reduction of 2-nitrophenol

CuNPs are prone to act as nanocatalysts for the reduction of nitroarene derivatives in the presence of a reducing agent, *i.e.* sodium borohydride (**Figure 3-3**). To this purpose, a solution of *o*-nitrophenol and $NaBH_4$ in a mixture of ACN and water (70/30 v/v) was injected through the loop of an HPLC pump into a 7 cm length capillary containing *in situ* generated CuNPs, as shown on **Figure 3-4**, at two different flow rates (4 µL.min^{-1} and 1.5 µL.min^{-1}). According to the UV spectra of the resulting incoming and outgoing solutions shown on **Figure 3-3 C & D**, the reaction yield of this catalytic reduction is dependent on the pump flowrate. Indeed, the lower the flowrate, the higher the reaction yields (40% at 4 µL.min^{-1} *vs.* 55% at 1.5 µL.min^{-1}). This can be easily explained by a longer contact

time of *o*-nitrophenol and $NaBH_4$ with the monolith-adsorbed nanometals when the flowrate is low. However, working at flow rates below 1.5 µL.min^{-1} do not allow sufficient internal pressure in order for the solution to percolate through the hybrid monolith. In all cases, the reaction yields were also better when longer copper nanoparticles adsorbed hybrid in-capillary monoliths were used, again demonstrating that a more prolonged contact time of the reactant solution with the adsorbed copper nanoparticles allows for more efficient catalysis (data not shown).

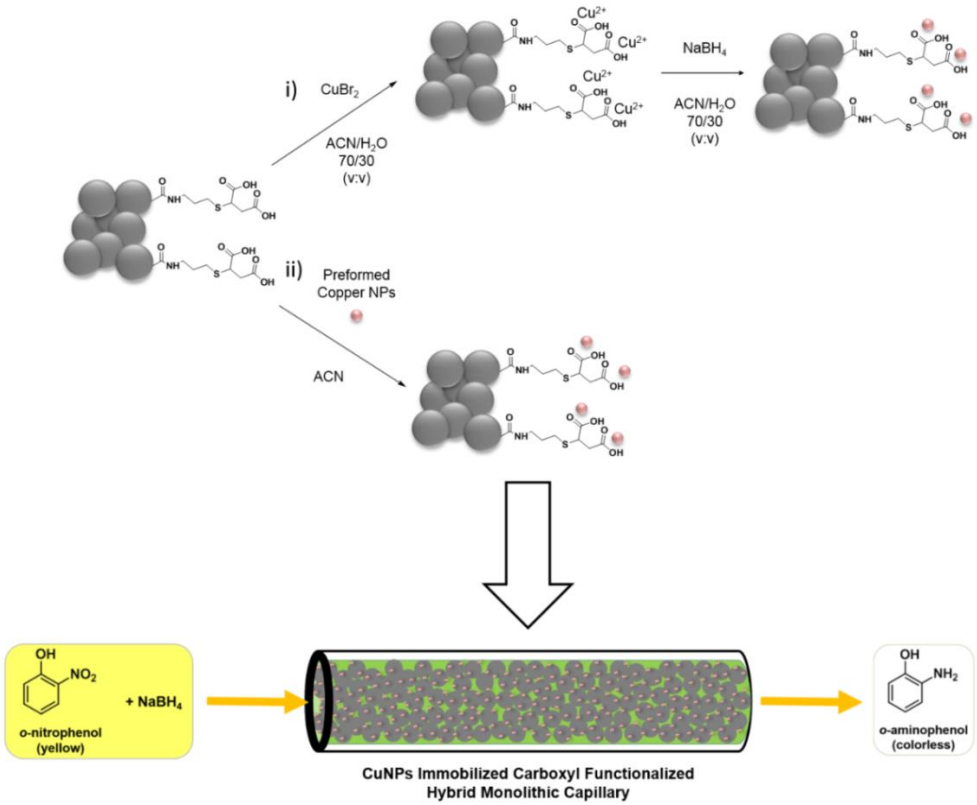

Figure 3-4: Schematic representation of the strategies applied for the surface immobilization of copper nanoparticles on carboxylic acid-functionalized monolith *via i)* surface chelation of copper ions and subsequent hydride-mediated formation of copper nanoparticles and *ii)* adsorption of colloidal solution of copper nanoparticles and subsequent flow-through reduction of nitroarene in the as-obtained in-capillary hybrid monolithic microreactors.

This catalytic reduction was also assessed with the hybrid capillary generated upon percolation of preformed CuNPs (7 cm length). Unfortunately, due to too high internal pressure in this capillary resulting most probably from CuNPs aggregation, the flow rate should be drastically reduced (0.3 µL.min^{-1}) to allow for the *o*-nitrophenol/$NaBH_4$ solution to percolate through the capillary. However, an UV spectrum was recorded and it demonstrated that the catalysis occurs with a rather satisfying 68.5% yield (cf. **Figure 3-5 B**).

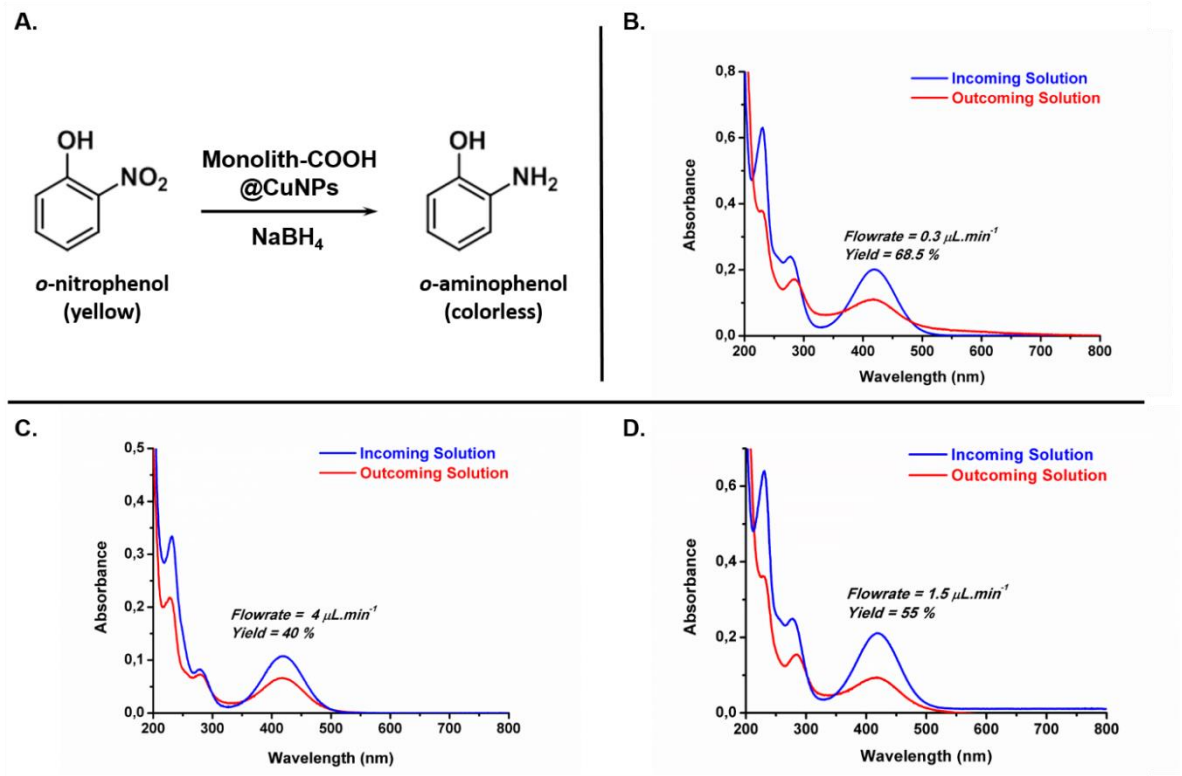

Figure 3-5: UV-visible investigation of the in-capillary monolith adsorbed CuNPs-mediated catalytic transformation of *A) o*-nitrophenol into the corresponding *o*-aminophenol. UV spectra recorded in the 200-800 nm wavelength range for $NaBH_4$/nitrophenol solutions before (blue trace, incoming) and after (red trace, outcoming) percolation through monolithic capillary microreactors with *B)* adsorbed preformed CuNPs or *C)* and *D) in situ*-generated CuNPs though reduction of copper ions. The flow rates applied for the catalytic reactions and the corresponding reaction yields are indicated directly in the figure.

3.4 Conclusion

In conclusion, a facile synthetic route towards CuNPs@carboxylic acid functionalized in-capillary polymeric monoliths has been developed *via* an atom economy-based thiol-ene "click" addition reaction and subsequent immobilization of CuNPs through either *in situ* or *ex situ* strategy. The hydride-mediated catalysed chemical reduction of *o*-nitrophenol through these hybrid monolithic microreactors was successfully demonstrated and evidenced in the case of both *in situ*- and *ex situ*-generated hybrid monoliths. It should pave the way towards other nanometal-catalyzed chemical reactions such as CuAAC reaction for instance.

3.5 References

(1) Panigrahi, S.; Basu, S.; Praharaj, S.; Pande, S.; Jana, S.; Pal, A.; Ghosh, S. K.; Pal, T. Synthesis and Size-Selective Catalysis by Supported Gold Nanoparticles: Study on Heterogeneous and Homogeneous Catalytic Process. *J. Phys. Chem. C* **2007**, *111* (12), 4596–4605.

(2) Gallon, B. J.; Kojima, R. W.; Kaner, R. B.; Diaconescu, P. L. Palladium Nanoparticles Supported on Polyaniline Nanofibers as a Semi-Heterogeneous Catalyst in Water. *Angew. Chem. Int. Ed.* **2007**, *46* (38), 7251–7254.

(3) Mandal, S.; Roy, D.; Chaudhari, R. V.; Sastry, M. Pt and Pd Nanoparticles Immobilized on Amine-Functionalized Zeolite: Excellent Catalysts for Hydrogenation and Heck Reactions. *Chem. Mater.* **2004**, *16* (19), 3714–3724.

(4) Jiang, Z.-J.; Liu, C.-Y.; Sun, L.-W. Catalytic Properties of Silver Nanoparticles Supported on Silica Spheres. *J. Phys. Chem. B* **2005**, *109* (5), 1730–1735.

(5) Han, J.; Liu, Y.; Guo, R. Facile Synthesis of Highly Stable Gold Nanoparticles and Their Unexpected Excellent Catalytic Activity for Suzuki−Miyaura Cross-Coupling Reaction in Water. *J. Am. Chem. Soc.* **2009**, *131* (6), 2060–2061.

(6) Campelo, J. M.; Luna, D.; Luque, R.; Marinas, J. M.; Romero, A. A. Sustainable Preparation of Supported Metal Nanoparticles and Their Applications in Catalysis. *ChemSusChem* **2009**, *2* (1), 18–45.

(7) Venkatesan, P.; Santhanalakshmi, J. Designed Synthesis of Au/Ag/Pd Trimetallic Nanoparticle-Based Catalysts for Sonogashira Coupling Reactions. *Langmuir* **2010**, *26* (14), 12225–12229.

(8) Cassol, C. C.; Umpierre, A. P.; Machado, G.; Wolke, S. I.; Dupont, J. The Role of Pd Nanoparticles in Ionic Liquid in the Heck Reaction. *J. Am. Chem. Soc.* **2005**, *127* (10), 3298–3299.

(9) Kuroda, K.; Ishida, T.; Haruta, M. Reduction of 4-Nitrophenol to 4-Aminophenol over Au Nanoparticles Deposited on PMMA. *J. Mol. Catal. Chem.* **2009**, *298* (1), 7–11.

(10) Saha, S.; Pal, A.; Kundu, S.; Basu, S.; Pal, T. Photochemical Green Synthesis of Calcium-Alginate-Stabilized Ag and Au Nanoparticles and Their Catalytic Application to 4-Nitrophenol Reduction. *Langmuir* **2010**, *26* (4), 2885–2893.

(11) Pradhan, N.; Pal, A.; Pal, T. Catalytic Reduction of Aromatic Nitro Compounds by Coinage Metal Nanoparticles. *Langmuir* **2001**, *17* (5), 1800–1802.

(12) Harish, S.; Mathiyarasu, J.; Phani, K. L. N.; Yegnaraman, V. Synthesis of Conducting Polymer Supported Pd Nanoparticles in Aqueous Medium and Catalytic Activity Towards 4-Nitrophenol Reduction. *Catal. Lett.* **2008**, *128* (1), 197.

(13) Esumi, K.; Isono, R.; Yoshimura, T. Preparation of PAMAM− and PPI−Metal (Silver, Platinum, and Palladium) Nanocomposites and Their Catalytic Activities for Reduction of 4-Nitrophenol. *Langmuir* **2004**, *20* (1), 237–243.

(14) Sethi, M.; Law, W.-C.; Fennell, W. A.; Prasad, P. N.; Knecht, M. R. Employing Materials Assembly to Elucidate Surface Interactions of Amino Acids with Au Nanoparticles. *Soft Matter* **2011**, *7* (14), 6532–6541.

(15) Ramezani-Dakhel, H.; Mirau, P. A.; Naik, R. R.; Knecht, M. R.; Heinz, H. Stability, Surface Features, and Atom Leaching of Palladium Nanoparticles: Toward Prediction of Catalytic Functionality. *Phys. Chem. Chem. Phys.* **2013**, *15* (15), 5488–5492.

(16) Coppage, R.; Slocik, J. M.; Ramezani-Dakhel, H.; Bedford, N. M.; Heinz, H.; Naik, R. R.; Knecht, M. R. Exploiting Localized Surface Binding Effects to Enhance the Catalytic Reactivity of Peptide-Capped Nanoparticles. *J. Am. Chem. Soc.* **2013**, *135* (30), 11048–11054.

(17) Cioffi, N.; Torsi, L.; Ditaranto, N.; Tantillo, G.; Ghibelli, L.; Sabbatini, L.; Bleve-Zacheo, T.; D'Alessio, M.; Zambonin, P. G.; Traversa, E. Copper Nanoparticle/Polymer Composites with Antifungal and Bacteriostatic Properties. *Chem. Mater.* **2005**, *17* (21), 5255–5262.

(18) Mary, G.; Bajpai, S. K.; Chand, N. Copper (II) Ions and Copper Nanoparticles-Loaded Chemically Modified Cotton Cellulose Fibers with Fair Antibacterial Properties. *J. Appl. Polym. Sci.* **2009**, *113* (2), 757–766.

(19) Kumar, A.; Aerry, S.; Saxena, A.; de, A.; Mozumdar, S. Copper Nanoparticulates in Guar-Gum: A Recyclable Catalytic System for the Huisgen [3 + 2]-Cycloaddition of Azides and Alkynes without Additives under Ambient Conditions. *Green Chem.* **2012**, *14* (5), 1298–1301.

(20) Duan, Z.; Ma, G.; Zhang, W. Preparation of Copper Nanoparticles and Catalytic Properties for the Reduction of Aromatic Nitro Compounds. *Bull. Korean Chem. Soc.* **2012**, *33* (12), 4003–4006.

(21) Saha, A.; Ranu, B. Highly Chemoselective Reduction of Aromatic Nitro Compounds by Copper Nanoparticles/Ammonium Formate. *J. Org. Chem.* **2008**, *73* (17), 6867–6870.

(22) Deka, P.; Deka, R. C.; Bharali, P. In Situ Generated Copper Nanoparticle Catalyzed Reduction of 4-Nitrophenol. *New J. Chem.* **2014**, *38* (4), 1789–1793.

(23) Kapoor, S.; Mukherjee, T. Photochemical Formation of Copper Nanoparticles in Poly(N-Vinylpyrrolidone). *Chem. Phys. Lett.* **2003**, *370* (1), 83–87.

(24) Li, Z.; Huang, H.; Wang, C. Electrostatic Forces Induce Poly(Vinyl Alcohol)-Protected Copper Nanoparticles to Form Copper/Poly(Vinyl Alcohol) Nanocables via Electrospinning. *Macromol. Rapid Commun.* **2006**, *27* (2), 152–155.

(25) Ikeda, S.; Akamatsu, K.; Nawafune, H.; Nishino, T.; Deki, S. Formation and Growth of Copper Nanoparticles from Ion-Doped Precursor Polyimide Layers. *J. Phys. Chem. B* **2004**, *108* (40), 15599–15607.

(26) Gotoh, Y.; Igarashi, (the late) Ryo; Ohkoshi, Y.; Nagura, M.; Akamatsu, K.; Deki, S. Preparation and Structure of Copper Nanoparticle/Poly(Acrylic Acid) Composite Films. *J. Mater. Chem.* **2000**, *10* (11), 2548–2552.

(27) Mallick, K.; Witcomb, M. J.; Scurrell, M. S. Preparation and Characterization of a Conjugated Polymer and Copper Nanoparticle Composite Material: A Chemical Synthesis Route. *Mater. Sci. Eng. B* **2005**, *123* (2), 181–186.

(28) Mallick, K.; Witcomb, M. J.; Scurrell, M. S. In Situ Synthesis of Copper Nanoparticles and Poly(o-Toluidine): A Metal–polymer Composite Material. *Eur. Polym. J.* **2006**, *42* (3), 670–675.

(29) Rodríguez, J. A.; Liu, P.; Hrbek, J.; Pérez, M.; Evans, J. Water–gas Shift Activity of Au and Cu Nanoparticles Supported on Molybdenum Oxides. *J. Mol. Catal. Chem.* **2008**, *281* (1), 59–65.

(30) Rodriguez, J. A.; Liu, P.; Wang, X.; Wen, W.; Hanson, J.; Hrbek, J.; Pérez, M.; Evans, J. Water-Gas Shift Activity of Cu Surfaces and Cu Nanoparticles Supported on Metal Oxides. *Catal. Today* **2009**, *143* (1), 45–50.

(31) Safiullah, S. M.; Wasi, K. A.; Basha, K. A. Preparation of Poly(Glycidyl Methacrylate)–copper Nanocomposite by in-Situ Suspension Polymerization – A Novel Synthetic Method. *Mater. Lett.* **2014**, *133*, 60–63.

(32) Buchmeiser, M. R. Polymeric Monolithic Materials: Syntheses, Properties, Functionalization and Applications. *Polymer* **2007**, *48* (8), 2187–2198.

(33) Svec, F. Porous Polymer Monoliths: Amazingly Wide Variety of Techniques Enabling Their Preparation. *J. Chromatogr. A* **2010**, *1217* (6), 902–924.

(34) Guerrouache, M.; Mahouche-Chergui, S.; Chehimi, M. M.; Carbonnier, B. Site-Specific Immobilisation of Gold Nanoparticles on a Porous Monolith Surface by Using a Thiol-Yne Click Photopatterning Approach. *Chem. Commun.* **2012**, *48* (60), 7486–7488.

(35) Han, J.; Du, Z.; Zou, W.; Li, H.; Zhang, C. Fabrication of Interfacial Functionalized Porous Polymer Monolith and Its Adsorption Properties of Copper Ions. *J. Hazard. Mater.* **2014**, *276*, 225–231.

(36) Tijunelyte, I.; Babinot, J.; Guerrouache, M.; Valincius, G.; Carbonnier, B. Hydrophilic Monolith with Ethylene Glycol-Based Grafts Prepared via Surface Confined Thiol-Ene Click Photoaddition. *Polymer* **2012**, *53* (1), 29–36.

(37) Guerrouache, M.; Millot, M.-C.; Carbonnier, B. Functionalization of Macroporous Organic Polymer Monolith Based on Succinimide Ester Reactivity for Chiral Capillary Chromatography: A Cyclodextrin Click Approach. *Macromol. Rapid Commun.* **2009**, *30* (2), 109–113.

(38) Guerrouache, M.; Mahouche-Chergui, S.; Mekhalif, T.; Dao, T. T. H.; Chehimi, M. M.; Carbonnier, B. Engineering the Surface Chemistry of Porous Polymers by Click Chemistry and Evaluating the Interface Properties by Raman Spectroscopy and Electrochromatography. *Surf. Interface Anal.* **2014**, *46* (10–11), 1009–1013.

Amine Functionalized In-Capillary Monoliths Supported Gold Nanoparticles Meant for Flow-Through Catalysis: A Comparative Study

Abstract: Monoliths functionalized with ethylene diamine-derived ligands were synthetized within micro-sized channel as permeable supports for the preparation of amine functionalized polymeric monoliths supported gold nanoparticles. The as-obtained hybrids, essentially differing on the grafted amine containing ligands were compared, notably regarding the immobilized nanoparticles morphology and their dispersion at the monolith pore surface. Further, such in-capillary hybrid monoliths were successfully applied as flow-through microreactors for the catalytic reduction of nitroaromatic compounds. The general synthetic route for preparing these composite materials consisted in a two-step procedure involving (*i*) UV-induced polymerization of *N*-acryloxysuccinimide and ethylene glycol dimethacrylate in toluene, (*ii*) surface grafting of a series of ethylene diamine derivatives through nucleophilic substitution of *N*-hydroxysuccinimide leaving groups, and (*iii*) successive *in situ* reduction of tetrachloroauric acid to generate monolith-adsorbed gold nanoparticles. The successful synthesis of such hybrid materials and of the intermediate monoliths was ascertained by *in-situ* Raman spectroscopy, EDX analysis and SEM observations. Microscopy notably demonstrated the key role of the grafted amine bearing ligand regarding the morphology, size and surface coverage of the immobilized gold nanoparticles at the monolith pore surface. Monolith adsorbed gold nanoparticles exhibited good catalytic activities towards the conversion of nitroaromatic compounds into the corresponding amino derivatives following a flow-through process.

3.6 Introduction

Miniaturization in materials chemistry had led to the development and the improvement of various strategies and methods to design and tailor performant microreactors. Among this type of reactors notably exist polymer-based systems that are very promising for flow-through catalytic processes.[1–5] The properties of the continuous interconnected porous polymer matrix, also called monolith, which can be easily prepared by polymerization of various commercially available styrenic or (meth)acrylic monomers can be tuned by grafting of ligands so as to change the interfacial features of the polymeric surface. For instance, the polymer matrix can be tuned with different chemical functions (*e.g.* amine, thiol, cyano or carboxylic acid among them) that notably allow for the grafting of several metallic nanoparticles. Svec *et al.*[6] pioneered the use of such cross-linked polymers as monolithic stationary phases for electrochromatographic and chromatographic applications.[7] Since, the technology has evolved and has been broadened to a plethora of solutes (hydrophobic, hydrophilic, ionic and chiral) that can be now efficiently separated.

On the other hand, metallic nanoparticles are well-known as supported nano-catalysts for various organic reactions: dyes reduction,[8] nitrocompounds reduction[9,10] or C-C cross-coupling such as Heck,[11,12] Sonogashira[13] or Suzuki-Miyaura[14] reactions. Noble metal-based nanoparticles relying on platinum,[12] palladium[9,15] or silver[16] have also been the subject of numerous studies. However, gold is so far the most commonly used noble metal for such hybrid-based heterogeneous catalyzed reactions.[17] One of the major advantages of such metallic nanoparticle-immobilized monolith relies on the facile supported catalyst recovery and the easy reusability of the hybrid systems. In the last years, such hybrids nanoparticles@polymer composites have been prepared into micro-sized capillary columns that allow for their use into flow-through systems. Svec research group reported for instance the preparation of poly(glycidyl methacrylate-*co*-ethylene glycol dimethacrylate)-based monoliths that were successively chemically modified with thiol functions.[18,19] Such sulfhydryl functions were used to tightly immobilize gold nanoparticles. Alternatively, our group took advantage of the amine functions of both cysteamine and ethylene diamine to anchor gold nanoparticles at the pore surface of *N*-acryloxysuccinimide-based monolithic columns.[20] On top of that, Liu *et al.* recently used another imidazole containing ligand, *i.e.* histamine, to the same purpose. Site-specific immobilization of commercially available preformed gold nanoparticles was achieved upon facile and straightforward dynamic loading of the functionalized monolithic capillary with a gold colloidal solution.[3] Other strategies to efficiently anchor gold nanoparticles onto porous materials rely on their preparation through an *in-situ* process involving percolation of a chloroauric acid solution as a GNP precursor and subsequent reduction of metallic ions with sodium borohydride[21] or *via* the Turkevitch method[22] involving citrate.[23]

As aforementioned, studies on nanometals immobilized at the pore surface of polymers generally focus their investigations on the ability of different chemical function (*e.g.* thiol, amine, *etc*) to chelate metallic ions.[18–20] Simultaneously, other efforts have been made to fully understand the nucleation and growth processes of the gold nanoparticles in colloidal solution.[24,25] However, no investigation regarding the shape of the metal ligand has been so far developed. In this context, we decided to investigate the effect of amine-derived ligand shape at the pore surface of such polymeric monolithic columns on the chelation of gold nanoparticles. Thus, ethylene diamine derivatives are prone to chelate a wide variety of metal ions.

Hence, we investigate in this work on the importance of the crucial role of chelating groups anchored at the monolith surface, notably in terms of gold nanoparticle morphology, dispersion and homogeneity. Experimentally, ethylenediamine (EDA), tetraethylenepentamine (TETRA), 1-(2-aminoethyl)piperazine (AEP) and tris(2-aminoethyl)amine (TRIS) were used as ligands of choice while *in situ* prepared gold nanoparticles were immobilized onto the amine-functionalized monolith *via* reduction of $HAuCl_4$ with sodium borohydride ($NaBH_4$). The as-obtained monoliths were finely characterized, notably by scanning electron microscopy (SEM) and Energy-dispersive X-ray spectroscopy (EDX). Finally, these hybrid monoliths were successfully applied to the flow-through reduction of nitro-compounds in the presence of $NaBH_4$. This work notably allowed to establish relationships between the shape of the ligand and that of the immobilized gold nanoparticles.

3.7 Materials and Methods

3.7.1 Experimental

N-Acryloxysuccinimide (NAS, ≥98%) and toluene (>99.5%) were obtained from TCI. 3-(Trimethoxysilyl)propyl methacrylate (γ-MAPS, 98%), sodium borohydride ($NaBH_4$, 98%), sodium hydroxide (NaOH, 0.1 M for HPCE), hydrochloric acid (HCl, 0.1 M for HPCE), ethylenediamine (EDA, ≥99.8%), tris(2-aminoethyl)amine (TRIS, 96%), tetraethylenepentamine (TETRA, 98%), 1-(2-aminoethyl)piperazine (AEP, 99%) and 4-nitroaniline (*p*-nitroaniline, ≥99%) were purchased from Sigma Aldrich. Ethylene glycol dimethacrylate (EGDMA, 98%) and 2,2'-azobisisobutyronitrile (AIBN, 98%) were obtained from Acros Organics. 2-Nitrophenol (*o*-nitrophenol, 98%) and 4-chloro-7-nitrobenzofurazan (99%) were purchased from Alfa Aesar. Acetone, and HPLC grade acetonitrile (ACN) were supplied by Carlo Erba. All reagents were used without any further purification except from AIBN that was recrystallized from MeOH and stored at 4 °C prior to use. 18.2 MΩ deionized water was filtered through a Milli-Q Plus purification pack. Fused silica capillaries with a UV-transparent external coating (100 µm I.D.) were obtained from Polymicro Technologies.

3.7.2 Instrumentation

An HPLC pump (Shimadzu LC-10ATVP) was used to flush monolithic columns with nitroarenes solutions along with mobile phase. Spectrolinker XL-1500 UV Crosslinker (Spectronics Corporation) equipped with eight lamps (8 × 15W, 365 nm) was used to photoinitiate the monolith polymerization. UV-Vis spectra were recorded on a Cary 60 UV-Vis Spectrophotometer from Agilent Technologies. Chemical Structure of the monoliths was investigated using a Raman apparatus XPlora One from Horiba Jobin Yvon equipped with a laser emitting at λ = 638 nm. Samples were investigated in different places of the cross sections to control the homogeneity of the monoliths. The acquisition time was fixed at 1 min. Scanning Electron Microscopy (SEM) investigations of the materials were performed with a MERLIN microscope from Zeiss equipped with InLens, EBSD and SE2 detectors using a low accelerating tension (2-3 kV) with a diaphragm aperture of 30 µm. Prior to analyses, the samples were coated with a 4-nm layer of palladium/platinum alloy in a Cressington 208 HR sputter-coater. Energy-dispersive X-ray spectroscopy (EDX) was performed using a SSD X-Max detector of 50 mm^2 from Oxford Instruments (127 eV for the Kα ray of Mn).

3.7.3 Synthesis of the monolithic capillaries

The synthesis of the separative monolithic columns relies on a two-step process involving *(i)* the synthesis of the macroporous acrylate-based matrix and *(ii)* the surface chemical modification of the matrix with one of the amine ligands, as shown on **Figure 3-6**.

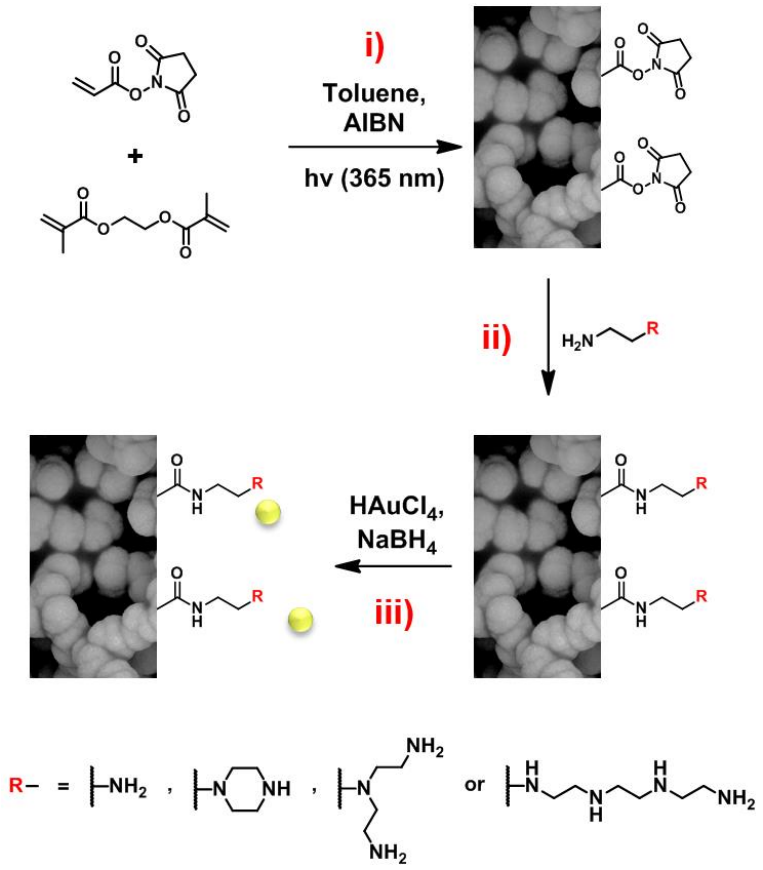

Figure 3-6: Schematic representation of the synthetic route applied to the design and synthesis of P(NAS-*co*-EGDMA) monoliths grafted with different ethylene diamine derivatives for the immobilization of *in-situ* generated gold nanoparticles: *i)* P(NAS-*co*-EGDMA) monolith synthesis, *ii)* functionalization of the P(NAS-*co*-EGDMA) with amine containing ligands and *iii)* immobilization of gold nanoparticles at the pore surface of amine functionalized P(NAS-*co*-EGDMA) monoliths *via* the *in-situ* strategy.

3.7.3.1 Surface pre-treatment of the capillaries

In order to ensure the stability of the monolithic column, the inner wall of the capillaries was submitted to a vinylization step. 3-(Trimethoxysilyl)propyl methacrylate was used as a bifunctional reagent allowing the covalent attachment of the polymeric material onto the inner wall of the capillaries. The procedure was as follows: fused silica capillaries were treated with 1.0 M NaOH for 1h at room temperature and subsequently heated for 2 h at a temperature of 100 °C. Capillaries were flushed with 0.1 M HCl for 10 min, rinsed with deionized water for 10 min and then with acetone for 15 min. thereafter, capillaries were purged with dry nitrogen gas for 2 h at a temperature of 120 °C. 3-(Trimethoxysilyl)propyl methacrylate 30% (v/v) solution in toluene was allowed to react overnight

with inner silanols at room temperature. Last, the capillaries were rinsed with toluene for 15 min and dried under a stream of nitrogen gas for 1 h. The capillaries thus treated were stored at 4 °C.

3.7.3.2 *In situ* synthesis of the porous monolith

The porous monolith was prepared through a polymerization reaction of a mixture consisting of the following combination: NAS as a functional monomer, EGDMA as a crosslinker, toluene as a porogenic solvent and AIBN as an initiator (1%, w/w, with respect of the total amount of monomers). The mixture was sonicated for about 15 min to obtain 15 min to obtain homogeneous solution. The pre-treated capillary was completely filled with the polymerization mixture by immersing the inlet of the capillary into a reservoir and by pushing through the solution under nitrogen pressure (3 bar). After flushing with a large excess of polymerization solution, both ends of the capillary were sealed with rubber septa and the capillary was placed within a Spectrolinker XL-1500 UV and irradiated under an overall intensity of 8 $J.cm^{-2}$ during 800s. After the polymerization was completed, the septa were removed and the monolith capillary was washed with ACN for 1 h (5 $\mu L.min^{-1}$) to remove the unreacted monomers and the porogenic solvent.

3.7.3.3 *In situ* functionalization of the porous monolith with amine ligands

The succinimide groups stemming from the NAS monomer were replace into different amines groups through nucleophilic substitution reaction. The reaction was performed *in-situ* by flushing the monolith capillary with a solution of EDA, TRIS or AEP (0.3 M ≈ 100 µL in 2 mL of ACN in a reservoir) or TETRA (0.3 M = 200 µL in 2 mL of ACN in a reservoir) pushed under nitrogen pressure (50 bar) during 3 h at room temperature. Thereafter, the monolithic capillary was washed with ACN for 1 h in order to remove the unreacted ligands. The nucleophilic substitution was evaluated through *in situ* Raman spectroscopy performed on monolithic capillary samples.

3.7.3.4 Formation of *in situ* gold nanoparticles (AuNPs)

The amine-modified capillary was primarily flushed by an HCl solution during 15 min to protonated the amine function into quaternary ammonium. Then it was flushed with a solution of 1% of $HAuCl_4$ in deionized water until all the capillary was totally coloured in yellow. It was then rinsed with deionized water during 1 h to remove the un-grafted gold ions. Then a solution of 7 mg of $NaBH_4$ in deionized water was flushed during 2 h. Finally the capillary was flushed 30 min by deionized water.

3.7.3.5 Reduction of nitroarenes by heterogeneous catalysis

Freshly prepared solution containing 200 µL of nitroarenes (*e.g. o*-nitrophenol, 4-chloro-7-nitrobenzofurazan or *p*-nitroaniline - 5 mg of the nitroarene in 10 mL H_2O), 200 µL of $NaBH_4$ (114 mg in 10 mL H_2O) in 5 mL of water was injected in the loop of a HPLC pump system, the solution coming out from the in capillary AuNPs decorated monoliths was collected and then analysed by UV-Vis spectrophotometry. This was done with the capillaries containing *in situ* generated AuNPs with a flow rate of 3 µL.min^{-1}.

3.8 Results and Discussions

3.8.1 Functionalization of the in-capillary polymer monolith

A two-step process was necessary for preparing an amine bearing porous monoliths within fused silica capillaries (inner diameter of 100 µm), as shown on **Figure 3-6** After activation of the inner wall of the capillary in the presence of γ-MAPS, a functional reactive acrylic monomer, *i.e. N*-acryloxysuccinimide (NAS), and EGDMA as a cross-linking agent were copolymerized in the presence of AIBN (1% w/w, with respect to the total amount of co-monomers) and toluene as a radical initiator and a porogenic solvent, respectively. Upon filling the pre-activated capillary with this polymerization mixture, sealing of the extremities with rubber septa and subsequent photo-initiated copolymerization within a UV oven at 356 nm, an in-capillary P(NAS-*co*-EGDMA) monolith was obtained with nucleophile-sensitive *N*-hydroxysuccinimide activated ester functionalities and well-defined interconnected pores in the micrometer-sized range, as observed in previously published results in the field.[26–32]

A post-polymerization modification was then investigated on the as-obtained P(NAS-*co*-EGDMA) monolith so as to functionalize the *N*-hydroxysuccinimide functions with nucleophilic amine derived from ethylene diamine. Four different of them were assessed, namely ethylene diamine (EDA), tris(2-aminoethyl)amine (TRIS), tetraethylenepentamine (TETRA) and 1-(2-aminoethyl)piperazine (AEP). Flushing of the different amine bearing ligands through the monolithic capillary allowed for a virtually total consumption of the *N*-hydroxysuccinimide activated ester moieties of the monolith. This was ascertained by *in-situ* Raman spectroscopy of the in-capillary monolith before and after post-polymerization modification that pointed out the complete disappearance of characteristic peaks of succinimidyl esters present in the pristine poly(NAS-*co*-EDMA) at 1730 (imide asymmetric stretching), 1780 (imide symmetric stretching) and 1810 cm^{-1} (activated ester stretching) corresponding to the carbonyl stretching modes, as already published elsewhere.[26–32] Additionally, appearing of peaks assigned to amide bonds (at 1300 cm^{-1}, 1550 cm^{-1}

and 1650 cm^{-1}), as shown on **Figure 3-7**, confirmed the covalent attachment of the four different ethylene diamine-based ligands at the surface of the monolith through amide bond coupling. Finally, peak assigned to the –NH stretching mode was observed at 3300 cm^{-1} in all the amino-containing ligand functionalized P(NAS-*co*-EGDMA) in capillary monoliths monitored by *in situ* Raman spectroscopy. This clearly demonstrated the efficiency of the grafting onto the functional reactive NAS functionalities by a facile and straightforward nucleophilic substitution.

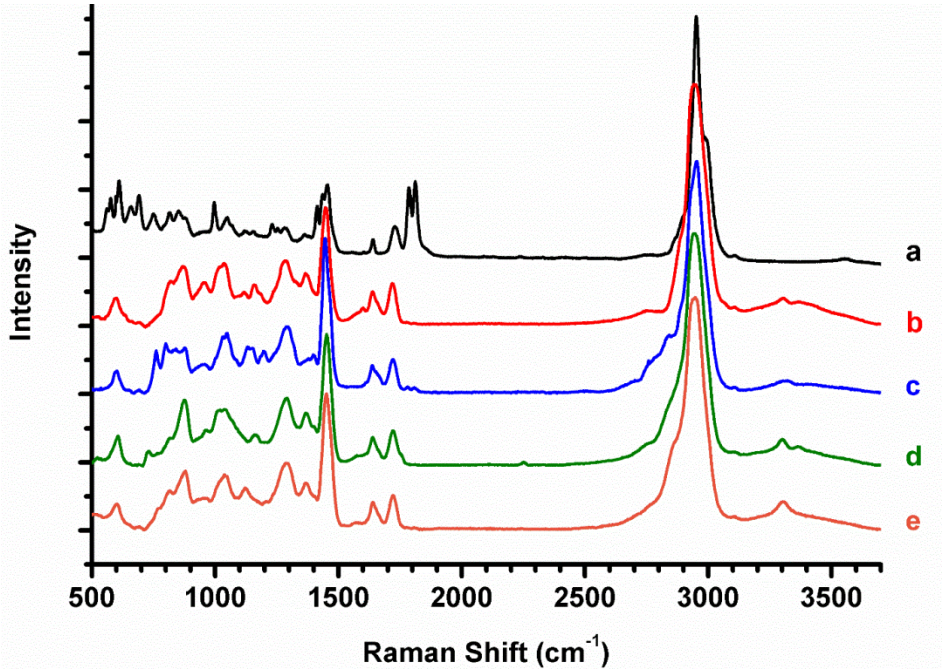

Figure 3-7: Raman spectra of the P(NAS-*co*-EGDMA)-based monoliths *a)* before or after functionalization with *b)* EDA, *c)* AEP, *d)* TRIS or *e)* TETRA ligands.

3.8.2 *In-situ* formation of AuNPs

Immobilization of AuNPs onto porous polymers has been well-described in the literature in the last decades, notably by taking advantage of the chemical functions exhibited at the pore surface such as thiol-,[33,34] cyano,[35] and amine[3,36] functions, to cite but a few. Surprisingly, even if some investigations on the crucial role of the chemical function on the AuNPs adsorption has been reported (thiol *vs.* amine for instance),[37] no such comparative study has been so far investigated on the influence of shape-like ligands over AuNPs adsorption. To fill this gap, we thus focused on the effect of different ethylenediamine-based amine ligands on the shape, morphology, dispersion and coverage of *in-situ* generated AuNPs over such amine functionalized P(NAS-*co*-EGDMA)-based monolithic capillaries. The adsorption of AuNPs was achieved through a two-step *in situ* strategy. In a first time, chloroauric acid solution ($HAuCl_4$) was percolated through the polymeric monolith. Then, the hydride-mediated reduction of Au^{3+} cations was achieved by flowing a $NaBH_4$ solution through the capillary

and allowed for the preparation of hybrid AuNPs@polymeric monoliths. Semi-quantitative EDX analyses (**Figure 3-8**) of the different resulting amine-functionalized hybrid monolithic capillaries were realized. Surprisingly, they clearly showed that similar gold content were immobilized at the pore surface of the NAS-based macroporous materials. However, SEM pictures (**Figure 3-9 & 3-10**) demonstrated the strong influence of the immobilized ethylene diamine-based ligands over the AuNP morphology. Indeed, *in-situ* formation of GNPs at the surface of EDA functionalized monoliths allowed for the obtention of two distinct populations of spherical AuNPs with diameters in the 30 nm and 100 nm range. Moreover, a tendency to aggregation was also observed a very inhomogeneous while. AEP functionalized monoliths presented also two distinct populations of "cubic" AuNPs with average diameters of 60 nm and 120 nm. At the opposite, a very homogeneous distribution of AuNPs over the monolith was observed in the case of AEP. TRIS functionalized monoliths also presented a homogeneous coverage of AuNPs, which displayed. Surprisingly, very small particle sizes were in that case observed, *i.e.* 2 nm and 20 nm. On the opposite, TETRA-functionalized monolith presents a rather inhomogeneous disparity of the nanoparticles diameter along with the presence of many aggregates.

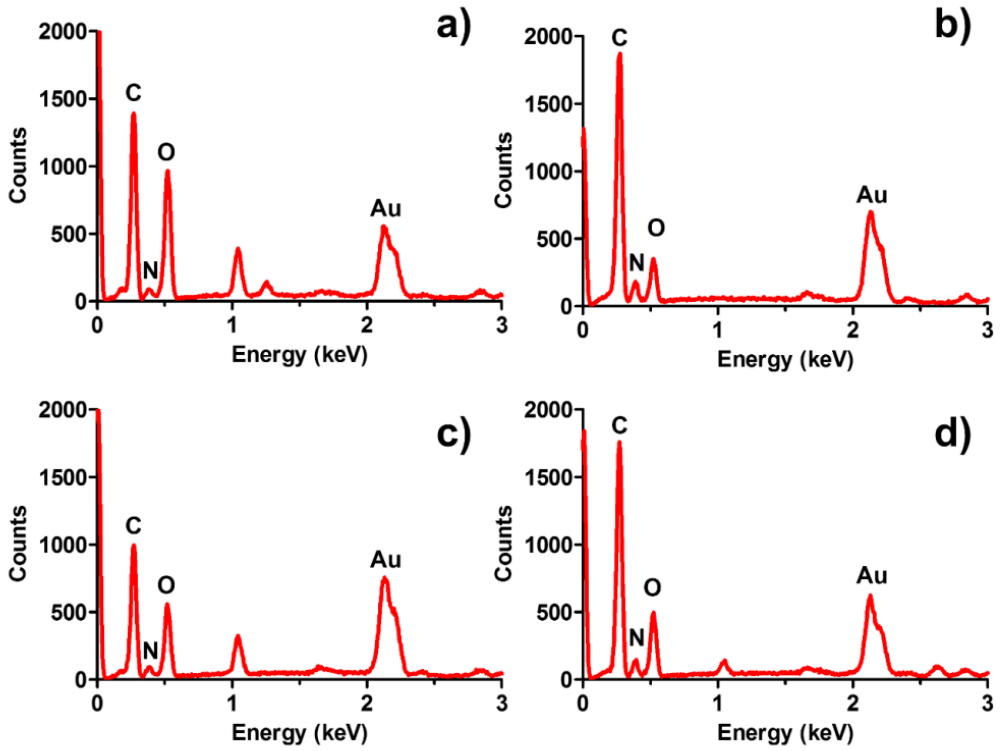

Figure 3-8: EDX spectra of hybrid *a)* EDA-, *b)* AEP-, *c)* TRIS- and *d)* TETRA-functionalized monoliths supported gold nanoparticles.

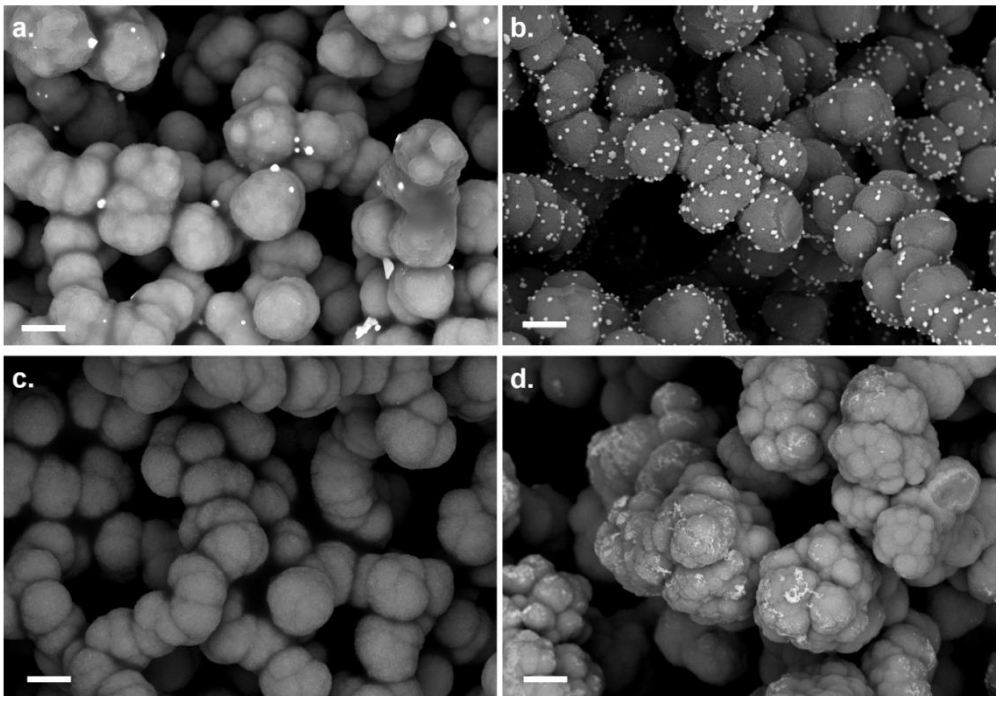

Figure 3-9: SEM pictures of the gold nanoparticles immobilized through the *in-situ* strategy over *a)* EDA-, *b)* AEP-, *c)* TRIS- and *d)* TETRA-functionalized P(NAS-*co*-EGDMA) monoliths. Scale bar = 1 µm.

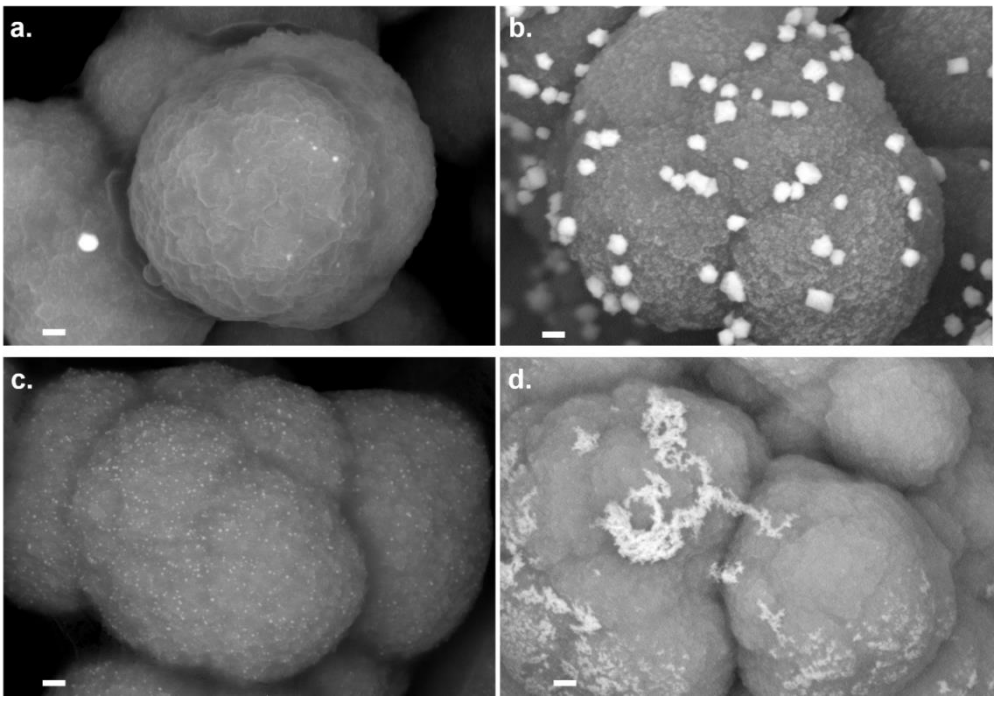

Figure 3-10: SEM pictures of the gold nanoparticles immobilized through the *in-situ* strategy over *a)* EDA-, *b)* AEP-, *c)* TRIS- and *d)* TETRA-functionalized P(NAS-*co*-EGDMA) monoliths. Scale bar = 100 nm.

3.8.3 Reduction of nitroarenes

AuNPs are prone to act supported catalyst for the reduction of nitroarenes compounds in the presence of sodium borohydride.[10] To this purpose, different solution of nitroarenes (namely *o*-nitrophenol, *p*-nitroaniline and 4-chloro-7-nitrobenzofurazan – **Figure 3-11**) along with $NaBH_4$ in water were freshly prepared and injected through the loop of an HPLC pump to a 10 cm length EDA-, AEP-, TRIS- or TETRA-functionalized NAS-based capillary containing *in-situ* generated AuNPs at a flow rate of 3 $\mu L.min^{-1}$. Solutions harvested at the outlet of the four different capillaries were analyzed by off-line UV-Visible spectrophotometry (**Figure 3-12**) and corresponding yields were calculated by comparing the maximum absorbance of the $\pi \rightarrow \pi^*$ of the substrate before and after percolation through the hybrid monolith, as can be shown in **Figure 3-12 d**. First, it was observed that reductions of *o*-nitrophenol and *p*-nitroaniline were completed upon percolation through each hybrid monolithic capillary at the flowrate of 3 $\mu L.min^{-1}$, as the signal corresponding to the $\pi \rightarrow \pi^*$ transition of these substrates vanished at 415 nm and 380 nm, respectively, as observed in **Figure 3-12 a & b**. According to the UV spectra (**Figure 3-12 c**) obtained after percolation of 4-chloro-7-nitrobenzofurazan, *i.e.* a fluorescent probe notably used for marking proteins, through each hybrid monolithic capillary, the reduction yield of this compound, *i.e.* from 32 to 76%, was rather low when compared to other nitroaromatic compounds investigated in this study. Especially the yield obtained upon catalytic reduction carried out with the TETRA functionalized hybrid monolithic capillary was twofold lower than that obtained with other amine functionalized hybrid capillaries. This is likely due to the presence of gold nanoparticle aggregates that are detrimental for the reaction to occur. This catalytic test reaction paves the way towards more complicated ones such as C-C homo- or cross-coupling reactions. Furthermore, the nature/shape of the chosen ligand seems to be a parameter to seriously take into consideration as it not only has an impact on the shape, morphology and dispersion of the *in situ* metallic nanoparticles at the pore surface of polymeric in-capillary monoliths but also on the yield of the catalytic reaction investigated in this study.

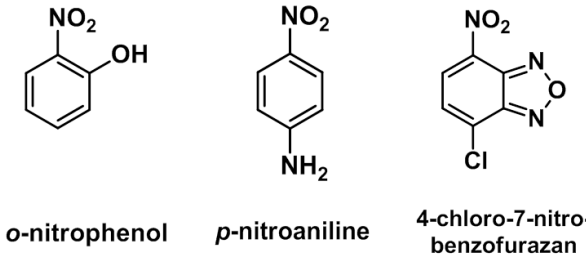

Figure 3-11: Chemical structure of the different nitro-containing aromatic organic compounds reduced by in-capillary flow-through GNP-catalyzed reaction in the presence of an excess of $NaBH_4$.

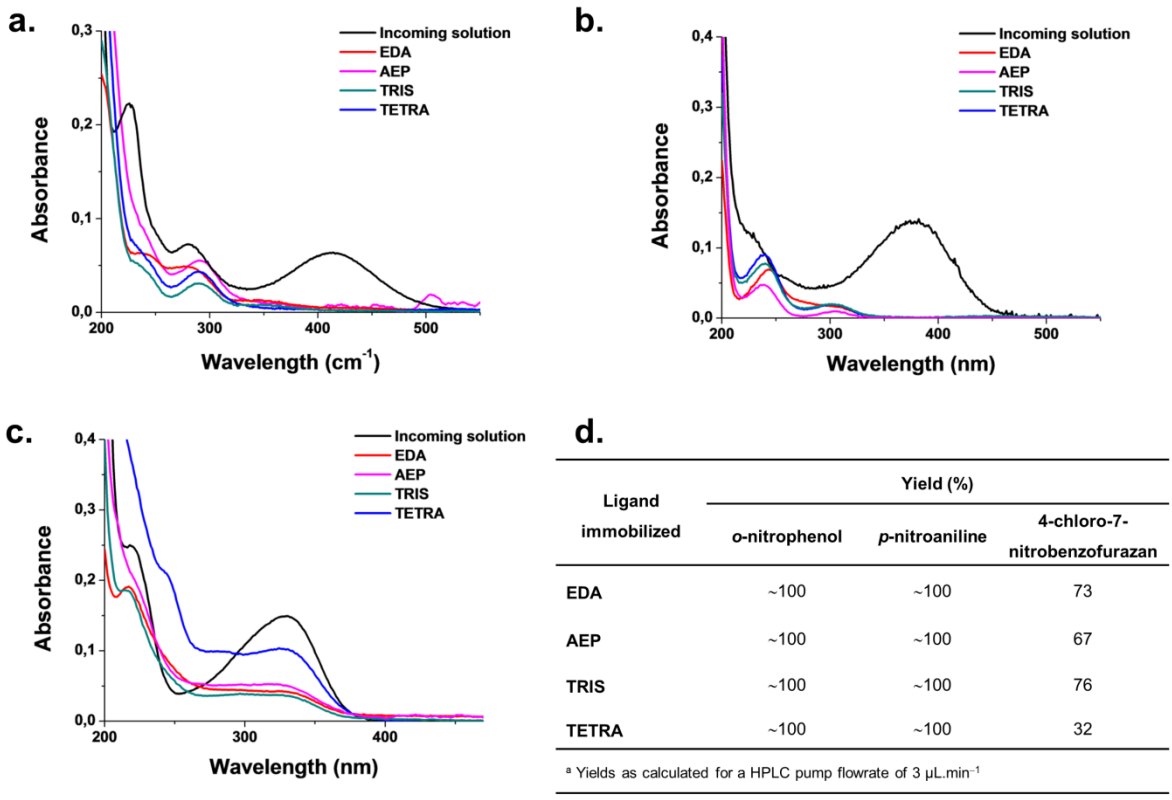

d.

Ligand immobilized	Yield (%)		
	o-nitrophenol	*p*-nitroaniline	4-chloro-7-nitrobenzofurazan
EDA	~100	~100	73
AEP	~100	~100	67
TRIS	~100	~100	76
TETRA	~100	~100	32

[a] Yields as calculated for a HPLC pump flowrate of 3 µL.min^{-1}

Figure 3-12: UV-visible absorption spectra recorded in the 200–500 nm wavelength range for reaction solutions of *a) o*-nitrophenol, *b) p*-nitroaniline and *c)* 4-chloro-7-nitrobenzofurazan in ethanol supplemented with an excess of $NaBH_4$ before (black trace) and after percolation through EDA- (red trace), AEP- (pink trace), TRIS- (green trace) or TETRA- (blue trace) functionalized monolithic capillaries supported gold nanoparticles and *d)* their corresponding yields gathered in a table.

3.9 Conclusions

In conclusion, the different amine ligands deriving from ethylenediamine exposed at the pore surface of in capillary monoliths play a key role regarding the subsequent immobilization of gold nanoparticles on such macroporous materials. Even if the gold content immobilized at the interface of such monoliths with the surrounding fluid, SEM micrographs clearly demonstrated that the shape and the diameter of adsorbed gold nanoparticles depend on the grafted ligand while the homogeneity of the dispersion of nanogold and/or the presence of aggregates at the pore surface is also impacted by the nature of the ligand grafted on such porous materials. Finally, such differences in the nanogold shape, diameter and dispersion homogeneity have a significative influence regarding the reduction of a variety of nitroarenes. Surprisingly, best nitroarene reduction yield were obtained with monoliths on which were immobilized the largest AuNPs (*i.e.* EDA and AEP).

3.10 References

(1) Poupart, R.; Djerir, N. E. H.; Chellapermal, D.; Guerrouache, M.; Carbonnier, B.; Le Droumaguet, B. Novel In-Capillary Polymeric Monoliths Arising from Glycerol Carbonate Methacrylate for Flow-through Catalytic and Chromatographic Applications. *RSC Adv.* **2016**, *6* (17), 13614–13617.

(2) Poupart, R.; Le Droumaguet, B.; Guerrouache, M.; Carbonnier, B. Copper Nanoparticles Supported on Permeable Monolith with Carboxylic Acid Surface Functionality: Stability and Catalytic Properties under Reductive Conditions. *Mater. Chem. Phys.* **2015**, *163*, 446–452.

(3) Liu, Y.; Guerrouache, M.; Kebe, S. I.; Carbonnier, B.; Le Droumaguet, B. Gold Nanoparticles-Supported Histamine-Grafted Monolithic Capillaries as Efficient Microreactors for Flow-through Reduction of Nitro-Containing Compounds. *J. Mater. Chem. A* **2017**, *5* (23), 11805–11814.

(4) Floris, P.; Twamley, B.; Nesterenko, P. N.; Paull, B.; Connolly, D. Agglomerated Polymer Monoliths with Bimetallic Nano-Particles as Flow-through Micro-Reactors. *Microchim. Acta* **2012**, *179* (1), 149–156.

(5) Floris, P.; Twamley, B.; Nesterenko, P. N.; Paull, B.; Connolly, D. Fabrication and Characterisation of Gold Nano-Particle Modified Polymer Monoliths for Flow-through Catalytic Reactions and Their Application in the Reduction of Hexacyanoferrate. *Microchim. Acta* **2014**, *181* (1), 249–256.

(6) Svec, F.; Fréchet, J. M. J. Continuous Rods of Macroporous Polymer as High-Performance Liquid Chromatography Separation Media. *Anal. Chem.* **1992**, *64* (7), 820–822.

(7) Svec, F. Quest for Organic Polymer-Based Monolithic Columns Affording Enhanced Efficiency in High Performance Liquid Chromatography Separations of Small Molecules in Isocratic Mode. *J. Chromatogr. A* **2012**, *1228*, 250–262.

(8) Féral-Martin, C.; Birot, M.; Deleuze, H.; Desforges, A.; Backov, R. Integrative Chemistry toward the First Spontaneous Generation of Gold Nanoparticles within Macrocellular PolyHIPE Supports (Au@polyHIPE) and Their Application to Eosin Reduction. *React. Funct. Polym.* **2007**, *67* (10), 1072–1082.

(9) Harish, S.; Mathiyarasu, J.; Phani, K. L. N.; Yegnaraman, V. Synthesis of Conducting Polymer Supported Pd Nanoparticles in Aqueous Medium and Catalytic Activity Towards 4-Nitrophenol Reduction. *Catal. Lett.* **2008**, *128* (1), 197.

(10) Kuroda, K.; Ishida, T.; Haruta, M. Reduction of 4-Nitrophenol to 4-Aminophenol over Au Nanoparticles Deposited on PMMA. *J. Mol. Catal. Chem.* **2009**, *298* (1), 7–11.

(11) Cassol, C. C.; Umpierre, A. P.; Machado, G.; Wolke, S. I.; Dupont, J. The Role of Pd Nanoparticles in Ionic Liquid in the Heck Reaction. *J. Am. Chem. Soc.* **2005**, *127* (10), 3298–3299.

(12) Mandal, S.; Roy, D.; Chaudhari, R. V.; Sastry, M. Pt and Pd Nanoparticles Immobilized on Amine-Functionalized Zeolite: Excellent Catalysts for Hydrogenation and Heck Reactions. *Chem. Mater.* **2004**, *16* (19), 3714–3724.

(13) Venkatesan, P.; Santhanalakshmi, J. Designed Synthesis of Au/Ag/Pd Trimetallic Nanoparticle-Based Catalysts for Sonogashira Coupling Reactions. *Langmuir* **2010**, *26* (14), 12225–12229.

(14) Han, J.; Liu, Y.; Guo, R. Facile Synthesis of Highly Stable Gold Nanoparticles and Their Unexpected Excellent Catalytic Activity for Suzuki−Miyaura Cross-Coupling Reaction in Water. *J. Am. Chem. Soc.* **2009**, *131* (6), 2060–2061.

(15) Gallon, B. J.; Kojima, R. W.; Kaner, R. B.; Diaconescu, P. L. Palladium Nanoparticles Supported on Polyaniline Nanofibers as a Semi-Heterogeneous Catalyst in Water. *Angew. Chem. Int. Ed.* **2007**, *46* (38), 7251–7254.

(16) Jiang, Z.-J.; Liu, C.-Y.; Sun, L.-W. Catalytic Properties of Silver Nanoparticles Supported on Silica Spheres. *J. Phys. Chem. B* **2005**, *109* (5), 1730–1735.

(17) Ma, Z.; Overbury, S. H.; Dai, S. Gold Nanoparticles as Chemical Catalysts. In *Encyclopedia of Inorganic Chemistry*; John Wiley & Sons, Ltd, 2006.

(18) Cao, Q.; Xu, Y.; Liu, F.; Svec, F.; Fréchet, J. M. J. Polymer Monoliths with Exchangeable Chemistries: Use of Gold Nanoparticles As Intermediate Ligands for Capillary Columns with Varying Surface Functionalities. *Anal. Chem.* **2010**, *82* (17), 7416–7421.

(19) Xu, Y.; Cao, Q.; Svec, F.; Fréchet, J. M. J. Porous Polymer Monolithic Column with Surface-Bound Gold Nanoparticles for the Capture and Separation of Cysteine-Containing Peptides. *Anal. Chem.* **2010**, *82* (8), 3352–3358.

(20) Guerrouache, M.; Mahouche-Chergui, S.; Chehimi, M. M.; Carbonnier, B. Site-Specific Immobilisation of Gold Nanoparticles on a Porous Monolith Surface by Using a Thiol-Yne Click Photopatterning Approach. *Chem. Commun.* **2012**, *48* (60), 7486–7488.

(21) DiScipio, R. G. Preparation of Colloidal Gold Particles of Various Sizes Using Sodium Borohydride and Sodium Cyanoborohydride. *Anal. Biochem.* **1996**, *236* (1), 168–170.

(22) Turkevich, J.; Stevenson, P. C.; Hillier, J. A Study of the Nucleation and Growth Processes in the Synthesis of Colloidal Gold. *Discuss. Faraday Soc.* **1951**, *11* (0), 55–75.

(23) Kimling, J.; Maier, M.; Okenve, B.; Kotaidis, V.; Ballot, H.; Plech, A. Turkevich Method for Gold Nanoparticle Synthesis Revisited. *J. Phys. Chem. B* **2006**, *110* (32), 15700–15707.

(24) Nguyen, D. T.; Kim, D.-J.; So, M. G.; Kim, K.-S. Experimental Measurements of Gold Nanoparticle Nucleation and Growth by Citrate Reduction of HAuCl4. *Adv. Powder Technol.* **2010**, *21* (2), 111–118.

(25) Polte, J.; Erler, R.; Thünemann, A. F.; Sokolov, S.; Ahner, T. T.; Rademann, K.; Emmerling, F.; Kraehnert, R. Nucleation and Growth of Gold Nanoparticles Studied via in Situ Small Angle X-Ray Scattering at Millisecond Time Resolution. *ACS Nano* **2010**, *4* (2), 1076–1082.

(26) Guerrouache, M.; Millot, M. C.; Carbonnier, B. Capillary Columns for Reversed-Phase CEC Prepared via Surface Functionalization of Polymer Monolith with Aromatic Selectors. *J. Sep. Sci.* **2011**, *34* (16–17), 2271–2278.

(27) Carbonnier, B.; Guerrouache, M.; Denoyel, R.; Millot, M.-C. CEC Separation of Aromatic Compounds and Proteins on Hexylamine-Functionalized N-Acryloxysuccinimide Monoliths. *J. Sep. Sci.* **2007**, *30* (17), 3000–3010.

(28) Guerrouache, M.; Millot, M.-C.; Carbonnier, B. Functionalization of Macroporous Organic Polymer Monolith Based on Succinimide Ester Reactivity for Chiral Capillary Chromatography: A Cyclodextrin Click Approach. *Macromol. Rapid Commun.* **2009**, *30* (2), 109–113.

(29) Khalil, A. M.; Georgiadou, V.; Guerrouache, M.; Mahouche-Chergui, S.; Dendrinou-Samara, C.; Chehimi, M. M.; Carbonnier, B. Gold-Decorated Polymeric Monoliths: In-Situ vs Ex-Situ Immobilization Strategies and Flow through Catalytic Applications towards Nitrophenols Reduction. *Polymer* **2015**, *77*, 218–226.

(30) Tijunelyte, I.; Babinot, J.; Guerrouache, M.; Valincius, G.; Carbonnier, B. Hydrophilic Monolith with Ethylene Glycol-Based Grafts Prepared via Surface Confined Thiol-Ene Click Photoaddition. *Polymer* **2012**, *53* (1), 29–36.

(31) Guerrouache, M.; Carbonnier, B.; Vidal-Madjar, C.; Millot, M.-C. In Situ Functionalization of N-Acryloxysuccinimide-Based Monolith for Reversed-Phase Electrochromatography. *J. Chromatogr. A* **2007**, *1149* (2), 368–376.

(32) Dao, T. T. H.; Guerrouache, M.; Carbonnier, B. Thiol-Yne Click Adamantane Monolithic Stationary Phase for Capillary Electrochromatography. *Chin. J. Chem.* **2012**, *30* (10), 2281–2284.

(33) Le Droumaguet, B.; Poupart, R.; Grande, D. "Clickable" Thiol-Functionalized Nanoporous Polymers: From Their Synthesis to Further Adsorption of Gold Nanoparticles and Subsequent Use as Efficient Catalytic Supports. *Polym. Chem.* **2015**, *6* (47), 8105–8111.

(34) Poupart, R.; Le Droumaguet, B.; Guerrouache, M.; Grande, D.; Carbonnier, B. Gold Nanoparticles Immobilized on Porous Monoliths Obtained from Disulfide-Based Dimethacrylate: Application to Supported Catalysis. *Polymer* **2017**, article in press, DOI: 10.1016/j.polymer.2017.04.034.

(35) Zhu, H.; Du, M.; Zou, M.; Xu, C.; Li, N.; Fu, Y. Facile and Green Synthesis of Well-Dispersed Au Nanoparticles in PAN Nanofibers by Tea Polyphenols. *J. Mater. Chem.* **2012**, *22* (18), 9301–9307.

(36) Poupart, R.; Benlahoues, A.; Le Droumaguet, B.; Grande, D. Porous Gold Nanoparticle-Decorated Nanoreactors Prepared from Smartly Designed Functional Polystyrene-Block-Poly(d,l-Lactide) Diblock Copolymers: Toward Efficient Systems for Catalytic Cascade Reaction Processes. *ACS Appl. Mater. Interfaces* **2017**, *article in press*, DOI: 10.1021/acsami.6b16157..

(37) Mahanta, N.; Valiyaveettil, S. Surface Modified Electrospun Poly(Vinyl Alcohol) Membranes for Extracting Nanoparticles from Water. *Nanoscale* **2011**, *3* (11), 4625–4631.

Novel In-Capillary Polymeric Monoliths Arising from Glycerol Carbonate Methacrylate for Flow-Through Catalytic and Chromatographic Applications

Abstract: In-capillary reactive polymer monoliths have been prepared from glycerol carbonate methacrylate functional monomer. Following functionalization with suitable ligands and eventually after immobilization of metallic nanoparticles, these materials can be successfully employed as microreactors for flow-through catalysis.

3.11 Introduction

Nowadays, the great challenge regarding polymeric monoliths, which relies on the control of their surface properties, has attracted an ever-growing interest in the world of material chemistry and analytic sciences. This concept notably requires that the functionalization of such porous materials should be fast, versatile, straightforward, as much quantitative as possible, simple to perform and achieved in mild experimental conditions. The commonly used strategy relies on the post-polymerization functionalization of reactive interfacial pendant moieties on monoliths. To this purpose, different macroporous materials based on functionalizable monomers have been developed, allowing for facile nucleophilic substitution/addition with organic grafts of interest. Historically, glycidyl methacrylate-(GMA) based monoliths were the first macroporous functional materials to be successfully modified with different organic molecules through ring-opening in the presence of amino compounds,[1–6] *etc.*[7–10] to afford a plethora of surface functionalities. Vinyl benzyl chloride-(VBC) based monoliths have also been notably modified by nucleophilic substitution of the chloride in the presence of different amines.[7,11] Other reactive monoliths based on 2-vinyl-4,4-dimethylazlactone (VDMA) were successfully used for the immobilization of amine bearing (macro)molecules such as ethylene diamine and cysteamine,[12,13] trypsin,[14,15] iminodiacetic acid[15] or anti-testosterone polyclonal antibodies[16] on azlactone pendant moieties for diverse bio-related sensing applications. More recently, porous monolithic micro-sized columns arising from *N*-acryloxysuccinimide (NAS) have been deeply investigated by our group. They can notably be easily functionalized with a a variety of amines.[17–19] On top of that, a two-step procedure can also be applied for the efficient grafting of thiol-appended organic (macro)molecules[20–23] *via* photo-initiated thiol-yne, thiol-ene addition or through copper-catalyzed azide-alkyne dipolar cycloaddition (CuAAC) reaction, respectively. Finally, IEM-based porous materials display a high reactivity towards alcohols and amines in the presence of dibutyltin dilaurate (DBTDL) catalyst.[24] Unfortunately, isocyanate moieties are highly sensitive to air moisture and, as a consequence, prone to hydrolysis. It is thus rather difficult to store them for long periods of time.

Despite their good reactivity and the numerous chemistries that can be undergone at the surface of such functional monoliths to produce diverse polymeric – from hydrophilic to hydrophobic – interfaces, all these reactive monomers originate from organic reagent precursors. Owing to today's major concerns of scientists for environment, polymers and polymeric materials stemming from renewable resources have gained a tremendous interest.

Herein, we report in this study a novel monolith based on glycerol carbonate methacrylate (GCMA), functional monomer arising from a bio-based precursor, *i.e.* glycerol.

Cyclic carbonates can undergo ring opening in the presence of nucleophilic compounds such as primary amines and eventually carboxylic acids. This may ensure for further easy and straightforward functionalization of the as-obtained porous matrix with organic compounds of interest (chelating molecules or selectors of different nature) and/or metallic nanoparticles (MNPs) for targeted applications such as flow-through catalysis or separation sciences.

3.12 Materials and Methods

3.12.1 Experimental

Glycerol carbonate methacrylate (GCMA) was supplied by Specific Polymers. Ethylene glycol dimethacrylate (EGDMA, 98%), 3-(Trimethoxysilyl)propyl methacrylate (γ-MAPS, 98%), Sodium borohydride ($NaBH_4$, ≥98%), Sodium hydroxide (NaOH, 1 M), Hydrochloric acid (HCl, 0.1 M for HPCE), , 2,2-Dimethoxy-2-phenylacetophenone (DMPA, 99%), Toluene (anhydrous, 99.8%), 1-Dodecanol (≥98%) and 4-Mercaptobutyric acid were purchased from Sigma Aldrich. 2,2'-Azobisisobutyronitrile (AIBN, 98%) was obtained from Acros Organics. 4-Nitrophenol (*p*-nitrophenol, 99%), Potassium tetrachloroplatinate (K_2PtCl_4, 99,9% metal basis), and Allylamine (98%+) were purchased from Alfa Aesar. Acetone, HPLC grade Acetonitrile (ACN) and Ethanol absolute (anhydrous) were supplied by Carlo Erba. *n*-Nonane comes from VWR Chemicals. All reagents were used without further purification. 18.2 MΩ deionized water was filtered through a Milli-Q Plus purification pack. Fused silica capillaries with a UV-transparent external coating (100 µm I.D.) were obtained from Polymicro Technologies.

3.12.2 Instrumentation

An HPLC pump (Shimadzu LC-10ATVP) was used to flush monolithic columns with 2-nitrophenol solutions along with mobile phase. Spectrolinker XL-1500 UV Crosslinker (Spectronics Corporation) equipped with eight lamps (8 × 15W, 365 nm) was used to photoinitiate the polymerization. UV-Vis spectra were recorded on a Cary 60 UV-Vis Spectrophotometer from Agilent Technologies. Chemical Structure of the monoliths was investigated using a Raman apparatus XPlora One from Horiba Jobin Yvon equipped with a laser at 638 nm. Samples were investigated in different places to control the homogeneity. The acquisition time was fixed at 1 min. Scanning Electron Microscopy (SEM) investigations of the materials were performed with a MERLIN microscope from Zeiss equipped with InLens, EBSD and SE2 detectors using a low accelerating tension (2-3 kV) with a diaphragm aperture of 30 µm. Prior to analyses, the samples were coated with a 4-nm layer of palladium/platinum alloy in a Cressington 208 HR sputter-coater. All chromatographic experiments

were carried out using a Dionex Ultimate 3000 HPLC RSLC nanosystem (Sunnyvale, CA, USA) equipped with a 10 nL In-line split loop manual injector and a Dionex VWD 3400 RS detection system operating at a fixed wavelength λ = 214 nm.

3.12.3 Synthesis of the GCMA-based functionalized monolithic capillaries

The synthesis of the (GCMA-*co*-EGDMA) monolithic columns relies on a three-step process involving *(i)* the synthesis of the porous methacrylate matrix ; *(ii)* the chemical modification of the matrix with allylamine and *(iii)* a thiol-ene reaction with either mercaptobutyric acid or 1-octane thiol.

3.12.4 Surface pre-treatment of the capillaries

In order to ensure the stability of the monolithic column, the inner wall of the capillaries was submitted to a vinylization step. 3-(Trimethoxysilyl)propyl methacrylate (γ-MAPS) was used as a bifunctional reagent allowing for the covalent attachment of the polymeric material onto the wall of the capillaries. The procedure was as follows: fused silica capillaries were treated with 1 M NaOH for 1h at room temperature and subsequently heated for 2 h at a temperature of 100 °C. Capillaries were flushed with 0.1 M HCl for 10 min, rinsed with deionized water for 10 min and then with acetone for 15 min. Thereafter, capillaries were purged with dry nitrogen gas for 2 h at a temperature of 120 °C. 30% (v/v) 3-(trimethoxysilyl)propyl methacrylate solution in toluene was allowed to react overnight with inner silanols at room temperature. Last, the capillaries were rinsed with toluene for 15 min and dried under a stream of nitrogen gas for 1 h. The capillaries thus treated were stored at 4 °C prior to use.

3.12.5 *In situ* synthesis of the porous monolith

In order to find the adequate mixture to realize further experiments, the porous monolith was prepared through a photochemically-driven free radical polymerization reaction. Different solutions were tested, consisting of variations of the following combination: GCMA as a functional monomer, EGDMA as a crosslinker, toluene and dodecanol (or nonane, depending of the samples) as porogenic solvents and AIBN as an initiator (4 mg, 1% w/w with respect to the total amount of monomers). Mixtures were sonicated for about 15 min to obtain homogeneous solution. The pre-treated capillary was completely filled with the polymerization mixture by immersing the inlet of the capillary into a reservoir and by pushing through the solution previously prepared under nitrogen pressure (3 bar). After flushing with a large excess of polymerization solution, both ends of the capillary were sealed

with rubber septa and the capillary was placed within a Spectrolinker XL-1500 UV and irradiated under an overall intensity of 8 $J.cm^{-2}$ (800 s). After the polymerization was completed, the septa were removed and the monolith capillary was washed with ACN for 1 h (5 $\mu L.min^{-1}$) to remove the unreacted monomers and the porogenic solvent. Subsequently, back pressure in the as-prepared capillaries was measured in order to determine their permeability.

3.12.6 *In situ* functionalization of the porous monolith with allylamine

The carbonate cycles stemming from the GCMA monomer were functionalized with alkene groups through nucleophilic substitution. The reaction was performed *in situ* by flushing the monolith capillary with a solution of allylamine (1 M = 160 µL in 2 mL of ACN in a reservoir) pushed under nitrogen pressure (50 bars) during 2 h at room temperature. Thereafter, the monolithic capillary was washed with ACN for 1 h in order to remove the unreacted allylamine. The nucleophilic substitution yield was evaluated through *in-situ* Raman spectroscopy performed on monolithic capillary samples.

3.12.7 Thiol-ene reaction with a thiol-based molecule

The capillary was flushed by anhydrous absolute ethanol for 1 h to remove the previous solvent. Then, the surface-grafted alkene moieties provided the reactive sites for the modification by 4-mercaptobutyric *via* thiol-ene-based "click" chemistry. Photochemical thiol-ene reaction was proceeded as follows: mercaptobutyric acid (0.1M) and DMPA (4 mg, 1 wt%) were dissolved in 2 mL of absolute ethanol. The solution was flushed into the capillary during 2 h under UV light (λ = 365 nm). Then the capillary was rinsed with pure absolute ethanol during 1 h to remove unreacted reagents. Conversion of double bonds was evaluated through *in situ* Raman spectroscopy performed on monolithic capillary samples.

3.12.8 *In situ* formation of platinum nanoparticles

The carboxyl-modified capillary was flushed first, with deionized water during 10 minutes, and then with a solution of 43 mg of K_2PtCl_4 into a 2 mL mixture of water during 30 min. it was then rinsed with H_2O during 10 minutes to remove the non-adsorbed platinum ions. Then a solution of 7 mg of $NaBH_4$ (0.1 M) in water was flushed during 1 h. Finally the capillary was washed 10 min deionized water.

3.12.9 Reduction of *p*-nitrophenol by heterogeneous catalysis

A freshly prepared solution containing 200 µL of *p*-nitrophenol (5 mg in 10 mL of H_2O), 200 µL of $NaBH_4$ (114 mg in 10 mL of water) in 5 mL of deionized water was injected in the loop (20 µL, Rheodyne) of a HPLC pump system, the solution coming out from the in-capillary PtNPs decorated monoliths was collected and then analysed by UV-Vis spectrophotometry. To undoubtedly evidence the catalytic effect of PtNPs, blank tests were performed with monolithic microreactors without nanoparticles.

3.13 Results and discussions

The synthetic route followed for the synthesis of the in-capillary monolith is depicted in the **Figure 3-13**. Prior to the polymerization of the GCMA-based monolith, an activation step, consisting in the grafting of methacrylic functions at the inner wall of the fused silica capillary, was necessary. This notably ensured the tight covalent attachment of the monolith to the inner wall of the 100-µm diameter capillary.

In order to obtain ideal porous characteristics of the GCMA-based monolith in terms of permeability and homogeneity all along the capillary, different polymerization mixtures were assessed. For instance, three different porogenic solvent mixtures were tested, namely toluene/dodecanol: 75/25 and 40/60 or toluene/nonane: 50/50 (v/v) among many others (see **Table S1 Annexes** for full polymerization mixture composition investigation), as shown in Table 1. In the same way, the GCMA/EGDMA and GCMA/porogenic solvent mixture (w/w) ratios were finely tuned. The micrometer-sized range porosity of such monoliths was demonstrated by mercury intrusion porosimetry on bulk materials that showed a bimodal porous distribution centred on 2.2 µm and 50 nm, respectively. This bimodal distribution was assumed to be likely due to the contribution of each porogenic solvent present in the polymerization mixture. The respective permeability of the as-obtained monolithic columns were calculated using the Darcy law equation (**Equation 6**), that measures their capacity to transmit a fluid driven by an imposed pressure drop:

$$B_0 = \frac{\eta \times L \times Q}{A \times \Delta P} \qquad \textbf{(Equation 6)}$$

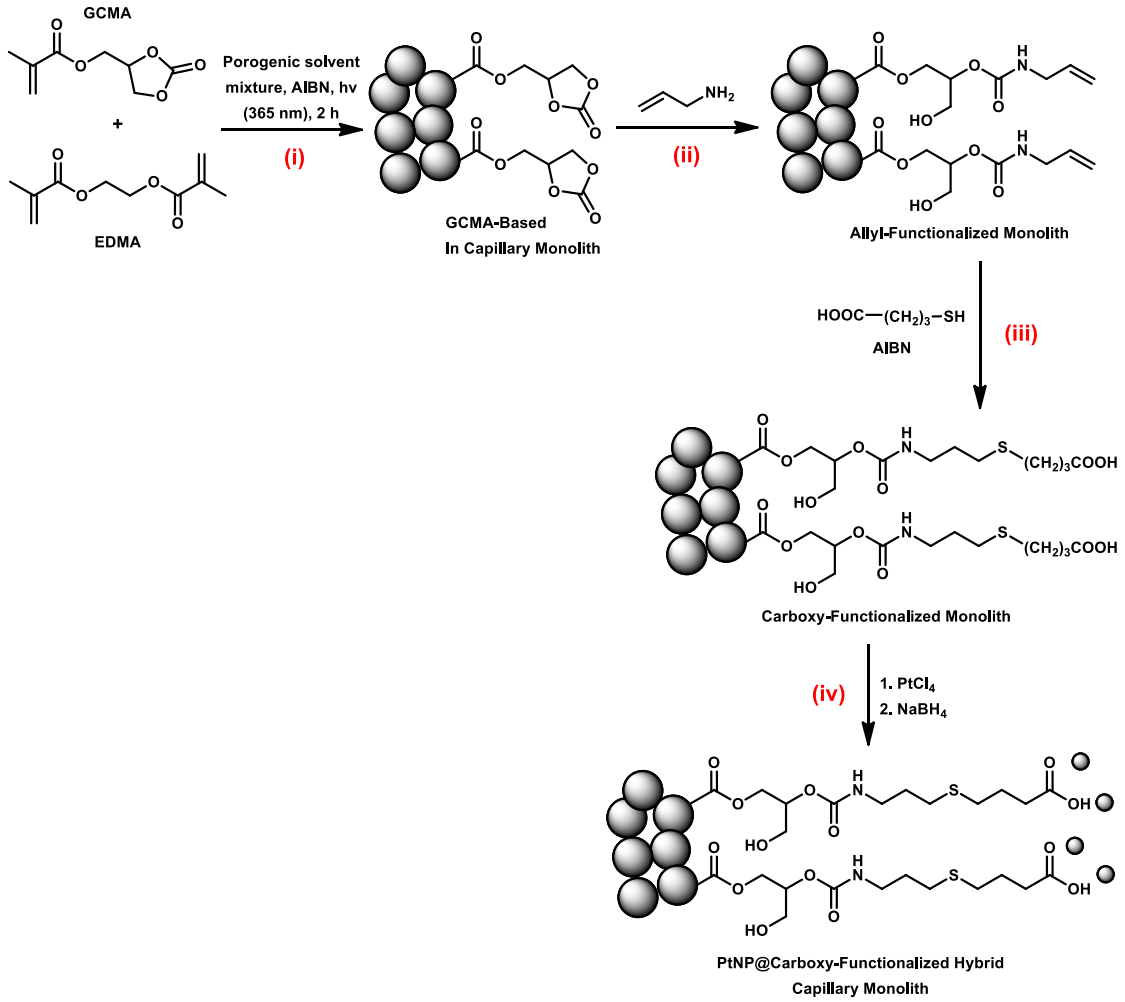

Figure 3-13: Schematic representation of the synthetic route applied to designing hybrid PtNPs@carboxylic acid functionalized GCMA-based in-capillary monolith *via* successive *i)* free-radical photopolymerization, *ii)* nucleophilic addition, *iii)* photo-triggered thiol-ene radical addition and *iv)* PtNPs immobilization step. The scheme is not to scale as the grey spheres corresponding to platinum nanoparticles have diameters of a few nanometers that are much larger than the size of a carboxylic unit.

In which B_0 stand for the permeability, η for the dynamic viscosity of the solvent (ACN), L for the length of the column, Q for ACN flowrate, A for the cross-sectional area, (A = 7.85×10^3 µm^2, knowing that the inner diameter of the capillary is 100 µm), and ΔP the pressure drop between the two extremities of the monolithic column. As seen from **Table 3-2**, the permeability of the monoliths greatly depends on the proportions of the different constituents of the polymerization feed. An optimum permeability value of 1.83×10^{-14} m^2 was obtained for the polymerization mixture 3, as observed from entry 3 in **Table 3-2**. The permeability features of such as-prepared in-capillary monoliths could also be deducted from

SEM micrographs (**Figure 3-14**). Indeed, the monolith generated from polymerization mixture 2 (**Table 3-2**, entry **2**) showed dense filling of the capillary with narrow pores, as shown on **Figure 3-14 A & B**, only permitting a limited permeability. On the opposite, using the polymerization mixture 1 (**Table 3-2**, entry **1**) generated a much permeable monolith with larger pores, as observed on MEB pictures of **Figure 3-14 C & D**. Finally, the best compromise in terms of permeability was obtained with the polymerization mixture 3 (**Table 3-2**, entry **3**) with an intermediate porous morphology, as shown on **Figure 3-14 E & F**.

Table 3-2: Composition of the three distinct polymerization feeds used for the preparation of in-capillary monoliths and their respective permeability.

Polymerization mixture	**% v/v toluene/DOH**[a]	**% v/v toluene/C_9H_{20}**	**% w/v monomers/solvents**	**% w/v GCMA/EGDMA**	**B_0**[b] **(10^{-14} µm²)**
1	75/25	-	36.2/33.8	34.4/65.6	4.31
2	-	50/50	36.2/63.8	34.4/65.6	0.89
3	60/40	-	39.2/60.8	34.4/65.6	1.83

[a] DOH: dodecanol

[b] B_0: permeability as calculated by the Darcy law

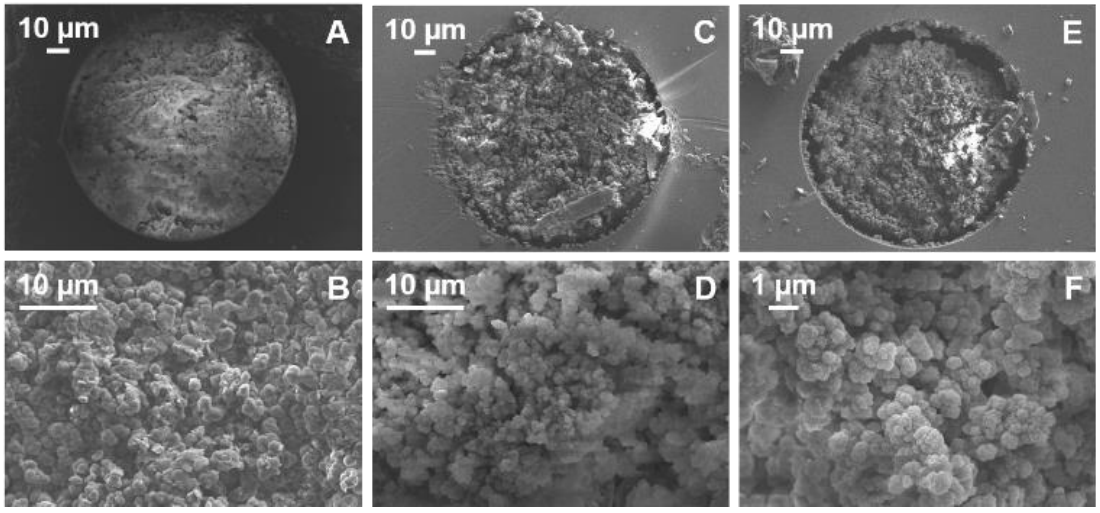

Figure 3-14: SEM micrographs of the in-capillary monolith prepared using different experimental conditions: *A)* and *B)* Polymerization mixture 2; *C)* and *D)* Polymerization mixture 1 and *E)* and *F)* Polymerization mixture 3.

The functionalization of the polymer monolithic capillary developed in this work relies on a strategy involving a nucleophilic addition of the pore surface glycerol carbonate functionalities with nucleophilic amino compounds. Indeed, different research groups reported in the past the possibility to easily functionalize such cyclic carbonates with good nucleophiles such as amines,[23,24] but also carboxylates.[25] Hence, we particularly focused our attention on the immobilization of allylamine at the pore surface of such GCMA-based in-capillary monolith as resulting interfacial alkene functionalities would generate a versatile, easy and straightforward platform for subsequent "click" photo-driven radical thiol-ene reaction[26] with chemical thiols of interest. Such a functionalization reaction was monitored by *in-situ* Raman spectroscopy as shown on **Figure 3-15**. The occurrence of the characteristic signal corresponding to the double bond arising from grafted allylamine was immediately noticed on the monolithic capillaries at 1636 cm^{-1} after functionalization reaction of the GCMA-based materials, when compared to pristine GCMA-based monoliths, while the cyclic carbonate characteristic band at 1800 cm^{-1} totally vanished.[27] Energy dispersive X-ray spectroscopy (EDX, **Figure S1 Annexes**) corroborated this finding with the appearing of the Kα ray of nitrogen (at 0.392 keV) in the resulting allyl-functionalized monolithic capillary. As already above-mentioned, a subsequent step was necessary to anchor metal chelating or hydrophobic functionalities at the monolith pore surface, depending on the targeted application, *i.e.* for flow-through catalysis or separation sciences, respectively. To that purpose, a photo-triggered radical thiol-ene addition of either 1-octane thiol or 4-mercaptobutyric acid was envisioned. Again, *in-situ* Raman spectroscopy ascertained the covalent grafting of both organic compounds at the pore surface. Indeed, the total disappearing of the band at 1636 cm^{-1} was noticed, thus demonstrating the efficiency of both photo-triggered radical thiol-ene "click" coupling reactions. These results (**Figure S1, Annexes**) were also confirmed by EDX semi-quantitative analysis that indicated the presence of an important sulfur content in the monoliths after thiol-ene reaction, as showed by the intense sulfur Kα ray at 2.307 keV.

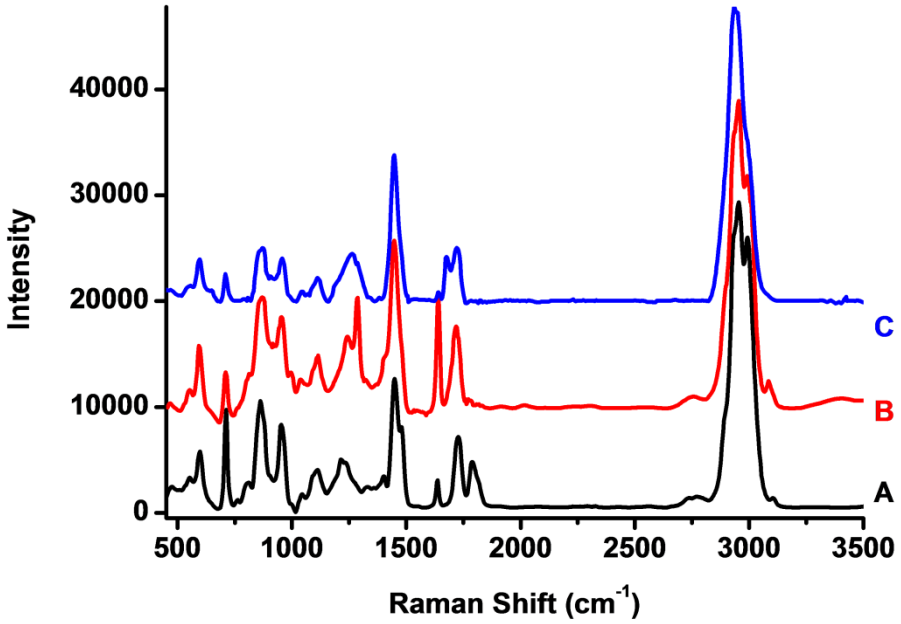

Figure 3-15: *In-situ* Raman spectra of GCMA-based in-capillary monolith *A)* before and *B)* after functionalization with allylamine, and *C)* subsequent "click" thiol-ene addition of 4-mercaptobutyric acid.

The immobilization of metallic nanoparticles at the surface of such polymer-based monolithic capillaries allows for the production of microreactors that can be applied in flow-through catalytic reactions.[22,28] Further immobilization of platinum nanoparticles was thus investigated through the *in situ* strategy consisting in the initial adsorption of metal cations over carboxyl-decorated monolithic surface and subsequent hydride-mediated reduction of metallic ions into the corresponding nanometals. Experimentally, a 1 wt. % Platinum salt ($PtCl_4^{2-}$) solution in ethanol was percolated through the carboxyl-functionalized GCMA-based capillary, thus allowing for Pt^{2+} ions pre-concentration at the pore surface of the carboxyl-functionalized monolith. In a second step, platinum nanoparticles (PtNPs) were generated *via* reduction of Pt^{2+} ion precursors in the presence of sodium borohydride ($NaBH_4$). SEM investigations onto the PtNPs@in-capillary GCMA-based monolith indicated a homogeneous and dense PtNPs coverage of the –COOH coated pore surface, as shown on **Figure 3-16 A**. As polymer-templated/-supported Pt NPs are prone to nitroarenes reduction.[29–31] In this context, the possibility to reduce *p*-nitrophenol (PNP) was investigated in the as-obtained hybrid PtNPs@in-capillary GCMA-based monolith. Upon dynamic loading (flowrate of 2 µL.min^{-1}) of a solution of PNP/$NaBH_4$ through the hybrid monolithic capillary, the solution harvested at the capillary outlet was observed to the naked eye. The yellow coloration of the solution loaded at the capillary inlet totally vanished and the obtained colorless solution was analyzed by UV-visible spectrophotometry.

The success of the reaction was immediately verified by the total disappearing of the π→π* transition band characteristic of PNP at 400 nm along with the appearing of a new π→π* transition band at higher energy (λ = 260 nm) corresponding to the expected product, *i.e. p*-aminophenol (PAP) as shown in **Figure 3-16 B**.

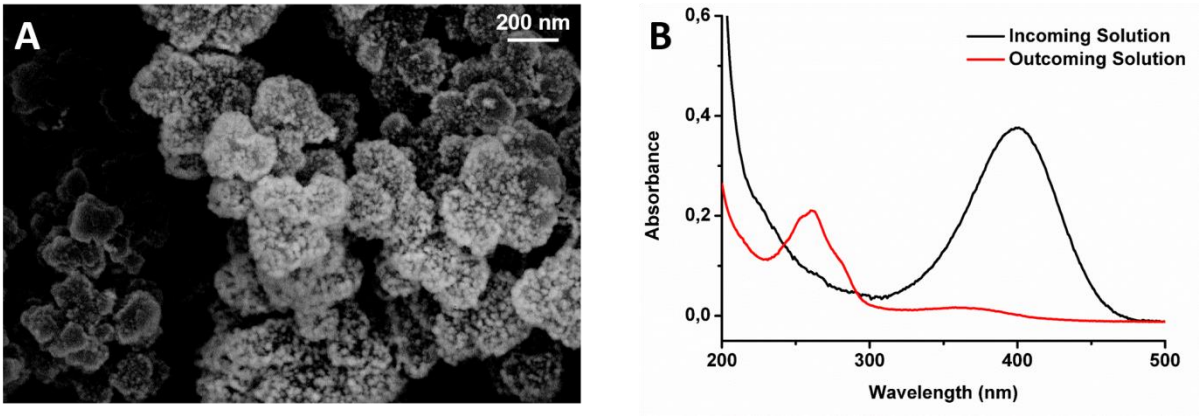

Figure 3-16: *A)* SEM micrographs of PtNPs@in-capillary GCMA-based monolith and *B)* UV-visible spectra of PNP/$NaBH_4$ solution before (black trace) and after (red trace) migration through the hybrid capillary.

3.14 Conclusions

In summary, this paper addresses the unprecedented preparation of monolithic columns from GCMA, a reactive functional monomer arising from renewable resources. Further surface modification of the pendant cyclic carbonate with allylamine afforded resulting alkene functionalized monoliths. A successive radical photo-triggered thiol-ene "click" addition allowed for the efficient grafting of mercaptobutyric acid. The full potential of such functional GCMA-based monolith was demonstrated flow-through catalysis with the efficient reduction of nitroarene model compound through PtNP-immobilized carboxylic acid-functionalized GCMA-based monoliths.

3.15 References

(1) Svec, F.; Fréchet, J. M. J. Modified Poly(Glycidyl Metharylate-Co-Ethylene Dimethacrylate) Continuous Rod Columns for Preparative-Scale Ion-Exchange Chromatography of Proteins. *J. Chromatogr. A* **1995**, *702* (1), 89–95.

(2) Cao, Q.; Xu, Y.; Liu, F.; Svec, F.; Fréchet, J. M. J. Polymer Monoliths with Exchangeable Chemistries: Use of Gold Nanoparticles As Intermediate Ligands for Capillary Columns with Varying Surface Functionalities. *Anal. Chem.* **2010**, *82* (17), 7416–7421.

(3) Xu, Y.; Cao, Q.; Svec, F.; Fréchet, J. M. J. Porous Polymer Monolithic Column with Surface-Bound Gold Nanoparticles for the Capture and Separation of Cysteine-Containing Peptides. *Anal. Chem.* **2010**, *82* (8), 3352–3358.

(4) Lv, Y.; Lin, Z.; Svec, F. "Thiol-Ene" Click Chemistry: A Facile and Versatile Route for the Functionalization of Porous Polymer Monoliths. *Analyst* **2012**, *137* (18), 4114–4118.

(5) Peters, E. C.; Svec, F.; Fréchet, J. M. J. Thermally Responsive Rigid Polymer Monoliths. *Adv. Mater.* **1997**, *9* (8), 630–633.

(6) Luo, Q.; Zou, H.; Xiao, X.; Guo, Z.; Kong, L.; Mao, X. Chromatographic Separation of Proteins on Metal Immobilized Iminodiacetic Acid-Bound Molded Monolithic Rods of Macroporous Poly (Glycidyl Methacrylate–co-Ethylene Dimethacrylate). *J. Chromatogr. A* **2001**, *926* (2), 255–264.

(7) Hutchinson, J. P.; Hilder, E. F.; Shellie, R. A.; Smith, J. A.; Haddad, P. R. Towards High Capacity Latex-Coated Porous Polymer Monoliths as Ion-Exchange Stationary Phases. *Analyst* **2006**, *131* (2), 215–221.

(8) Slater, M.; Snauko, M.; Svec, F.; Fréchet, J. M. J. "Click Chemistry" in the Preparation of Porous Polymer-Based Particulate Stationary Phases for μ-HPLC Separation of Peptides and Proteins. *Anal. Chem.* **2006**, *78* (14), 4969–4975.

(9) Sun, X.; He, X.; Chen, L.; Zhang, Y. In-Column "Click" Preparation of Hydrophobic Organic Monolithic Stationary Phases for Protein Separation. *Anal. Bioanal. Chem.* **2011**, *399* (10), 3407–3413.

(10) Ueki, Y.; Umemura, T.; Li, J.; Odake, T.; Tsunoda, K. Preparation and Application of Methacrylate-Based Cation-Exchange Monolithic Columns for Capillary Ion Chromatography. *Anal. Chem.* **2004**, *76* (23), 7007–7012.

(11) Gusev, I.; Huang, X.; Horváth, C. Capillary Columns with in Situ Formed Porous Monolithic Packing for Micro High-Performance Liquid Chromatography and Capillary Electrochromatography. *J. Chromatogr. A* **1999**, *855* (1), 273–290.

(12) Connolly, D.; Twamley, B.; Paull, B. High-Capacity Gold Nanoparticle Functionalised Polymer Monoliths. *Chem. Commun.* **2010**, *46* (12), 2109–2111.

(13) Floris, P.; Twamley, B.; Nesterenko, P. N.; Paull, B.; Connolly, D. Fabrication and Characterisation of Gold Nano-Particle Modified Polymer Monoliths for Flow-through Catalytic Reactions and Their Application in the Reduction of Hexacyanoferrate. *Microchim. Acta* **2014**, *181* (1), 249–256.

(14) Xie, S.; Svec, F.; Fréchet, J. M. J. Design of Reactive Porous Polymer Supports for High Throughput Bioreactors: Poly(2-Vinyl-4,4-Dimethylazlactone-Co-Acrylamide-Co-Ethylene Dimethacrylate) Monoliths. *Biotechnol. Bioeng.* **1999**, *62* (1), 30–35.

(15) Peterson, D. S.; Rohr, T.; Svec, F.; Fréchet, J. M. J. Enzymatic Microreactor-on-a-Chip: Protein Mapping Using Trypsin Immobilized on Porous Polymer Monoliths Molded in Channels of Microfluidic Devices. *Anal. Chem.* **2002**, *74* (16), 4081–4088.

(16) Chen, H.-X.; Huang, T.; Zhang, X.-X. Immunoaffinity Extraction of Testosterone by Antibody Immobilized Monolithic Capillary with On-Line Laser-Induced Fluorescence Detection. *Talanta* **2009**, *78* (1), 259–264.

(17) Carbonnier, B.; Guerrouache, M.; Denoyel, R.; Millot, M.-C. CEC Separation of Aromatic Compounds and Proteins on Hexylamine-Functionalized N-Acryloxysuccinimide Monoliths. *J. Sep. Sci.* **2007**, *30* (17), 3000–3010.

(18) Guerrouache, M.; Carbonnier, B.; Vidal-Madjar, C.; Millot, M.-C. In Situ Functionalization of N-Acryloxysuccinimide-Based Monolith for Reversed-Phase Electrochromatography. *J. Chromatogr. A* **2007**, *1149* (2), 368–376.

(19) Guerrouache, M.; Millot, M. C.; Carbonnier, B. Capillary Columns for Reversed-Phase CEC Prepared via Surface Functionalization of Polymer Monolith with Aromatic Selectors. *J. Sep. Sci.* **2011**, *34* (16–17), 2271–2278.

(20) Dao, T. T. H.; Guerrouache, M.; Carbonnier, B. Thiol-Yne Click Adamantane Monolithic Stationary Phase for Capillary Electrochromatography. *Chin. J. Chem.* **2012**, *30* (10), 2281–2284.

(21) Tijunelyte, I.; Babinot, J.; Guerrouache, M.; Valincius, G.; Carbonnier, B. Hydrophilic Monolith with Ethylene Glycol-Based Grafts Prepared via Surface Confined Thiol-Ene Click Photoaddition. *Polymer* **2012**, *53* (1), 29–36.

(22) Poupart, R.; Le Droumaguet, B.; Guerrouache, M.; Carbonnier, B. Copper Nanoparticles Supported on Permeable Monolith with Carboxylic Acid Surface Functionality: Stability and Catalytic Properties under Reductive Conditions. *Mater. Chem. Phys.* **2015**, *163*, 446–452.

(23) Guerrouache, M.; Millot, M.-C.; Carbonnier, B. Functionalization of Macroporous Organic Polymer Monolith Based on Succinimide Ester Reactivity for Chiral Capillary Chromatography: A Cyclodextrin Click Approach. *Macromol. Rapid Commun.* **2009**, *30* (2), 109–113.

(24) Lv, Y.; Hughes, T. C.; Hao, X.; Hart, N. K.; Littler, S. W.; Zhang, X.; Tan, T. A Novel Route to Prepare Highly Reactive and Versatile Chromatographic Monoliths. *Macromol. Rapid Commun.* **2010**, *31* (20), 1785–1790.

(25) Ghandi, M.; Mostashari, A.; Karegar, M.; Barzegar, M. Efficient Synthesis of α-Monoglycerides via Solventless Condensation of Fatty Acids with Glycerol Carbonate. *J. Am. Oil Chem. Soc.* **2007**, *84* (7), 681–685.

(26) Guerrouache, M.; Mahouche-Chergui, S.; Chehimi, M. M.; Carbonnier, B. Site-Specific Immobilisation of Gold Nanoparticles on a Porous Monolith Surface by Using a Thiol-Yne Click Photopatterning Approach. *Chem. Commun.* **2012**, *48* (60), 7486–7488.

(27) Huang, C. C.; Lin, C. H.; Dai, S. A. Synthesis of Poly(Isopropenylphenoxy Propylene Carbonate) and Its Facile Side-Chain Functionalization into Hydroxy-Polyurethanes. *J. Polym. Sci. Part Polym. Chem.* **2016**, *54* (6), 802–808.

(28) Nandi, M.; Uyama, H. Porous Acrylate Monolith Supported Pd Nanoparticles: Highly Active and Reusable Catalyst for Suzuki-Miyaura Reaction in Water. *RSC Adv.* **2014**, *4* (40), 20847–20855.

(29) Liu, H.; Wan, D.; Du, J.; Jin, M. Dendritic Amphiphile Mediated One-Pot Preparation of 3D Pt Nanoparticles-Decorated PolyHIPE as a Durable and Well-Recyclable Catalyst. *ACS Appl. Mater. Interfaces* **2015**, *7* (37), 20885–20892.

(30) Pandey, S.; Mishra, S. B. Catalytic Reduction of P-Nitrophenol by Using Platinum Nanoparticles Stabilised by Guar Gum. *Carbohydr. Polym.* **2014**, *113*, 525–531.

(31) Noh, J.-H.; Meijboom, R. Synthesis and Catalytic Evaluation of Dendrimer-Templated and Reverse Microemulsion Pd and Pt Nanoparticles in the Reduction of 4-Nitrophenol: The Effect of Size and Synthetic Methodologies. *Appl. Catal. Gen.* **2015**, *497*, 107–120.

Chapter 4:

Nanoporous Polystyrene Frameworks as New Nanoparticles-Decorated Supports for Heterogeneous Catalysis

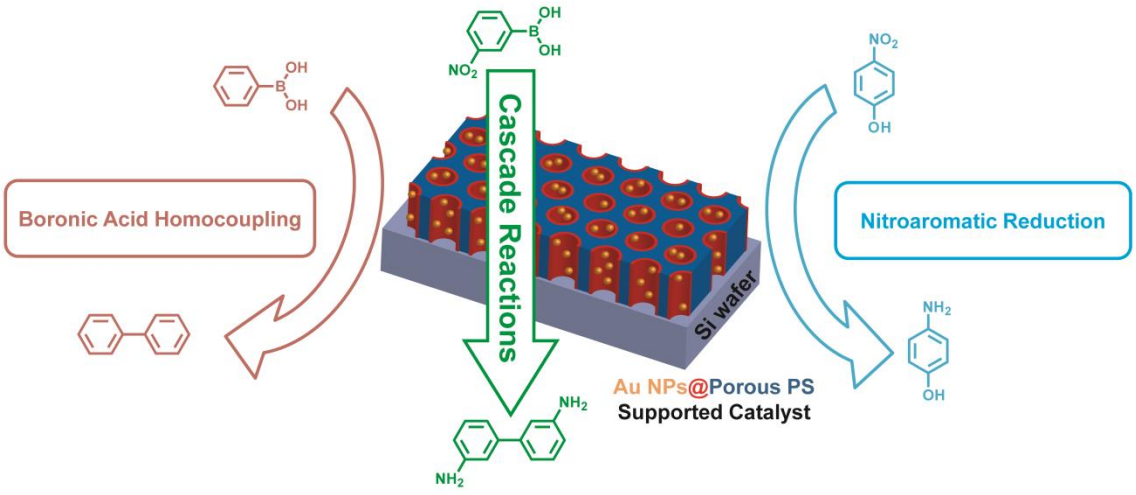

Contexte

Comme décrit précédemment dans le chapitre bibliographique, les membranes polymères peuvent présenter un intérêt majeur pour la catalyse supportée. Si des exemples de membranes nanoporeuses capables de catalyser des réactions ont déjà été présentés dans la littérature, elles sont bien souvent commerciales et éventuellement préalablement modifiées chimiquement de manière à immobiliser des nanoparticules. Par ailleurs, des voies de synthèses originales ont été développées afin de générer des polymères nanoporeux servant de membranes, soit par la technique « track-etching » mais encore par élimination sélective d'un bloc sacrificiel dans des copolymères à blocs nanostructurés.

Cette dernière méthode permet notamment l'accès à différentes morphologies à microséparation de phases. L'exemple le plus concret provient des copolymères diblocs qui permettent d'obtenir des lamelles, des gyroïdes, des cylindres ou des sphères en fonction de la fraction volumique de chacun des blocs constituant le copolymère. Conjointement au polystyrène comme bloc principal, de nombreux blocs sacrificiels ont été utilisés comme le polyisoprène, le poly(méthacrylate de méthyle) ou le poly(acide lactique) dégradables par ozonolyse, rayonnement ultra-violet et hydrolyse, respectivement. De plus, depuis quelques années, des recherches se concentrent sur l'utilisation de copolymères diblocs présentant une jonction clivable entre les deux blocs, afin de faciliter non seulement l'élimination du bloc sacrificiel mais aussi la fonctionnalisation de la surface des pores avec des fonctions d'intérêts. Malgré ces récents développements et les multiples possibilités déjà offertes par ces polymères nanoporeux, ils n'ont encore jamais été utilisés comme supports de nanoparticules métalliques pour la catalyse hétérogène.

C'est pourquoi, nous avons développé des polymères poreux à partir de copolymères diblocs polystyrène-*bloc*-poly(acide D,L-lactique) (PS-*b*-PLA) possédant une rotule chimique pouvant être aisément et sélectivement clivée. Nous avons d'abord synthétisé un amorceur difonctionnel possédant un pont disulfure central, une liaison terminale C^{IV}-Br permettant d'amorcer la polymérisation radicalaire par transfert d'atome (ATRP) du styrène et un alcool primaire terminal afin d'amorcer la polymérisation par ouverture de cycle (ROP) du D,L-lactide. Après polymérisations séquentielles du styrène et du D,L-lactide, en contrôlant la composition finale des copolymères de manière à ce qu'ils développent une morphologie constituée de cylindres de PLA dans une matrice de PS, une étape d'orientation des copolymères dans une cellule de cisaillement a été opérée afin d'aligner les nanodomaines de PLA perpendiculairement au plan membranaire. Les échantillons de copolymères orientés ont ensuite été placés dans une solution d'éthanol contenant de la triphénylphosphine, connue pour être un agent réducteur efficace des ponts disulfure. Les pores cylindriques générés possèdent

ainsi des groupements fonctionnels thiols en surface et ont été utilisés pour l'adsorption de nanoparticules d'or générées *in situ*. Ces systèmes nanoporeux hybrides ont permis la réduction catalytique du 4-nitrophénol sur plusieurs cycles. Ce travail a été publié dans l'article suivant : **"Clickable" thiol-functionalized nanoporous polymers: from their synthesis to further adsorption of gold nanoparticles and subsequent use as efficient catalytic support**, B. Le Droumaguet, R. Poupart, D. Grande, *Polymer Chemistry* **2015**, *6*, 8105-8111.

En outre, nous avons aussi synthétisé un amorceur difonctionnel asymétrique tout à fait original possédant cette fois-ci une jonction acétal dans sa structure. Après la formation séquentielle du bloc de PS et de celui de PLA, les copolymères diblocs ainsi générés ont été déposés sous la forme de films minces sur des supports de silicium. L'orientation des domaines a été effectuée par recuit par vapeur de solvant et a été suivie d'un clivage de la jonction acétal en présence d'acide trifluoroacétique, révélant ainsi les pores dans la matrice de PS. Ces pores, possédant un aldéhyde en surface, ont été post-fonctionnalisés par amination réductrice avec une polyamine, la tétraéthylènepentamine. Les fonctions amine nouvellement présentes à la surface des pores ont été utilisées pour l'ancrage de nanoparticules d'or générées *in situ* par réduction d'acide tétrachloroaurique. Le catalyseur supporté ainsi généré a ensuite servi de catalyseur efficace dans diverses réactions organiques modèles : tout d'abord, la réduction du 4-nitrophénol, puis l'homocouplage boronique de l'acide phénylboronique, et finalement, une réaction en cascade inédite avec l'homocouplage de l'acide 3-nitrophénylboronique suivie de la réduction du 3,3'-dinitrobiphényl intermédiaire. Ce travail original a été publié dans l'article suivant : **Porous gold nanoparticle-decorated nanoreactors prepared from smartly designed functional polystyrene-*block*-poly(D,L-lactide) diblock copolymers: Toward efficient systems for cascade reaction processes**, R. Poupart, A. Benlahoues, B. Le Droumaguet, D. Grande, *ACS Applied Materials & Interfaces*, **2017**, article sous presse, DOI : 10.1021/acsami.6b16157.

"Clickable" Thiol-Functionalized Nanoporous Polymers: From their Synthesis to Further Adosrption of Gold Nanoparticles and Subsequent Use as Efficient Catalytic Supports

Abstract: A straightforward and versatile approach towards thiol-functionalized nanoporous polystyrene frameworks is reported through the selective cleavage of a disulfide bridge at the junction between both blocks of newly synthesized polystyrene-*block*-poly(D,L-lactide) (PS-*b*-PLA) diblock copolymer precursors. This methodology requires the synthesis of a disulfide-bearing heterodifunctional initiator that allows for the production of well-defined diblock copolymers by combining atom transfer radical polymerization (ATRP) of styrene and ring-opening polymerization (ROP) of D,L-lactide. After macroscopic orientation of the copolymer precursors through channel die processing and subsequent quantitative degradation of the disulfide bridge *via* triphenylphosphine-mediated reduction, thiol-functionalized porous polymers are obtained. Further, "click" thiol-ene-mediated functionalization of thiol-coated pore walls within nanoporous frameworks is implemented. More interestingly, adsorption of *in-situ* generated gold nanoparticles and subsequent and unprecedented supported catalytic reduction of a model nitroaromatic compound, *i.e. para*-nitrophenol, are successfully achieved. Reusability of the hybrid catalyst is also proved over a 5 run-cycle with conversion of nearly 70% within only two hours.

4.1 Introduction

Due to the large variety of properties and applications of organic porous materials,[1] nanoporous polymer-based systems have attracted significant attention within the research community. The applications for these materials are diverse, *i.e.* filtration and separation techniques, heterogeneous supported catalysis, as well as diagnosis or drug delivery.[2,3] Organic porous materials present unique properties compared to their inorganic nanostructured analogues,[4] such as simplicity of functionalization, tunable mechanical properties, and above all low-cost production. The preparation of porous polymeric materials has been reported with pore sizes ranging from some nanometers to some micrometers. More interestingly, block copolymers (BCPs) develop well-defined equilibrium domain morphologies (*i.e.*, for linear diblock copolymers, alternating lamellae, hexagonally close-packed cylinders, bicontinuous gyroids, and body-centered cubic spheres), and thus constitute arguably ideal nanostructured precursors for the formation of ordered mesoporous polymers.[5–7] In this particular case, the copolymer is composed of at least one sacrificial block that should allow for well-defined porosity after a selective etching process. The removal of the sacrificial block can be achieved using two main strategies. The first one relies on the degradation of the expendable segment itself. In this case, etching conditions are clearly dictated by the nature of the concerned block. The sacrificial components used to generate nanopores in BCP precursors are diversified and include poly(dimethylsiloxane) (PDMS),[8–10] poly(propylene glycol) (PPG),[11] polyisoprene (PI)[12] or poly(methyl methacrylate) (PMMA)[13,14] that can be degraded by reaction with HF or tetrabutyl ammonium fluoride, oxygen plasma treatment (or degradation in presence of fuming nitric acid), ozonolysis or UV irradiation followed by acetic acid extraction, respectively. In addition, the selective hydrolysis of the polyester block associated with polystyrene-*block*-poly(D,L-lactide) (PS-*b*-PLA) diblock copolymers has allowed for controlling the porosity and the functionality of resulting nanoporous polymers, in previous contributions.[15–18] Alternatively, ongoing research concerns the development of more efficient and environmentally benign etching strategies. In this context, the insertion of an easily cleavable linker group at the junction between the microphase-separated blocks of BCPs seems to be a promising route, since it allows for site-specific scission between both blocks. This elegant strategy does not require degradation of the entire backbone of the polymer segment in the sacrificial minor phase. The chemical nature of the linker should thus be suitably chosen so as to allow for its subsequent cleavage under experimental conditions that do not alter/destroy the morphology of BCPs obtained during the self-organization process. “Smart” methodologies involving the cleavage of the chemical junction between incompatible blocks have been successfully put forward in the literature for the generation of nanoporous polymeric frameworks. For instance, a hetero-Diels-Alder adduct,[19] orthonitrobenzyl,[20,21] or trityl ether[22] functional groups can be inserted at the junction between both blocks of diblock copolymers, and such groups can be specifically cleaved under rather mild conditions. A ruthenium (II)-terpyridine bis-complex[23] or a $-SO_3^-@-NH_3^+$ ionic pair[24] have also

been introduced into "pseudo" BCPs, allowing for further facile degradation of the interfacial junction moiety. Such design strategies for the incorporation of a functional junction essentially do not alter the self-organization behaviour of the BCPs because of the negligible volume fraction of the linking entities. Moreover, they pave the way for decoration of pore walls with reactive functional groups and expand the choice of components for the BCP precursors. Especially, the chemical reduction of a disulfide bridge at the junction between incompatible polystyrene (PS) and poly(ethylene oxide) (PEO) segments in PS-*b*-PEO copolymers has afforded well-defined nanoporous polystyrene frameworks.[25] Nevertheless, the preparation of such advanced materials requires many synthetic steps so as to introduce the disulfide bridge within the diblock copolymer precursors.

In this context, we describe the synthesis of PS-*b*-PLA diblock copolymers possessing a disulfide group at the junction point between both blocks *via* a novel and straightforward methodology from a purposely designed disulfide-bearing dual initiator. Their macroscopic orientation, followed by the reduction of the disulfide bridge joining both blocks leads to the formation of nanoporous polymeric materials with thiol-coated pore walls. The subsequent "click" thiol-ene coupling with a model allyl-functionalized PEG evidences the presence of chemically accessible and modifiable thiol functions on the pore surface. Furthermore, *in-situ* generated gold nanoparticles (GNPs) are immobilized at the surface of nanochannels, and these innovative hybrid systems can efficiently be used as supported catalysts. To the best of our knowledge, such GNP@nanoporous polymer hybrid materials have not found any application as nanoreactors in heterogeneous catalysis so far.

4.2 Experimental

4.2.1 Materials

All polymerizations were carried out using standards Schlenk techniques under nitrogen atmosphere. THF (99.9%, SDS) and anisole (99%, SDS) were stored upon 4 Å molecular sieves, and used without any further purification. Prior to use, Cu(I)Br (99%, Aldrich) was purified as reported by Keller and Wycoff.[26] Styrene (Aldrich) was passed through a column filled with basic alumina in order to remove any polymerization inhibitor. Pentamethyldiethylenetriamine (PMDETA, 99%, Aldrich), 3,6-dimethyl-1,4-dioxane-2,5-dione (D,L-lactide, LA), bis(2-hydroxyethyl) disulfide (technical grade, 90%), α-bromoisobutyryl bromide (98%), tin(II) 2-ethylhexanoate ($Sn(Oct)_2$, 95%), triethylamine (99%), gold(III) chloride hydrate ($AuCl_3 \bullet xH_2O$, 99.999%), $NaBH_4$ and allyl bromide (ReagentPlus®, 99%) were purchased from Aldrich and used as received. 4-nitrophenol was supplied by Alfa Aesar. Triphenylphosphine (99%, Acros), dichloromethane (99.9%, Carlo Erba), anhydrous toluene (99.8%, Aldrich), and methanol (MeOH, 99%, SDS) were used without any further purification. α-methoxy poly(ethylene glycol) (Mn NMR = 590 g.mol–1) was obtained from Aldrich and used as received.

18.2 MΩ deionized water was filtered through a Milli-Q Plus purification pack.

4.2.2 Synthesis of 2-[(2-hydroxyethyl)dithio]ethyl 2-bromoisobutyrate

2-[(2-hydroxyethyl)dithio]ethyl 2-bromoisobutyrate was synthesized according to a modified literature procedure.[27] 15.39 g (0.099 mol) of bis(2-hydroxyethyl) disulfide, 100 mL of THF, and 12.54 mL (0.090 mol) of triethylamine were introduced into a three-neck round bottom flask kept under nitrogen atmosphere. The reaction mixture was cooled to 0 °C. 11 mL (0.089 mol) of α-bromoisobutyryl bromide were added dropwise overnight. The reaction mixture was finally stirred at 50 °C for 5 h. After removal of the solvent, the crude product was purified by silica gel column chromatography with an eluent mixture, *i.e.* dichloromethane/cyclohexane (1/3 to 1/1 v/v). The pure product was obtained as a viscous yellowish oil. Yield: 58%. ^{1}H NMR ($CDCl_3$, 400 MHz, 298 K): δ (ppm): 1.92 (s, 6H, –C*(CH₃)₂*–Br), 2.88 (t, 2H, HO–CH_2–C*H₂*–S–, ^{3}J = 5.8 Hz), 2.96 (t, 2H, –CO–O–CH_2–C*H₂*–S–, ^{3}J = 6.7 Hz), 3.88 (t, 2H, HO–C*H₂*–, ^{3}J = 5.8 Hz), 4.39(t, 2H, –C=O–O–C*H₂*–, ^{3}J = 6.7 Hz); ^{13}C NMR ($CDCl_3$, 100 MHz, 298 K): δ (ppm): 31.07 (2C, C–(*C*H_3)$_2$), 36.87 (1C, HO–CH_2-*C*H_2–), 41.80 (1C, –S–*C*H_2–CH_2–O–CO–), 55.95 (1C, HO–*C*H_2–), 68.73 (1C, –*C*H_2–O–CO–), 171.97 (1C, –*C*O_2–). Elemental analysis calculated for $C_8H_{15}BrO_3S_2$: C 31.69%, H 4.99%, Br 26.35%, O 15.83%, S 21.15%; found C 31.41%, H 4.68%, Br 25.60%, O 19.51%, S 18.80%.

4.2.3 Preparation of polystyrene macroinitiator (PS_{104}-OH)

Styrene (11 g, 0.105 mol), 2-[(2-hydroxyethyl)dithio]ethyl 2-bromoisobutyrate (0.304 g, 1 mmol), anisole (4 mL), CuBr (145 mg, 1 mmol) and DMSO (2 mL) were added in a dry Schlenk flask carefully purged with nitrogen. The reaction mixture was degassed by three freeze-pump-thaw cycles before adding PMDETA (120 µL, 1 mmol) under N_2 atmosphere. The initial ratio [monomer]:[initiator]:[ligand]:[catalyst] of the atom transfer radical polymerization (ATRP) feed was fixed at 100:1:1:1 so as to obtain a PS_{104}-OH macroinitiator with a theoretical M_n ~ 10 kg.mol^{-1} after virtually total conversion of the monomer. The flask was immersed in an oil bath at 110 °C. After 36 h, the reaction medium was diluted with CH_2Cl_2, passed through a small pad of neutral alumina and precipitated at least twice into a large volume of cold methanol. The as-obtained PS-OH macroinitiator was dried under vacuum to afford a fine white off powder that was further characterized by ^{1}H NMR and SEC analyses.

4.2.4 Microwave-assisted synthesis of PS-*b*-PLA diblock copolymers

The microwave-assisted ring-opening polymerization (ROP) of LA was carried out using an Anton-Paar monomode 300 microwave reactor. The microwave source was a magnetron with a 2.45 GHz frequency powered by a 900 W power generator, which could be operated at different power levels. Typically, 500 mg (4.8 mmol) of PS_{104}-OH and 660 mg (4.6 mmol) of LA were dissolved in 1 mL of anhydrous toluene in a 10 mL microwave-transparent quartz vial, and the mixture was freeze-dried overnight.[28,29] After freeze-drying, 1 mL of anisole and 50 µL of $Sn(Oct)_2$ (4.8 mmol) were added under a dried nitrogen flow, and the vial was closed with a silicon cap. The internal reaction temperature (120 °C) was monitored and controlled with a fiber-optic sensor (Ruby thermometer) immersed in the reaction solution under vigorous stirring. The polymerization was terminated by cooling the vial with compressed air. The product was diluted with CH_2Cl_2, and precipitated at least twice into a large volume of methanol. The as-obtained PS-*b*-PLA copolymer was dried under vacuum. It was further analyzed by SEC and ^{1}H NMR analyses.

4.2.5 Orientation of PS-*b*-PLA diblock copolymers

A home-made channel die (3 mm wide and 60 mm long) was used to align the nanodomains in the block copolymers. Previously pressed pieces of PS-*b*-PLA were placed in the center of the channel die which was then heated to 140 °C in a laboratory press. The samples were subjected to compression upon constant load (compression ratio of ~ 10) and quenched under load to room temperature over a period of 1 h. The samples were post-annealed overnight at 160 °C to reach thermodynamic equilibrium, before removing them from the channel die with a sample thickness between 0.5 and 1.0 mm.

4.2.6 Removal of PLA segment in diblock copolymers by reduction of disulfide bond

In order to selectively get rid of the PLA block, PS-*b*-PLA pieces (200 mg) were immersed in a mixture containing 6 mL of ethanol and 600 mg of triphenylphosphine at 65 °C for 5 days. The as-obtained porous samples were washed abundantly with ethanol. After dissolution of the sample in $CDCl_3$, the selective removal of the PLA block by reduction of the disulfide bridge was confirmed by ^{1}H NMR.

4.2.7 Synthesis of allyl-terminated poly(ethylene glycol)

An allyl-functionalized poly(ethylene glycol) (PEG) sample was prepared following a previously reported experimental procedure: It was synthesized by reacting a 590 $g.mol^{-1}$ PEG oligomer (1 g, 1.82 mmol) with an excess of allyl bromide (440 mg, 3.64 mmol) over 145 mg of NaOH powder in 5 mL toluene for 12 h at 45 °C.[30] At the end of the reaction, toluene was removed under reduced pressure. The residue was dissolved with 10 mL of deionized water. The aqueous phase was extracted with 4 × 20 mL water. Pooled organic fractions were dried over $MgSO_4$, and CH_2Cl_2 was finally removed under reduced pressure. The pure product was obtained as a pale yellow oil (yield ~ 100%). ^{1}H NMR ($CDCl_3$, 400 MHz, 298 K) δ (ppm): 5.96–5.82 (m, 1H, CH_2=C*H*–CH_2–), 5.20 (dd, 2H, C*H*$_2$=CH–CH_2–, J = 16 & 40 Hz), 3.99 (d, 2H, CH_2=CH–C*H*$_2$–), 3.48–3.75 (m, 52 H, –O–C*H*$_2$–C*H*$_2$–O–), 3.35 (s, 3H, –O–C*H*$_3$).

4.2.8 End-group functionalization by thiol-ene "click" chemistry

In a 10 mL round-bottom flask, 20 mg of PS_{104}-SH ($1.45.10^{-4}$ mol, 1 equiv.) was suspended in a 1 mol % AIBN solution in ethanol (3 mL). 6 mg of allyl-terminated PEG ($5.8.\ 10^{-4}$ mol, 5 equiv.) was added to the suspension. The reaction mixture was stirred for 24 h at 90 °C. The product was recovered by filtration after abundant washing with ethanol and analyzed by ^{1}H NMR.

4.2.9 *In-situ* generation of gold nanoparticles by reducing $HAuCl_4$

21.7 mg of nanoporous polystyrene were put into 1 mL of a 0.1 wt% $HAuCl_4$ solution over 3 days. 5 mg of $NaBH_4$ in 10 mL of water was added dropwise and permitted to react for 2 h. The sample was vigorously washed with water to remove unadsorbed gold nanoparticles (GNPs). SEM pictures of the samples were recorded to check the nanoparticle immobilization.

4.2.10 Reduction of 4-nitrophenol by supported heterogeneous catalysis

A freshly prepared solution containing 200 µL of 4-nitrophenol (5 mg in 10 mL of deionized water), 200 µL of $NaBH_4$ (114 mg in 10 mL of water) in 4 mL of water was mixed with 10 mg of the as-obtained supported GNP-based catalyst for 2 h at room temperature in dark conditions. UV-Vis spectra were recorded before the catalyst addition and 2 h after addition in order to determine the reaction yield. For the sake of comparison, a 4 mL solution containing 200 µL of $NaBH_4$ (114 mg in

10 mL of water) and 200 µL of a 4-nitrophenol solution (5 mg in 10 mL of water) was left for 2 h in the presence of thiol-functionalized nanoporous frameworks as a blank experiment. An iteration of 5 successive cycles was achieved through the same process, again in dark conditions. UV-Vis spectra were recorded in the same ways.

4.2.11 Instrumentation

Size Exclusion Chromatography (SEC) analyses were performed on a system equipped with a Spectra Physics P100 pump with two PL gel 5 µm mixed-C columns from Polymer Laboratories, and a Shodex RI 71 refractive index detector. The eluent was tetrahydrofuran at a flow rate of 1 $mL.min^{-1}$. The system was calibrated by using polystyrene standards from Polymer Source. ^{1}H and ^{13}C NMR spectra were recorded at room temperature on a Bruker Avance II spectrometer operating at a resonance frequency of 400 and 100 MHz, respectively. For ^{1}H NMR analysis, the sample concentration was ~10 $mg.mL^{-1}$, while it was ~ 30 $mg.mL^{-1}$ for ^{13}C NMR experiments. $CDCl_3$ was used as solvent and internal standard (7.27 ppm in ^{1}H NMR; 77.2 ppm in ^{13}C NMR). Scanning Electron Microscopy (SEM) was performed on a LEO 1530 microscope equipped with InLens and Secondary Electron detectors using low accelerating voltage (3 kV). Prior to analyses, the samples were cryo-fractured and coated with a 3-nm layer of palladium/platinum alloy in a Cressington 208 HR sputter-coater. Energy-dispersive X-ray spectroscopy (EDX) was performed using an SSD X-Max detector of 50 mm^2 from Oxford Instruments (127 eV for the Kα of Mn). Inductively coupled plasma optical emission spectrometry (ICP-OES) analysis was performed using a Varian Vista-PRO CCD Simultaneous spectrometer. UV-Vis spectra were recorded between 200 and 600 nm on a Cary 60 UV-Vis Spectrophotometer from Agilent Technologies.

4.3 Results and discussion

4.3.1 Synthesis of PS-*b*-PLA diblock copolymers

PS-*b*-PLA diblock copolymers with a disulfide bridge at the junction between both blocks were newly synthesized by an orthogonal tandem approach combining two distinct polymerization mechanisms, *i.e.* ATRP[31,32] and ROP[33] (**Figure 4-1**).

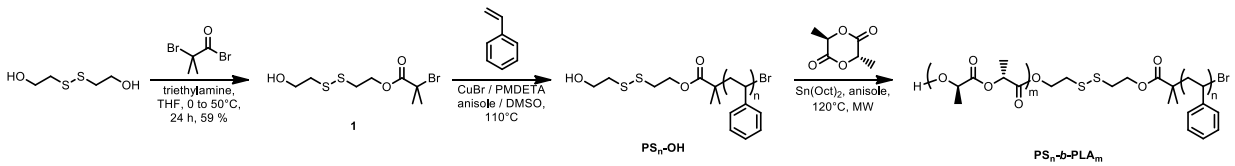

Figure 4-1: Synthetic pathway towards PS-*b*-PLA diblock copolymer precursors by a tandem approach combining ATRP of styrene and MW-assisted ROP of D,L-lactide initiated by 2-[(2-hydroxyethyl)dithio]ethyl 2-bromoisobutyrate.

Such a methodology required the employment of an asymmetric difunctional initiator for the generation of both blocks. For this purpose, we specifically prepared 2-[(2-hydroxyethyl)dithio]ethyl 2-bromoisobutyrate (HDBI **1**, **Figure 4-1**) because it contains *(i)* a disulfide bridge that can be easily cleaved *via* chemical reduction, *(ii)* a tertiary alkyl halide (C^{IV}–Br) that can initiate styrene ATRP, and *(iii)* a terminal primary hydroxyl group (–CH_2OH) that should ensure fast initiation for ROP of LA. This initiator (**1**) was prepared using an adapted literature procedure,[27,34] and it was obtained in nearly 60% yield through a simple nucleophilic substitution by reaction of bis(2-hydroxyethyl) disulfide with 2-bromoisobutyryl bromide in the presence of triethylamine. ^{1}H and^{13}C NMR analyses (**Figure S2 Annexes**) along with elemental analysis of the pure compound confirmed the successful formation of the heterodifunctional initiator necessary to the synthesis of PS-*b*-PLA copolymer precursors. A polystyrene macroinitiator was obtained (PS_{104}-OH) from the initiator (**1**) and displayed an experimental M_n value close to the theoretical one along with a low molar mass dispersity $Đ$ (**Table 4-1**), thus confirming the controlled character of the ATRP of styrene. Further SEC (**Figure S3 Annexes**) and ^{1}H NMR (**Figure 4-2 a**) analyses corroborated the previous results. D,L-lactide was then polymerized from the as-obtained PS_{104}-OH macroinitiator (**Table 4-1**).

The use of microwave-assisted ring-opening of D,L-lactide permitted to proceed with a fast polymerization kinetics (120 °C, 45 min),[28,29] while the polymerization lasted at least 5 days using a conventional heating process.[17] These PS-*b*-PLA copolymers where fully characterized by SEC (**Figure S3 Annexes**) and ^{1}H NMR (**Figure 4-2 b**); their main molecular characteristics are gathered in Table 1. It is noteworthy that these copolymer were synthesized with a PLA volume fraction (f_{PLA}) around 0.3–0.4 in order to develop a morphology of hexagonally close-packed PLA cylinders in a PS matrix, according to Hillmyer's previous investigations.[16] The ^{1}H NMR spectra displayed the typical chemical shifts of PS and PLA, the signals in the 6–7 ppm area being attributed to the aromatic protons of PS, and the resonance bands in the 5–5.5 ppm region arising from –CH– groups of PLA repeating units (**Figure 4-2 b**)

Table 4-1: Molecular features of PS macroinitiator and PS-*b*-PLA precursors obtained using the asymmetric difunctional initiator HDBI.

PS_n[a] or PS_n-*b*-PLA_m[a]	Conversion[b] (%)	$M_{n\ theor}$[c] [kg/mol]	$M_{n\ NMR}$[d] [kg/mol]	$M_{n\ SEC}$[e] [kg/mol]	$Đ$[e]	Polymerization time [h]	f_{PLA}[f]
$PS_{104\text{-}OH}$	79	9.0	10.8	11.8	1.2	36	-
PS_{104}-*b*-PLA_{39}	35	15.9	16.5	23.6	1.3	0.75	0.29
PS_{104}-*b*-PLA_{47}	41	16.9	18.8	17.9	1.2	0.75	0.34
PS_{104}-*b*-PLA_{59}	54	18.8	20.0	20.8	1.2	0.75	0.38

[a] n, m : number-average polymerization degrees of PS or PLA blocks as determined by ^{1}H NMR

[b] Conversion as determined by gravimetry

[c] $M_{n\ theor}$ = conversion × DP_n × M_o(styrene) or $M_{n\ theor}$ = conversion × DP_n × M_o (LA) + $M_{n\ NMR}$ (PS-OH)

[d] $M_{n\ NMR}$: number-average molar mass evaluated by ^{1}H NMR

[e] SEC measurements with polystyrene standards

[f] Volume fraction of PLA as calculated by ^{1}H NMR, assuming that the densities of PS and PLA are 1.02 and 1.25, respectively

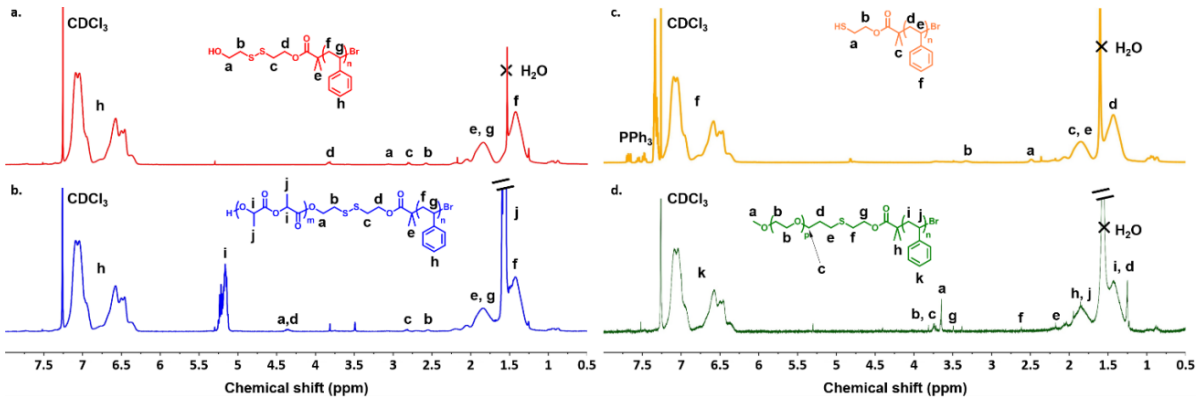

Figure 4-2: ^{1}H NMR spectra: *a)* PS_{104}-OH macroinitiator prepared *via* ATRP, *b)* PS_{104}-*b*-PLA_{47} diblock copolymer prepared *via* the tandem ATRP-ROP approach, *c)* PS_{104}-SH specimen after reductive degradation, *d)* PS-SH coupled with PEG_{14}-allyl.

Furthermore, **Figure S3 Annexes** displays the typical SEC traces obtained for the PS macroinitiator and a PS-*b*-PLA copolymer. The SEC chromatogram of the copolymer exhibited a monomodal distribution and a peak shift toward a lower retention time, thus confirming the formation of a diblock copolymer, while the molar mass dispersity of the as-obtained PS-*b*-PLA copolymer remained rather narrow ($Đ < 1.3$).

4.3.2 Macroscopic orientation of diblock copolymers

The macroscopic orientation of PS-*b*-PLA copolymer nanodomains in bulk materials was realized using a channel die processing technique, as reported elsewhere.[35] During this procedure, diblock copolymers were subjected to shear flow that induced a stress in the materials. This shear stress could then be relieved by a rearrangement of copolymers in such a way that the nanodomains might orientate along the shear direction.

4.3.3 Generation of functionalized nanoporous polymeric materials

Phosphines, *e.g.* tributylphosphine, tris(2-carboxyethyl) phosphine and triphenylphosphine, are prone to efficiently reduce disulfide bridges, especially when inserted in the chemical structure of macromolecular architectures.[27,36–40] As a consequence, triphenylphosphine (PPh_3) was used to reduce the disulfide bridge at the junction between PS and PLA segments of the newly synthesized copolymers. This degradation was conducted in mild conditions, at 65 °C, namely an intermediate temperature between the T_g of PLA (around 50 °C) and that of PS (around 100 °C) in ethanol, *i.e.* a non-solvent for PS, and a solvent for PLA. The completion of this chemical cleavage was monitored by ^{1}H NMR after abundant washing of the resulting materials, drying, and subsequent solubilization in $CDCl_3$. Experimentally, within 5 days of reaction, the total disappearance of typical PLA bands (in particular the signal associated with –CH– protons of repeating units at 5.1–5.2 ppm), was observed as shown in **Figure 4-2 c,** thus confirming the relatively fast completion of the chemical reduction. The experimental conditions selected afforded thiol-functionalized porous PS suitable for further coupling of model compounds *via* thiol-ene "click" chemistry.

4.3.4 Morphological and pore surface chemical characterization of nanoporous polymer frameworks

Upon disulfide reduction, the resulting materials obtained after removal of the PLA block

displayed nanoporous frameworks as observed by SEM. The occurrence of well-defined nanoporosity (D_p = 10 nm) was confirmed by SEM with the observation of cylindrical nanopores (**Figure 4-3**), demonstrating the gain of the expected hexagonally close-packed cylindrical morphology. More importantly, an EDX analysis revealed the presence of sulfur atoms on the pore surface, as observed in **Figure 4-4** with the presence of a weak signal for sulfur at 2.307 keV. Concomitantly, elemental analysis was conducted on the PS_{104}-OH macroinitiator, the PS_{104}-*b*-PLA_{47} copolymer sample, and the corresponding PS material after reduction of disulfide bridge. The sulfur contents found by this technique were in good agreement with those theoretically calculated, *i.e.* 0.56, 0.32, and 0.28 wt.% for the experimental values found for the macroinitiator, the copolymer precursor, and the nanoporous polymer after reduction, and respectively 0.60, 0.34, and 0.30 wt.% for the expected values. These results thus corroborated the quantitative removal of PLA block during the disulfide bridge reduction step. In order to further demonstrate the availability of unmodified thiol groups on pore walls, a post-functionalization reaction was implemented.

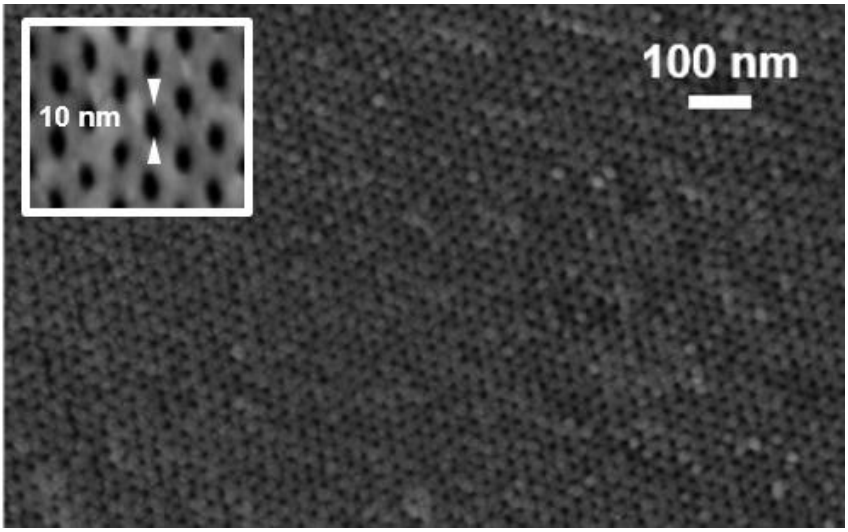

Figure 4-3: Cross-sectional SEM micrograph of the porous polymeric material obtained from PS_{104}-*b*-PLA_{59} after channel die processing and removal of the PLA sacrificial block by selective PPh_3-mediated reduction of disulfide junction. Inset: zoom of the nanopore array (D_p = 10 nm).

4.3.5 Thiol-ene mediated functionalization of nanoporous PS frameworks

The presence of thiol functional groups as chain ends was confirmed through a post-modification "click" thiol-ene addition[41] in a heterogeneous medium. The –SH groups in the as-obtained porous PS frameworks were reacted with allyl-terminated PEG, thus leading to the formation of grafted PEG chains onto the pore walls with a 50% yield, as calculated by ^{1}H NMR (**Figure 4-2 d**). Such a low yield was assumed to be likely due to the steric hindrance of the PEG_{14}-allyl

macromolecule that did not allow for quantitative reaction yields. This functionalization assay illustrates the potential of such thiol-functionalized porous frameworks in the development of functional nanoreactors by thiol-ene "click" ligation with suitable ligands, *e.g.* imidazolyl moieties, allowing for further insertion of metallic nanoparticles within reactive supports for instance.

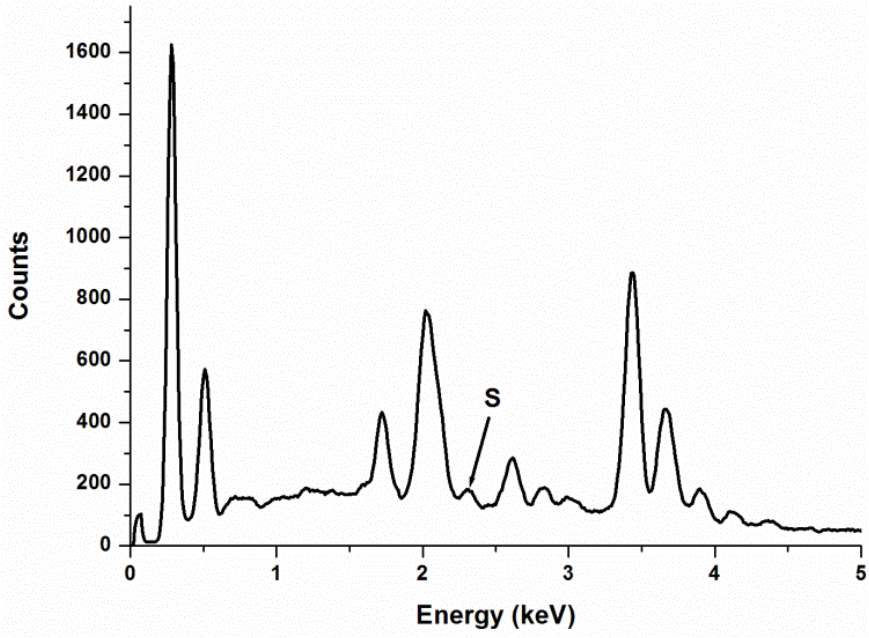

Figure 4-4: EDX spectrum of the pore surface of a thiol functionalized porous polystyrene obtained from a PS_{104}-*b*-PLA_{47} diblock copolymer precursor.

4.3.6 *In-situ* generation of gold nanoparticles adsorbed on porous polystyrene and supported catalytic reduction

It is well-known that thiol-containing organic (macro)molecules have a strong affinity for gold surfaces.[42–45] In addition, supported gold nanoparticles (GNPs) are widely used as nanocatalysts for the reduction of nitro-containing compounds.[42] Notably, it has recently been reported by Barner-Kowollik's research group that thiol-coated nanoporous polystyrene obtained from PS-*b*-PEO diblock copolymers can tightly adsorb GNPs.[19] In this context, GNPs were *in-situ* generated on the surface of the as-obtained thiol-functionalized porous polystyrene frameworks. Nanoporous polymers were immersed for 3 days in a 1 wt. % chloroauric acid ($HAuCl_4$) solution, and then immediately subjected to hydride-mediated reduction in the presence of a solution of sodium borohydride in water. The presence of GNPs was verified by SEM (data not shown), and a quantification of gold in the hybrid system was realized by ICP-MS. It was observed that nanoporous polystyrene could adsorb ~ 1.5 wt. % of gold nanoparticles.

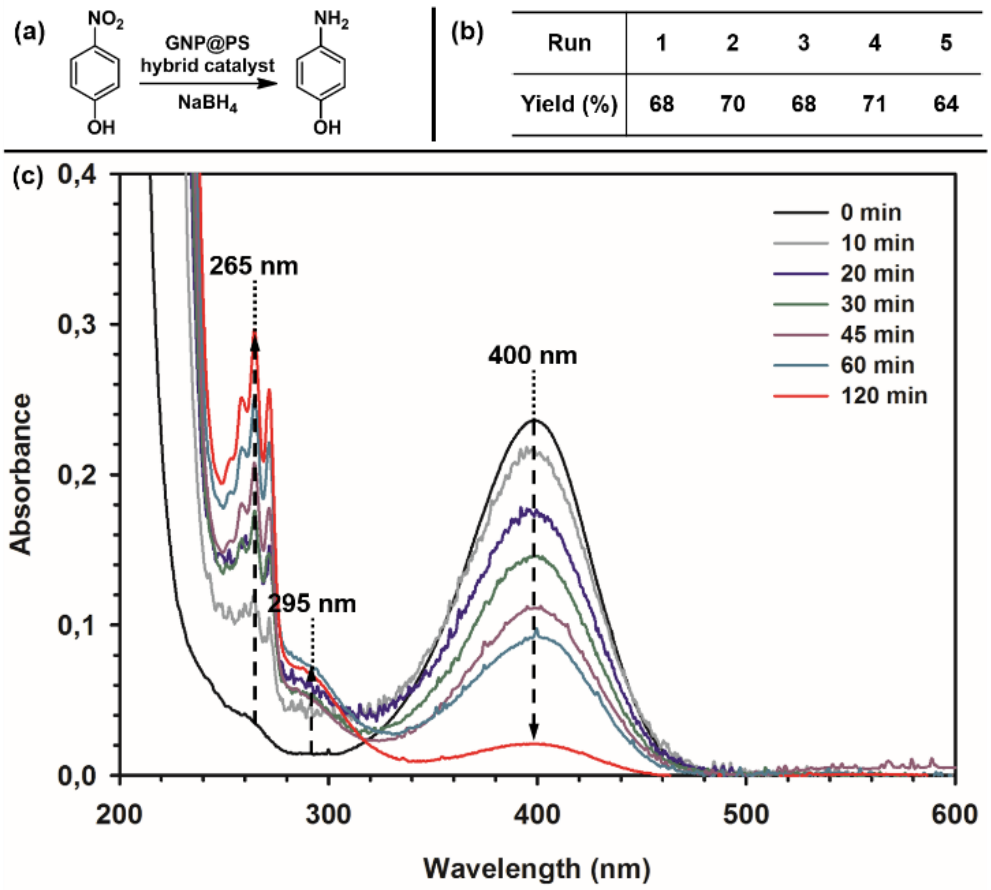

Figure 4-5: *a)* Schematic reaction of the hydride-mediated GNP-catalyzed reduction of 4-nitrophenol. *b)* Stability of the hybrid catalyst after 5 runs of the same reduction reaction. *c)* UV-Vis spectra associated with the reduction of 4-nitrophenol into the corresponding 4-aminophenol as a function of reaction time in the presence of GNP@nanoporous PS hybrid catalyst

Further, the catalytic behaviour of such hybrid porous systems was investigated. To this purpose, $NaBH_4$ and 4-nitrophenol were solubilized in water in the presence of the nanoporous GNP-adsorbed polystyrene hybrid catalyst (**Figure 4-5 a**). The first run of 4-nitrophenol reduction into 4-aminophenol was achieved with a 68% yield over a 1 h period, as demonstrated by the dramatic decrease in the characteristic $\pi \rightarrow \pi^*$ transition band of 4-nitrophenol at 400 nm (**Figure 4-5 c**). This clearly demonstrated the efficiency of the as-obtained catalyst. The UV-Vis spectrum corresponding to the blank experiment showed no reduction of the nitroaromatic compound, even after prolonged contact time with the thiol functionalized nanoporous frameworks (data not shown). Additionally, 4 successive reduction cycles were repeated following the same procedure. The catalyst efficiency was maintained, even after 5 runs (**Figure 4-5 b**). These features clearly demonstrated that the nanoporous hybrid catalyst was very efficient and highly reusable.

4.4 Conclusions

Thiol-functionalized nanoporous materials could be engineered from novel PS-*b*-PLA diblock copolymers containing a disulfide bridge at the interface between the two distinct blocks. These copolymers were synthesized from a new asymmetric difunctional initiator, *i.e.* 2-[(2-hydroxyethyl)dithio]ethyl 2-bromoisobutyrate. After macroscopic orientation of the precursor copolymers and quantitative reduction of the disulfide bridge in a suitable solvent, well-defined nanoporous materials were obtained. The presence of thiol functions on the pore surface was demonstrated by EDX, and it allowed for further "click" thiol-ene-mediated functionalization of the resulting porous materials with an olefin-bearing model compound, *i.e.* allyl-terminated PEG. More interestingly, thiol-coated nanoporous polymeric frameworks allowed for the robust immobilization of gold nanoparticles at the surface of the nanochannels, and such hybrid systems could efficiently be used as supported catalysts for the reduction of nitro compounds.

This investigation paves the way for further functionalization of thiol-coated porous nanoreactors with interesting model compounds that could find applications in the design of innovative catalytic supports or nanofiltration membranes.

4.5 References

(1) Wu, D.; Xu, F.; Sun, B.; Fu, R.; He, H.; Matyjaszewski, K. Design and Preparation of Porous Polymers. *Chem. Rev.* **2012**, *112* (7), 3959–4015.

(2) Guan, J.; Fujimoto, K. L.; Sacks, M. S.; Wagner, W. R. Preparation and Characterization of Highly Porous, Biodegradable Polyurethane Scaffolds for Soft Tissue Applications. *Biomaterials* **2005**, *26* (18), 3961–3971.

(3) Hentze, H.-P.; Antonietti, M. Porous Polymers and Resins for Biotechnological and Biomedical Applications. *Rev. Mol. Biotechnol.* **2002**, *90* (1), 27–53.

(4) Martin, C. R. Nanomaterials: A Membrane-Based Synthetic Approach. *Science* **1994**, *266* (5193), 1961.

(5) Hillmyer, M. A. Nanoporous Materials from Block Copolymer Precursors. In *Block Copolymers II*; Abetz, V., Ed.; Advances in Polymer Science; Springer Berlin Heidelberg: Berlin, Heidelberg, 2005; pp 137–181.

(6) Olson, D. A.; Chen, L.; Hillmyer, M. A. Templating Nanoporous Polymers with Ordered Block Copolymers. *Chem. Mater.* **2008**, *20* (3), 869–890.

(7) Pietsch, T.; Gindy, N.; Mahltig, B.; Fahmi, A. Fabrication of Functional Nano-Objects via Self-Assembly of Nanostructured Hybrid Materials. *J. Polym. Sci. Part B Polym. Phys.* **2010**, *48* (14), 1642–1650.

(8) Cavicchi, K. A.; Zalusky, A. S.; Hillmyer, M. A.; Lodge, T. P. An Ordered Nanoporous Monolith from an Elastomeric Crosslinked Block Copolymer Precursor. *Macromol. Rapid Commun.* **2004**, *25* (6), 704–709.

(9) Hansen, M. S.; Vigild, M. E.; Berg, R. H.; Ndoni, S. Nanoporous Crosslinked Polyisoprenefrom Polyisoprene—Polydimethylsiloxane BlockCopolymer. *Polym. Bull.* **2004**, *51* (5), 403–409.

(10) Szewczykowski, P. P.; Andersen, K.; Schulte, L.; Mortensen, K.; Vigild, M. E.; Ndoni, S. Elastomers with Reversible Nanoporosity. *Macromolecules* **2009**, *42* (15), 5636–5641.

(11) Hedrick, J. L.; Miller, R. D.; Hawker, C. J.; Carter, K. R.; Volksen, W.; Yoon, D. Y.; Trollsås, M. Templating Nanoporosity in Thin-Film Dielectric Insulators. *Adv. Mater.* **1998**, *10* (13), 1049–1053.

(12) Chen, S.-Y.; Huang, Y.; Tsiang, R. C.-C. Ozonolysis Efficiency of PS-b-PI Block Copolymers for Forming Nanoporous Polystyrene. *J. Polym. Sci. Part Polym. Chem.* **2008**, *46* (6), 1964–1973.

(13) Sekine, R.; Sato, N.; Matsuyama, T.; Akasaka, S.; Hasegawa, H. Radiation-Induced Fabrication of Polymer Nanoporous Materials from Microphase-Separated Structure of Diblock Copolymers as a Template. *J. Polym. Sci. Part Polym. Chem.* **2007**, *45* (24), 5916–5922.

(14) Li, Y.; Ito, T. Surface Chemical Functionalization of Cylindrical Nanopores Derived from a Polystyrene−Poly(Methylmethacrylate) Diblock Copolymer via Amidation. *Langmuir* **2008**, *24* (16), 8959–8963.

(15) Zalusky, A. S.; Olayo-Valles, R.; Taylor, C. J.; Hillmyer, M. A. Mesoporous Polystyrene Monoliths. *J. Am. Chem. Soc.* **2001**, *123* (7), 1519–1520.

(16) Zalusky, A. S.; Olayo-Valles, R.; Wolf, J. H.; Hillmyer, M. A. Ordered Nanoporous Polymers from Polystyrene−Polylactide Block Copolymers. *J. Am. Chem. Soc.* **2002**, *124* (43), 12761–12773.

(17) Grande, D.; Penelle, J.; Davidson, P.; Beurroies, I.; Denoyel, R. Functionalized Ordered Nanoporous Polymeric Materials: From the Synthesis of Diblock Copolymers to Their Nanostructuration and Their Selective Degradation. *Microporous Mesoporous Mater.* **2011**, *140* (1), 34–39.

(18) Majdoub, R.; Antoun, T.; Le Droumaguet, B.; Benzina, M.; Grande, D. Original Route to Polylactide–polystyrene Diblock Copolymers Containing a Sulfonyl Group at the Junction between Both Blocks as Precursors to Functional Nanoporous Materials. *React. Funct. Polym.* **2012**, *72* (8), 495–502.

(19) Glassner, M.; Blinco, J. P.; Barner-Kowollik, C. Formation of Nanoporous Materials via Mild Retro-Diels-Alder Chemistry. *Polym. Chem.* **2011**, *2* (1), 83–87.

(20) Kang, M.; Moon, B. Synthesis of Photocleavable Poly(Styrene-Block-Ethylene Oxide) and Its Self-Assembly into Nanoporous Thin Films. *Macromolecules* **2009**, *42* (1), 455–458.

(21) Zhao, H.; Gu, W.; Thielke, M. W.; Sterner, E.; Tsai, T.; Russell, T. P.; Coughlin, E. B.; Theato, P. Functionalized Nanoporous Thin Films and Fibers from Photocleavable Block Copolymers Featuring Activated Esters. *Macromolecules* **2013**, *46* (13), 5195–5201.

(22) Zhang, M.; Yang, L.; Yurt, S.; Misner, M. J.; Chen, J.-T.; Coughlin, E. B.; Venkataraman, D.; Russell, T. P. Highly Ordered Nanoporous Thin Films from Cleavable Polystyrene-Block-Poly(Ethylene Oxide). *Adv. Mater.* **2007**, *19* (12), 1571–1576.

(23) Fustin, C.-A.; Lohmeijer, B. G. G.; Duwez, A.-S.; Jonas, A. M.; Schubert, U. S.; Gohy, J.-F. Nanoporous Thin Films from Self-Assembled Metallo- Supramolecular Block Copolymers. *Adv. Mater.* **2005**, *17* (9), 1162–1165.

(24) Takahashi, A.; Rho, Y.; Higashihara, T.; Ahn, B.; Ree, M.; Ueda, M. Preparation of Nanoporous Poly(3-Hexylthiophene) Films Based on a Template System of Block Copolymers via Ionic Interaction. *Macromolecules* **2010**, *43* (11), 4843–4852.

(25) Ryu, J.-H.; Park, S.; Kim, B.; Klaikherd, A.; Russell, T. P.; Thayumanavan, S. Highly Ordered Gold Nanotubes Using Thiols at a Cleavable Block Copolymer Interface. *J. Am. Chem. Soc.* **2009**, *131* (29), 9870–9871.

(26) Keller, R. N.; Wycoff, H. D.; Marchi, L. E. Inorganic Syntheses. In *Inorganic Syntheses*; New York, 1946; Vol. 2, pp 1–4.

(27) Tsarevsky, N. V.; Matyjaszewski, K. Combining Atom Transfer Radical Polymerization and Disulfide/Thiol Redox Chemistry: A Route to Well-Defined (Bio)Degradable Polymeric Materials. *Macromolecules* **2005**, *38* (8), 3087–3092.

(28) Ramier, J.; Renard, E.; Grande, D. Microwave-Assisted Ring-Opening Polymerization of D,L-Lactide: A Probe for the Nonexistence of Nonthermal Microwave Effects. *Macromol. Chem. Phys.* **2012**, *213* (7), 784–788.

(29) Ramier, J.; Renard, E.; Grande, D. Microwave-Assisted Synthesis and Characterization of Biodegradable Block Copolyesters Based on Poly(3-Hydroxyalkanoate)s and Poly(D,L-Lactide). *J. Polym. Sci. Part Polym. Chem.* **2012**, *50* (7), 1445–1455.

(30) Kurian, P.; Zschoche, S.; Kennedy, J. P. Synthesis and Characterization of Novel Amphiphilic Block Copolymers Di-, Tri-, Multi-, and Star Blocks of PEG and PIB. *J. Polym. Sci. Part Polym. Chem.* **2000**, *38* (17), 3200–3209.

(31) Wang, J.-S.; Matyjaszewski, K. Controlled/"living" Radical Polymerization. Atom Transfer Radical Polymerization in the Presence of Transition-Metal Complexes. *J. Am. Chem. Soc.* **1995**, *117* (20), 5614–5615.

(32) Kato, M.; Kamigaito, M.; Sawamoto, M.; Higashimura, T. Polymerization of Methyl Methacrylate with the Carbon Tetrachloride/Dichlorotris- (Triphenylphosphine)Ruthenium(II)/Methylaluminum Bis(2,6-Di-Tert-Butylphenoxide) Initiating System: Possibility of Living Radical Polymerization. *Macromolecules* **1995**, *28* (5), 1721–1723.

(33) Kricheldorf, H. R.; Kreiser-Saunders, I.; Boettcher, C. Polylactones: 31. Sn(II)Octoate-Initiated Polymerization of L-Lactide: A Mechanistic Study. *Polymer* **1995**, *36* (6), 1253–1259.

(34) Tsarevsky, N. V.; Matyjaszewski, K. Reversible Redox Cleavage/Coupling of Polystyrene with Disulfide or Thiol Groups Prepared by Atom Transfer Radical Polymerization. *Macromolecules* **2002**, *35* (24), 9009–9014.

(35) Drzal, P. L.; Barnes, J. D.; Kofinas, P. Path Dependent Microstructure Orientation during Strain Compression of Semicrystalline Block Copolymers. *Polymer* **2001**, *42* (13), 5633–5642.

(36) Tsarevsky, N. V.; Huang, J.; Matyjaszewski, K. Synthesis of Hyperbranched Degradable Polymers by Atom Transfer Radical (Co)Polymerization of Inimers with Ester or Disulfide Groups. *J. Polym. Sci. Part Polym. Chem.* **2009**, *47* (24), 6839–6851.

(37) Gao, H.; Tsarevsky, N. V.; Matyjaszewski, K. Synthesis of Degradable Miktoarm Star Copolymers via Atom Transfer Radical Polymerization. *Macromolecules* **2005**, *38* (14), 5995–6004.

(38) Burns, J. A.; Butler, J. C.; Moran, J.; Whitesides, G. M. Selective Reduction of Disulfides by Tris(2-Carboxyethyl)Phosphine. *J. Org. Chem.* **1991**, *56* (8), 2648–2650.

(39) Chujo, Y.; Sada, K.; Naka, A.; Nomura, R.; Saegusa, T. Synthesis and Redox Gelation of Disulfide-Modified Polyoxazoline. *Macromolecules* **1993**, *26* (5), 883–887.

(40) Wang, W.; Murray, R. W. Reaction of Triphenylphosphine with Phenylethanethiolate-Protected Au38 Nanoparticles. *Langmuir* **2005**, *21* (15), 7015–7022.

(41) Lowe, A. B. Thiol-Ene "Click" Reactions and Recent Applications in Polymer and Materials Synthesis. *Polym. Chem.* **2010**, *1* (1), 17–36.

(42) Pradhan, N.; Pal, A.; Pal, T. Catalytic Reduction of Aromatic Nitro Compounds by Coinage Metal Nanoparticles. *Langmuir* **2001**, *17* (5), 1800–1802.

(43) Panigrahi, S.; Basu, S.; Praharaj, S.; Pande, S.; Jana, S.; Pal, A.; Ghosh, S. K.; Pal, T. Synthesis and Size-Selective Catalysis by Supported Gold Nanoparticles: Study on Heterogeneous and Homogeneous Catalytic Process. *J. Phys. Chem. C* **2007**, *111* (12), 4596–4605.

(44) Kuroda, K.; Ishida, T.; Haruta, M. Reduction of 4-Nitrophenol to 4-Aminophenol over Au Nanoparticles Deposited on PMMA. *J. Mol. Catal. Chem.* **2009**, *298* (1), 7–11.

(45) Saha, S.; Pal, A.; Kundu, S.; Basu, S.; Pal, T. Photochemical Green Synthesis of Calcium-Alginate-Stabilized Ag and Au Nanoparticles and Their Catalytic Application to 4-Nitrophenol Reduction. *Langmuir* **2010**, *26* (4), 2885–2893.

Porous Gold Nanoparticles-Decorated Reactors Prepared from Smartly Designed Functional Polystyrene-*block*-Poly(D,L-Lactide) Diblock Copolymers: Towards Efficient Systems for Catalytic Cascade Reaction Processes

Abstract: Original nanoporous catalytic supports can be engineered *via* an effective and straightforward synthetic route to polystyrene-*block*-poly(D,L-lactide) diblock copolymer precursors displaying an acid-cleavable acetal junction between both blocks. To this purpose, an acetal-containing hetero-difunctional initiator was synthesized, thus enabling to combine two different polymerization methods, *i.e.* first Atom Transfer Radical Polymerization (ATRP) of styrene, and then Ring-Opening Polymerization (ROP) of D,L-lactide. Thanks to the labile nature of the acetal junction, oriented nanoporous frameworks could be obtained upon trifluoroacetic acid-mediated cleavage of the latter, after orientation of the block copolymer nanodomains by solvent vapor annealing. The resulting nanoporous materials bearing a reactive aldehyde function at the pore surface allowed for further chemical modification *via* reductive amination with amino-containing compounds, such as tetraethylenepentamine, thus leading to amine-functionalized nanoporous polystyrene. *In-situ* generated gold nanoparticle could then be immobilized within such functionalized porous nanoreactors, and these hybrid materials could find interesting applications in heterogeneous supported catalysis. In this regard, model catalytic reactions, including C-C homocoupling of benzeneboronic acid derivatives, hydride-mediated reduction of nitroaromatic compounds, and especially unprecedented "one-pot" cascade reactions consisting of the latter consecutive reactions from 3-nitrobenzeneboronic acid, were successfully monitored by different chromatographic and spectroscopic techniques.

4.6 Introduction

Research on porous polymers has witnessed a rapid expansion in the last decades because of the plethora of applications offered by these peculiar materials. Among them, nanoporous polymeric frameworks have encountered specific applications in filtration and separation techniques, heterogeneous supported catalysis, gas transport, as well as in diagnosis or drug delivery.[1-5] They present unique intrinsic properties when compared to their inorganic counterparts that make them really appealing, including tunable mechanical properties, ease of functionalization, high compatibility toward organic and biological molecules, and more importantly chemical processing/engineering associated with low-cost production. Nanoporous polymer-based materials obtained from block copolymer (BCP) precursors have notably been the subject of intense research and widespread interest in the last decade.[6-9] Indeed, BCPs develop well-defined equilibrium domain morphologies (*i.e.*, for linear diblock copolymers, alternating lamellae, hexagonally close-packed cylinders, bicontinuous gyroids, and body-centered cubic spheres), and thus constitute ideal nanostructured precursors for the formation of ordered mesoporous polymers. In such a case, the copolymer precursor is composed of at least one sacrificial block that should allow for well-defined nanoporosity after a selective etching process. The removal of the sacrificial block can be achieved using two main strategies. The first one relies on the degradation of the expendable block itself, etching conditions being dictated by the nature of the block. The sacrificial segments in BCP precursors used to generate nanopores are diversified and may include poly(dimethyl siloxane) (PDMS),[10-13] poly(propylene glycol) (PPG),[14] poly(isoprene) (PI)[15-17] or poly(methyl methacrylate) (PMMA)[18-20] that can be degraded by reaction with HF or tetrabutyl ammonium fluoride, oxygen plasma treatment (or degradation in presence of fuming nitric acid), ozonolysis or UV irradiation, respectively. In addition, the selective alkaline hydrolysis of the polyester block associated with polystyrene-*block*-poly(D,L-lactide) (PS-*b*-PLA) diblock copolymers has permitted to control the porosity and the functionality of the resulting nanoporous polymers in miscellaneous contributions.[21-25]

Alternatively, ongoing research concerns the development of more efficient and environmentally benign etching strategies. In this context, the insertion of an easily cleavable linker group at the junction between both blocks of diblock copolymers seems to be a promising route, since it readily allows for site-specific scission between both blocks and does not require degradation of the entire backbone of the sacrificial polymer segment. The chemical nature of the linker should thus be suitably chosen so as to allow for its subsequent cleavage under mild experimental conditions that do not alter/destroy the morphology of the resulting porous polymeric scaffolds. “Smart” methodologies have thus been successfully put forward by different research groups for the generation of nanoporous polymeric frameworks. For instance, a hetero-Diels-Alder adduct,[26] orthonitrobenzyl,[27-28] trityl ether[29] or disulfide bridge[30-31] functional groups can be inserted between both blocks of BCP precursors, and such groups can be specifically cleaved under rather mild conditions. The acetal function, which can

be easily cleaved under mild acidic conditions to afford aldehyde and diol functions then appears as a potential promising junction between BCPs blocks. A decade ago, Taubmann *et al* [32] presented the synthesis of poly(oxazoline)-based copolymers bearing acetal side chains that can react chemoselectively with *O*-benzylhydroxylamine hydrochloride to yield the corresponding oxime-based functionalized copolymers. More recently, Legros *et al.* [33] reported on the synthesis of poly(oxazoline)-based random copolymers exhibiting acetal pendant chains. The latter were then deprotected in the presence of trifluoroacetic acid (TFA) and the resulting aldehyde functions were subjected to aminolysis in the presence of primary amines, such as benzylamine and subsequent reduction of the corresponding Schiff base by sodium cyanoborohydride ($NaCNBH_3$) to afford functionalized copolymers. Finally, another elegant strategy based on the facile and straightforward TFA-based hydrolysis of the acetal moiety was recently adopted for the preparation of polystyrene-*block*-poly(*tert*-butyl methacrylate) (PS-*b*-P*t*BA) diblock copolymers. It relied notably on a two-step polymerization process from an acetal-containing difunctional initiator through a combination of Reversible Addition-Fragmentation chain-Transfer (RAFT) polymerization and Atom Transfer Radical Polymerization (ATRP).[34] The subsequent acidic cleavage of the acetal moiety allowed for the generation of two homopolymers with either terminal aldehyde or diol functions.

In the present paper, we describe an original synthetic route to engineer functionalized nanoporous PS frameworks from newly synthetized PS-*b*-PLA precursors possessing an acetal function at the junction between both blocks. After proper orientation of the diblock copolymers and removal of the PLA sacrificial block *via* TFA-based hydrolysis of the acetal junction, nanoporous ordered materials with aldehyde functions on the pore surface can be obtained allowing for further functionalization. In this context, reductive amination of the aldehyde moieties with a multidentate amine, *i.e.* tetraethylenepentamine, is achieved. Furthermore, the possibility to immobilize *in-situ* generated gold nanoparticles (GNPs) on the as-obtained amine-decorated pore walls is investigated. Finally, the resulting GNP@porous PS hybrid materials can be efficiently used as supported catalysts in model reactions, including C-C homocoupling of benzeneboronic acid derivatives, hydride-mediated reduction of nitroaromatic compounds, and especially unprecedented "one-pot" cascade reactions consisting of the latter consecutive reactions from 3-nitrobenzeneboronic acid.

4.7 Materials and Methods

4.7.1 Materials

All polymerizations were carried out using standard Schlenk techniques under nitrogen atmosphere. Anisole (99 %, Aldrich) was stored upon 4 Å molecular sieves, and used without any further purification. Styrene (99 %, Aldrich) was passed through a pad of neutral alumina to removed

radical inhibitor prior to use. Prior to use, Cu(I)Br (99 %, Aldrich) was purified as reported by Keller and Wycoff.[35] 3,6-Dimethyl-1,4-dioxane-2,5-dione (D,L-lactide, Aldrich) was recrystallized from ethyl acetate, and stored at 4 °C prior to use. 4-Hydroxybenzaldehyde (98 %), tin(II) 2-ethylhexanoate ($SnOct_2$, 95 %), anhydrous toluene (99.8 %), *N,N,N',N'',N''*-pentamethyldiethylenetriamine (PMDETA, 99 %), tetraethylenepentamine (TEPA, technical grade), methanol (99.8 %), sodium borohydride ($NaBH_4$, ≥ 98 %) and sodium cyanoborohydride ($NaCNBH_3$, 99 %) were purchased from Aldrich and used as received. Benzeneboronic acid (98 %+, Alfa Aesar), 3-nitrobenzeneboronic acid (98 %, Alfa Aesar), *α*-bromoisobutyrylbromide (97 %, Alfa Aesar), trimethylamine (TEA, 99 %, Alfa Aesar), 4-nitrophenol (4-NP, 99 %), potassium carbonate (K_2CO_3, 99 %, Alfa Aesar), trifluoroacetic acid (TFA, 99 %, SDS), and dichloromethane (99.8 %, VWR) were used as received. Ethyl acetate (99.9 %), tetrahydrofuran (THF, 99 %) and cyclohexane (99.8 %) were obtained from SDS and used without any further purification

4.7.2 Synthesis of ATRP initiator

2.44 g (20 mmol) of *p*-hydroxybenzaldehyde, and 5.5mL (40 mmol) of TEA were mixed with 25 mL of dichloromethane in a three-neck round bottom flask immerged in an ice/water bath. 9.4 mL (22 mmol) of *α* -bromoisobutyryl bromide diluted in 13 mL of dichloromethane were added dropwise overnight into the latter flask under nitrogen atmosphere. After the reaction, the solution was filtered off to remove the white precipitate and washed successively with HCl (1 M) and K_2CO_3 saturated solution. The organic layer was dried over $MgSO_4$ and purified by silica gel chromatography column eluting with a solvent gradient of a cyclohexane/dichloromethane mixture from 90/10 (v/v) to 50/50. The product was obtained as a slightly brown oil (yield: 90 %). ^{1}H NMR ($CDCl_3$, 400 MHz): *δ* (ppm) 2.07 (s, 6H), 7.26 (d, 2H, *J* = 8 Hz), 7.98 (d, 2H, *J* = 8 Hz), 10.00 (s, 1H).^{13}C NMR ($CDCl_3$, 400 MHz): *δ* (ppm) 30.50 ((CH_3)-C-), 54.95 ((CH_3)-*C*-), 121.94 (2 C_{ortho}), 131.28 (2 C_{meta}), 134.31 ($C_{aromatic}$), 137.90 ($C_{aromatic}$), 169.63 (-O-*C*(=O)-), 190.83 (-*C*(=O)-H).

4.7.3 Synthesis of glycerol-protected dual initiator

1.36 g (4.97 mmol) of ATRP initiator, 2.80 g (28.8 mmol) of glycerol, and 30 mL of toluene were introduced in a 100 mL three-necked round bottom flask equipped with a Dean Stark apparatus and a water condenser. A catalytic amount of 4-methylbenzenesulfonyl chloride was added to the flask. The mixture was allowed to react under reflux and stirring for 24 h. After the reaction, the mixture was washed with K_2CO_3 saturated solution, and the organic layer was dried over $MgSO_4$ and dried under vacuum. The product was obtained as a yellowish oil (yield: 85 %). ^{1}H NMR ($CDCl_3$, 400

MHz): δ (ppm) 2.07 (s, 6H), 3.60-4.40 (m, 5H), 5.20-6.00 (m, 1H), 7.13 (d, 2H, J = 12 Hz), 7.53 (d, 2H, J = 12 Hz).

4.7.4 ATRP of styrene

345 mg (1 mmol) of dual initiator, 12.6 mL (100 mmol) of styrene, 143 mg (1 mmol) of Cu(I)Br, 173 mg (1 mmol) of *N*,*N*,*N′*,*N′*,*N″*-pentamethyldiethylenetriamine, and 20 mL of anisole were added in a Schlenk tube. The flask was submitted to three freeze-pump-thaw cycles. The polymerization was triggered by immersing the Schlenk tube into an oil bath at 110 °C. After 24 h, the reaction medium was diluted in dichloromethane, put back under normal atmosphere to oxidize Cu(I)Br and passed through a short alumina column to eliminate the residual copper. The solution was then precipitated at least twice into a large volume of methanol and the precipitate was isolated by filtration. The resulting acetal-functionalized polymer was recovered as a white powder that was dried under vacuum, and then analyzed by ^{1}H NMR and SEC.

4.7.5 ROP of D,L-lactide

250 mg (1.8×10^{-2} mmol) of acetal-functionalized PS (PS_{104}-OH) and 259 mg (1.8 mmol) of D,L-lactide were introduced in a Schlenk flask. The powders were freeze-dried in the presence of a minimum of anhydrous toluene to eliminate possible water traces. The flask was then filled with nitrogen, and 400 µL of anhydrous toluene and 100 µL of $SnOct_2$ were introduced with a syringe through a septum. The reaction was allowed to react for 3 h at 120 °C. The resulting mixture was dissolved in dichloromethane, precipitated twice in methanol and filtered. The white solid was then recovered, dried under vacuum overnight, and then analyzed by ^{1}H NMR and SEC.

4.7.6 Solvent vapor annealing orientation of PS-*b*-PLA copolymers

20 mg of PS-*b*-PLA copolymer were solubilized in 1 mL of THF. One drop of this solution was spin-coated onto a Si wafer first at 400 rpm for 15 s, and then at 2000 rpm for 40 s. Films were put in a closed chamber containing saturating THF vapors for different periods of times in order to optimize the film nanostructuration. The films were finally vacuum-dried at room temperature.

4.7.7 Selective acidic cleavage of acetal junction in oriented PS-*b*-PLA

The oriented copolymers were introduced into a mixture of 2 mL of ethanol and 500 µL of TFA for 4 h, *i.e.* up to quantitative hydrolysis of the acetal junction. The resulting materials were then washed with ethanol, dried under vacuum, and analyzed by means of ^{1}H NMR and SEM to ascertain the total disappearance of the PLA block.

4.7.8 Functionalization of porous materials

The aldehyde-functionalized porous PS film on Si wafer was immerged in 5 mL of ethanol. 500 µL of a primary amine (*i.e.* TEPA) were added dropwise to the solution and left under stirring for 1 h. Then, 10 mg of sodium cyanoborohydride ($NaCNBH_3$) were added to the solution that was left under stirring for 1 h. The polymer film was then washed with a large volume of ethanol and dried under vacuum before being analyzed by ^{1}H NMR.

4.7.9 Immobilization of gold nanoparticles

A sample of the TEPA-functionalized porous polystyrene was inserted in a round-bottom flask under vacuum. Then, 3 mL of an aqueous solution of $HAuCl_4$ (1.7 mg.mL^{-1}) were added in the flask and stirred for 1 h. 10 mg of sodium borohydride ($NaBH_4$) were then added to the solution and left under stirring for 2 h. The resulting GNP-supported material was washed with deionized water and dried under vacuum overnight.

4.7.10 Heterogeneous supported catalysis of boronic acid homocoupling

A 9 mL mixture of ethanol containing benzeneboronic acid (14 mg, 0.12 mmol) and 500 µL of K_2CO_3 hydro-alcoholic solution (50 mg in 2 mL of deionized water and 3 mL of ethanol) was freshly prepared. 1 mL of this solution was sampled out and put into a round-bottom flask containing the GNP-loaded porous PS_{178} sample. The C-C homocoupling reaction was carried out at 65 °C. After different reaction times (15 min, 30 min, 45 min, 1 h, and 2 h), the reaction medium was cooled down to room temperature, diluted with CH_2Cl_2, and the supported catalyst was withdrawn from the solution. Following an extraction step with water to remove all inorganic salts, GC-MS analyses were performed on the crude reaction mixtures to determine the reaction progress and kinetics. Naphthalene was used as an internal standard (retention time equal to 4.24 min).

4.7.11 Heterogeneous supported catalysis of 4-nitrophenol reduction

A freshly prepared mixture containing 200 µL of 4-nitrophenol solution (7 mg, *i.e*. 0.05 mmol, in 10 mL deionized water) and 200 µL of $NaBH_4$ solution (114 mg in 10 mL of deionized water) in 5 mL of deionized water was introduced in a round-bottom flask containing the GNP-decorated porous PS_{178} sample. The reaction was carried out at room temperature during 1 h. Following the reaction, UV-Vis spectroscopy was performed to assess the reaction completion.

4.7.12 Heterogeneous supported catalysis of cascade reactions

A 9 mL mixture of ethanol containing 20 mg (0.12 mmol) of 3-nitrobenzeneboronic acid and 500 µL of K_2CO_3 hydro-alcoholic solution (50 mg in 2 mL deionized water and 3 mL ethanol) was freshly prepared. 1 mL of this solution was sampled out and placed into a 5 mL round-bottom flask containing the GNP-loaded porous PS_{178} thin film. The C-C homocoupling reaction of boronic acid was carried out at 65 °C. After 24 h, the reaction medium was cooled down to room temperature, and 3 mL of a $NaBH_4$ solution (114 mg in a 10 mL solution of 80/20 vol. % ethanol/deionized water) were further introduced. The nitro reduction reaction then took place during 24 h. The supported catalyst was finally withdrawn from the solution. ^{1}H NMR analyses of the products were performed after completion of the boronic acid homocoupling and after the subsequent nitro reduction step.

4.7.13 Instrumentation

Size Exclusion Chromatography (SEC) analyses were performed on a system equipped with a Spectra Physics P100 pump with two PL gel 5 µm mixed-C columns from Polymer Laboratories, and a Shodex RI 71 refractive index detector. The eluent was tetrahydrofuran at a flow rate of 1 mL.min^{-1}. The system was calibrated using polystyrene standards from Polymer Source.

^{1}H and ^{13}C NMR spectra were recorded at room temperature on a Bruker Avance II spectrometer operating at a resonance frequency of 400 and 100 MHz, respectively. For ^{1}H NMR analysis, the sample concentration was equal to ~10 mg.mL^{-1}, while it was equal to ~30 mg.mL^{-1} for ^{13}C NMR. $CDCl_3$ was used as a solvent and internal standard (7.26 ppm in ^{1}H NMR; 77.2 ppm in ^{13}C NMR).

Scanning Electron Microscopy (SEM) was performed on a MERLIN microscope from Zeiss equipped with InLens and SE2 detectors using low accelerating voltage (3-10 kV). Prior to analyses, the samples were coated with a 4-nm layer of palladium/platinum alloy in a Cressington 208 HR

sputter-coater. Energy dispersive X-ray spectroscopy (EDX) was performed using an SSD X-Max detector of 50 mm² from Oxford Instruments (127 eV for the Kα of Mn).

UV-Vis spectra were recorded in UV quartz cuvette (1 mm length × 10 mm width × 45 mm height) on a Cary 60 UV-Vis spectrophotometer from Agilent Technologies using a 5 $nm.s^{-1}$ scanning speed.

Gas chromatography (GC) was performed using a Shimadzu GC-2025 chromatograph equipped with a Phenomenex ZB-SemiVolatiles capillary column (L = 5.5 m). Helium was used as a carrier gas and column head pressure was fixed at 3 bar. The injector temperature was fixed at 270 °C, whereas that of the FID detector was fixed at 280 °C. The column temperature started at 50 °C and increased at a rate of 10 $°C.min^{-1}$ up to 270 °C, followed by an isotherm during 10 min.

4.8 Results and Discussions

4.8.1 Synthesis and nanostructuration of functional diblock copolymer precursors

PS-*b*-PLA copolymers possessing an acetal function at the junction between both blocks were synthesized by combining two well-known polymerization methods, namely Atom Transfer Radical Polymerization (ATRP) of styrene[36-37] and Ring-Opening Polymerization (ROP) of D,L-lactide,[38] as depicted in **Figure 4-6**. To this purpose, the strategy required the use of an asymmetric difunctional initiator so as to generate both blocks.

A hetero-difunctional initiator was specifically prepared through a two-step synthetic route (**Figure 4-6**), as already reported elsewhere.[34] It contained *(i)* an acetal linker easily cleavable *via* acidic hydrolysis, *(ii)* a tertiary alkyl halide (C^{IV}-Br bond) able to initiate styrene ATRP, and *(iii)* a terminal hydroxyl group capable of triggering D,L-lactide ROP. The first step of the synthesis involved the esterification of 4-hydroxybenzaldehyde with *α*-bromoisobutyryl bromide. The corresponding ester was obtained with a 85 % yield after purification on a silica gel column. This intermediate product was characterized by ^{1}H NMR, as shown in **Figure 4-7**. The appearance of a new band integrating for 6 protons was ascribed to the protons of methyl residues linked to the terminal tertiary carbon tethered during this synthetic step. A slight shift of the signal arising from the aromatic protons was also noticeable towards lower magnetic fields, likely due to the presence of electron-withdrawing ester moiety when compared to the electron-donating alcohol group. The second synthetic step implied the acetalization of the as-obtained aldehyde in the presence of glycerol and a catalytic amount of 4-methylbenzenesulfonyl chloride. The success of the synthesis was demonstrated again by means of ^{1}H NMR (**Figure 4-7**) that displayed the total vanishing of the characteristic signal arising from the aldehyde proton at 10 ppm, while the specific signals of the acetal function could be

observed at 3.6-4.4 ppm (-CH_2-) and 5.2-6.0 ppm (-CH-). A slight shift of the aromatic protons was also observed towards higher magnetic fields, likely due to the replacement of the aldehyde moiety (electron-withdrawing group) by the acetal moiety (electron-donating group). It is worth mentioning that two distinct regioisomers were obtained during this acetalization step depending on the location of the electrophilic attack of the carbonyl group of the aromatic aldehyde onto the hydroxyl groups of glycerol. The 5-membered ring (1,2-regioisomer) to 6-membered (1,3-regioisomer) ring acetal molar ratio has been calculated by comparing the integration of signals at 5.44 and 5.56 ppm (corresponding to the trans and cis isomers of the 6-membered ring acetal, respectively) and that of the signals at 5.84 and 5.99 (corresponding to the trans and cis isomers of the 5-membered ring acetal, respectively). In this way, we found out that the 1,3- and 1,2-regioisomers were obtained in a 40/60 molar ratio, as observed by ^{1}H NMR (**Figure 4-7**).

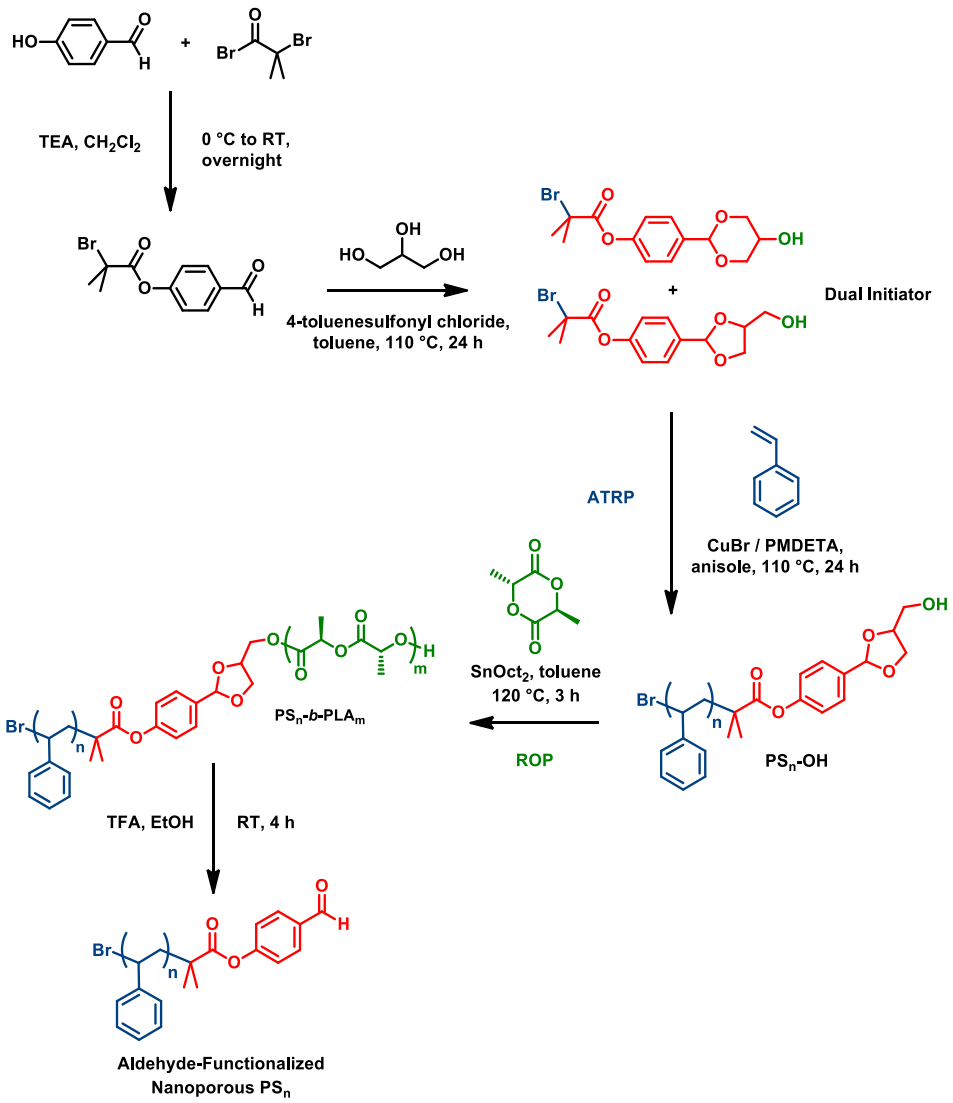

Figure 4-6: Synthetic pathway towards PS-*b*-PLA diblock copolymers from the acetal-containing difunctional macroinitiator and corresponding aldehyde functionalized porous polystyrene after acidic cleavage of the acetal group.

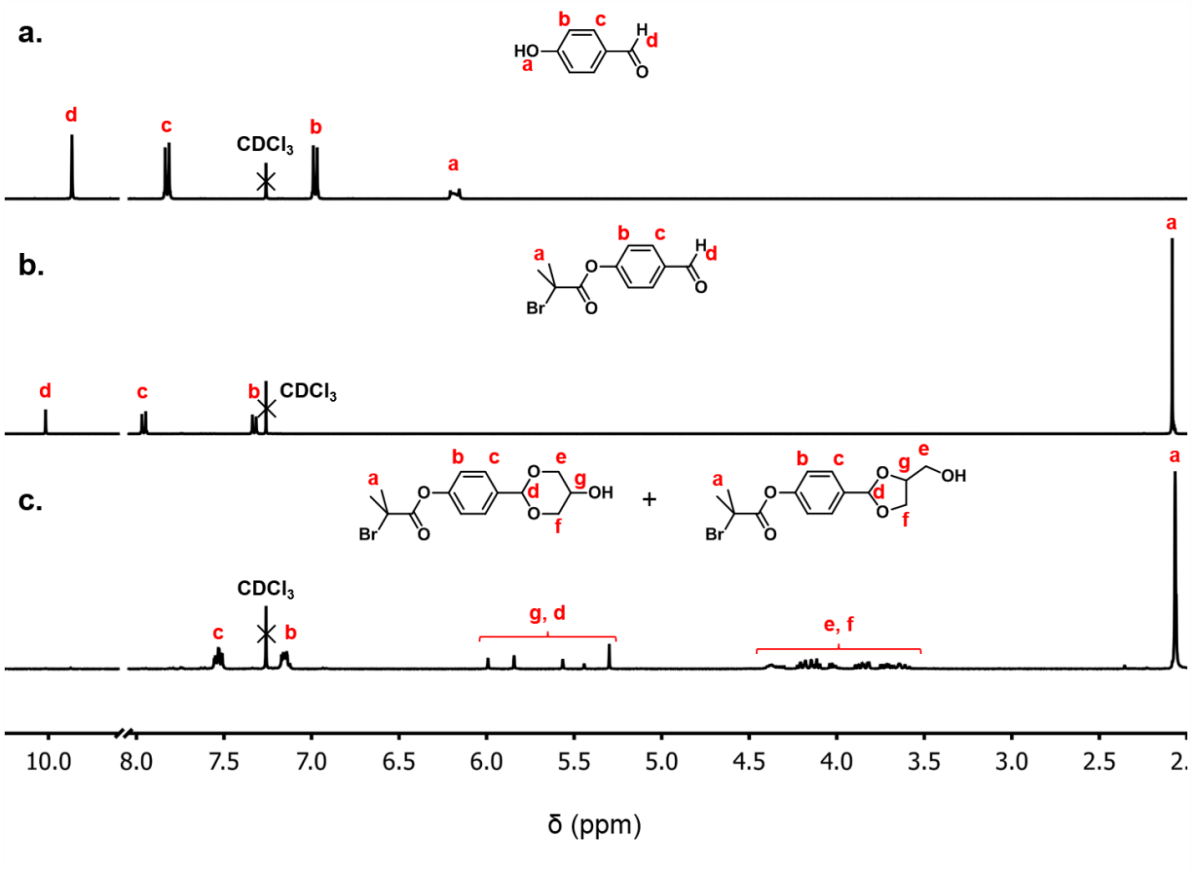

Figure 4-7: ^{1}H NMR ($CDCl_3$) spectra of *a)* starting reactant, *i.e.* 4-hydroxybenzaldehyde, *b)* difunctional precursor, and *c)* corresponding hetero-difunctional initiator after protection of the aldehyde function with glycerol.

The hetero-difunctional initiator was obtained with an overall yield of nearly 80 %. It is noteworthy that a mixture of two different acetals was obtained depending on whether the acetal ring was formed by reaction of the glycerol hydroxyl functions in 1,2- or 1,3- positions, as shown in **Figure 4-7**. Unfortunately, these two isomers could not be separated on silica gel chromatography column, and both were used subsequently.

Various PS macroinitiators were then prepared (PS_{44}-OH, PS_{104}-OH, PS_{178}-OH) from the hetero-difunctional initiator. They exhibited experimental M_n values as determined by ^{1}H NMR close to theoretical ones as well as relatively low polydispersity index $Đ$ (**Table 4-2**), thus confirming the controlled character of styrene ATRP.

Table 4-2: Molecular features of PS macroinitiators.

PS_n[a]	Conv.[b] (%)	$M_{n\ theor}$[c] (kg/mol)	$M_{n\ NMR}$[d] (kg/mol)	$M_{n\ SEC}$[e] (kg/mol)	$Đ$[e]
PS_{44}-OH	65	4.0	4.6	13.5	1.35
PS_{104}-OH	89	10.5	11.0	20.0	1.30
PS_{178}-OH	91	21.0	17.8	17.5	1.30

[a] n: number-average polymerization degree of PS as determined by ^{1}H NMR

[b] conversion as determined by gravimetry

[c] $M_{n\ theor}$ = conversion × DP_n × M_o (styrene)

[d] $M_{n\ RMN}$: number-average molar mass as evaluated by ^{1}H NMR

[e] values from SEC/RI measurements with PS standards

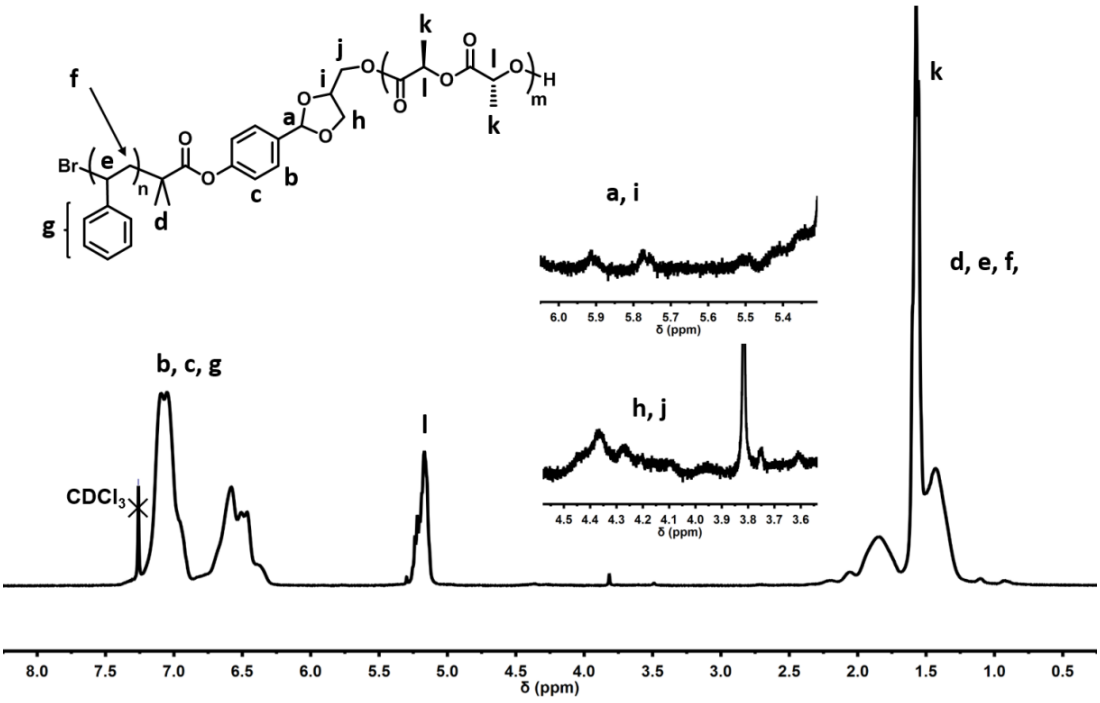

Figure 4-8: ^{1}H NMR ($CDCl_3$) spectrum of PS_{104}-*b*-PLA_{56} copolymer.

Starting from the as-synthesized PS-based macroinitators, PS-*b*-PLA copolymers were prepared by ROP of D,L-lactide (**Figure 4-6**). These PS-*b*-PLA copolymers were then characterized by SEC and ^{1}H NMR. The ^{1}H NMR spectra of the resulting block copolymers displayed the typical chemical shifts of PS and PLA (**Figure 4-8** as an example), the broad signals between 6 and 7.25 ppm being attributed to the aromatic protons of PS and those at 5-5.3 ppm being ascribed to the –CH– groups of PLA repeating units. It is noteworthy that such diblock copolymers were synthesized with PLA volume fractions (f_{PLA}) ranging from 0.35 to 0.45 (**Table 4-3**) in order to develop morphologies consisting of hexagonally close-packed PLA cylinders in a PS matrix, according to the equilibrium phase diagram established by Hillmyer's group.[21-22]

Table 4-3: Molecular features of PS_n-*b*-PLA_m obtained *via* ROP of D,L-lactide from PS_n macroinitiators.

PS_n-*b*-PLA_m[a]	**Conv.**[b] **(%)**	**$M_{n\ theor}$**[c] **(kg/mol)**	**$M_{n\ NMR}$**[d] **(kg/mol)**	**$M_{n\ SEC}$**[e] **(kg/mol)**	**$Đ$**[e]	**f_{PLA}**[f]
PS_{44}-*b*-PLA_{31}	25	16.8	15.6	7.0	1.30	0.44
PS_{104}-*b*-PLA_{50}	53	23.8	17.8	11.8	1.50	0.35
PS_{104}-*b*-PLA_{56}	40	21.9	20.0	11.4	1.50	0.38
PS_{178}-*b*-PLA_{118}	40	21.2	31.7	26.3	1.50	0.43
PS_{178}-*b*-PLA_{130}	50	22.5	25.6	26.0	1.35	0.45

[a] n, m: number-average polymerization degrees of PS an PLA, respectively, as determined by ^{1}H NMR

[b] conversion as determined by gravimetry

[c] $M_{n\ theor}$ = conversion × DP_n × $M_{o\ lactide}$ + $M_{n\ RMN\ (PSn\text{-}OH)}$

[d] $M_{n\ RMN}$: number-average molar mass as calculated by ^{1}H NMR

[e] values as obtained from SEC equipped with RI detection (PS standards)

[f] volume fraction of PLA as determined by ^{1}H NMR, assuming that densities of PS and PLA are 1.02 and 1.25, respectively

Moreover, the SEC chromatograms of PS-*b*-PLA copolymers display a monomodal distribution along with a peak shift toward lower retention time, compared to the corresponding PS macroinitiator, thus confirming the formation of diblock copolymers (**Figure 4-9** as an example). The polydispersity index values were also rather low ($Đ$ < 1.50) in accordance with the controlled character of ROP of D,L-lactide.

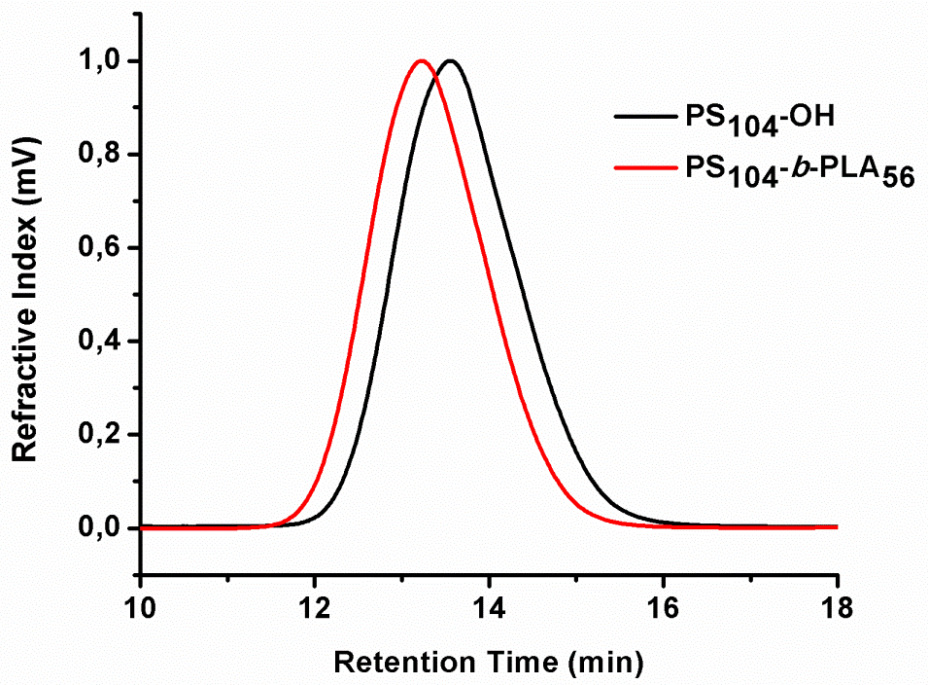

Figure 4-9: SEC chromatograms of PS_{104}-OH macroinitiator and resulting PS_{104}-*b*-PLA_{56} diblock copolymer.

The macroscopic orientation of PS-*b*-PLA copolymer nanodomains was previously implemented using a channel die processing technique.[21-25, 31] Nevertheless, this technique is time-consuming, and in some instances it is difficult to achieve long-range order.[39] An alternative technique that has largely been developed in the recent literature is based on solvent vapor annealing.[40] This versatile method could efficiently be applied to a wide range of PS-based diblock copolymers, such as polystyrene-*block*-poly(ethylene glycol) (PS-*b*-PEO),[41] polystyrene-*block*-poly(4-vinylpyridine) (PS-*b*-P4VP),[42] polystyrene-*block*-poly(methyl methacrylate) (PS-*b*-PMMA),[43] polystyrene-*block*-polydimethylsiloxane (PS-*b*-PDMS),[44] PS-*b*-PLA[45-50] or even polystyrene-*block*-maltoheptaose (PS-*b*-MH).[51] In our study, the spin-coated films were typically introduced into a sealed chamber saturated with THF vapors during 3, 16, and 24 h. Afterward, films were vacuum-dried at room temperature, and they developed domains perpendicular to their plan.

4.8.2 Generation of functionalized porous polymeric materials

The acetal function inserted between both blocks of PS-*b*-PLA diblock copolymer is prone to facile hydrolysis under acidic conditions.[32-34] Accordingly, TFA was used to cleave the junction between the two blocks of the synthesized copolymers, as shown in **Figure 4-6**. This degradation was conducted in ethanol, which is a non-solvent for PS but a good solvent for rather small PLA fragments. The PLA etching from the as-obtained PS-*b*-PLA materials was monitored for 4 h. Experimentally, a small piece of the material was withdrawn from the heterogeneous reaction mixture, washed with an abundant volume of ethanol in order to remove potential adsorbed PLA residues, and finally analyzed by ^{1}H NMR as shown in **Figure 4-10 a & b**. The kinetics of PLA etching was monitored by sampling out pieces of thin films during the acidic hydrolysis and analyzing them by ^{1}H NMR to determine the hydrolysis yield, as illustrated in **Figure 4-10 c**.

After 4 h of acidic hydrolysis, a complete removal of the PLA block was observed by the total disappearance of the signal associated with –CH– motif in the PLA repeating unit at 5.2 ppm. Moreover, the characteristic signal of the proton of the aldehyde function appeared at 10 ppm (**Figure 4-10 b**), thus confirming the complete hydrolysis of the acetal function and the recovery of the initial functionality at the pore surface which should ensure post-polymerization functionalization of the aldehyde with amines of interest through reductive amination. Although PLA could be potentially hydrolyzed by TFA,[52] the polyester degradation took several weeks to be complete, thus strongly suggesting that PLA etching mainly occurred *via* the cleavage of the acetal junction within our experimental conditions.

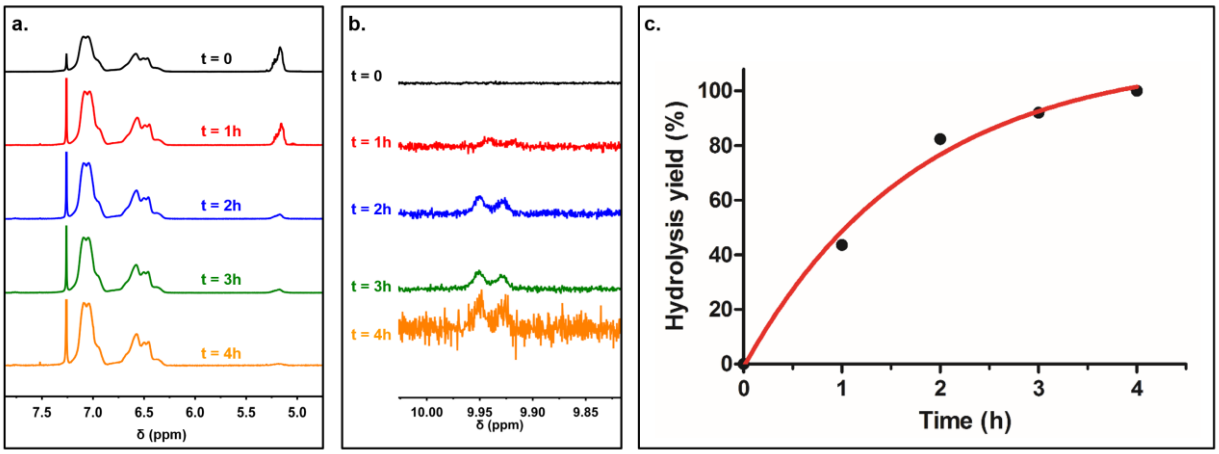

Figure 4-10: ^{1}H NMR spectra of PS_{104}-*b*-PLA_{56} diblock copolymer during acidic hydrolysis of the acetal junction: *a)* 5.0-7.5 ppm spectral zone, *b)* zoom of 9.85-10.00 ppm spectral zone. *c)* Time dependence of hydrolysis yield as determined by ^{1}H NMR.

4.8.3 Morphological and pore surface chemical characterization of porous frameworks

SEM investigation of porous polystyrene resulting from the acidic cleavage of the acetal in the PS_{178}-*b*-PLA_{130} precursor clearly indicated the occurrence of pores within the thin films with diameters in the 1-2 µm range. It is noteworthy that the best orientation for the generated pores was obtained after 24 h of solvent vapor annealing, as shown in **Figure 4-11**.

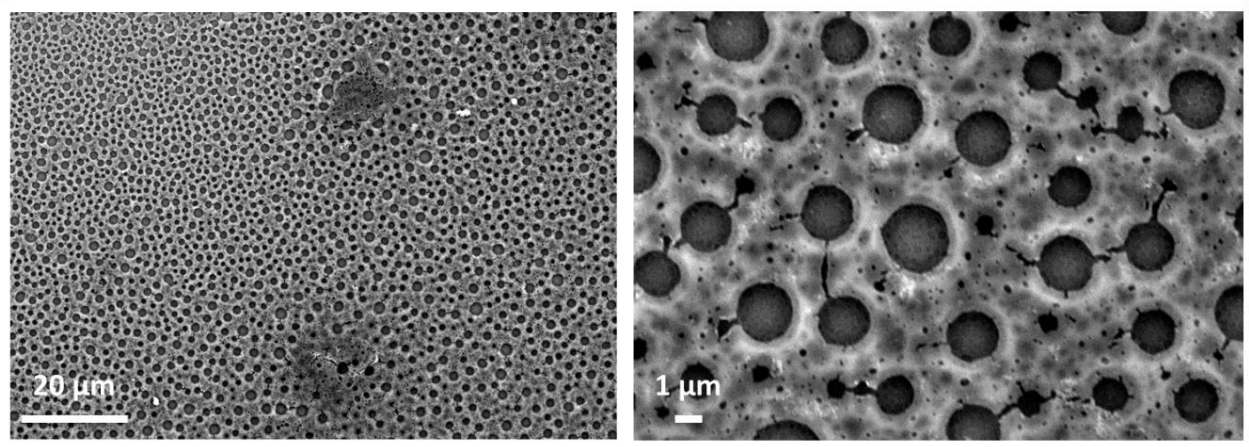

Figure 4-11: SEM micrographs of aldehyde-functionalized porous polystyrene stemming from PS_{178}-*b*-PLA_{130} diblock copolymer precursor after 24 h vapor solvent annealing orientation.

Further, the possibility to chemically modify the available aldehyde functions was envisioned. To this purpose, the aldehyde-functionalized polymers on Si wafers were immersed in ethanol and reacted with a large excess of tetraethylenepentamine (TEPA). Finally, hydride-mediated reduction of the corresponding Schiff base was achieved in the presence of $NaCNBH_3$ as an efficient reductive agent, as depicted in **Figure 4-12 a**. After extensive washing of the films, ^{1}H NMR analyses were performed so as to ascertain the complete amine-functionalization of polystyrene. As shown in **Figure 4-12 b**, the total disappearance of the aldehyde characteristic band at ~ 10 ppm was observed along with the appearance of new signals attributed to the -CH_2- protons of covalently attached amine (~ 2.75 ppm for TEPA fragments). Moreover, the signal arising from the -CH_2- proton in the alpha position of phenyl and amine moieties is displayed at ~5.2 ppm, thus asserting the success of the reductive amination.

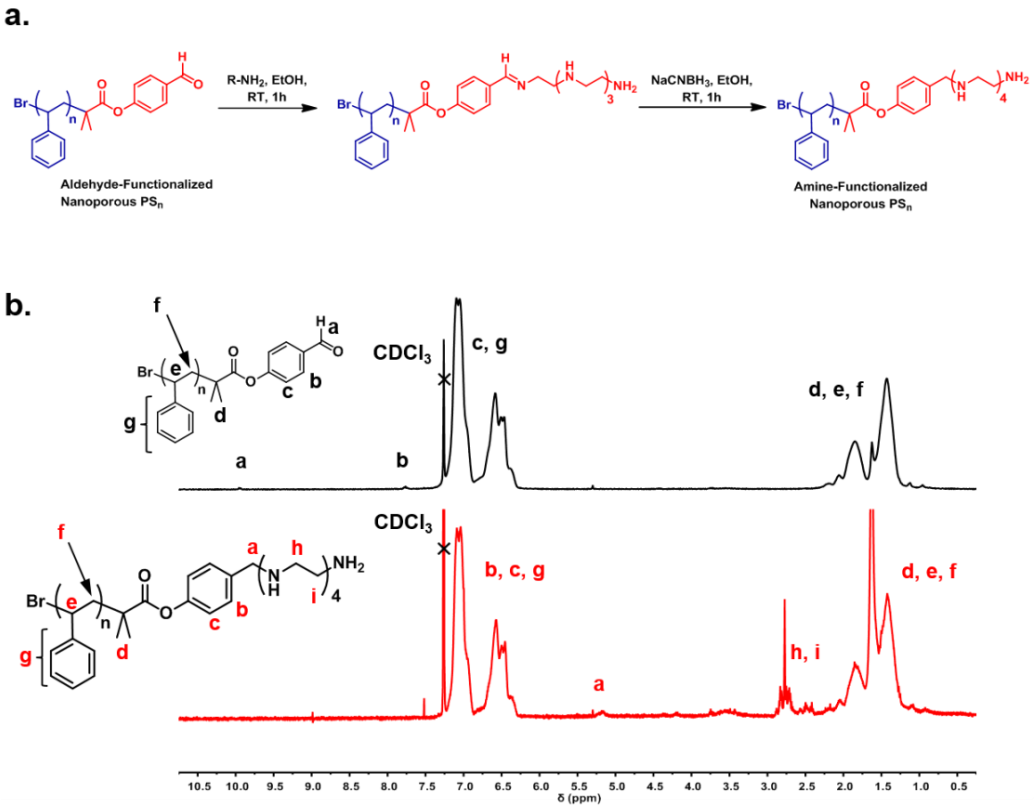

Figure 4-12: *a)* Synthetic pathway adopted for the functionalization of porous PS_n by reductive amination; *b)* ^1H NMR spectra ($CDCl_3$) of aldehyde-functionalized PS_{178} sample before and after reductive amination.

4.8.4 Immobilization of *in-situ* generated gold nanoparticles

GNP-based supported systems are already well-known in the literature as efficient catalysts for the C-C boronic homocoupling of aromatic compounds[53] and nitroarene reduction.[54] To this purpose, the possibility to immobilize GNPs at the pore surface of amine-functionalized porous polystyrene-based materials was investigated. Experimentally, thin films of porous polystyrene were immersed in a tetrachloroauric acid solution. A successive hydride-mediated reduction of Au^{3+} metallic cations was achieved in the presence of $NaBH_4$. The presence of *in-situ* generated GNPs within the porous structure of polystyrene was illustrated by SEM and confirmed by EDX (**Figure 4-13**). As shown in **Figure 4-13 a**, a quite sparse dispersion of GNPs was obtained within the channels of porous polystyrene material, while a rather narrow dispersion in size was observed (around 100 nm, as determined using the ImageJ® freeware).

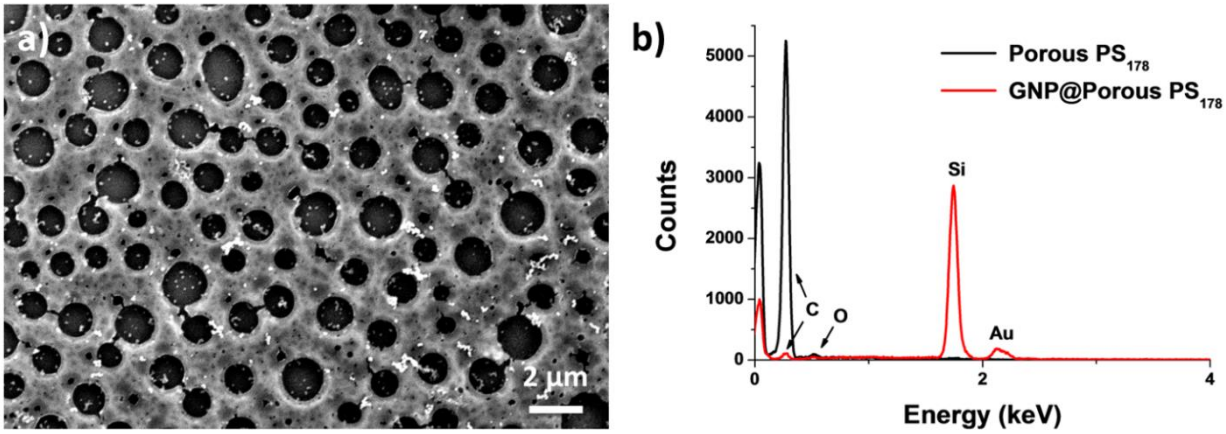

Figure 4-13: *a)* SEM micrograph of GNP-decorated amine-functionalized porous PS_{178} sample, *b)* EDX spectra of amine-functionalized porous PS_{178} sample and corresponding GNP@porous PS_{178} sample on Si wafers.

4.8.5 Investigation of heterogeneous supported catalysis

To further evaluate the catalytic behavior of the as-prepared hybrid systems, two different model reactions were assessed. Boronic acid derivatives are indeed well-known to be involved in a plethora of catalytic reactions,[55] such as Suzuki cross-coupling, Suzuki-Miyaura C-C cross-coupling that requires the use of aryl halides (*i.e.*, bromine or iodine) and trifluoroborates[56-57] or boronic acid derivatives[58] as the substrates and either palladium[59-60] or gold[61] as noble metal-based catalysts. Additionally, gold is prone to catalyze allylation of boronic acid[62] as well as homocoupling of boronic acids. The latter reaction is useful to create symmetric phenyl derivatives, and it can be performed either with gold salts[63] or with gold nanoparticles.[64] In addition, it is also well-established that GNPs, either suspended in solution or immobilized on porous materials, can efficiently catalyze the reduction of nitroaromatic compounds into corresponding amines.[65-66] Considering this, we decided to focus our attention on the possibility to achieve two consecutive GNP-catalyzed chemical reactions in a row on the same substrate with our newly prepared GNP@porous PS supported catalysts. The starting chemical reagent was carefully chosen so as to *(i)* first generate a biphenyl derivative through C-C homocoupling, and *(ii)* then reduce nitro moieties substituted on aromatic rings. Therefore, a substrate of choice that could be envisioned for such cascade reactions was 3-nitrobenzeneboronic acid.

As a starting point of our catalytic studies, the possibility to efficiently complete each reaction independently was assessed. First, the GNP-loaded porous PS_{178} material was immersed in a solution of benzeneboronic acid (BA), and the C-C homocoupling reaction of BA was carried out at 65 °C. Small aliquots of the reaction mixture were withdrawn at different times and analyzed by GC after proper treatment. As observed in **Figure 4-14 a**, throughout the course of the catalytic reaction, a

progressive vanishing of the BA peak (retention time: 16.60 min) was observed concomitantly to an increasing appearance of a peak assigned to the resulting biphenyl product (retention time: 6.05 min). The GC results clearly indicated that the desired product was obtained in a quantitative way within only 2 h, as no BA was present anymore in the reaction mixture. As shown from **Figure 4-14 b** that displays the plot of $\ln[BA]_t$ *vs.* reaction time, the GNP-catalyzed C-C homocoupling reaction followed a first-order kinetics with a reaction rate constant equal to 3.2×10^{-4} s^{-1}.

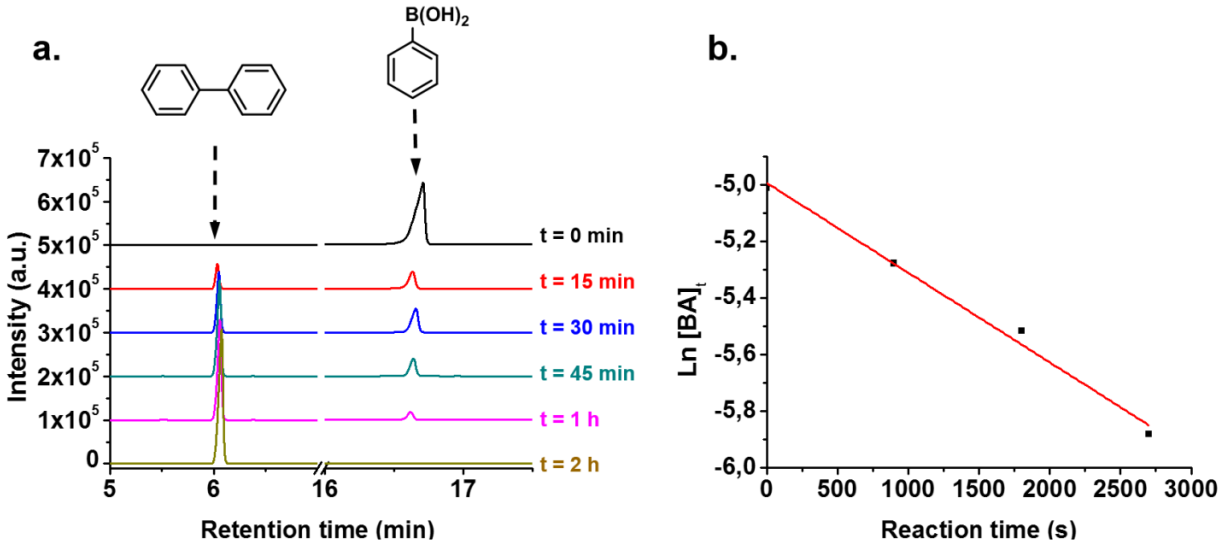

Figure 4-14: *a)* GC monitoring of C-C homocoupling of benzeneboronic acid as a function of reaction time. Only expanded regions of the chromatogram corresponding to the elution of the reactant (16-17.5 min) and the product (5-7 min) are displayed. *b)* Time dependence of $\ln[BA]_t$ in the reaction mixture.

We then investigated the GNP-catalyzed reduction of a nitroaromatic compound, namely 4-nitrophenol (4-NP). The reaction was carried out in ethanol in the presence of a large excess of $NaBH_4$ at room temperature and was triggered by the introduction of the GNP-loaded porous PS_{178} material into the solution (t = 0, yellow color). After 1 h reaction, the solution turned colorless and it was then analyzed by UV-Visible spectrophotometry. As shown in **Figure 4-15**, the characteristic $\pi \rightarrow \pi^*$ transition band of the reactant, *i.e.* 4-NP, completely vanished at 400 nm, while a new low-absorbance band appeared at 320 nm that was ascribed to the $\pi \rightarrow \pi^*$ transition of the resulting product, *i.e.* 4-aminophenol (4-AP), thus proving the efficiency of this reaction.[31, 65, 67-68] It should be stressed that no reduction of 4-NP occurred when an amine-functionalized porous PS_{178} sample (without adsorbed GNPs) was in contact with a $NaBH_4$ solution, even after prolongated times (data not shown).

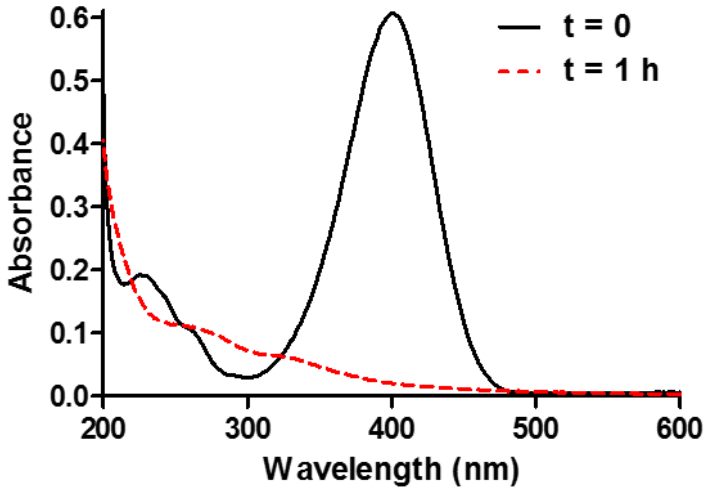

Figure 4-15: UV-Vis spectra of the starting solution (constituted of 4-NP and $NaBH_4$) and the resulting solution obtained after 1 h reaction in contact with a GNP@porous PS supported catalyst.

Finally, "one-pot" cascade reactions consisting of the C-C homocoupling of 3-nitrobenzeneboronic acid and subsequent reduction of the nitro moieties of the intermediate product were investigated. As a matter of fact, GC/MS could not be properly implemented due to the absence of appropriate standards for intermediate and final products needed for the calibration curves. On the other hand, UV/Vis spectra of biphenyl products were not easily assigned, even though some shifts of maxima associated with $\pi \rightarrow \pi^*$ transition bands were detected (data not shown). Accordingly, the completion of each successive reaction was monitored by means of ^{1}H NMR. Experimentally, the reaction was analyzed after the first step (C-C homocoupling at 65 °C) without purification of the intermediate. As shown in **Figure 4-16**, clear shifts of the signals assigned to aromatic protons were observed when compared to those of the reactant (*i.e.*, 3-nitrobenzeneboronic acid), thus demonstrating the efficient formation of the intermediate product (*i.e.*, 3,3'-dinitrobiphenyl, yellowish color). The ^{1}H NMR shifts of the 3,3'-dinitrobiphenyl intermediate were indeed in agreement with those previously reported for this compound in the literature.[69] After the second step consisting of the $NaBH_4$-mediated reduction of the nitro moieties at room temperature, the solution turned brown. ^{1}H NMR again showed some significant shifts of the bands that could be attributed to the aromatic protons of the final diamino biphenyl compound (**Figure 4-16**). As conclusion, "one-pot" cascade reactions consisting of boronic acid C-C homocoupling, followed by nitroaromatic compound reduction, was successfully accomplished for the first time. It is also noteworthy that several successive cycles were repeated following the same procedure, and the catalyst efficiency was maintained. These features clearly illustrated that newly designed GNP@porous PS supported catalysts were highly efficient and recyclable.

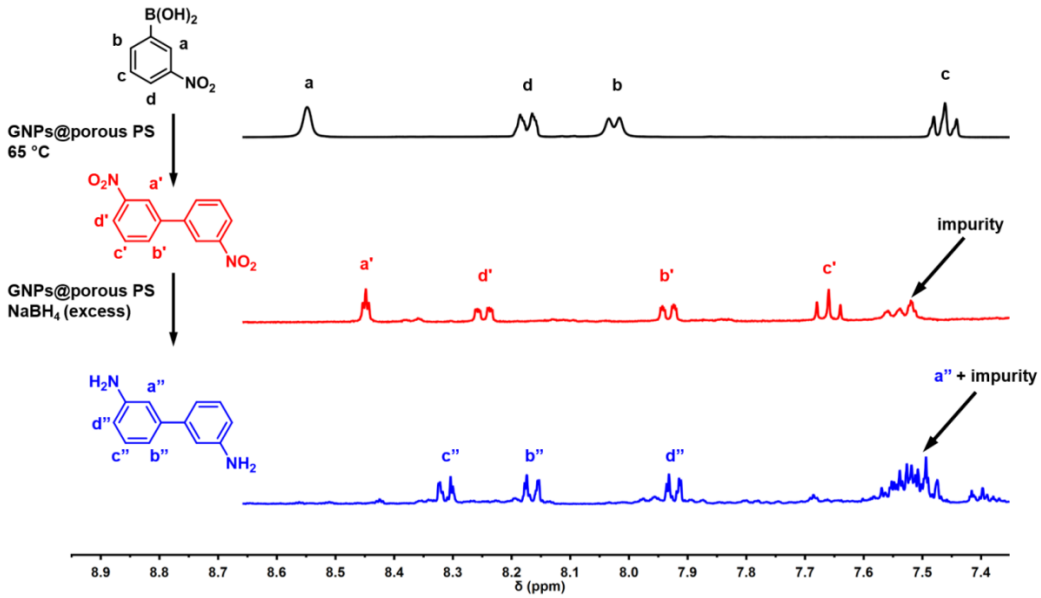

Figure 4-16: ^{1}H NMR ($CDCl_3$) monitoring of the cascade reactions consisting of the C-C homocoupling of 3-nitrobenzeneboronic acid and subsequent reduction of 3,3'-dinitrobiphenyl intermediate in contact with a GNP@porous PS_{178} supported catalyst.

4.9 Conclusions

Novel porous catalytic supports could be engineered from functional PS-*b*-PLA precursors possessing a cleavable acetal junction between both blocks. The newly synthesized PS-*b*-PLA diblock copolymers were oriented by the solvent vapor annealing methodology, and the sacrificial PLA segment was successfully etched by an easy and rapid degradation of the labile acetal junction under TFA-mediated acidic conditions. The as-obtained porous PS-based materials bore chemically accessible and modifiable aldehyde functions at the pore surface, which enabled further functionalization with multidentate amines, such as TEPA, through reductive amination. This TEPA functionalization reaction allowed for subsequent adsorption of *in-situ* generated gold nanoparticles within porous PS-based films, and heterogeneous supported catalytic systems could thus be engineered. Very interestingly, the possibility of proceeding "one-pot" cascade reactions consisting of boronic acid C-C homocoupling and subsequent nitroaromatic reduction was successfully accomplished for the first time.

This investigation paves the way for further development of advanced porous reactors from smartly designed diblock copolymers bearing cleavable junctions that could find diverse nanotechnology applications, more particularly in heterogeneous supported catalysis or confined chemistry.

4.10 References

(1) Koros, W. J.; Fleming, G. K.; Jordan, S. M.; Kim, T. H.; Hoehn, H. H. Polymeric membrane materials for solution-diffusion based permeation separations. *Prog. Polym. Sci.* **1988,** *13*, 339-401.
(2) Thomas, J. D. R. Selective membrane electrodes for analysis. *Analyst* **1994,** *119*, 203-208.
(3) Dunleavy, M. Polymeric membranes. A review of applications. *Med. Device Technol.* **1996,** *7*, 14.
(4) Svec, F.; Peters, E. C.; Sykora, D.; Yu, C.; Frechet, J. Monolithic stationary phases for capillary electrochromatography based on synthetic polymers: designs and applications. *J. High. Resolut. Chromatogr.* **2000,** *23*, 3-18.
(5) Hentze, H. P.; Antonietti, M. Porous polymers and resins for biotechnological and biomedical applications. *Rev. Mol. Biotechnol.* **2002,** *90*, 27-53.
(6) Hillmyer, M. A. Nanoporous Materials from Block Copolymer Precursors. *Adv. Polym. Sci.* **2005,** *190*, 137-181.
(7) Wu, D.; Xu, F.; Sun, B.; Fu, R.; He, H.; Matyjaszewski, K. Design and Preparation of Porous Polymers. *Chem. Rev.* **2012,** *112*, 3959-4015.
(8) Gamys, C. G.; Schumers, J.-M.; Mugemana, C.; Fustin, C.-A.; Gohy, J.-F. Pore-Functionalized Nanoporous Materials Derived from Block Copolymers. *Macromol. Rapid Commun.* **2013,** *34*, 962-982.
(9) Olson, D. A.; Chen, L.; Hillmyer, M. A. Templating Nanoporous Polymers with Ordered Block Copolymers. *Chem. Mater.* **2008,** *20*, 869-890.
(10) Cavicchi, K. A.; Zalusky, A. S.; Hillmyer, M. A.; Lodge, T. P. An Ordered Nanoporous Monolith from an Elastomeric Crosslinked Block Copolymer Precursor. *Macromol. Rapid Commun.* **2004,** *25*, 704-709.
(11) Hansen, M. S.; Vigild, M. E.; Berg, R. H.; Ndoni, S. Nanoporous Crosslinked Polyisoprenefrom Polyisoprene—Polydimethylsiloxane BlockCopolymer. *Polym. Bull.* **2004,** *51*, 403-409.
(12) Ndoni, S.; Li, L.; Schulte, L.; Szewczykowski, P. P.; Hansen, T. W.; Guo, F.; Berg, R. H.; Vigild, M. E. Controlled Photooxidation of Nanoporous Polymers. *Macromolecules* **2009,** *42*, 3877-3880.
(13) Szewczykowski, P. P.; Andersen, K.; Schulte, L.; Mortensen, K.; Vigild, M. E.; Ndoni, S. Elastomers with Reversible Nanoporosity. *Macromolecules* **2009,** *42*, 5636-5641.
(14) Hedrick, J. L.; Miller, R. D.; Hawker, C. J.; Carter, K. R.; Volksen, W.; Yoon, D. Y.; Trollsås, M. Templating Nanoporosity in Thin-Film Dielectric Insulators. *Adv. Mater.* **1998,** *10*, 1049-1053.
(15) Lee, J. S.; Hirao, A.; Nakahama, S. Polymerization of monomers containing functional silyl groups. 5. Synthesis of new porous membranes with functional groups. *Macromolecules* **1988,** *21*, 274-276.
(16) Lee, J. S.; Hirao, A.; Nakahama, S. Polymerization of monomers containing functional silyl groups. 7. Porous membranes with controlled microstructures. *Macromolecules* **1989,** *22*, 2602-2606.
(17) Adachi, M.; Okumura, A.; Sivaniah, E.; Hashimoto, T. Incorporation of Metal Nanoparticles into a Double Gyroid Network Texture. *Macromolecules* **2006,** *39*, 7352-7357.
(18) Thurn-Albrecht, T.; Steiner, R.; DeRouchey, J.; Stafford, C. M.; Huang, E.; Bal, M.; Tuominen, M.; Hawker, C. J.; Russell, T. P. Nanoscopic Templates from Oriented Block Copolymer Films. *Adv. Mater.* **2000,** *12*, 787-791.
(19) Xu, T.; Kim, H.-C.; DeRouchey, J.; Seney, C.; Levesque, C.; Martin, P.; Stafford, C. M.; Russell, T. P. The influence of molecular weight on nanoporous polymer films. *Polymer* **2001,** *42*, 9091-9095.
(20) Li, Y.; Ito, T. Surface Chemical Functionalization of Cylindrical Nanopores Derived from a Polystyrene−Poly(methylmethacrylate) Diblock Copolymer via Amidation. *Langmuir* **2008,** *24*, 8959-8963.
(21) Zalusky, A. S.; Olayo-Valles, R.; Taylor, C. J.; Hillmyer, M. A. Mesoporous Polystyrene Monoliths. *J. Am. Chem. Soc.* **2001,** *123*, 1519-1520.
(22) Zalusky, A. S.; Olayo-Valles, R.; Wolf, J. H.; Hillmyer, M. A. Ordered Nanoporous Polymers from Polystyrene−Polylactide Block Copolymers. *J. Am. Chem. Soc.* **2002,** *124*, 12761-12773.
(23) Gorzolnik, B.; Davidson, P.; Beurroies, I.; Denoyel, R.; Grande, D. Novel Functional Mesoporous Materials Obtained from Nanostructured Diblock Copolymers. *Macromol. Symp.* **2010,** *287*, 127-134.
(24) Grande, D.; Penelle, J.; Davidson, P.; Beurroies, I.; Denoyel, R. Functionalized ordered nanoporous polymeric materials: From the synthesis of diblock copolymers to their nanostructuration and their selective degradation. *Microporous Mesoporous Mater.* **2011,** *140*, 34-39.

(25) Majdoub, R.; Antoun, T.; Droumaguet, B. L.; Benzina, M.; Grande, D. Original route to polylactide–polystyrene diblock copolymers containing a sulfonyl group at the junction between both blocks as precursors to functional nanoporous materials. *React. Funct. Polym.* **2012,** *72*, 495-502.
(26) Glassner, M.; Blinco, J. P.; Barner-Kowollik, C. Formation of nanoporous materials via mild retro-Diels-Alder chemistry. *Polym. Chem.* **2011,** *2*, 83-87.
(27) Zhao, H.; Gu, W.; Thielke, M. W.; Sterner, E.; Tsai, T.; Russell, T. P.; Coughlin, E. B.; Theato, P. Functionalized Nanoporous Thin Films and Fibers from Photocleavable Block Copolymers Featuring Activated Esters. *Macromolecules* **2013,** *46*, 5195-5201.
(28) Kang, M.; Moon, B. Synthesis of Photocleavable Poly(styrene-block-ethylene oxide) and Its Self-Assembly into Nanoporous Thin Films. *Macromolecules* **2009,** *42*, 455-458.
(29) Zhang, M.; Yang, L.; Yurt, S.; Misner, M. J.; Chen, J. T.; Coughlin, E. B.; Venkataraman, D.; Russell, T. P. Highly Ordered Nanoporous Thin Films from Cleavable Polystyrene-block-poly(ethylene oxide). *Adv. Mater.* **2007,** *19*, 1571-1576.
(30) Ryu, J.-H.; Park, S.; Kim, B.; Klaikherd, A.; Russell, T. P.; Thayumanavan, S. Highly Ordered Gold Nanotubes Using Thiols at a Cleavable Block Copolymer Interface. *J. Am. Chem. Soc.* **2009,** *131*, 9870-9871.
(31) Le Droumaguet, B.; Poupart, R.; Grande, D. "Clickable" thiol-functionalized nanoporous polymers: from their synthesis to further adsorption of gold nanoparticles and subsequent use as efficient catalytic supports. *Polym. Chem.* **2015**, *6* (47), 8105–8111.
(32) Taubmann, C.; Luxenhofer, R.; Cesana, S.; Jordan, R. First Aldehyde-Functionalized Poly(2-oxazoline)s for Chemoselective Ligation. *Macromol. Biosci.* **2005,** *5*, 603-612.
(33) Legros, C.; De Pauw-Gillet, M.-C.; Tam, K. C.; Lecommandoux, S.; Taton, D. Aldehyde-functional copolymers based on poly(2-oxazoline) for post-polymerization modification. *Eur. Polym. J.* **2015,** *62*, 322-330.
(34) Sui, X.; Zhang, Z.; Guan, S.; Xu, Y.; Li, C.; Lv, Y.; Chen, A.; Yang, L.; Gao, L. A facile strategy for the synthesis of block copolymers bearing an acid-cleavable junction. *Polym. Chem.* **2015,** *6*, 2777-2782.
(35) Keller, R. N.; Wycoff, H. D., Inorganic Synthesis. 1946 ed.; John Wiley: New York, pp 1–4.
(36) Wang, J.-S.; Matyjaszewski, K. Controlled/"living" radical polymerization. atom transfer radical polymerization in the presence of transition-metal complexes. *J. Am. Chem. Soc.* **1995,** *117*, 5614-5615.
(37) Kato, M.; Kamigaito, M.; Sawamoto, M.; Higashimura, T. Polymerization of Methyl Methacrylate with the Carbon Tetrachloride/Dichlorotris- (triphenylphosphine)ruthenium(II)/Methylaluminum Bis(2,6-di-tert-butylphenoxide) Initiating System: Possibility of Living Radical Polymerization. *Macromolecules* **1995,** *28*, 1721-1723.
(38) Kricheldorf, H. R.; Kreiser-Saunders, I.; Boettcher, C. Polylactones: 31. Sn(II)octoate-initiated polymerization of L-lactide: a mechanistic study. *Polymer* **1995,** *36*, 1253-1259.
(39) Drzal, P. L.; Barnes, J. D.; Kofinas, P. Path dependent microstructure orientation during strain compression of semicrystalline block copolymers. *Polymer* **2001,** *42*, 5633-5642.
(40) Sinturel, C.; Vayer, M.; Morris, M.; Hillmyer, M. A. Solvent Vapor Annealing of Block Polymer Thin Films. *Macromolecules* **2013,** *46*, 5399-5415.
(41) Yu, K.; Eisenberg, A. Bilayer Morphologies of Self-Assembled Crew-Cut Aggregates of Amphiphilic PS-b-PEO Diblock Copolymers in Solution. *Macromolecules* **1998,** *31*, 3509-3518.
(42) van Zoelen, W.; Asumaa, T.; Ruokolainen, J.; Ikkala, O.; ten Brinke, G. Phase Behavior of Solvent Vapor Annealed Thin Films of PS-b-P4VP(PDP) Supramolecules. *Macromolecules* **2008,** *41*, 3199-3208.
(43) Kim, K.; Park, S.; Kim, Y.; Bang, J.; Park, C.; Ryu, D. Y. Optimized Solvent Vapor Annealing for Long-Range Perpendicular Lamellae in PS-b-PMMA Films. *Macromolecules* **2016,** *49*, 1722-1730.
(44) Son, J. G.; Gotrik, K. W.; Ross, C. A. High-Aspect-Ratio Perpendicular Orientation of PS-b-PDMS Thin Films under Solvent Annealing. *ACS Macro Lett.* **2012,** *1*, 1279-1284.
(45) Baruth, A.; Seo, M.; Lin, C. H.; Walster, K.; Shankar, A.; Hillmyer, M. A.; Leighton, C. Optimization of Long-Range Order in Solvent Vapor Annealed Poly(styrene)-block-poly(lactide) Thin Films for Nanolithography. *ACS Appl. Mater. Interfaces* **2014,** *6*, 13770-13781.
(46) Phillip, W. A.; O'Neill, B.; Rodwogin, M.; Hillmyer, M. A.; Cussler, E. L. Self-Assembled Block Copolymer Thin Films as Water Filtration Membranes. *ACS Appl. Mater. Interfaces* **2010,** *2*, 847-853.
(47) Sinturel, C.; Grosso, D.; Boudot, M.; Amenitsch, H.; Hillmyer, M. A.; Pineau, A.; Vayer, M. Structural Transitions in Asymmetric Poly(styrene)-block-Poly(lactide) Thin Films Induced by Solvent Vapor Exposure. *ACS Appl. Mater. Interfaces* **2014,** *6*, 12146-12152.

(48) Vayer, M.; Hillmyer, M. A.; Dirany, M.; Thevenin, G.; Erre, R.; Sinturel, C. Perpendicular orientation of cylindrical domains upon solvent annealing thin films of polystyrene-b-polylactide. *Thin Solid Films* **2010,** *518*, 3710-3715.
(49) Cummins, C.; Mokarian-Tabari, P.; Andreazza, P.; Sinturel, C.; Morris, M. A. Solvothermal Vapor Annealing of Lamellar Poly(styrene)-block-poly(d,l-lactide) Block Copolymer Thin Films for Directed Self-Assembly Application. *ACS Appl. Mater. Interfaces* **2016,** *8*, 8295-8304.
(50) Wu, Y.-H.; Lo, T.-Y.; She, M.-S.; Ho, R.-M. Morphological Evolution of Gyroid-Forming Block Copolymer Thin Films with Varying Solvent Evaporation Rate. *ACS Appl. Mater. Interfaces* **2015,** *7*, 16536-16547.
(51) Otsuka, I.; Tallegas, S.; Sakai, Y.; Rochas, C.; Halila, S.; Fort, S.; Bsiesy, A.; Baron, T.; Borsali, R. Control of 10 nm scale cylinder orientation in self-organized sugar-based block copolymer thin films. *Nanoscale* **2013,** *5*, 2637-2641.
(52) Rashkov, I.; Manolova, N.; Li, S. M.; Espartero, J. L.; Vert, M. Synthesis, Characterization, and Hydrolytic Degradation of PLA/PEO/PLA Triblock Copolymers with Short Poly(l-lactic acid) Chains. *Macromolecules* **1996,** *29*, 50-56.
(53) Dhital, R. N.; Murugadoss, A.; Sakurai, H. Dual Roles of Polyhydroxy Matrices in the Homocoupling of Arylboronic Acids Catalyzed by Gold Nanoclusters under Acidic Conditions. *Chem. Asian J.* **2012,** *7*, 55-59.
(54) Corma, A.; Serna, P. Chemoselective Hydrogenation of Nitro Compounds with Supported Gold Catalysts. *Science* **2006,** *313*, 332-334.
(55) Lennox, A. J. J.; Lloyd-Jones, G. C. Selection of boron reagents for Suzuki-Miyaura coupling. *Chem. Soc. Rev.* **2014,** *43*, 412-443.
(56) Butters, M.; Harvey, J. N.; Jover, J.; Lennox, A. J. J.; Lloyd-Jones, G. C.; Murray, P. M. Aryl Trifluoroborates in Suzuki–Miyaura Coupling: The Roles of Endogenous Aryl Boronic Acid and Fluoride. *Angew. Chem. Int. Ed.* **2010,** *49*, 5156-5160.
(57) Ren, W.; Li, J.; Zou, D.; Wu, Y.; Wu, Y. Palladium-catalyzed Suzuki–Miyaura cross-coupling reaction of potassium 2-pyridyl trifluoroborate with aryl (heteroaryl) halides. *Tetrahedron* **2012,** *68*, 1351-1358.
(58) Sawoo, S.; Srimani, D.; Dutta, P.; Lahiri, R.; Sarkar, A. Size controlled synthesis of Pd nanoparticles in water and their catalytic application in C–C coupling reactions. *Tetrahedron* **2009,** *65*, 4367-4374.
(59) Canty, A. J.; Deverell, J. A.; Gömann, A.; Guijt, R. M.; Rodemann, T.; Smith, J. A. Microfluidic Devices for Flow-Through Supported Palladium Catalysis on Porous Organic Monolith. *Aust. J. Chem.* **2008,** *61*, 630-633.
(60) Mahouche Chergui, S.; Ledebt, A.; Mammeri, F.; Herbst, F.; Carbonnier, B.; Ben Romdhane, H.; Delamar, M.; Chehimi, M. M. Hairy Carbon Nanotube@Nano-Pd Heterostructures: Design, Characterization, and Application in Suzuki C−C Coupling Reaction. *Langmuir* **2010,** *26*, 16115-16121.
(61) Han, J.; Liu, Y.; Guo, R. Facile Synthesis of Highly Stable Gold Nanoparticles and Their Unexpected Excellent Catalytic Activity for Suzuki−Miyaura Cross-Coupling Reaction in Water. *J. Am. Chem. Soc.* **2009,** *131*, 2060-2061.
(62) Levin, M. D.; Toste, F. D. Gold-Catalyzed Allylation of Aryl Boronic Acids: Accessing Cross-Coupling Reactivity with Gold. *Angew. Chem. Int. Ed.* **2014,** *53*, 6211-6215.
(63) Matsuda, T.; Asai, T.; Shiose, S.; Kato, K. Homocoupling of arylboronic acids catalyzed by simple gold salts. *Tetrahedron Lett.* **2011,** *52*, 4779-4781.
(64) Carrettin, S.; Guzman, J.; Corma, A. Supported Gold Catalyzes the Homocoupling of Phenylboronic Acid with High Conversion and Selectivity. *Angew. Chem. Int. Ed.* **2005,** *44*, 2242-2245.
(65) Pradhan, N.; Pal, A.; Pal, T. Catalytic Reduction of Aromatic Nitro Compounds by Coinage Metal Nanoparticles. *Langmuir* **2001,** *17*, 1800-1802.
(66) Adhikari, B.; Biswas, A.; Banerjee, A. Graphene Oxide-Based Hydrogels to Make Metal Nanoparticle-Containing Reduced Graphene Oxide-Based Functional Hybrid Hydrogels. *ACS Appl. Mater. Interfaces* **2012,** *4*, 5472-5482.
(67) Panigrahi, S.; Basu, S.; Praharaj, S.; Pande, S.; Jana, S.; Pal, A.; Ghosh, S. K.; Pal, T. Synthesis and Size-Selective Catalysis by Supported Gold Nanoparticles: Study on Heterogeneous and Homogeneous Catalytic Process. *J. Phys. Chem. C* **2007,** *111*, 4596-4605.

(68) Poupart, R.; Nour El Houda, D.; Chellapermal, D.; Guerrouache, M.; Carbonnier, B.; Le Droumaguet, B. Novel in-capillary polymeric monoliths arising from glycerol carbonate methacrylate for flow-through catalytic and chromatographic applications. *RSC Adv.* **2016,** *6*, 13614-13617.
(69) Kirai, N.; Yamamoto, Y. Homocoupling of Arylboronic Acids Catalyzed by 1,10-Phenanthroline-Ligated Copper Complexes in Air. *Eur. J. Org. Chem.* **2009,** *2009*, 1864-1867.

Conclusions

Cette thèse s'est attachée à développer de nouveaux catalyseurs supportés hybrides à base de polymères poreux et de nanoparticules métalliques. L'originalité de nos études réside notamment dans la variété des supports catalytiques, de monolithes polymères à des films nanoporeux issus de copolymères à blocs originaux en passant par des microréacteurs monolithiques pour la catalyse supportée en flux continu. Nous avons également fait varier les fonctionnalités à l'interface entre les nanoparticules et les supports polymères. Nous nous sommes aussi intéressés à faire varier les métaux utilisés pour les nanoparticules mais également à tester différentes réactions catalytiques, comme la réduction de composés nitrés ou de colorants et finalement les couplages Carbone-Carbone.

Pour ce faire, nous avons structuré notre investigation en trois grandes parties. La première s'est tournée vers la synthèse de matériaux monolithiques. Nous avons préparé et finement caractérisé des réseaux méthacryliques comprenant des ponts disulfures sélectivement clivables. Une fois réduits, les thiols obtenus ont servi de points d'ancrage à des nanoparticules d'or générées *in-situ* par réduction des sels métalliques correspondants en solution. Ces catalyseurs supportés ont été utilisé pour réduire efficacement un colorant largement employé dans l'industrie textile, l'éosine Y. Nous avons aussi testé une méthode alternative pour la génération de nanoparticules par voie sèche. Sur des réseaux à base de méthacrylate de glycidyle, nous avons immobilisé des sels d'or et/ou de palladium qui ont été réduits en utilisant l'hydrogène gazeux. Grâce aux nanoparticules formées, des couplages de Suzuki-Miyaura ont été réalisés, et l'influence de la nature du métal choisi sur la structure des produits obtenus a été démontrée. Les matériaux massiques sont ainsi très utiles pour des expériences préliminaires de catalyse hétérogène supportée. Faisant fi de la mise en forme du support, nous avons ainsi fondé nos études sur la chimie elle-même en faisant varier soit la structure des monomères fonctionnalisés, soit la nature du métal, soit le mode d'immobilisation des nanoparticules. En outre, en tant que blocs de polymères de tailles macroscopiques, une simple filtration permet de recycler les catalyseurs supportés. Malgré tout, leur faible résistance mécanique est une limite si une forte agitation est requise durant les réactions catalytiques.

Pour tenter de pallier ce problème, une deuxième partie s'est focalisée sur l'élaboration de microréacteurs à base de polymères méthacryliques. Ainsi, la matrice de *N*-acryloyloxysuccinimide, largement connue dans la littérature, a permis de nous familiariser avec les procédés de catalyse supportée en flux continu, en immobilisant d'abord des nanoparticules de cuivre par différentes voies possibles. Nous avons également étudié l'influence que différents ligands aminés greffés sur la matrice polymère pourraient avoir sur la génération des nanoparticules ainsi que sur le rendement catalytique

de la réduction de composés nitro-aromatiques. Par ailleurs, nous avons élaboré de nouveaux monolithes en utilisant un monomère tout à fait original, le méthacrylate de carbonate de glycérol, et les avons utilisés comme supports de NPs de platine. Ces catalyseurs supportés ont été exploités pour la réduction du 4-nitrophénol. L'intérêt des microréacteurs est bien sûr celui de la chimie en flux continu qui permet la récupération directe, aisée, du produit désiré en sortie de réacteur, sans étape supplémentaire de filtration. Par ailleurs les temps de réactions sont très courts, de l'ordre de quelques secondes et le catalyseur supporté peut être réutilisé après une simple étape de rinçage. Ces atouts sont majeurs d'un point de vue technologique, tout comme les faciles changements d'échelle qui permettrait de multiplier les volumes traités. Un point crucial est celui de la perte de charge générée en conditions dynamiques. Il faut en effet, contrôler finement la distribution des NPs à la surface des supports polymères et éviter tout phénomène d'agrégation qui serait préjudiciables à des utilisations en conditions douces, *i.e.* faible pression, du fait du colmatage des microréacteurs. Une compréhension fine de l'interface polymère/nanoparticules ainsi que l'optimisation des conditions de flux continu (débit, température, rapport massique entre réactifs, …) sont donc nécessaires en vue de diminuer les pertes de charge dans ces systèmes miniaturisés et d'améliorer les rendements de réactions.

Enfin, la dernière partie a permis d'explorer la catalyse hétérogène supportée en utilisant comme supports catalytiques des polymères nanoporeux issus de copolymères diblocs fonctionnalisés. Selon une approche originale faisant appel au clivage sélectif d'une jonction chimique spécifique entre les deux blocs, nous avons généré des matériaux nanoporeux à base de polystyrène possédant des fonctions chimiques thiol ou amine à la surface des pores. Différents procédés d'orientation ont permis la mise en forme des matériaux, soit sous forme massique, soit sous forme de films. Dans les deux cas, l'immobilisation de nanoparticules d'or générées *in-situ* a été réalisée avec succès et ces nouveaux catalyseurs supportés ont été testés dans différentes réactions organiques modèles avec une excellente efficacité. Dans le cas des films poreux fonctionnalisés par des amines, nous avons réalisé une réaction en cascade en « one-pot » constituée par un couplage carbone-carbone d'un acide boronique, suivie d'une réduction du composé nitré intermédiaire. Cependant, malgré l'originalité de ces systèmes, il n'en reste pas moins que la synthèse des copolymères précurseurs demeure relativement longue. Les amorceurs hétérobifonctionnels requis sont d'abord synthétisés en laboratoire en une ou plusieurs étapes selon la fonction désirée et les disponibilités de précurseurs commerciaux. De plus, les étapes nécessaires à l'orientation des copolymères et à la génération des pores peuvent aussi être consommatrices de temps. Malgré ces limites, ils ont l'avantage indéniable de permettre le contrôle de la morphologie poreuse ainsi que des tailles de pores en jouant sur la longueur du bloc sacrificiel des précurseurs. Ces atouts expliquent pourquoi les matériaux nanoporeux issus de copolymères à blocs sont exploités dans divers domaines des nanotechnologies.

L'ensemble de ces résultats intéressants ouvrent des perspectives prometteuses. Dans le cas des microréacteurs, outre le fait de s'attaquer à une échelle de colonne plus grande, c'est à de nouvelles applications que l'on pourrait penser. En effet, comme nous l'avons vu, en chimie en flux continu, la récupération des produits est aisée. Cela ne s'applique néanmoins qu'aux réactions ne générant qu'un seul produit. Dans le cas général de réactions donnant lieu à un mélange de produits, les systèmes de type microréacteur monolithique pourraient être judicieusement exploités pour d'une part, effectuer un suivi en ligne du rendement de la réaction et d'autre part, séparer les produits de réaction, permettant leur récupération séquentielle en sortie de réacteur. Ainsi, un microréacteur multifonctionnel pourrait intégrer une zone en entrée de réacteur destinée à la réaction, en y accrochant des nanoparticules *via* des sélecteurs greffés, suivi d'une zone possédant un greffon jouant le rôle de sélecteur pour séparation des produits issus de la réaction. Nous pourrions donc, en théorie, collecter séparément les produits d'intérêt et les sous-produits non désirés.

Concernant les copolymères à blocs, même si l'on peut encore penser au développement de nouvelles jonctions chimiques entre les blocs, il est aussi tout à fait possible d'envisager d'autres axes de développement. Si les différentes méthodes de polymérisations utilisées sont maîtrisées, il est toujours délicat d'intégrer des fonctions chimiques dans les amorceurs. En effet, ces différentes fonctions peuvent interagir de manière inopinée lors des étapes de polymérisation et, en conséquence, doivent éventuellement être protégées. De manière à développer une approche plus polyvalente, nous pourrions envisager une jonction capable de lier les blocs de manière efficace, en utilisant possiblement des blocs commerciaux. Une tentative réalisée durant cette thèse à donner lieu à la synthèse d'une jonction très originale, possédant d'une part une double liaison susceptible de subir une réaction « click » thiol-ène et d'autre part une benzodioxinone diphénylée pouvant accepter un alcool primaire sous UV pour former un ester (**Schéma A**). Une série de copolymères diblocs divers et variés peut alors être envisagée par double réaction de condensation en « one-pot » en présence de la jonction difonctionnelle présentant des groupements antagonistes à ceux des blocs, en faisant varier la nature et/ou la longueur des blocs. La jonction entre les blocs devient facilement clivable grâce à une simple hydrolyse de l'ester formé (**Schéma B**).

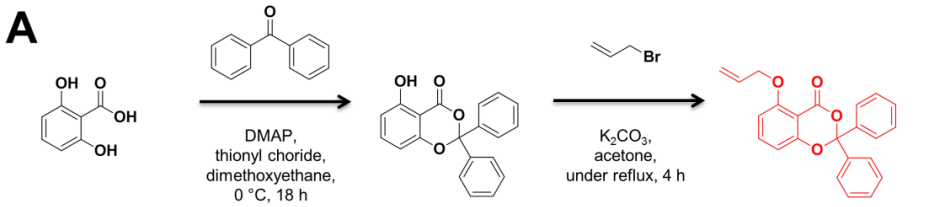
A
OH
O
OH
OH
DMAP,
thionyl choride,
dimethoxyethane,
0 °C, 18 h
Br
K_2CO_3,
acetone,
under reflux, 4 h

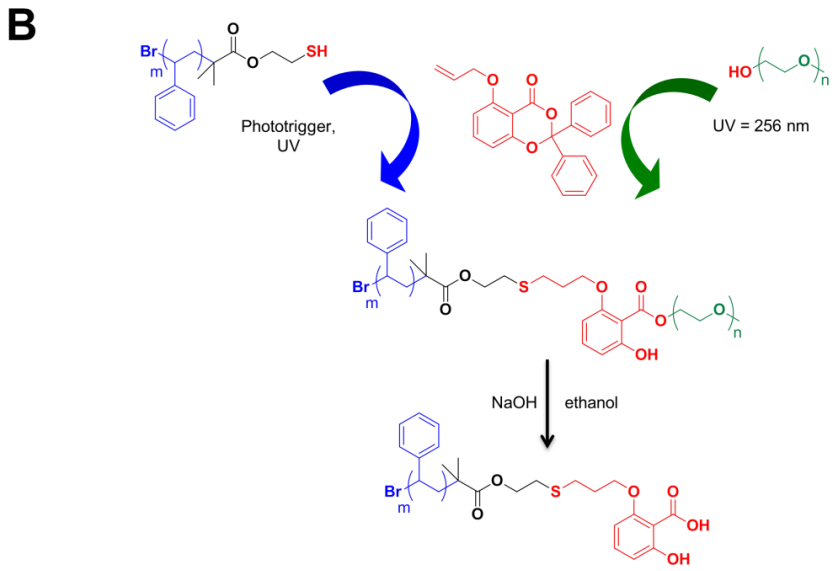
B
Br
m
SH
Phototrigger,
UV
HO
n
UV = 256 nm
S
NaOH
ethanol

Annexes

Supplementary Information of Article 5

Table S1: Composition of polymerization mixtures used for the preparation of in-capillary monoliths with the corresponding permeabilities.

Polymerization Mixture	% v/v toluene/DOH[a]	% v/v toluene/C_9H_{20}	% w/w monomers/solvents	% w/w GCMA/EGDMA	B_0[b] (10^{-14} µm²)
1	75/25	-	36.2/33.8	34.4/65.6	4.31
2	-	50/50	36.2/63.8	34.4/65.6	0.89
3	40/60	-	39.2/60.8	34.4/65.6	1.83
4	100/0	100/0	36.2/63.8	34.4/65.7	12,21
5	0/100	-	36.2/63.8	34.4/65.8	[a]
6	50/50	-	36.2/63.9	34.4/65.9	3,56
7	25/75	-	36.2/63.10	34.4/65.10	[a]
8	60/40	-	36.2/63.11	34.4/65.11	5,23
9	-	0/100	36.2/63.12	34.4/65.12	[a]
10	40/60	-	36.2/63.13	34.4/65.13	[a]
11	40/60	-	44,2/55.8	34.4/65.14	1,08
12	40/60	-	49,8/50,2	34.4/65.15	1,78
13	40/60	-	39,2/60,8	25,1/74,9	11,60
14	40/60	-	39,2/60,8	43,8/56,2	16,74

[a] Permeability impossible to measure due to monolithic capillary clogging

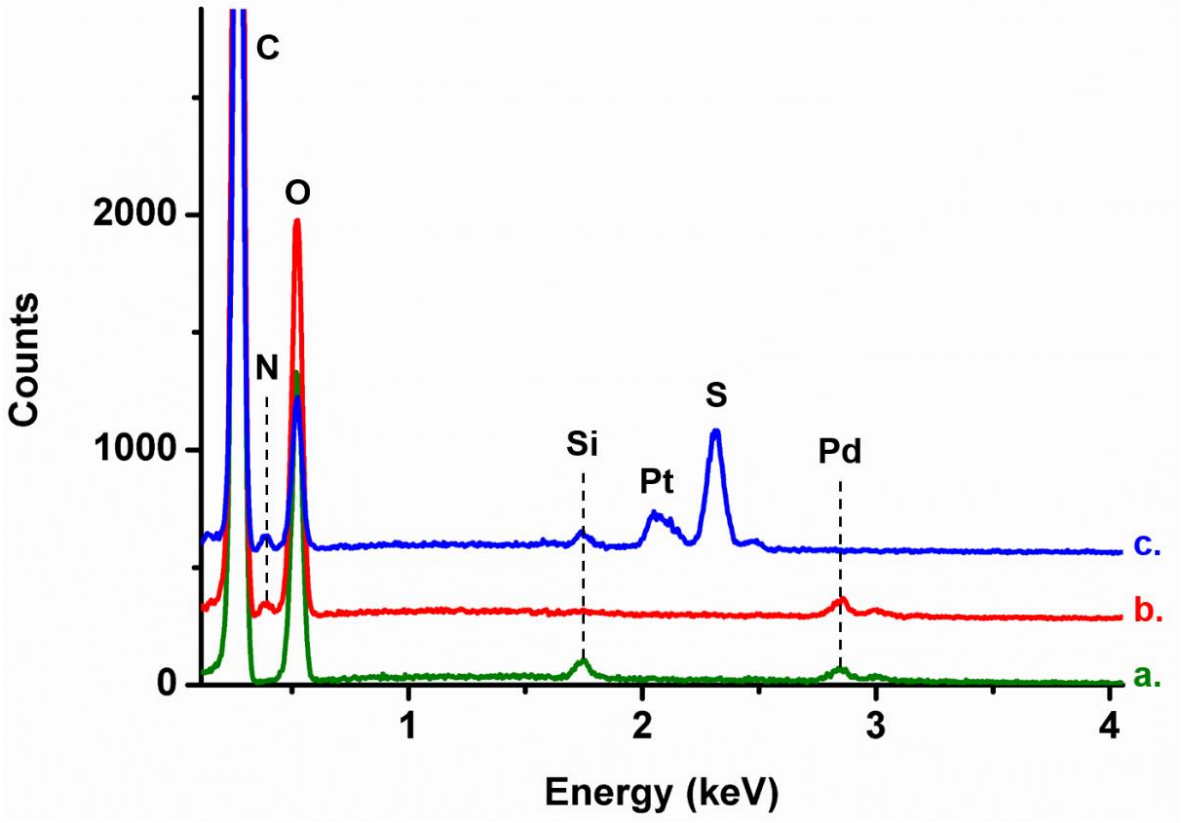

Figure S1: *In-situ* EDX semi-quantitative analysis of monolithic GCMA-based capillary *a)* before and after functionalization with *b)* allylamine and subsequent thiol-ene addition of *c)* 1-octane thiol.

Supplementary Information of Article 6

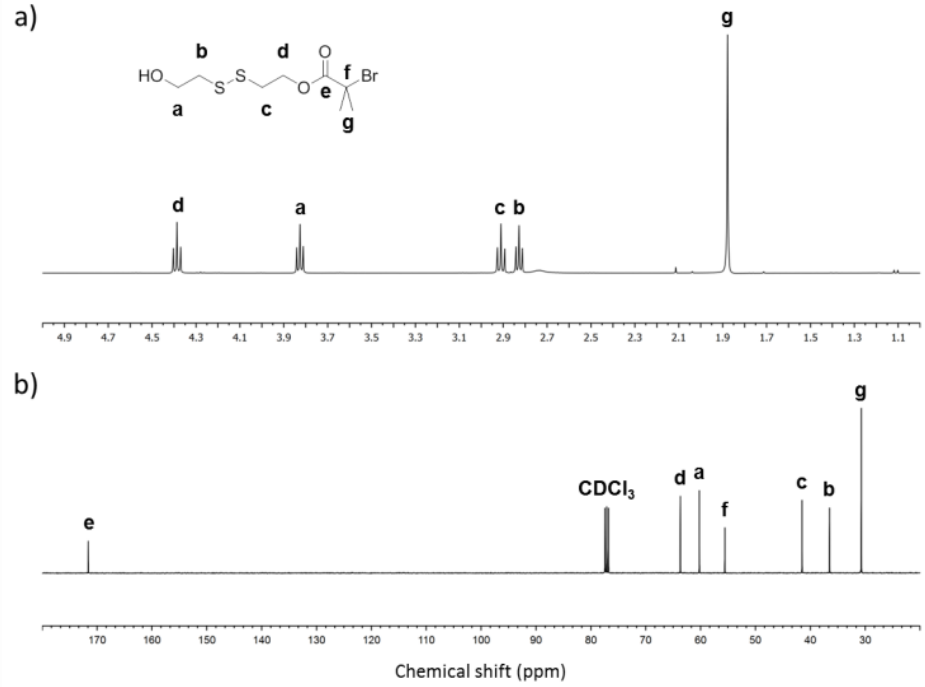

Figure S2: *a)* ^{1}H NMR and *b)* ^{13}C NMR of the new asymmetric difunctional initiator, *i.e.* 2-[(2-hydroxyethyl)dithio]ethyl 2-bromoisobutyrate (**1**).

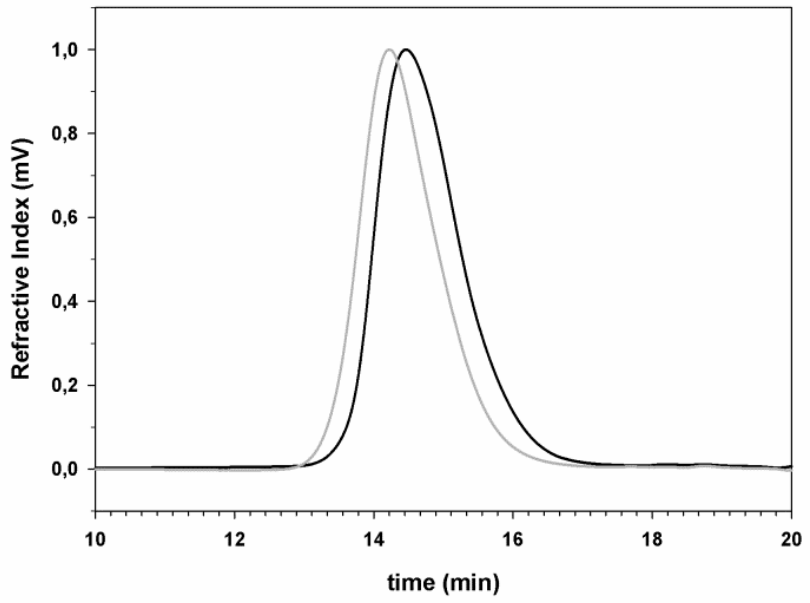

Figure S3: SEC traces of PS_{104}-OH macroinitiator (black line) and corresponding PS_{104}-*b*-PLA_{47} copolymer (grey line).

Résumé

Les matériaux poreux issus de polymères organiques ont fait l'objet, depuis leur découverte, d'intenses recherches dans divers champs d'application. Leurs propriétés intrinsèques uniques, comme par exemple leur facilité de fonctionnalisation, leur large gamme de porosité accessible, ainsi que leur faible coût de production les ont ainsi rendu particulièrement attrayants. La catalyse hétérogène supportée, permettant de se débarrasser du catalyseur métallique une fois la réaction achevée et également de facilement le recycler, est en plein essor, notamment depuis l'avènement des nanoparticules métalliques. Durant ce travail de thèse, nous avons développé différents matériaux polymères pouvant servir de supports robustes pour l'immobilisation de nanoparticules métalliques en nous focalisant majoritairement sur trois types de matériaux distincts: des charpentes polymères macroporeuses monolithiques, des monolithes polymères poreux confinés dans des microcanaux ainsi que des structures (nano)poreuses provenant de la dégradation sélective de copolymères diblocs nanostructurés et fonctionnalisés.

L'immobilisation de nanoparticules métalliques de différentes natures a généralement nécessité une étape de fonctionnalisation post-polymérisation avec des greffons chimiques de manière à favoriser la chélation de nanoparticules métalliques générées *in situ* ou *ex situ*. Finalement, différentes réactions catalysées par ces nanoparticules métalliques supportées ont été testées en utilisant les matériaux hybrides ainsi préparés. Nous avons notamment démontré que la réduction de dérivés nitroaromatiques ou de colorants et des homo- ou hétéro-couplages C-C ont été menés avec une bonne efficacité catalytique. Le caractère recyclable de certains de ces matériaux hybrides a également été facilement démontré en réalisant plusieurs cycles catalytiques avec des efficacités constantes.

Mots-clefs : polymères poreux, nanoparticules métalliques, catalyse supportée.

Abstract

Since their discovery, porous materials stemming from organic polymers have been the subject of intense research in diverse application fields. Their unique intrinsic properties, such as their facile functionalization, their large porosity range accessible as well as their low production cost for instance have thus made them particularly attractive. Supported heterogeneous catalysis permits to remove the metallic catalyst once the reaction completed and also to easily recycle it; it is a still growing area, especially since the emergence of metallic nanoparticles. During this Ph.D. work, different porous polymeric materials have thus been designed so as to be implemented as robust supports for the immobilization of metallic nanoparticles. We mainly focused our investigations on three distinct types of materials: macroporous polymeric monoliths, in-microchannels porous polymeric monoliths as well as (nano)porous frameworks arising from selective degradation of diblock copolymers.

The immobilization of metallic nanoparticles of different natures generally required a post-polymerization functionalization step with suitable chemical grafts so as to improve the chelation of *in-situ* or *ex-situ* generated metallic nanoparticles. Finally, different supported metallic nanoparticle-based catalytic reactions have been assessed using such as-prepared hybrid materials. We notably demonstrated that reduction of nitroaromatic derivatives, reduction of dyes and C-C homo- and cross-coupling were successfully achieved with high catalytic efficiency. The recyclability of some of these porous hybrid materials was also easily ascertained by realizing different catalytic runs with constant efficiency values.

Keywords: porous polymers, metallic nanoparticles, supported catalysis.